Uplink Capacity Enhancement in WCDMA

Multi Cell Admission Control, Synchronised Schemes and Fast Packet Scheduling

Outes Carnero, José

Publication date:
2004

Document Version
Publisher's PDF, also known as Version of record

Ph.D. Thesis

Uplink Capacity Enhancement in WCDMA

Multi Cell Admission Control, Synchronised Schemes and Fast Packet Scheduling

March 2004

ISBN 87-90834-54-2

ISSN 0908-1224

R04-1011

Department of Communication Technology

Institute of Electronic Systems

Aalborg University

Niels Jernes Vej 12, DK-9220 Aalborg Øst, Denmark

Abstract

The large expectances created for WCDMA are based on its flexibility for multimedia capabilities and the high capacity it will provide. However, the demanded traffic grows rapidly, and new capacity enhancements are required in order to satisfy the future needs. This thesis analyses the potential for three advanced features to enhance the capacity in the uplink (from mobile station to base station) of WCDMA systems: multi cell admission control, synchronised schemes and fast packet scheduling.

First, a power-based multi cell admission control algorithm is studied as an alternative to the existing single cell algorithms. With a single cell algorithm the power increase caused by a new user is only evaluated in the serving cell before admission is granted/rejected. If the new user is close to the cell edge and requires high transmission power, it might also create excessive interference in neighbouring cells, leading to potential network instability. Multi cell admission control algorithms prevent these situations by also estimating the power increase at the neighbouring cells. The results reveal that under non-homogeneous load conditions, the uplink multi cell admission control offers 34% more cell throughput compared to a single cell scheme for a 5% probability of reaching an overload situation.

The second capacity enhancing feature consists of reaching uplink orthogonality by means of synchronised schemes. The performance of an uplink synchronous WCDMA system is evaluated at network level. According to the results generated for speech service, the main problem in uplink synchronous WCDMA systems is the code shortage. For ITU Pedestrian A environments with the most realistic assumptions, uplink synchronous WCDMA only provides a 10% capacity gain in terms of cell throughput. However, a high potential exists for situations where this code shortage can be solved, e.g. 36% capacity gain can be obtained assuming no code restriction. Variable modulation and coding is introduced as a solution to improve the channelisation code utilisation and thereby increase the capacity of uplink synchronous WCDMA. A 29% capacity gain is obtained in terms of cell throughput for a Pedestrian A environment.

Finally, a fast scheduling concept for packet data traffic over uplink dedicated channels is investigated including physical layer Hybrid ARQ (HARQ). Two algorithms for fast scheduling based on blind data rate detection and time division multiplexing with shorter scheduling period are considered. For comparable network load and user quality of service, the cell throughput becomes up to 9% higher with HARQ. The total gain of HARQ with a fast scheduling strategy based on channel quality information is 52% compared to 3GPP/Release 99-based packet scheduler implementations in a macro-cell scenario. In the case of a pedestrian micro-cell environment, the scheduling based on time division multiplexing can be combined with uplink synchronous WCDMA, providing a higher capacity increase. With an unfair scheduling policy there is a cell throughput increase of 108%, whereas with a strategy that allocates the same average throughput for all the users, the throughput increase remains as high as 95%.

The research has been carried out having as a reference study case the UMTS Terrestrial Radio Access (UTRA) Frequency Division Duplex (FDD) mode, standardised by the 3rd Generation Partnership Project (3GPP). The results provided in this thesis are supported by theoretical analysis and/or extensive system level simulations with multi cell scenarios, including the effect of many relevant mechanisms that have an impact on the radio access.

Dansk Resumé

Translated by Troels B. Sørensen

De store forventninger til WCDMA er baseret på teknologiens fleksibilitet for multimedia transmission og trafikkapaciteten som tilvejebringes med denne teknologi. Trafikbelastningen vil dog vokse kraftigt og for at imødekomme fremtidige krav er det nødvendigt med nye teknikker til kapacitetsforøgelse. Denne afhandling analyserer potentialet i tre avancerede kapacitetsforøgende teknikker for uplink retningen (fra mobil enhed til basisstation) i WCDMA: multicelle netacces (’admission control’), synkroniseret transmission og pakkeskedulering (’packet scheduling’).

Indledningsvis studeres multicelle netacces baseret på modtagen effekt som et alternativ til de eksisterende enkeltcelle algoritmer. For enkeltcelle algoritmerne baseres netaccessen for en ny bruger udelukkende på forøgelsen af den modtagne effekt i den enkelte celle. Hvis den nye bruger er tæt på cellegrænsen og derfor kræver et højt transmitteret effektniveau er det sandsynligt at der også genereres kraftig interferens i nabocellerne; en sådan situation kan skabe et ustabilt netværk. Multicelle baseret netacces forhindrer sådanne situationer ved også at estimere effektforøgelsen i nabocellerne. Resultaterne viser at uplink multicelle netacces kan give en forøgelse i den supporterede trafikbelastning på 34% i sammenligning med enkeltcelle netacces under ikke-homogen trafik og 5% sandsynlighed for et overbelastet netværk.

Den anden kapacitetsforøgende teknik går ud på at opnå ortogonalitet i WCDMA uplink ved hjælp af synkroniseret transmission. Teknikken er i denne afhandling evalueret på netværksniveau. Som tydeliggjort med resultaterne for transmission af tale er det centrale problem for uplink synkroniseret transmission begrænsningen i antallet af spredningskoder: Med de mest realistiske antagelser og udbredelsesmiljø i henhold til ITU ’Pedestrian A’ giver uplink synkroniseret transmission en beskeden kapacitetsforøgelse på 10% større supporteret trafikbelastning. Teknikken har dog et stort potentiale hvis det er muligt at omgå begrænsningen i antallet af spredningskoder – ideelt uden begrænsning i antal koder er kapacitetsforøgelsen på 36%. Variabel modulation og kodning er i denne afhandling anvendt til at forøge udnyttelsen af spredningskoderne og dermed forøge kapaciteten for uplink synkroniseret transmission i WCDMA. For ’Pedestrian A’ udbredelsesmiljøet er kapacitetsforøgelsen aktuelt på 29%.

Som den tredje og sidste teknik er der fokuseret på et hurtigt pakkeskeduleringskoncept for pakkedata trafik over dedikerede uplink kanaler, inkluderende retransmission på fysisk lag i form af ’Hybrid ARQ (HARQ)’. Specifikt er der fokuseret på to algoritmer baseret på henholdsvis ’blind data rate detection’, og ’time division multiplexing’ med kort pakkeskeduleringsperiode. For samme netværks trafikbelastning og bruger ’Quality of Service’ giver HARQ en forøgelse af den supporterede trafikbelastning på 34%. Kombineret med pakkeskedulering baseret på ’time division multiplexing’ og brug af ’Channel Quality Information’ er kapacitetsforøgelsen i makro-celle udbredelsesmiljø på 52% i sammenligning med pakkeskedulering baseret på 3GPP/Release 99. For mikrocelle udbredelsesmiljø kan skedulering baseret på ’time division multiplexing’ kombineres med uplink synkroniseret transmission og deraf følgende yderligere kapacitetsforøgelse. Anvendes en skeduleringsmetode der tillader differentiering af brugerne er kapacitetsforøgelsen på 108%, mens en metode der ikke differentierer brugerne giver en kapacitetsforøgelse på op til 95%.

Forskningen i denne afhandling er konkretiseret med UMTS Terrestrial Radio Access

(UTRA) Frequency Division Duplex (FDD) standarden som reference. Denne standard er udviklet i 3rd Generation Partnership Project (3GPP). Afhandlingens resultater er genereret på baggrund af teoretisk analyse og/eller omfattende systemniveau simuleringer af multicelle radionetværk hvori er medtaget flere relevante aspekter med indflydelse på radiogrænsefladen.

Preface and Acknowledgement

This Ph.D. thesis is the result of a three-year project carried out at the Center for PersonKommunikation (CPK), now integrated in the Department of Communication Technology of Aalborg University. The thesis work has been completed in parallel with the mandatory courses and teaching/working obligations required in order to obtain the Ph.D. degree. The research project has been accomplished under the supervision of Research Professor Ph.D. Preben E. Mogensen (Aalborg University) and the co-supervision of Ph.D. Klaus I. Pedersen (Nokia Networks) and Associate Professor Ph.D. Troels B. Sørensen (Aalborg University). This Ph.D. research has been fully sponsored by Nokia Networks.

The thesis investigates new techniques to increase the uplink capacity in WCDMA systems, concretely for UTRA FDD mode as specified by the 3rd Generation Partnership Project (3GPP). The study is mainly based on computer simulations, taking many practical system aspects into account. Theoretical analyses are also carried out in order to corroborate the results from the simulations. The reader is expected to have a basic knowledge about system level aspects of UMTS Terrestrial Radio Access Network (UTRAN) Frequency Division Duplex (FDD) as well as radio propagation.

The thesis is divided into three main parts, which can be read independently. Each of them is covered in a single chapter, except the one covering uplink synchronous WCDMA, which is relatively wider and is therefore distributed in three chapters. A list of abbreviations is provided at the beginning of the report. A large number of references are quoted throughout the dissertation. All of them are listed at the end of the report. A number of appendices have been included with additional information to clarify certain aspects associated with the main chapters of the report. Some of the appendices also include extra investigations that, although they do not directly lead to the final target, they provide interesting results related to the core of the Ph.D. thesis.

The work presented in Sections 6.3-6.5 has been jointly carried out together with Ph.D. student Claudio Rosa (Aalborg University), to whom I must recognise fifty percent of the work, as well as unnumbered very interesting and productive discussions. The contribution of other colleagues to this thesis is described in Section 1.5.

I am deeply grateful to my supervisor Preben E. Mogensen for his support, advice and guidance, as well as for encouraging me to finish my Ph.D. thesis during the most difficult moments of the project.

From a technical point of view, I would also like to express my gratitude to Klaus I. Pedersen, who, apart from dedicating an important part of his time to the co-supervision of my thesis, has provided me with his excellent vision to conduct investigations and concentrate on the important matters. Distinctive gratitude is also paid to Troels B. Sørensen, who participated in the review process of this thesis report together with the rest of my supervisors, as well as for his wise pieces of advice during the study period, especially in the last phase. The contribution by Troels E. Kolding is very much appreciated, thanks to his technical support during part of the research, as well as his personal attention.

The support by all my colleagues and former colleagues from the Cellular Systems group of the University of Aalborg is highly appreciated. I would like to thank Lars Berger and Laurent Schumacher for their personal and technical support. The contribution of Claudio Rosa and Konstantinos Dimou, who I have worked in close cooperation with during the last part of my thesis, is not forgotten. Thanks also to Lisbeth S. Larsen for taking good care of me and for

making my life easier during the moments when it was most necessary. A special acknowledgement is given to Pablo Ameigeiras, Isaías López and Juan Ramiro, who together with me studied at the University of Málaga and afterwards decided to continue tailoring our working future by trying new experiences in Aalborg.

I am also thankful to the rest of colleagues at Nokia Networks in Aalborg for their contribution to the elaboration of the Ph.D. study. I would like to dedicate a special acknowledgement to Jytte Larsen for reviewing the use of English in the report. Lise M. Hansen's assistance and good humour during the first two years of my Ph.D. study period are deeply appreciated.

I owe a special distinction to Gema, who decided to follow me to Aalborg, staying by my side, taking care of me and giving me all her love. I am infinitely thankful to my parents Pepe and Mercedes and my brother Daniel, to whom I have been in contact practically every day since I moved to Aalborg, and who have given me their unconditional love, advice, care and emotional support in the most difficult moments. I would also like to express my gratitude to the rest of my family and my friends in Málaga, who have never forgotten me and have made me feel closer to home thanks to their phone calls, letters, emails and visits to Aalborg.

José Outes Carnero

March 2004

Contents

Abbreviations

16QAM	16-symbol Quadrature Amplitude Modulation
3G	3rd Generation of mobile communications
3GPP	3rd Generation Partnership Project
64QAM	64-symbol Quadrature Amplitude Modulation
8PSK	8-symbol Phase Shift Keying
AC	Admission Control
AVI	Actual Value Interface
AWGN	Additive White Gaussian Noise
BER	Bit Error Rate
BLER	Block Error Rate
BPSK	Binary Phase Shift Keying
BRD	Blind data Rate Detection
BS	Base Station
BSC	Base Station Controller
BTS	Base Transceiver Station
CCDF	Complementary Cumulative Distribution Function
CDF	Cumulative Distribution Function
CDMA	Code Division Multiple Access
CL	Code Load
CN	Core Network
DCH	Dedicated Channel
DPCCH	Dedicated Physical Control Channel
DPDCH	Dedicated Physical Data Channel
DS-CDMA	Direct Sequence Code Division Multiple Access
DTX	Discontinuous Transmission
Eb/No	Energy-per-bit to Noise ratio
Ec/Io	Energy-per-chip to Interference-power-density ratio
E-DCH	Enhanced Dedicated Channel
Es/No	Energy-per-symbol to Noise ratio
FACH	Forward Access Channel
FDD	Frequency Division Duplex

GPRS	General Packet Radio Service
HSDPA	High Speed Downlink Packet Access
iid	Independent, identically distributed
IPI	Inter-Path Interference
I-Q	In-phase and Quadrature-phase
L1	Layer 1 (physical layer)
L2	Layer 2 (link layer)
L3	Layer 3 (network layer)
LC	Load Control
MAC	Medium-Access Control
MAI	Multiple Access Interference
MC	Multi Cell
MCS	Modulation and Coding Scheme
ME	Mobile Equipment
MRC	Maximal Ratio Combining
MS	Mobile Station
MSC	Mobile Services Switching Centre
MTPE	Maximise Transmit Power Efficiency
NBAP	Node B Application Part
NR	Noise Rise
NRT	Non-Real Time
OVSF	Orthogonal Variable Spreading Factor
PAR	Peak-to-Average (power) Ratio
PC	Power Control
PDE	Power Decrease Estimator
PDF	Probability Density Function
PDP	Power Delay Profile
PFT	Proportional Fair Throughput
PIE	Power Increase Estimator
QoS	Quality of Service
QPSK	Quadrature Phase Shift Keying
RLC	Radio Link Control
RM	Resource Manager
RNC	Radio Network Controller
RNS	Radio Network Subsystem

RRC	Radio Resource Control
RRFT	Round-Robin Fair Throughput
RRM	Radio Resource Management
RT	Real Time
RTPD	Round Trip Propagation Delay
RUF	Resource Utilisation Factor
SC	Single Cell
SF	Spreading Factor
SGNS	Serving GPRS Support Node
SHO	Soft Handover
SIR	Signal-to-Interference (power) Ratio
SNR	Signal-to-Noise (power) Ratio
TAB	Time Alignment Bit
TDD	Time Division Duplex
TDM	Time Division Multiplexing
TDMA	Time Division Multiple Access
TFC	Transport Format Combination
TFCI	Transport Format Combination Indicator
TFCS	Transport Format Combination Set
TTI	Transmission Time Interval
TVM	Traffic Volume Measurements
UE	User Equipment
UMTS	Universal Mobile Telecommunications System
USIM	UMTS Subscriber Identity Module
USTS	Uplink Synchronous Transmission Scheme
UTRA	UMTS Terrestrial Radio Access
UTRAN	UMTS Terrestrial Radio Access Network
VMC	Variable Modulation and Coding
WCDMA	Wideband Code Division Multiple Access

Chapter 1

Introduction

1.1 Preliminaries

Since the first analog cellular system was deployed in the beginning of the 80s [1], the mobile communication systems have been continuously evolving. The trend has been towards new technologies that offer more advanced services and an anticipated solution to the users' demands. Currently two third generation of mobile communication (3G) systems are specified: the Universal Mobile Telecommunication System (UMTS) and cdma2000. UMTS is based on Wideband CDMA (WCDMA) and is composed of two different but related modes: UMTS Terrestrial Radio Access (UTRA) Frequency Division Duplex (FDD), and UTRA Time Division Duplex (TDD); cdma2000 consists of multicarrier CDMA [1].

The 3rd Generation Partnership Project (3GPP) is in charge of the specifications of the UTRA FDD, whereas a second body, 3GPP2, was established around cdma2000 [2].

In the beginning of this Ph.D. study, the 3GPP had already frozen the Release 99 specifications, and the preparation of a new release (Release 4) had already begun. Release 4 and 5 are currently frozen, whereas new releases (Release 6 and 7) are ongoing [3].

The evolution from the 3GPP/Release 99 is oriented to the increase of the cell capacity and peak data rate and the decrease of the delay associated with packet services [4].

Figure 1.1 illustrates the demanded data rates over the years for the uplink (connection from the mobile terminal to the base station) and the downlink (connection from the base station to the mobile terminal) [5]. Due to the asymmetrical properties of the traffic, most of the efforts to include a high data rate packet access in the 3GPP specifications are dedicated to the downlink. High Speed Downlink Packet Access (HSDPA) is the evolution of the Release 99

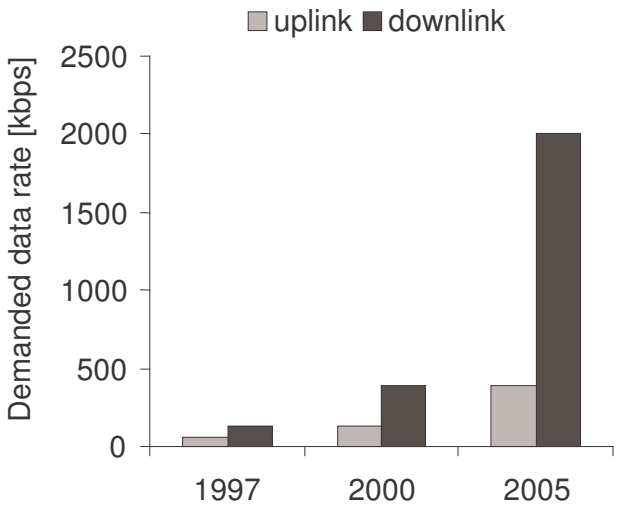

Figure 1.1. Evolution of the traffic demand [5].

for downlink and provides peak data rates of up to 10 Mbps [6].

On the contrary, this thesis will focus on the uplink of WCDMA, but will consider the evolution of UTRA FDD mode as a reference study case. The main motivations for the selection of the scope of this Ph.D. thesis originate from the little attention paid to the uplink in the open literature compared to the downlink evolution of UMTS.

1.2 Overview of the UTRA FDD Release 99

1.2.1 Summary of WCDMA

WCDMA is a network-asynchronous wideband direct-sequence CDMA (DS-CDMA) scheme. The use of orthogonal variable spreading factors (OVSF) allows for the accommodation of highly variable user data rates and facilitates a flexible introduction of new services. The used chip rate of 3.84 Mcps leads to a carrier bandwidth of approximately 5 MHz. In UTRA FDD two separate bandwidth of 5 MHz are used for uplink and downlink. A user bit rate of up to 2 Mbps can be reached [7].

1.2.2 The Uplink in WCDMA

Due to their inherent properties, the design of the uplink and the downlink in WCDMA require different approaches. This sub-section describes the main characteristics of the uplink in WCDMA. The aim is to facilitate a better comprehension of techniques and approaches commonly used for the uplink, as well as to clarify the ways to proceed for the enhancement of the uplink. WCDMA defines two types of dedicated physical channels for the uplink, the Dedicated Physical Data Channel (DPDCH) and the Dedicated Physical Control Channel (DPCCH). Each connection is allocated one DPCCH and zero, one or several DPDCHs [8]. In addition, common physical channels are also defined. The channels use a 10 ms radio frame structure, divided into 15 slots. Within each slot, the DPDCHs and the DPCCH are transmitted in parallel I-Q branches, using different codes and spreading factors (SF). Figure 1.2 presents the generic structure of an uplink transmitter according to 3GPP [9], [10]. The

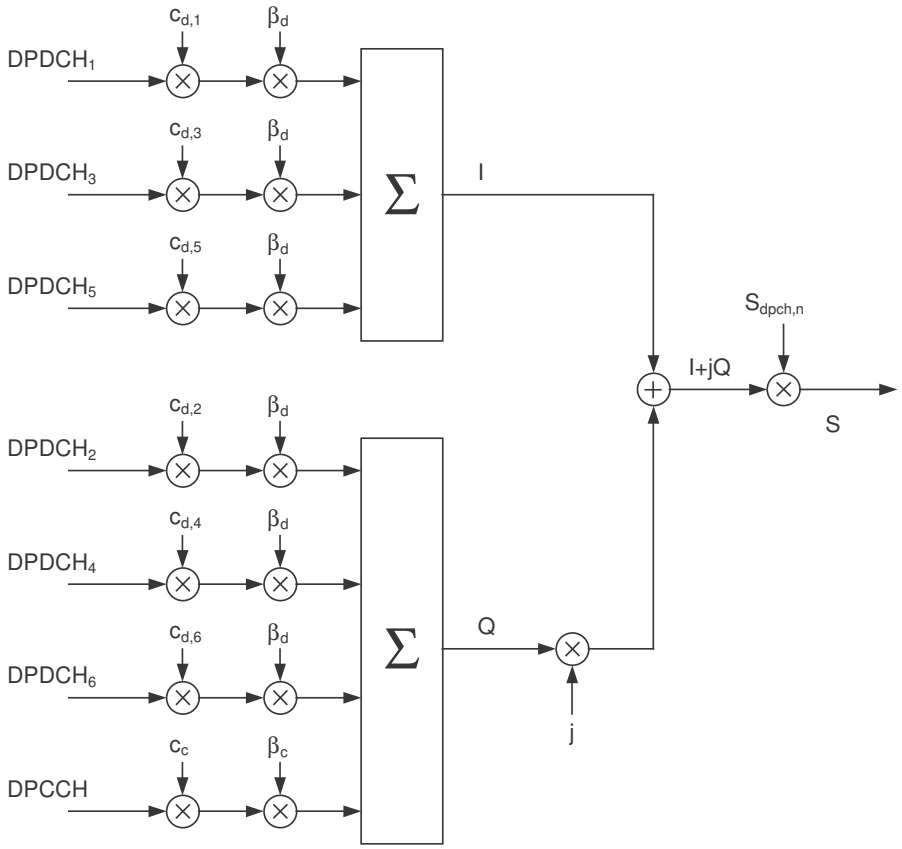

Figure 1.2. Transmission of data through one or more DPDCHs and one DPCCH according to 3GPP [9].

signals are multiplied by a channelisation code (c) for channel discrimination and a scrambling code (S) for user discrimination. Additionally, the channels are given different relative power strengths by means of the power scale factor β. In the uplink the SFs can vary between 4 and 256 [7].

One inherent problem in the uplink is the so-called near-far effect: users near the receiver are received at higher power than those far away, which suffer degradation in performance. Power control (PC) is the most common solution to solve the near-far effect. As a result, the signals received at the cell site from all the mobile units within a cell remain at the same level assuming equal bit rate [11]. In WCDMA fast closed-loop PC is run at slot basis, i.e. with a frequency of 1500 Hz.

In the uplink the reception of the signals in the same cell is performed in a centralised way by a unique entity, the base station (BS). Therefore, the equipment for reception is common for all the users and not distributed among the mobile stations (MS) as in the downlink case. This fact makes the use of advanced receivers in the uplink very attractive, since all the MSs can benefit from the technology upgrades made at the BS side.

The fact that the transmission is distributed among the MSs, with different physical locations, brings about both pros and cons. On one hand, the uplink of the WCDMA systems is not typically power limited, but interference limited.

On the other hand, since the signals from the different users in the cell arrive asynchronously at the BS, it is not possible to use orthogonal codes to reduce the multiple access interference

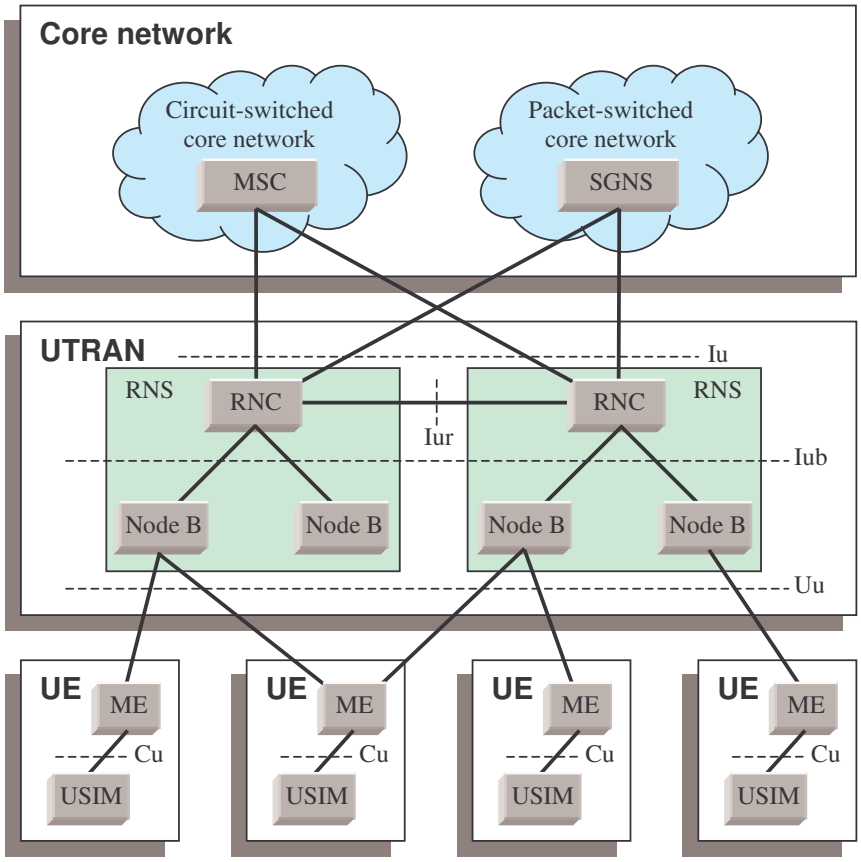

Figure 1.3. UMTS architecture.

(MAI), as it is done for the downlink. Furthermore, the packet scheduling gets complicated, as the users have to signal the information about their buffer occupancy.

The investigations in this thesis are carried out by assuming conventional Rake receivers. The Rake receivers are employed to exploit the multi-path diversity of the signals subject to multi-path fading. A Rake receiver consists of a bank of correlators, each of which correlates to a particular multi-path component of the desired signal. The correlator outputs may be weighted according to their relative strengths and summed to obtain the final estimate [12]. In this study, maximal ratio combining (MRC) is considered, which means that each of the branches associated with every multi-path component are used in a co-phased and weighted manner so that the highest achievable signal-to-noise ratio (SNR) is always available at the receiver.

Despite the fact that other advanced techniques can largely boost the overall performance of CDMA system, the Rake is still the receiver structure of choice for the first round of low-complexity receivers for 3G systems [13].

1.2.3 UTRAN Architecture

The UMTS system consists of a number of logical network elements, each of them with a defined functionality. The network elements are grouped in the UMTS Terrestrial Radio Access Network (UTRAN), the Core Network (CN), and the MSs, which in 3GPP are called user equipments (UE), as shown in Figure 1.3 [7]. The UTRAN handles all radio-related functionalities. The CN is responsible for switching and routing calls and data connections to external networks. The UE interfaces with the user and the radio interface.

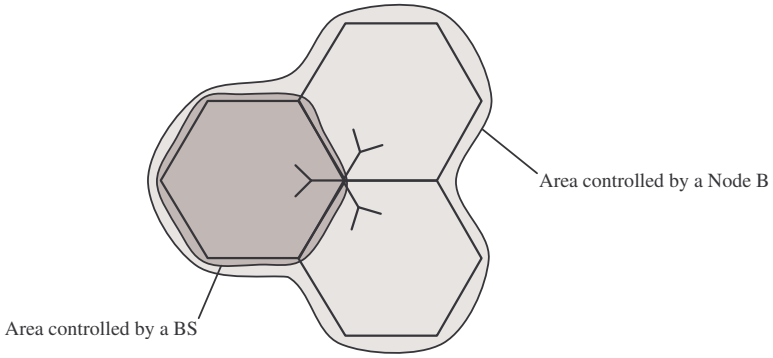

Figure 1.4. Difference between the concepts Node B and BS as defined in this Ph.D. thesis.

The UMTS network elements can also be grouped in subnetwork elements. The UMTS standard is structured so that the internal functionality of the subnetwork elements is not specified in detail. Instead, the interfaces between the logical network elements have been defined.

The UTRAN consists of one or more Radio Network Subsystems (RNS) connected to the CN through the Iu interface. An RNS is composed of a Radio Network Controller (RNC) and one or more base stations, which in 3GPP are called Node Bs. A Node B is connected to the RNC through the Iub interface, and may serve one or multiple cells. It converts the data flow between the Iub and Uu interfaces and also participates in the radio resource management (RRM). The RNC owns and controls the radio resources in the Node Bs connected to it. In this thesis the term Node B is considered to refer to a site controlling one or more sectors. The term BS refers to the logical division of the Node B that controls one single sector. The difference between both concepts is illustrated in Figure 1.4.

The UTRAN permits, under certain circumstances, the use of multiple radio links across multiple cells in support of a single UTRAN-UE connection. This concept is referred to as soft handover (SHO).

In the CN, the Mobile Services Switching Centre (MSC) and the Serving GPRS Support Node (SGNS), serve the UE in its current location for circuit-switched and packet-switched services, respectively.

The UE consists of the Mobile Equipment (ME), which is the radio terminal used for radio communication over the Uu interface, and the UMTS Subscriber Identity Module (USIM).

1.2.4 Radio Resource Management

As the number of subscribers of mobile and wireless services raises, as well as the data rates required by their applications, the available resources have to be utilised efficiently.

RRM is thus a major concern for current as well as future network configurations. The main objective of the RRM is to efficiently utilise the available radio resources, while maintaining the quality of service (QoS) requirements from the users and the planned coverage area.

The RRM algorithms are: admission control (AC), load control (LC), packet scheduler (PS), resource manager (RM), handover control (HC) and PC. Figure 1.5 shows the location of the different RRM algorithms according to [7].

AC handles all the new incoming traffic and checks whether new connections can be admitted to the system. LC manages the situation in which the system load exceeds the planned value,

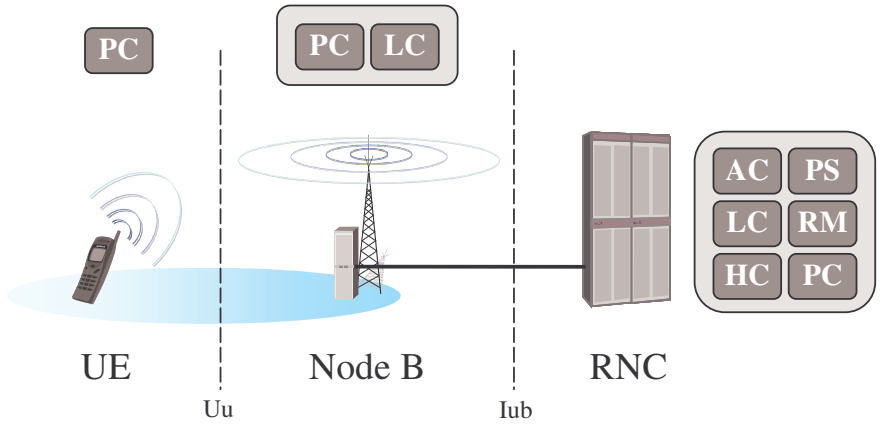

Figure 1.5. Location of the different RRM algorithms.

and takes measures in order to get the system back to a feasible load. PS handles all the non-real traffic (NRT), i.e. packet data users, and decides when a packet transmission is initiated and what bit rate is to be used. RM controls the logical resources in the Node B and the RNC, and reserves resources in the terrestrial network. HC handles and makes the handover decisions, as well as controls the users' active set of Node Bs. PC is responsible for keeping the radio link quality and minimising the power used in the radio interface by adjusting the transmission power. PC usually consists of a fast closed-loop PC algorithm and an outer-loop PC algorithm.

AC, LC, PS and RM are network based functions, since they are located in the RNC and control the resources of a Node B. Some fast actions associated with LC are run at the Node B side. PC and HC are connection based functions, since they handle the resources of one connection. HC is implemented in the RNC, while PC operates at the RNC, the Node B and the UE.

1.3 Techniques to Enhance the Uplink Capacity

So far, plenty of effort has been dedicated to the research of new techniques that increase the capacity of WCDMA. However, most of the work is concentrated in the downlink part, due to the asymmetrical properties of the traffic. The most important example is found to be HSDPA. Nevertheless, in spite of the asymmetry of the traffic between uplink and downlink there are reasons for investigating new capacity enhancing techniques for the uplink. On one hand, with the arrival of the application of the mobile communication systems to the multimedia communications, new services are getting into the picture. These services which will very likely require higher throughput and/or instantaneous data rate in the uplink direction from what the current implementations are able to provide: videoconferences, gaming, multimedia messaging, etc. Some examples of such services are included in Figure 1.6 [14]. On the other hand, the high peak data rate provided by HSPDA would have difficulties offering full service without an associated high speed reverse channel.

There are several approaches to exploit the peculiarities of the uplink in WCDMA and thus increase the capacity by means of new advanced techniques. The use of two receive antennas

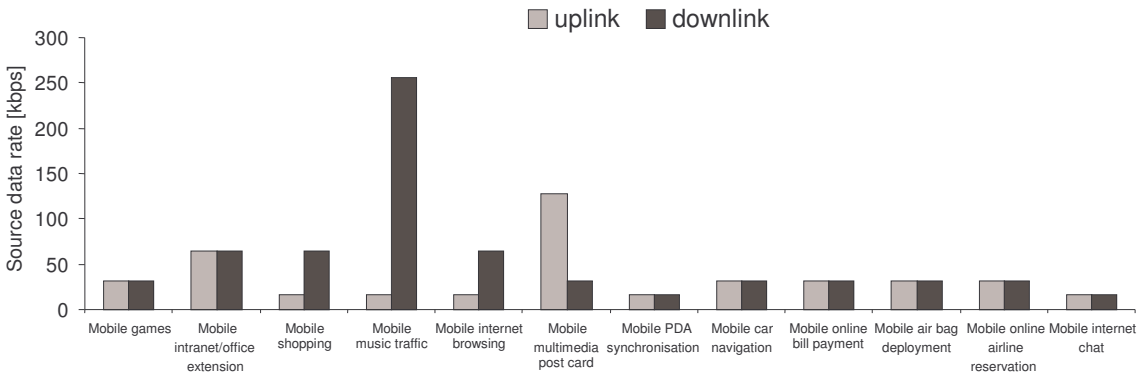

Figure 1.6. Traffic characteristics of 3G wireless data for advanced multimedia services [14].

provides coverage gain by coherently combining the signals collected at each antenna. Additionally antenna diversity provides gain against fast fading, since fast fading typically correlates poorly between the diversity antennas [7]. According to [7], the diversity gain in the ITU Pedestrian A channel is 7.5 dB in terms of required energy-per-bit to noise ratio (Eb/No) in the case without PC. In the ITU Vehicular A channel the diversity gain is smaller, 4.3 dB, because there is more multi-path diversity.

The performance of four-branch receiver antenna diversity is studied in [15], showing a 4 dB capacity gain with respect to two receiver antennas in Pedestrian A. In Vehicular A the gain is 3 dB. The more diversity is available, the smaller the diversity gain from an additional source of diversity [7]; e.g. in [16] it is concluded that with two receive antennas and fast closed-loop PC, multi-path diversity does not result in a capacity gain in micro-cells.

Another way to use antenna arrays is to form narrow beams towards the desired users, by means of the so-called beam-forming techniques [17]. This approach shows real promise for substantial capacity enhancement with the use of spatial and/or time processing at the cell site antenna array [18], [19], [20]. In [17], up to 350% capacity gain is obtained with eight antenna elements compare to the one antenna case from simulations with realistic assumptions. However, this gain is at the expense of an increased cost in the reception complexity as well as in hardware investment.

The enhancement of the RRM is also a solution to increase the uplink capacity in WCDMA systems. One of the ways is by means of the control of the received power at the Node B. There are three algorithms involved in the control of the received power level: AC, LC and PS. These algorithms do not necessarily have to operate based on the received power level, but it is the most common approach for WCDMA systems [26], [27], [28], [29]. With a power based AC, users are accepted in the system if the estimated power increase due to the admission is not expected to exceed a certain value, i.e. if

$$P < P_{threshold}, \tag{1.1}$$

where P is the total received power at the BS where the capacity is being requested, and $P_{threshold}$ is a power theshold chosen as a security margin, to prevent the system from reaching an instable state. By improving the liability of the AC algorithm it would be possible to reduce the security margin while keeping the same instability probability, and therefore increase the cell capacity. In [28] a power based AC is proposed for the uplink that evaluates the interference caused by the admission of the candidate user not only at the serving cell (single cell AC), but also at the neighbouring cells (multi cell AC). A multi cell AC algorithm can potentially avoid the problem of admitting a user that generates excessive interference in

an adjacent cell. However this typically happens when the user is close to the cell border and transmitting with a higher power level. In [30] a SIR based multi cell AC approach is presented; the final results do not show a significant capacity gain compared to an equivalent single cell AC under hot spot traffic. However, the results are obtained for speech services, which require a lower transmission power compared to higher data rate services. Hence, there is some potential from investigating the use of multi cell AC algorithms to increase the cell capacity in scenarios with high data rate services.

The mobile station (MS) has only information about its own chip sequence, while the BS has the knowledge of all the chip sequences for the own cell UEs. This opens for the utilisation of multi-user detection (MUD) in the uplink. With a MUD receiver, the information about multiple users is jointly used to better detect each individual user [21]. While in a conventional CDMA system all the users interfere with each other, in MUD all the users are considered as signals for each other [22]. MUD is a very attractive option to provide capacity increase in the uplink of WCDMA systems [21], [22], [23]. Furthermore, the use of MUD can also reduce the near-far effect [21]. The drawback of using optimal MUD is the increased complexity, so suboptimal approaches are commonly being sought [22].

Synchronising the received signals at the Node B can potentially increase the capacity in the uplink. The idea behind uplink synchronisation is to use a similar approach as in the downlink, where the signals from the same cell are separated by means of orthogonal codes, which allow reducing the MAI. The link level simulations in [24] show a 9 dB gain in signal-to-interference ratio (SIR) compared to an asynchronous scheme in an ITU Pedestrian A channel. However, these results are obtained for single cell, and they do not consider the blocking caused by the limited number of orthogonal codes. In [25] a theoretical value of 400% capacity gain is obtained by means of theoretical estimations in a pedestrian environment with two receive antenna diversity. These results are again based on a single-cell, without considering background noise. It seems quite obvious that there is some potential on the use of uplink synchronisation for capacity improvement. However, more thorough investigations with realistic assumptions are required in order to get a more exhaustive knowledge on the potential of such a scheme.

A potential capacity enhancement also exists for uplink packet access by improving the PS. There are some investigations on the packet access for the uplink of WCDMA systems [29], [31], although in general it has been paid less attention than for the downlink case. One of the reasons is the already mentioned traffic asymmetry, as most of the demanded packet traffic is for the downlink. Furthermore, performing PS in the uplink is more complex, as the transmission is started from the users, and network needs signalled information on their buffer occupancy. Moreover, in order to perform power-based PS, the RNC needs measurements of the received power level at the Node B, which require some time until they are finally reported. This information is sent through Node B Application Part (NBAP) signalling at network layer. Hence, there is some significant delay from the moment in which the PS decisions are taken till they are actually effective. In [29], the potential of performing a faster PS is considered, showing some potential capacity gain. However this requires moving the PS to the Node B. This option, which is currently being considered in 3GPP [32], admits the design of new algorithms and advanced techniques for promising capacity increase of the uplink packet access.

1.4 Objective of the Ph.D. Thesis

The objective of this Ph.D. study is to identify and analyse different methods for capacity enhancement in the uplink of WCDMA systems. Some of the most promising study frames from all those listed in Section 1.3 have been selected as study cases for this Ph.D. research. Features such as multiple receive antenna diversity or MUD have already been investigated in detail. Therefore, the selection has been made taking into account the amount of work that has previously been done, as well as the potential for further investigations in each of the areas.

The goal is to provide results that help illustrating the potential of the chosen methods for capacity increase, but always taking into account the main issues derived from deploying such schemes. UTRA FDD mode is considered as a reference study case throughout the thesis.

The overall study includes the following general capacity enhancing schemes for the uplink of WCDMA:

- Multi cell admission control

  In WCDMA systems the total received power generated in every cell gives a measurement of the uplink resources. A power-based AC allows access to the new users in the system provided that the estimated new power after the admission does not create excessive interference in the cell. However, with the arrival of the new services that require higher data rates, users might also create excessive interference in the adjacent cells. This problem has been formulated in the literature and some ideas have been proposed to solve it. In the beginning of the Ph.D. study no results showing a significant capacity increase existed from deploying a power based multi cell AC algorithm. However, a higher potential is expected in non-homogenous load conditions with high data rate services. In this thesis a new power-based multi cell AC is proposed and investigated, by identifying the situations in which it might be profitable to deploy.

- Uplink synchronisation

  Preliminary studies on uplink synchronisation show a huge capacity increase by means of introducing uplink orthogonality and thus reduce the own cell MAI. However, the existing results on this topic were obtained under not very realistic assumptions, like the absence of thermal noise, perfect synchronisation or the use of single cell scenarios. Moreover, there are other aspects that have direct impact on the performance of uplink synchronisation and have not been investigated yet, like the constraints in the number of orthogonal codes. If such aspects are taken into consideration, the gain is expected to decrease.

  In this Ph.D. dissertation the performance of uplink synchronous WCDMA is investigated by considering the most realistic assumptions. The goal is to calculate the real potential capacity gain while identifying the main issues that have an impact on it.

- Advanced fast packet scheduling

  As already mentioned in Section 1.3, most of the efforts to improve the packet access in WCDMA systems have been concentrated on the downlink, on the so-called HSDPA within 3GPP. This thesis proposes and investigates several schemes that aim at increasing the capacity for uplink packet services and may potentially be included in

the uplink evolution for packet access in UMTS. Many of the studied ideas are based on techniques that have already been demonstrated to provide a very high capacity gain with HSDPA, like moving the PS functionality from the RNC to the Node B or the use of Hybrid ARQ (HARQ).

To sum up, this Ph.D. investigation aims at evaluating the system level performance of the three above-mentioned capacity enhancing methods for the uplink of WCDMA. Moreover, it will try to provide an answer to the question of whether it is worth deploying each one of them for different situations.

The results included in this Ph.D. thesis are based on theoretical analyses as well as static and dynamic computer simulations. The analysis of the cell capacity is more accurate and faster with theoretical calculations, but it complicates and sometimes is not feasible to carry out when considering realistic assumptions or advanced features, such as SHO, fast fading, traffic models, etc. This justifies the use of both static and dynamic system level simulators. A customised implementation of all the required simulators employed in this Ph.D. thesis has been carried out as part of the Ph.D. work. The system level simulations include link level results which are not part of this Ph.D. investigation and have been provided by others.

1.5 Structure of the Thesis and Novelty

Part of the Ph.D. work has been published in references [P1]-[P8], which are listed in Section 1.6.

The main part of the thesis is organised as follows:

Chapter 2 studies a multi cell AC approach as an alternative to the conventional single cell-based algorithm typically employed in WCDMA systems. Although the multi cell approach has already been addressed in the open literature, this thesis contributes with new system level results that explicitly compare its performance to a realistic reference case for the single cell admission control approach. Moreover, a new method has been derived to estimate the power increase that the admission of a new user causes in the neighbouring cells. The results have been obtained by means of static simulations. The elaboration of such a simulator implied both the implementation and design of a realistic network model. Part of the work is included in [P1]. The second author of the paper derived a modified version of the single cell power increase estimator (PIE), whereas the first author derived the multi cell PIE, developed the simulator and obtained the results. The rest of the authors provided guidance and corrections.

Chapters 3, 4 and 5 cover the investigation on uplink synchronous WCDMA.

Chapter 3 presents uplink synchronisation as a method to reduce the MAI in WCDMA systems. An overview of the scheme is given, and the main issues in the achievement of perfect synchronisation in the uplink are discussed. The study takes as a starting point the proposal made within 3GPP in [24]. This chapter of the thesis contributes with a feasibility study for uplink synchronous WCDMA, evaluating the problems related to the lack of synchronism as well as the impact of the radio channel on the orthogonality. Some of these issues are included in a 3GPP contribution [P6]. All the research work included both in Chapter 3 and [P6], counting theoretical studies, simulator development and results, has been performed by Ph.D. student José Outes, under the supervision of Klaus I. Pedersen and Preben E. Mogensen.

Chapter 4 analyses the performance of uplink synchronisation at system level, evaluating the

impact on the results when it is applied in combination with other conventional capacity enhancing techniques, like SHO or discontinuous transmission (DTX). The lack of available channelisation codes is found to be the main drawback to reach a high capacity gain.

Prior to this Ph.D. research some system level results existed on potential gain of uplink synchronous WCDMA. However, such studies were only focused on the single cell case and neglected the background noise power. Chapter 4 provides both theoretical and dynamic simulation results at system level for realistic scenarios. The new research is included in [P2] and [P5]. The first author performed the analytical study, carried out the network model design and the implementation of the dynamic system level simulator; finally he obtained the results. The implementation of the dynamic system level simulator also required an exhaustive network design in order to model a realistic scenario. The simulator relies on link level results, which have been provided by other colleagues. The rest of the authors contributed with guidance and a major part of the text writing and edition. Some of the preliminary results obtained from this investigation were also published in [P7] and [P8], and contributed to the decision made in 3GPP to discard uplink synchronisation from the standard.

Chapter 5 investigates the performance of uplink synchronisation combined with higher order modulation and coding rate as a solution to the channelisation code constriction problem. The evaluation is performed with the help of a theoretical analysis and an updated version of the system level simulator employed for the results in Chapter 4. New RRM algorithms for dynamic allocation of codes and modulation and coding schemes (MCS) have been designed and implemented in the simulator. Further link level modelling was necessary in order to also consider the new MCSs for the dynamic simulations. The work was published in [P3], and has been performed by the first author, with the guidance and corrections of the rest of the authors. The link level modelling was carried out with the support of Troels E. Kolding and Frank Frederiksen.

Chapter 6 presents and analyses the performance of advanced strategies for capacity enhancement of uplink packet access. The techniques are mostly based on moving part of the RNC functionality to the Node B, and include HARQ and fast scheduling based on blind data rate detection and on time division multiplexing with a shorter transmission time interval (TTI). Some of these techniques can also be combined in order to reach a higher capacity gain, as shown in this thesis. The novelty in this chapter consists of providing new results on the system level performance of HARQ with fast physical layer retransmissions, based on theoretical and dynamic simulation results at system level. Moreover, new algorithms to perform Node B PS in the uplink have been evaluated by means of the dynamic simulations. The simulator employed to obtain the results is an upgraded version of the one used for Chapter 4, including traffic modelling and packet access, and has been jointly developed by Ph.D. students Claudio Rosa, Konstantinos Dimou and José Outes. Part of the work has been published in [P4]. The research has been carried out by the first two authors with equal contribution. Finally, a combined scheme for enhanced packet access including uplink synchronous WCDMA has been considered as well. All the work associated with the simulation results including uplink synchronous WCDMA have been provided by Ph.D. student José Outes, under the guidance of his supervisors.

Chapter 7 summarises the main conclusions of the Ph.D. investigation.

Nine appendices have been included with additional information to clarify certain aspects associated with the main chapters of the report. Some of the appendices also include extra investigations that, although they do not directly lead to the final target, they provide interesting results related to the core of the Ph.D. thesis.

Appendix A investigates the performance of a multi cell admission control approach for the downlink case. The followed steps are the same as those presented in Chapter 1 for the uplink. A new multi cell PIE for downlink has been derived by Ph.D. student José Outes; he also carried out the implementation of the static system level simulator, the required associated network model design, and the generation of the results. The reference single cell PIE for downlink was provided by Klaus Pedersen, who also supervised such a research together with Preben Mogensen.

Appendix B presents a new method to obtain uplink actual value interface (AVI) tables for different MCSs, which are essential to accomplish the simulation study in Chapter 5. The generation of the AVI tables relies on downlink results at link level provided by Frank Frederiksen. The procedure to obtain the uplink AVI tables has been derived by Ph.D. student José Outes under the guidance of Troels Kolding, Klaus Pedersen and Preben Mogensen.

Appendix C studies the impact of using a higher order modulation than BPSK on the peak-to-average power ratio (PAR) at the output of the uplink transmitter; the purpose of such a study is to better understand the inconveniences of using different MCSs for the investigation in Chapter 5. Statistical results on the PAR are provided for different transmission configurations based on Montecarlo simulations. The implementation of the simulator as well as the associated modelling of the uplink transmitters and the generation of the results have been carried out by Ph.D. student José Outes, under the guidance of Troels Kolding.

Appendix D proposes the use of an effective noise rise when uplink synchronisation is supported as a novel and more realistic load measurement compared to the conventional noise rise, normally employed for the uplink. The capacity gain of uplink synchronisation was evaluated theoretically in Chapter 5 by using the effective noise rise as a reference load measurement. The concept was proposed by Preben Mogensen, whereas the practical definition and theoretical expression of the effective noise rise have been provided by Ph.D. student José Outes.

Appendix E describes the PIE for uplink presented in [26]; such a PIE has been used for the system level simulators in Chapter 2, Chapter 5 and Chapter 6.

Appendix F presents a new PIE for BSs supporting uplink synchronisation, serving both asynchronous and synchronous UEs simultaneously; such a PIE has been used for the system level simulators in Chapter 5 and Chapter 6. The PIE for uplink synchronisation has been derived by Ph.D. student José Outes.

Appendix G explains the basis behind the new uplink power decrease estimators (PDE) employed for the PS implemented in the system level simulator in Chapter 6. The PDEs have been derived by Ph.D. student José Outes.

Appendix H analyses the impact of using uplink AVI tables that include the effect of one DPDCH and one DPCCH on the simulations performed with HARQ in Chapter 6. The appendix also addresses the impact of using the same AVI tables for different data rates. The study has been carried out by Ph.D. student José Outes.

Appendix I summarises the source uplink traffic model implemented for the system level simulations with packet services in Chapter 6. The chosen traffic model has been obtained from a 3GPP technical report [32].

1.6 Publications

The following articles have been written as part of the Ph.D. study:

[P1] J. Outes, L. Nielsen, K. Pedersen and P. Mogensen, "Multi-Cell Admission Control for UMTS", *IEEE Vehicular Technology Conference*, Vol. 2, pp. 987-991, Rhodes (Greece), May 2001.

[P2] J. Outes, K. Pedersen and P. Mogensen, "Performance of uplink synchronous WCDMA at network level", *IEEE Vehicular Technology Conference*, Vol. 1, pp. 105-109, Birmingham (Alabama), May 2002.

[P3] J. Outes, K. Pedersen, P. Mogensen and T. Kolding, "Uplink synchronous WCDMA combined with variable modulation and coding", *IEEE Vehicular Technology Conference*, Vol. 1, pp. 24-28, Vancouver (Canada), September 2002.

[P4] C. Rosa, J. Outes, K. Dimou et al, "Performance of Fast Node B Scheduling and L1 HARQ Schemes in WCDMA Uplink Packet Access", Accepted for publication in the *IEEE Vehicular Technology Conference*, Milan (Italy), May 2004.

[P5] J. Outes, K.I. Pedersen and P.E. Mogensen, "Capacity Gain of an Uplink Synchronous WCDMA System Under Channelization Code Constraints", Accepted for publication in the *IEEE Transactions on Vehicular Technology*.

Moreover, some of the preliminary results obtained during the Ph.D. study were presented as report documents to contribute in two 3GPP meetings:

[P6] TSGR1 (01) 0892: "System Level Performance of USTS", by SK Telecom and Nokia.

[P7] TSGR1 (01) 1181: "System Level Performance of USTS" by Nokia.

The results included in [P7] have subsequently been included in the following 3GPP Technical Report:

[P8] 3rd Generation Partnership Project, "Study report for Uplink Synchronous Transmission Scheme (USTS)", TR 25.854, Version 5.0.0, Release 5, Available at www.3gpp.org, December 2001.

Chapter 2

Multi Cell Admission Control for Uplink

2.1 Preliminaries

The radio resource management (RRM) is responsible for the utilisation of the air interface resources, and it is necessary to guarantee a certain QoS, maintain the planned coverage area and offer a high capacity. Although most of the required RRM algorithms have already been designed (i.e. admission control, load control, power control, packet scheduler, etc.) not all of them have been optimised considering the nature of these new services [7]. This is the current situation of the admission control (AC) functionality, which has been studied widely, but there are still some aspects that could be refined in order to improve its performance.

From previous studies it is well known that power is a robust integral measure of the network load for WCDMA systems and normally used by AC [26], [27], [28], [30], [33]. In conventional single cell (SC) AC, users are allowed access and resources to the system provided that $P<P_{threshold}$, where $P_{threshold}$ is a known power threshold obtained from network dimensioning, and P is the total transmitted/received power at the base station (BS) where capacity is being requested. If the condition is not kept, the network might reach an unstable situation, and the cell range is reduced; this only refers to the uplink case, which is typically interference limited, unlike the downlink case, which is mostly power limited. In order to decide whether a user should be granted capacity or not, the new power level at the BS of interest needs to be estimated, i.e. a power increase estimator (PIE) is required.

However, one of the shortcomings of this method is that the interference rise in the system

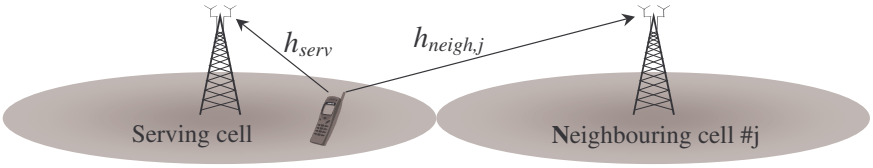

Figure 2.1. Situation where a new UE generates extra interference at a neighbouring cell.

due to the new user is only evaluated for the cell of interest before admission is granted/rejected. In some cases a new user might also create excessive interference in the neighbouring cells (Figure 2.1), leading to potential network instability and resulting in dropped connections or lower quality of service (QoS). This is likely to happen in situations where the load in the cell of interest is low, while all the neighbouring cells are highly loaded, particularly if the new user is requesting a high bit rate. Such cases are especially critical in the uplink, where, as it has already been mentioned, the systems are mostly limited by the interference.

A new AC procedure is therefore investigated to prevent these situations from happening, which finally turns into making the system more stable and increasing the capacity while reducing the probability of reaching an overload situation. This is achieved by using a multi cell (MC) AC scheme, where information from the neighbouring BSs is considered in order to decide whether a new request should be accepted or not. Using such an approach is also discussed in [28], [30], [33]. In [28], the information from the neighbouring BSs is the pilot power received by the user equipments (UE), and in [30], the uplink signal-to-interference ratio (SIR) measurements at the adjacent BSs. In [33] the AC is carried out based on an empirical model where the measured received power is correlated with the traffic in the serving and the neighbouring cells.

In this chapter we propose an alternative power based MC AC algorithm for the uplink that takes into account the level of interference power received at the neighbouring BSs. The serving BS performs the AC by estimating the power increase that a new user would cause in the neighbouring BSs. The power increase estimation is carried out based on the information of the average interference level measured by the adjacent BSs and the information contained in the pilot report measurements that the UEs periodically send to the closest BSs [34].

The objective of this chapter is to analyse the benefit of the proposed MC AC method compared to an equivalent scheme exclusively based on SC information. This study focuses on the uplink case, although the same principles apply for the downlink; a similar approach for the downlink case is addressed in Appendix A.

The chapter is organised as follows: The MC AC algorithm is introduced in Section 2.2. The model used for simulating the operation of this procedure is outlined in Section 2.3. Simulation results are shown and discussed in Section 2.4. Concluding remarks are presented in Section 2.5.

2.2 Power Based Multi Cell Admission Control

The noise rise (NR) is a parameter usually employed for uplink AC and is defined as the total received wideband power at the BS relative to the background noise power. Let us define a

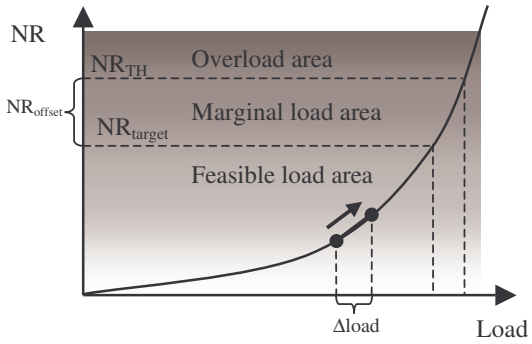

Figure 2.2. Uplink operating areas in a BS.

SC power based admission criterion for the uplink as

$$NR_{serv} < NR_{TH}\,, \tag{2.1}$$

where NR_{serv} is the noise rise at the serving BS after the user has been admitted to the system, and NR_{TH} is the noise rise value where the system is considered to reach the overload situation, set from network dimensioning. The serving BS is chosen as the BS with the lowest propagation path loss to the UE. Since it is not possible to know the final NR before the addition of the user, the following condition is assessed to take the admission decision

$$NR^{est}_{serv} < NR_{TH} - NR_{offset} = NR_{target}\ [\text{dB}], \tag{2.2}$$

where NR^{est}_{serv} is an estimate of NR_{serv}, and NR_{offset} is a noise rise offset set to compensate for potential estimation errors. If NR_{TH} is exceeded, load control (LC) actions have to be carried out. Figure 2.2 shows the areas in which a BS can operate. While the BS is working in the feasible area, new users can be admitted according to the AC algorithm. When the system is operating in the marginal load area, then preventive LC actions are taken, which means that no more users are accepted in the system. If the BS receives power to such an extent that it reaches the overload area, LC actions are taken to reduce the system load.

Nevertheless, this AC algorithm does not consider the problem of making an adjacent BS reach an overload situation because of the admission of a new user in the serving cell. To avoid these situations an MC AC algorithm is proposed, where a new user is admitted to the system if the noise rises of the serving and all its adjacent BSs do not exceed the target value, i.e. provided that

$$\begin{aligned} &NR_{serv} < NR_{TH}\,, \text{and} \\ &NR_{neigh,j} < NR_{TH} \quad \forall j \,|\, 1 \le j \le N_{adj}\,, \end{aligned} \tag{2.3}$$

where $NR_{neigh,j}$ is the noise rise at the j-th adjacent BS after the user has been added to the system, and N_{adj} is the number of adjacent BSs. The serving BS is the one labelled as *serv*, and the N_{adj} adjacent ones from *neigh,1* to *neigh,*N_{adj}, as shown in Figure 2.3 for a grid with 1-sector sites.

Again, as it is not possible to know the final NR beforehand, an estimate is applied and the admission criterion is modified to

$$\begin{aligned} &NR^{est}_{serv} < NR_{target}\,, \text{and} \\ &NR^{est}_{neigh,j} < NR_{target} \quad \forall j \,|\, 1 \le j \le N_{adj}\,, \end{aligned} \tag{2.4}$$

where $NR^{est}_{neigh,j}$ is an estimation of $NR_{neigh,j}$.

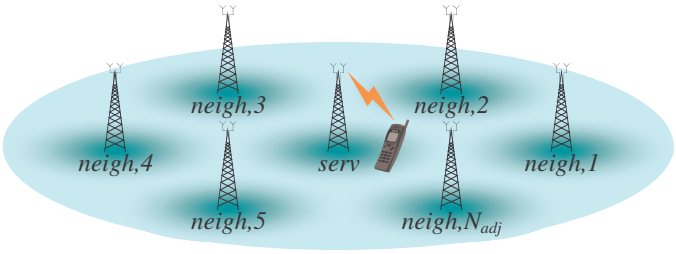

Figure 2.3. Numbering of the BSs for a grid with 1-sector sites.

In order to deploy both the SC and the MC AC algorithms, it is necessary to have an estimate of the NR that the serving and the surrounding BSs are going to receive after the new UE is admitted.

2.2.1 Multi Cell Power Increase Estimator for Uplink

This section presents an algorithm to estimate the power increase caused by a new UE at the serving BS before the admission decision is taken. Then a new algorithm is proposed to estimate the interference increase that the acceptance of the new user would generate in the adjacent BSs beforehand. For simplicity, let us call SC PIE the algorithm that estimates the power increase in the serving cell and MC PIE the estimation of the power increase in an adjacent cell. The SC PIE has been taken from the literature, whereas the MC PIE is a new contribution of the Ph.D. thesis.

Let us recall that the noise rise is defined as

$$\mathrm{NR} = \frac{P_{RX}}{P_{noise}}, \tag{2.5}$$

where P_{RX} is the total received wideband power at the BS and P_{noise} is the background noise power. The noise rise after the admission of a new user can be expressed as

$$NR = \frac{P_{RX} + \Delta P}{P_{noise}}, \tag{2.6}$$

where ΔP is the wideband power increase at the BS caused by the admission of the new user. Notice that ΔP includes both the power of the new user and the power increase of the existing users in the system, assuming that the network is power controlled. The noise rise after the admission is estimated as

$$NR^{est} = \frac{P_{RX} + \Delta P^{est}}{P_{noise}}, \tag{2.7}$$

where ΔP^{est} is an estimate of ΔP.

Let us use an SC PIE based on the expression proposed in [26] (and derived in Appendix E) to estimate the power increase at the serving BS caused by the admission of a new UE

$$\Delta P_{serv}^{est} = \frac{P_{RX}\Delta\eta^{est}}{1-\eta-\Delta\eta^{est}}, \tag{2.8}$$

where η is the fractional load, defined as

$$\eta = \frac{P_{RX} - P_{noise}}{P_{RX}}, \tag{2.9}$$

and $\Delta\eta^{est}$ is an estimate of the fractional load increment at the serving BS if it admits the new user, defined as in [35]

$$\Delta\eta^{est} = \omega \cdot \Delta\eta_o^{est} + (1-\omega) \cdot \Delta\eta_u^{est}. \tag{2.10}$$

In (2.10), ω is a weight parameter within the range [0,1], and $\Delta\eta_o{}^{est}$ and $\Delta\eta_u{}^{est}$ are an overestimate and an underestimate of the increment of load respectively, given by

$$\Delta\eta_o^{est} = \frac{1}{1 + \frac{R_c}{R_i \rho_i}}, \tag{2.11}$$

$$\Delta\eta_u^{est} = \Delta\eta_o^{est} \frac{P_{noise}}{P_{noise} + P_{other}}, \tag{2.12}$$

where R_c is the chip rate, R_i is the bit rate demanded by the user, ρ_i is the required energy-per-bit to noise ratio (Eb/No), and P_{other} is the wideband power from other cells. $\Delta\eta_o{}^{est}$ gives an overestimation of the increment of load because it assumes that the power received from other cells exactly increases by the same fraction as the own cell power. $\Delta\eta_u{}^{est}$ underestimates the increment of load because it assumes no rise in other cell interference after the admission.

The increment of power received at BS #*j* can be expressed in the following way

$$\Delta P_{neigh,j} = \Delta P_{neigh,j}^{new\_UE} + \Delta P_{neigh,j}^{other\_UEs} = \Delta P_{serv}^{new\_UE} \frac{h_{neigh,j}}{h_{serv}} + \Delta P_{serv}^{other\_UEs} K_{neigh,j}, \tag{2.13}$$

where $\Delta P^{new\_UE}{}_{neigh,j}$ and $\Delta P^{new\_UE}{}_{serv}$ are the initial power increase generated by the new UE at the adjacent BS #*j* and in the serving BS, respectively; $\Delta P^{other\_UEs}{}_{neigh,j}$ and $\Delta P^{other\_UEs}{}_{serv}$ are the power increment caused in the adjacent BS #*j* and in the serving BS by the rest of the users in the network in order to compensate for the extra interference; $K_{neigh,j}$ is the ratio of power increase caused in the adjacent BS #*j* by the rest of the users in the network to the power increase caused in the serving BS by such users; and h_{serv} and $h_{neigh,j}$ are the path gain from the new UE to the serving BS and to the adjacent BS #*j*, respectively (see Figure 2.1).

By assuming $\Delta P_{serv} \approx \Delta P_{serv}{}^{est}$ and $K_{neigh,j} \approx h_{neigh,j}/h_{serv}$, it is possible to derive an MC PIE that allows estimating the power increase that a user would cause in the adjacent BS #*j*, which is expressed as

$$\Delta P_{neigh,j}^{est} = \Delta P_{serv}^{est} \frac{h_{neigh,j}}{h_{serv}}. \tag{2.14}$$

Pilot reports from the UE to the nearest BSs are available at the serving BS, and give information on the downlink (from BS to UE) path gain [36]. This can be utilised to estimate $h_{neigh,j}$ and h_{serv}. The only factor that makes downlink and uplink path gains different is the fast fading. If the UE averages over fast fading, it is possible to approximate the uplink path gain to the downlink path gain derived from the pilot report.

Based on these assumptions, let us deduct the value of $h_{neigh,j}$ and h_{serv}. The pilot report related to every link starting from the UE and ending at any BS can be described in the following way:

$$\rho_k^{Pilot} = \frac{P_k^{Pilot} \cdot h_k}{P_{RX\_UE}}, \tag{2.15}$$

where $\rho^{Pilot}{}_k$ is the energy-per-chip to interference-power-density ratio (Ec/Io) reported by the new UE for the link to the BS labelled as k, $P^{Pilot}{}_k$ is the pilot power transmitted by the BS labelled as k, h_k is path gain from the UE to the BS labelled as k, and P_{RX_UE} is the total power received by the new UE.

Rearranging (2.15) yields

$$h_k = \frac{\rho_k^{Pilot} \cdot P_{RX\_UE}}{P_k^{Pilot}}. \tag{2.16}$$

Notice that the value of P_{RX_UE} does not depend on the BS, as it is a downlink measurement and according to the definition of $\rho^{Pilot}{}_k$ made in (2.15) it includes all the received interference, including the pilot powers. The received power increase at all the neighbouring BSs can be estimated by using (2.14) and (2.16)

$$\Delta P_{neigh,j}^{est} = \Delta P_{serv}^{est} \frac{P_{serv}^{Pilot} \rho_{neigh,j}^{Pilot}}{P_{neigh,j}^{Pilot} \rho_{serv}^{Pilot}}. \tag{2.17}$$

2.3 Model for Simulations

With the aim of evaluating the performance of the MC AC algorithm, a set of simulations has been carried out. This section summarises the network layout, the propagation conditions and the parameters employed for the static simulations of the uplink MC AC, followed by a brief description of the network simulator operation. Finally, the particular cases that have been simulated to illustrate the advantages of using the MC AC algorithm will be described.

2.3.1 Cellular System Model and Radio Propagation Model

The whole service area is divided into seven cells with a radius R, as it is shown in Figure 2.4. UEs are distributed inside a circle whose area equals $3R$. A BS with an omni directional antenna is located at the centre of each cell. A UE arriving in the system will choose its

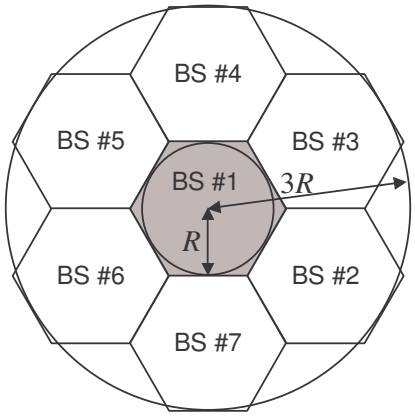

Figure 2.4. Network layout.

Parameter	Value
Cell radius (R)	1 km
Antenna gain at the BSs	12 dBi
Chip rate	3.84 Mbps
Standard deviation of the shadow fading	8 dB
Fast PC iterations between admissions	20
Fast PC step size	1 dB
Required Eb/No (ρ)	6 dB
Maximum power transmitted by the UEs	Unlimited
Thermal noise level (P_{noise})	-102.9 dBm
Standard deviation of the pilot report error	1 dB
Mean value of the pilot report error	0 dB
NR threshold (NR_{TH})	6 dB
NR target (NR_{target}) range	3.5 - 6 dB
Weight factor for SC PIE (ω)	0.5

Table 2.1. Default parameters employed for the simulations.

serving cell so that the radio propagation attenuation between the UE and the BS of its serving cell is minimised. The radio propagation attenuation is composed of two factors, the path loss with distance and a lognormal shadow fading. The Okumura-Hata model has been employed to describe the path loss effect, taking the particular case of an urban macro-cell with a BS antenna height of 30 m, a UE antenna height of 1.5 m and a carrier frequency of 1950 MHz [26]. Thus, when the UE is at a distance r from its serving BS, the attenuation is

$$Att = \left(137.4 + 35.2 \cdot \log(r)\right) + \xi \ \text{[dB]}, \tag{2.18}$$

where ξ (in dB) has a normal distribution with zero mean that represents the effect of shadow fading, and r is given in km. Fast fading is not modelled. The model is static, i.e. the UEs do not move. The UEs are power controlled by their serving BSs; an algorithm that simulates the effect of fast closed-loop power control (PC) is executed a fixed number of times between consecutive admissions to stabilise the network. This number of iterations must be long enough so that the Eb/No of all links has converged and remains oscillating around their Eb/No target at the end of it. The initial transmitted power for a new user is set so that it allows the link of this UE to reach the Eb/No target before the fast closed-loop PC starts to be executed. Errors in pilot report measurements are considered, and simulated as Gaussian distributed in decibels. No limit is considered for the maximum power that the UEs are able to transmit; this implies that the system is assumed to be capacity limited more than coverage limited.

Table 2.1 contains the default parameters used for all the simulations.

2.3.2 Network Simulator Operation

The purpose of the network simulator is to supply some statistics on the available system capacity when using different AC algorithms as a function of the probability of having unstable situations (which, as it was already mentioned, might lead to dropped connections).

These statistics are based on the probability of having two kinds of errors: Type 1 errors and Type 2 errors.

- *Type 1 error*: This error occurs when a new user is admitted to the system and this provokes an unstable state in the network that might lead to the dropping of an already

established connection. We consider that a Type 1 error has occurred when a new request is accepted and

$$NR_{serv} > NR_{TH} \text{ or } NR_{neigh,j} > NR_{TH} \quad for\ some\ \ j \mid 1 \le j \le N_{adj}. \tag{2.19}$$

- *Type 2 error*: This error occurs when a new user is not accepted in the system although it could have been admitted. In this study, it is considered that a Type 2 error has occurred when the request made by a new user to enter the system is rejected and

$$NR_{serv} < NR_{TH} \text{ and } NR_{neigh,j} < NR_{TH} \quad \forall j \mid 1 \le j \le N_{adj}. \tag{2.20}$$

Type 1 errors are obviously more dangerous than Type 2 errors, since it is preferable to make a mistake by wrongly rejecting a user rather than admitting a user which might lead to the dropping of existing calls.

Let us also define the Type 3 errors as the particular case of the Type 1 errors that occur when a BS reaches the overload area due to an incorrect admission made by a neighbouring BS. This kind of errors comes from wrong AC decisions of users in a different BS from the affected one, and should therefore be avoided.

Figure 2.5 describes the procedure used by the network simulator in order to measure the probability of having the different types of errors when performing AC functions.

The steps are the following ones:

- First, starting from an empty network, users are added to the system until the initial target fractional load is reached at every cell. After every admission, fast closed-loop PC is performed so that all the links reach their target Eb/No.
- Once the network is loaded as it was planned, the system receives a request for a new connection.
- Then the AC is carried out, and the decision on whether to grant or not to grant resources is taken.
- Afterwards, the user is admitted regardless of the decision made, and fast closed-loop PC is performed again so that all the links reach their target Eb/No. Then, the state of the BSs in the network is checked and, depending on it, a certain action is taken:
  - If a Type 1 error or a Type 2 error occurs, the simulation is counted as it is finished like that. If a Type 1 error is also a Type 3 error, it is counted.
  - If the user is admitted and there were no errors, the NR level at the serving BS is checked. If this NR level is smaller than the NR target a new request is received, and the whole process is carried out again; otherwise, the simulation is finished and counted as it has no errors.
  - If the user was rejected successfully, the simulation is finished and counted as it has no errors.

Finally, the probability of having Type 1, Type 2 and Type 3 errors is calculated as the result of dividing the number of simulations finished in such types of errors by the total number of executed simulations.

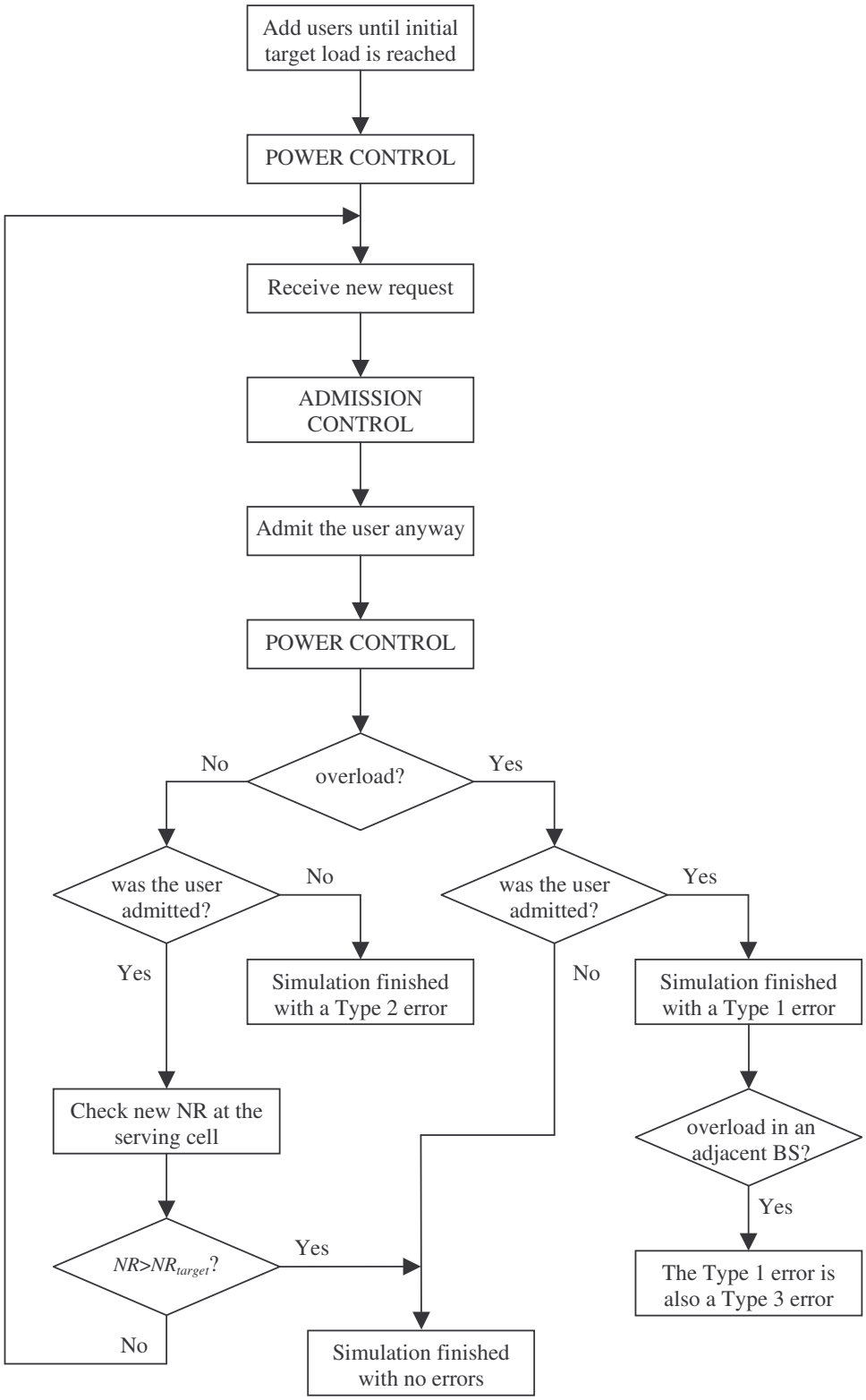

Figure 2.5. Simulator operation.

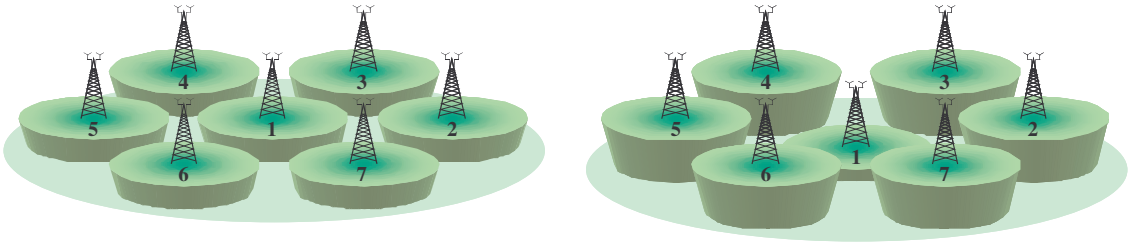

Figure 2.6. Initial configuration of the network with homogeneous load (left) and non-homogeneous load (right).

2.3.3 Cases under Study

This section describes the different conditions in which the system has been simulated in order to assess the efficiency of the MC AC algorithm.

There are two general patterns that have been used to perform the simulations, defined by the initial configuration of the network and the location selected for adding the new users afterwards. The initial condition of the network is fixed by a certain load measured in every cell.

The general cases used in the simulations are the following:

- *Simulation case 1: Homogeneous load*

  In this situation users are added consecutively in every cell which has not reached a fractional load η=0.3. Notice that in this case the other cell interference is higher in the central cell, as in the model the rest of them only have three adjacent cells. In order to obtain the same other-to-own cell interference factor (i) for all the cells and thus have a realistic homogenous case, an extra constant interference has been added to BSs #2-7.

  A user is randomly added in a cell according to a uniform distribution in area. Then new users are located anywhere in the network, also following a uniform distribution in area.

  The purpose of considering this case is to simulate a typical operation of the system, in principle a bit far away from those in which the MC AC algorithm is supposed to provide a bigger advantage.

- *Simulation case 2: Non-homogeneous load*

  In this case, before starting the simulations, the network must be in the condition depicted on the right side of Figure 2.6, where the central cell (BS #1 in Figure 2.4) is in low load conditions and the neighbours are in high load conditions.

  The initial value of the load is reached by adding users, also following a uniform distribution in area for each cell of the network separately (except for BS #1) until their fractional load is over the target value η=0.55. Thereafter, new users are only added in the central cell until a target fractional load of η=0.15 is reached.

  In order to let BSs #2-7 reach a high target load, a fixed interference power level has also been added to all of them. In this case this extra interference should be higher than in the homogenous load case to reach the situation depicted in Figure 2.6 and keep a higher i in the central cell than in the rest.

Load	Traffic	Extra P_{other}	Average i	
			BS #1	BSs #2-7
Spot	Case 1	$0.50P_{noise}$	1.4	1.2
	Case 2	$0.40P_{noise}$	1.2	1.0
Homogeneous	Case 1	$0.14P_{noise}$	1.0	1.0
	Case 2	$0.12P_{noise}$	0.7	0.7

Table 2.2. Extra constant power added to BSs #2-7 to simulate the other cell interference for the different cases; it also includes the average other-to-own cell interference ratio from simulations.

In both cases, every user transmits over a circuit-switched connection with one of these bit rates:

- *Traffic case 1*: 16 kbps, 64 kbps, 128 kbps and 384 kbps, with probabilities 0.4, 0.4, 0.1 and 0.1 respectively.
- *Traffic case 2*: 16 kbps and 64 kbps, with probabilities 0.6 and 0.4 respectively.

The MC AC is presumed to show a better performance compared to the SC AC algorithm when simulating the traffic case 1. The reason is that the impact of adding high bit rate users on the NR at the neighbouring cells is expected to be bigger than with low data rates, as higher data rates typically require higher transmission power.

Table 2.2 shows the values of the constant power added to all the cells except for the central one in order to reach the desired i; the average value of i from the simulations is also included.

2.4 Simulation Results

This section presents and discusses the results on the performance of both the uplink MC PIE and the uplink MC AC algorithm for the study cases presented in Section 2.3.3.

2.4.1 Results on the Performance of the Multi Cell Power Increase Estimator

In order to evaluate the performance of the uplink MC PIE, statistics on the estimation error have been collected from the simulations. The PIE estimation error is defined as

$$\text{error}\,[\%] = \frac{\text{Estimated Power} - \text{Accurate Power}}{\text{Accurate Power}} \cdot 100. \tag{2.21}$$

The performance of the MC PIE derived in (2.17) is assessed and compared to the case in which no estimation is performed; this case is considered as an MC PIE where the power increase at the neighbouring BSs is estimated to be zero.

Figure 2.7 shows the cumulative distribution function (CDF) of the estimation error when MC PIE and no MC PIE is used for homogeneous and non-homogeneous load and for traffic case 1. Table 2.3 summarises the values of the estimation error for CDF values of 10% and 90%, including both the traffic case 1 and 2. The negative values of the errors correspond to underestimations. Notice how in all the cases the underestimation error for a CDF value of 10% is reduced when using the MC PIE.

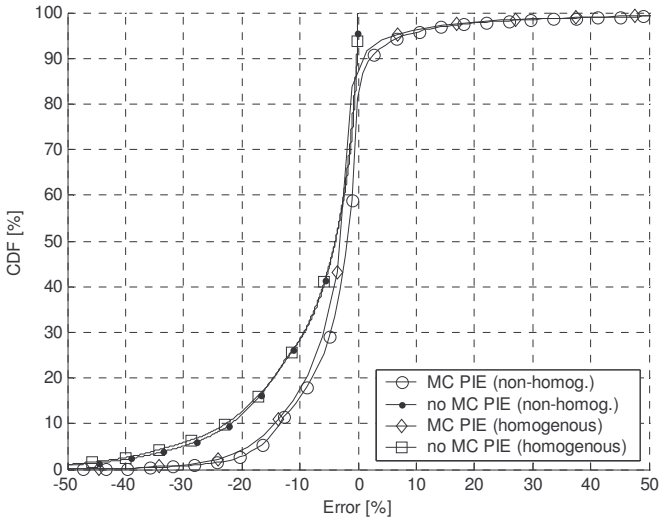

Figure 2.7. CDF of the estimation error when using different AC approaches for traffic case 1.

On the contrary, some overestimation errors are obtained by using the MC PIE. However, these kinds of errors (positive values) are not very frequent; the worst case happens for non-homogenous load with traffic case 1, where the MC PIE estimation error is smaller than 2.2% for 90% of the cases.

2.4.2 Results on the Performance of the Multi Cell Admission Control Algorithm

The results presented next show the outcome of performing a set of simulations based on the scheme described in Section 2.3. They allow comparing both the SC AC algorithm described in equation (2.2) and the MC AC algorithm described in equation (2.4).

Figure 2.8 shows the probability of having Type 1 and Type 2 errors for SC and MC AC. In all the cases the probability of Type 2 errors when the MC AC algorithm is used is always higher or equal to the SC AC. On the other hand, the probability of Type 1 errors is always smaller or equal to the SC AC. The MC AC is therefore more conservative than the SC AC approach. To make a fair comparison it is necessary to set the NR_{target} values so that the SC and the MC AC algorithms provide the same probability of Type 1 errors. In such a situation,

Traffic case	Load	MC PIE	CDF at 10%	CDF at 90%
1	Spot	ON	-13.4 %	2.2 %
		OFF	-21.8 %	-0.3 %
	Homogeneous	ON	-14.5 %	1.1 %
		OFF	-22.7 %	-0.2 %
2	Spot	ON	-4.1 %	1.7 %
		OFF	-6.9 %	-0.1 %
	Homogeneous	ON	-5.2 %	0.3 %
		OFF	-7.7 %	-0.1 %

Table 2.3. Estimation error for CDF values of 10 and 90%.

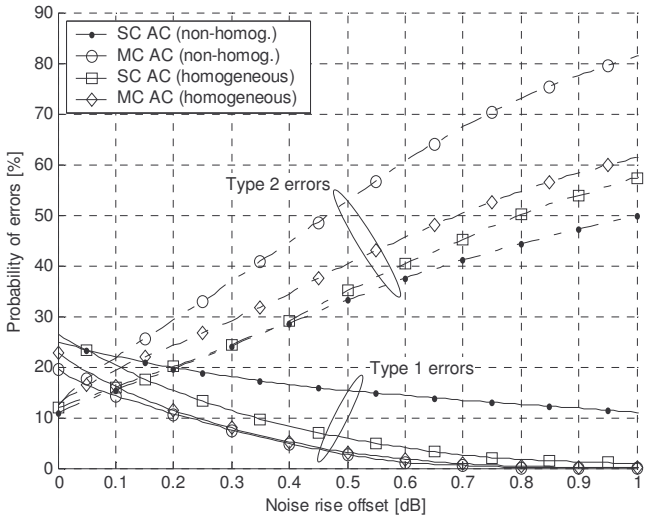

Figure 2.8. Probability of Type 1 and Type 2 errors when using different AC approaches for traffic case 1.

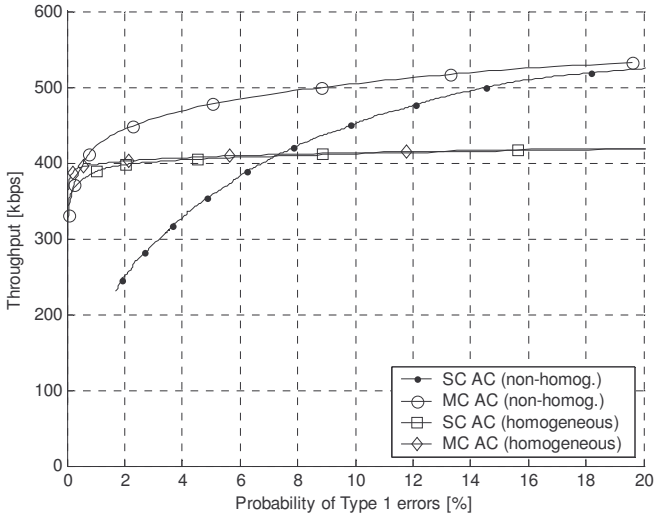

Figure 2.9. Average throughput at BS #1 when using different AC approaches for traffic case 1.

the MC AC always has a smaller or equal probability of Type 2 errors compared to the SC AC for all the cases. This means that the MC always allows dealing with a higher or equal throughput per cell while keeping the same probability of Type 1 errors as the SC AC.

Figure 2.9 shows the average throughput reached at the central cell (BS #1) as a function of the probability of Type 1 errors for the traffic case 1, while Figure 2.10 depicts the percentage of the Type 1 errors that are due to AC errors in an adjacent cell (i.e. they are also Type 3 errors) for both the SC and the MC AC algorithms.

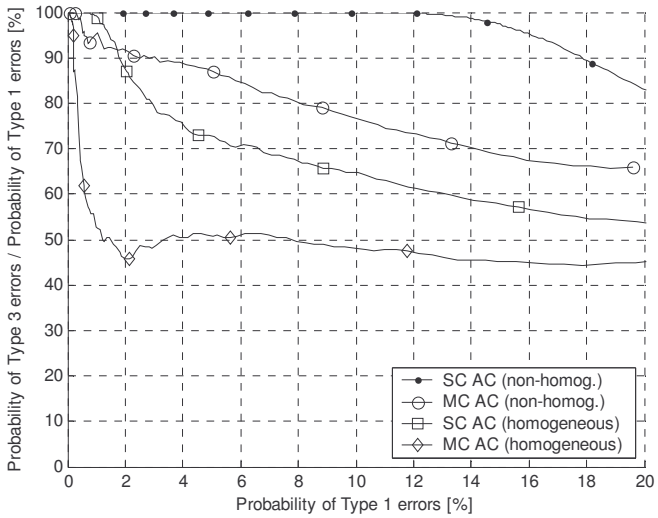

Figure 2.10. Ratio of the probability of Type 3 errors to the probability of Type 1 errors when using different AC approaches for traffic case 1.

The four possible cases derived from combining the situations described in Section 2.3.3 are considered next.

In the homogenous load case all the cells are equally loaded in the beginning, and then new users are added everywhere. This is a very general case where all the BSs are initially quite far away from reaching the overload situation, and the MC AC algorithm does not offer a significant increase of capacity. However, with the MC AC scheme the percentage of the Type 1 errors that occur in the adjacent cells is reduced by 22.1% and 18.8% for a 5% probability of Type 1 errors and traffic cases 1 and 2, respectively.

The study presented in [33] estimates a 10-20% capacity gain when using an AC algorithm based on MC information for a 2% call blocking rate under homogenous conditions with conversational services. However, the reference SC AC algorithm from which the gain is assessed only uses estimates of the intra cell load to take the admission decision. Thus, the SC AC algorithm does not have information from other cells, nor does it explicitly consider the inter cell load (the SC AC approach presented in Section 2.2 estimates the inter cell load from the receive power measurements). Furthermore, the results are obtained by setting the NR threshold to 13.5 dB; although in the paper a homogenous situation is presumed, the cells are allowed to operate at an extremely high load (up to η=0.96), where the network operates in a very unstable state in which the very simple SC AC commits lots of errors, which are easier to eliminate with the MC AC.

The case of non-homogeneous load with traffic case 1 is the only one where the MC AC provides some significant capacity gain. In such a case the MC AC gives cell throughput increases of 11.8%, 33.7% and 63.8% compared to the SC case for probabilities of Type 1 errors of 10%, 5% and 2.5%, respectively. Furthermore, the percentage of the Type 1 errors that occur in the adjacent cells is reduced by 13.0% for a 5% probability of Type 1 errors.

In the situation where non-homogeneous load is simulated with the traffic case 2 (only two possible bit rates), the initial load in all the neighbouring BSs is very close to the target value, since they only serve low data rate users. This, together with the fact that they do not add new users, leaves the load of the adjacent BSs a bit far from the overload limit during the whole

simulation. Furthermore, the interference generated by the users transmitting at low data rates in the serving BS during one simulation does not let them reach this limit. Therefore, no capacity gain is obtained when using the MC AC algorithm in this specific case. However, the simulation results are quite interesting as long as no capacity losses are made. On the other hand, no Type 3 errors occur in this case when using the SC AC approach, and therefore no improvements were possible by using the MC AC algorithm, whose purpose is basically to reduce them.

2.5 Concluding Remarks

An uplink power based MC AC approach has been proposed to increase the system capacity and stability in networks with high-speed data users.

An MC PIE has also been derived in order to make the operation of the MC AC algorithm possible. Although both the SC and the MC PIE provide estimations with a small variance of error, they are slightly biased, as it is not feasible to maintain a null mean for a large variety of bit rates and for all load levels in the BS. Moreover, in the homogeneous load case it was not possible to have a much greater capacity gain even with better PIEs, since the throughput provided by the SC AC algorithm is already quite close to the available limit.

A simulation procedure has been developed to compare the operation and efficiency of the SC and the MC AC algorithms. Results show that the number of Type 2 errors tends to increase when the MC AC algorithm is used. Nevertheless, the probability of Type 1 errors linked to them is much smaller than with the SC AC algorithm. This means that it is possible to increase the value for the admission decision so that, having the same probability of Type 1 errors, the MC AC algorithm provides a higher capacity.

In homogeneous load cases the MC AC algorithm does not give any appreciable gain. The same outcome is concluded from the results for the hot spot load case with low data rate users. These results are in consonance with those in [30], where no capacity gain is obtained under hot spot and homogenous load conditions with low data rate users.

A significant capacity increase is obtained under non-homogeneous conditions with respect to a SC AC scheme when considering both low and high data rate users (34% more cell throughput for Type 1 error probability of 5%).

An important outcome that should be remarked is that the MC AC algorithm also reduces the probability of Type 1 errors in the adjacent cells due to erroneous AC decisions in the serving BS.

The other-to-own cell interference factor can give an idea of the coupling between cells. The higher this factor is, the higher the coupling, and the higher the probability of overloading an adjacent cell by allocating resources to a new UE. However, the SC AC presented in Section 2.2 may still maintain robustness if the adjacent cells are equally loaded or moderate data rates are allocated to the UEs. The use of an MC AC approach is therefore favourable for systems with a high degree of interference coupling between cells, high probability of hot spots situations and allocation of high data rates to the UEs; notice that the two latter conditions are inherent to UMTS.

The extra cost introduced by using the MC AC approach is of minor concern, and basically consists of running the MC PIE for the neighbouring BSs whenever there is a new admission request. Furthermore, although the MC AC algorithm requires new measurements they are

already available at the Radio Network Controller (RNC), which is the place where the AC algorithm is executed. These new measurements are the pilot report measurements sent from the UE to the serving and the neighbouring BSs, the transmit pilot powers at the serving and the neighbouring BSs, and the NR level at the neighbouring BSs.

As the UMTS systems are expected to operate in situations with non-homogeneous load and high data rate, the use of the MC AC for uplink is therefore recommended, since the extra associated cost is very small.

As mentioned in Section 2.1, the MC AC approach can also be applied to the downlink case, which has been investigated in Appendix A. The results show similar performance in terms of capacity gain with respect to an equivalent SC AC approach.

Chapter 3

Uplink Synchronisation in WCDMA

3.1 Introduction

It is well known that orthogonal codes are a powerful method to reduce the multiple access interference (MAI) and thereby increase the network capacity in WCDMA systems. In the downlink of the UMTS, the signals from the same cell are separated by time-synchronised orthogonal codes derived from the set of Walsh codes [7]. However, maintaining the synchronisation at the Node B in the uplink is not straightforward, since the transmission is started from different user equipments (UE).

A potential capacity enhancing technique is to synchronise the uplink, so that the signals transmitted from different UEs within the same cell are time-aligned at the base station (BS). This admits the utilisation of orthogonal codes for own cell UE separation, so the own cell interference is in principle completely mitigated.

Previous studies have demonstrated that it is possible to achieve accurate symbol synchronisation in the uplink by using a maximum likelihood acquisition algorithm [37] or a simple delay-tracking loop for low mobility UEs [24]. Reliable synchronisation can also be obtained in environments with temporal dispersion in the radio channel by estimating both the line-of-sight component and the multi-path parameters [38]. Further, the uplink synchronised WCDMA has been discussed as a candidate feature within the standardisation body; 3GPP [24]. In 3GPP, uplink synchronised WCDMA is denoted Uplink Synchronous Transmission Scheme (USTS). The deployment of USTS requires changes in the specifications to allow the

uplink synchronism, but also to define a new code allocation rule. In this thesis, the uplink synchronisation is studied for the particular case of UMTS.

This chapter presents an overview of the method proposed by the 3GPP to reach uplink synchronisation in WCDMA systems. The main causes of non-perfect synchronisation are studied, as well as the impact that they have on the performance of the uplink synchronous WCDMA. Later in Chapter 4 and Chapter 5, the performance of the uplink synchronous WCDMA is evaluated at system level, investigating the main factors that have impact on obtaining a high capacity gain.

The present chapter is organised as follows. Section 3.2 gives an overall description of the USTS, specifying the main changes that such a scheme requires in the specifications with respect to the 3GPP/Release 99. The impact of the lack of synchronism in the performance of the uplink synchronous WCDMA systems is studied in Section 3.3, taking into consideration the main factors influencing the synchronisation. The conclusions are finally summarised in Section 3.4.

3.2 Overview of the Uplink Synchronous Transmission Scheme

This section describes the method proposed by the 3GPP to reach uplink synchronisation, as well as the scheme to allocate codes to the different users. The main problems related to this technique are addressed.

3.2.1 Time Synchronisation

In order to preserve the uplink orthogonality between the signals it is necessary that the symbols sent from the different UEs arrive time-synchronised at the BS. With this purpose the USTS contemplates that the BS sets a continuous series of time references separated by 256 chips, which correspond to the longest symbol period allowed for the uplink in UMTS. As illustrated in Figure 3.1, these reference instants determine the time in which the BS must receive a symbol from every synchronised UE.

The sub-chip level synchronisation is reached in USTS by means of a conventional tracking loop procedure, which is suitable for low mobility terminals in low dispersive environments. The time alignment process is composed of an initial synchronisation phase and a tracking phase. The initial synchronisation is made based on the Round Trip Propagation Delay (RTPD) information, which is sent by the BS through a common downlink physical channel called Forward Access Channel (FACH). According to the 3GPP specifications, the UMTS Terrestrial Radio Access Network (UTRAN) obtains the RTPD and sets the amount of adjustment for initial synchronisation to compensate for the difference between the RTPD and the reference time [36]. The UEs adjust their transmission according to the information received through the FACH from UTRAN. This information has a resolution of 3 chips. Assuming that the maximum variation of the transmitting time for the UE is $\pm 1/4$ chip every 200 ms [34], and considering that the BS takes 200 ms before comparing the reception time until it starts transmitting the information associated with it to the user, every UE needs between 200 ms and 1400 ms to get synchronised.

The tracking process consists of a closed-loop timing control procedure, where the UEs adjust the transmission time according to the Time Alignment Bits (TAB). The BS compares the

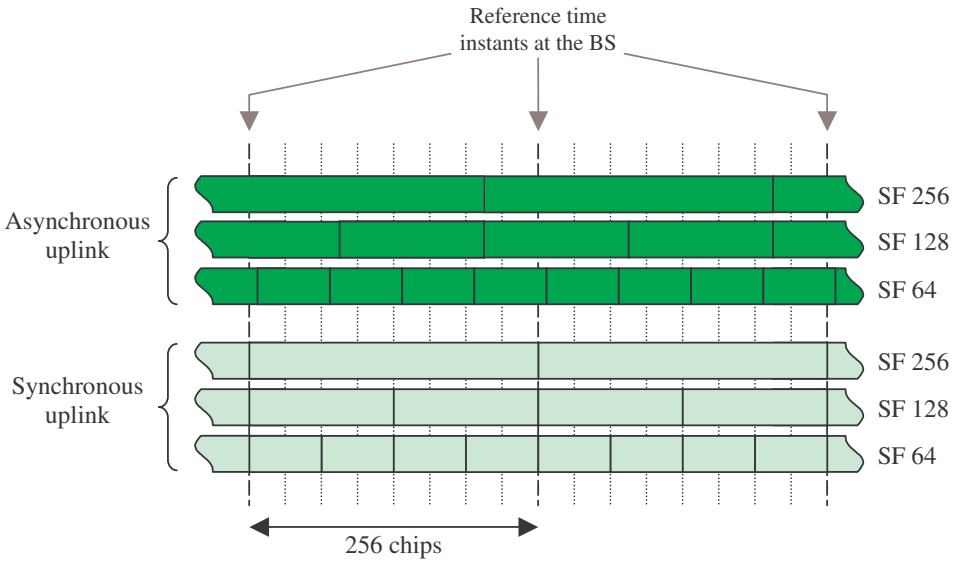

Figure 3.1. Symbol arrival instants at the BS with asynchronous and synchronous uplink.

arrival time of the received signal from the UE with the desired arrival time every 200 ms, and then decides the value of the TABs, which are sent once every 30 slots (20 ms) by replacing the bit reserved for fast power control (PC) information. Hence, this procedure slightly reduces the frequency of the fast PC updates; however, this is of minor concern, since the USTS is aimed at low mobility terminals.

Perfect synchronisation is not possible in the uplink because of the multi-path effect and other factors that have impact on the propagation delay of the signals transmitted from the different UEs. The lack of synchronisation is translated into a reduction of the orthogonality among the signals received by the BS, and therefore of the capacity gain provided by USTS. Only one of the detected paths of every signal received by the BS can be aligned in time. Furthermore, the alignment of the first path is not perfect, due to the finite timing control resolution, the errors in the transmission of the TABs, and the maximum frequency allowed for timing updates. Moreover, the BS is subject to errors in the estimation of the symbol arrival time due to the channel variation and the MAI. Some of these issues are further investigated in Section 3.3.

3.2.2 Code Allocation

In a conventional uplink asynchronous WCDMA system, like the one specified in the 3GPP/Release 99, a unique pseudo random sequence is allocated to every UE. Adopting the UMTS terminology, we will refer to the pseudo random sequences as scrambling codes[1]. The signals from different physical channels associated with the same UE arrive synchronously at the BS, and can be separated by using different orthogonal channelisation codes, derived from the set of Walsh codes. Hence, the narrow-band signal from a UE associated with a physical channel is both multiplied by a channelisation code and a scrambling code, as depicted in the block diagram of Figure 3.2. An example of scrambling and channelisation code allocation for the uplink of WCDMA according to 3GPP/Release 99 is shown in Figure 3.3. In uplink

[1] In UMTS the scrambling sequences are complex values. 3GPP contemplates long scrambling sequences, generated from segments of Gold sequences, and short scrambling sequences, defined from the family of periodically extended S(2) codes [9]. The investigation carried out in this Ph.D. thesis is based on the long scrambling sequences.

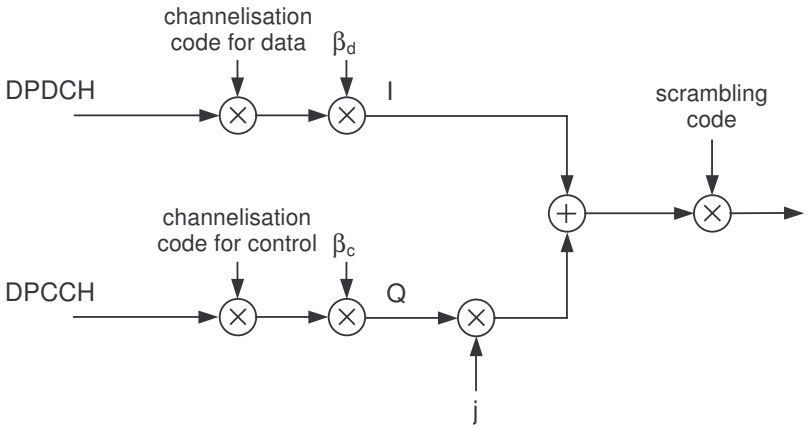

Figure 3.2. Spreading and scrambling of signals associated with uplink physical channels.

synchronised WCDMA, UEs within the same cell share the same scrambling code, while using different orthogonal channelisation codes, as illustrated in Figure 3.4. The channelisation codes are utilised to separate physical channels from different UEs. The scrambling code is therefore cell specific.

The number of available channelisation codes establishes an upper limit on the maximum number of UEs per cell in uplink synchronous WCDMA. Unlike the downlink case, the Dedicated Physical Data Channel (DPDCH) and its associated Dedicated Physical Control Channel (DPCCH) are not time-multiplexed in the uplink and use different channelisation codes. This is done because the discontinuous transmission could cause audible interference to any audio equipment that is very close to the terminal, such as hearing aids [7]. This restriction makes the UE use a higher number of channelisation codes in general than in the downlink. However, this limitation can be lifted by introducing several scrambling code groups within a cell. This implies that a certain set of UEs is transmitted under one scrambling code while another set of UEs is transmitted under different scrambling codes. Introduction of multiple scrambling codes within a cell eliminates the constraint on the maximum number of UEs due to channelisation code shortage. However, this is obtained at the expense of an increased MAI, since signals transmitted under different scrambling codes are non-orthogonal. As it will be demonstrated in Chapter 4, the limited number of channelisation codes under a single scrambling code is a major limitation for the capacity gain provided by uplink synchronisation in UMTS.

3.3 Effect of the Misalignment

As mentioned in Section 3.2.1, the lack of synchronisation is translated into a reduction of the orthogonality among the signals received by the BS, and therefore of the capacity gain provided by uplink synchronisation in WCDMA systems.

In this section the impact of the misalignment on the performance of the uplink synchronisation for WCDMA systems is investigated. First, the uplink orthogonality factor is introduced as a parameter to characterise the effect of the misalignment among the signals from different UEs operating in synchronous mode. Afterwards the factors that make a perfect uplink synchronisation among the UEs impossible are analysed.

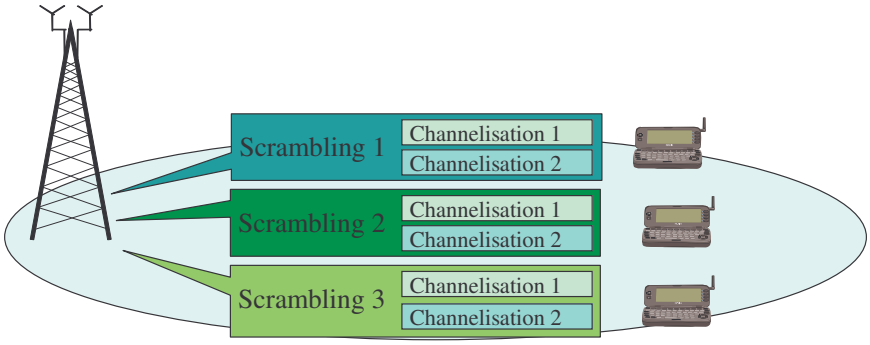

Figure 3.3. UE scrambling and channelisation code allocation according to 3GPP/Release 99.

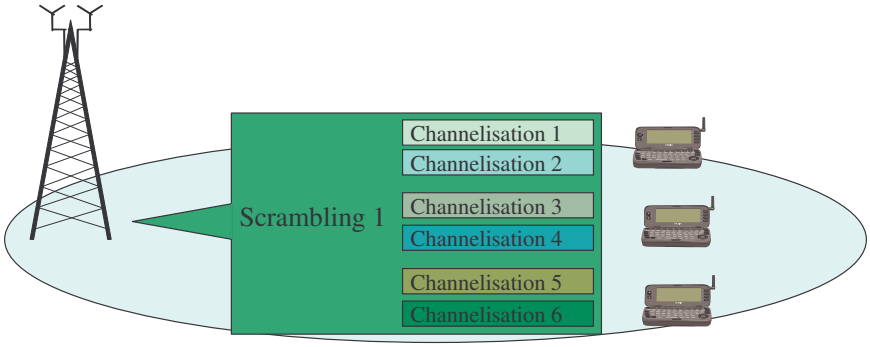

Figure 3.4. UE scrambling and channelisation code allocation for USTS.

3.3.1 The Uplink Orthogonality Factor

Assuming that all the signals from the own cell BS are transmitted under the same scrambling code, the energy-per-bit to noise ratio (Eb/No) after Rake finger combining for a user in the downlink direction can be approximately calculated as in [39]

$$\rho_{DL} = G_p \frac{P_{UE}}{P_{noise} + P_{other} + P_{own}(1-\alpha)}, \tag{3.1}$$

where G_p is the spreading processing gain, P_{UE} is the received power of the desired signal, P_{noise} is the background noise power, P_{other} is the total received wideband power from other BSs, P_{own} is the total received wideband power from the own BS, and $\alpha \in [0,1]$ is the orthogonality factor. The orthogonality factor gives the proportion of the interference from a UE served by the own BS that is cancelled after despreading, compared to the interference that would be obtained if that UE used a different scrambling code. According to this, the orthogonality factor can have values between zero (non-orthogonality at all) and one (full orthogonality).

In the downlink, the orthogonality factor is identical for every couple of UEs served by the same BS.

In the uplink, since the transmission is started from the UEs, which are located in different places and move at different speeds, their radio paths are different, which means that their power delay profiles (PDP) are not identical. Therefore, the uplink orthogonality is different for every couple of UEs. The Eb/No after Rake finger combining for a particular user in the uplink direction can be calculated as

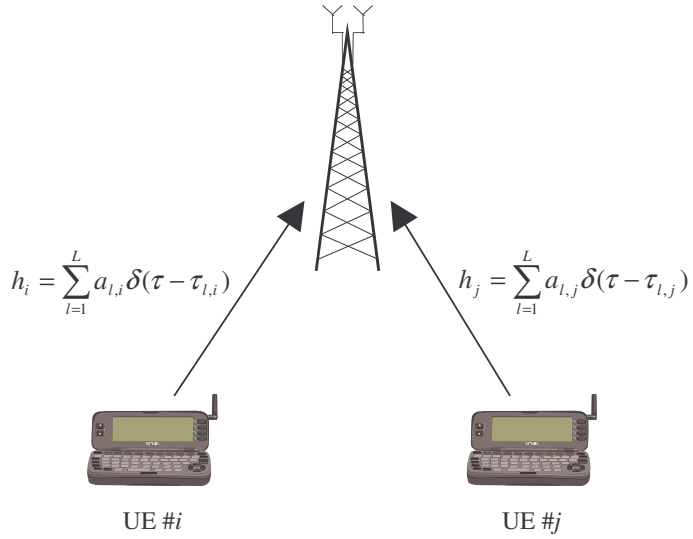

Figure 3.5. Multi-path channel scenario with two UEs transmitting to the same BS.

$$\rho_{UL} = G_p \frac{P_{UE}}{P_{noise} + P_{other} + \sum_{i=1}^{N} P_i\left(1 - \alpha_{UE,i}\right)}, \tag{3.2}$$

where P_i is the received power of the signal associated with the i-th UE served by the own BS, $\alpha_{UE,i}$ is the orthogonality factor between the signal of the desired UE and the signal associated with the i-th UE served by the own BS, and N is the number of UEs served by the own BS.

Next, a method to characterise uplink orthogonality factor is investigated. Let us consider a scenario with two UEs as in Figure 3.5. In this situation, a desired signal from a UE #*i* is received at the BS together with a signal from an interferer UE #*j*. The PDPs from UE #*i* and UE #*j* are denoted h_i and h_j, respectively; $a_{l,k}$ and $\tau_{l,k}$ are the random power and delay associated with the l-th path of UE #*k*, respectively. The paths are normalised so that the sum of the average powers of the PDP equals one.

Let us define the orthogonality factor between the signals from a desired UE #*i* and an interferer UE #*j* based on the expression provided in [40]

$$\alpha_{i,j} \equiv 1 - \frac{\Gamma_T}{\Gamma_S}, \tag{3.3}$$

where Γ_T is the signal-to-total-interference power ratio between that couple of UEs before despreading; and Γ_S is the signal-to-interference power ratio before despreading by considering only the part of the total interference power that cannot be cancelled after despreading and is only reduced by the processing gain.

Assuming a Rake receiver, where maximal ratio combining (MRC) is applied with equal noise power per branch, the resulting signal-to-noise ratio (SNR) is given as the sum of the SNRs at the different Rake fingers [41]

$$\Gamma = \sum_{l=1}^{L} \Gamma_l, \tag{3.4}$$

where L is the number of resolvable paths at the Rake receiver. A sufficient number of Rake fingers is here assumed to resolve all the paths of the PDP. The value of Γ_S associated with the l-th Rake finger can be approximated as

$$\Gamma_{S,l} \approx \frac{a_{l,i}}{\sum_{m=1}^{L} a_{m,j}\gamma(\tau_{m,j}-\tau_{l,i})}, \tag{3.5}$$

where $\gamma(\tau_{m,j}-\tau_{l,i})$ is the proportion of the power from the m-th interferer path that cannot be cancelled in the reception of the l-th path of the desired signal. This function $\gamma(\tau_{m,j}-\tau_{l,i})$ depends on the delay between the m-th path of UE #j and the l-th path of UE #i. It is approximately equal to one if the delay is larger than one chip period, and zero if they are fully aligned. The expression in (3.4) is an approximation because the Rake fingers must have equal noise power [40]. The SNRs for the signal-to-total interference ratio calculation at the Rake finger associated to the l-th path is given by

$$\Gamma_{T,l} = \frac{a_{l,i}}{\sum_{m=1}^{L} a_{m,j}}. \tag{3.6}$$

The orthogonality factor can therefore be approximated as

$$\alpha_{i,j} = 1 - \frac{\sum_{l=1}^{L} \frac{a_{l,i}}{\sum_{m=1}^{L} a_{m,j}}}{\sum_{l=1}^{L} \frac{a_{l,i}}{\sum_{m=1}^{L} a_{m,j}\gamma(\tau_{m,j}-\tau_{l,i})}}. \tag{3.7}$$

Notice that with this definition $\alpha_{i,j}$ is not necessarily equal to $\alpha_{j,i}$.

Let us assume for this study an identical PDP for all the UEs, with a power a_l and a delay τ_l associated with every path #l equal to the average values of the PDP. A relative delay τ between the PDPs from different UEs is kept. The orthogonality factor under these assumptions is

$$\alpha = 1 - \frac{1}{\sum_{l=1}^{L} \frac{a_l}{\sum_{m=1}^{L} a_m \gamma_{l,m}}}, \tag{3.8}$$

where, $\gamma_{l,m}=\gamma(\tau_m-\tau_l-\tau)$.

Note that the orthogonality as defined in (3.8) is equivalent to the expression provided in [39], [42] for the downlink.

Let us now consider a scenario in which only one path from an interferer UE #j arrives in the receiver associated with the desired signal sent by UE #i, similarly received in a one-path channel. The baseband block diagram for the physical layer in this situation is equivalent to the one described in Figure 3.6.

The data signals b_i[n] and b_j[n] sent by the UEs are constant during a bit period, with values of ±1. The base-band signals at the output of UE #i and UE #j are

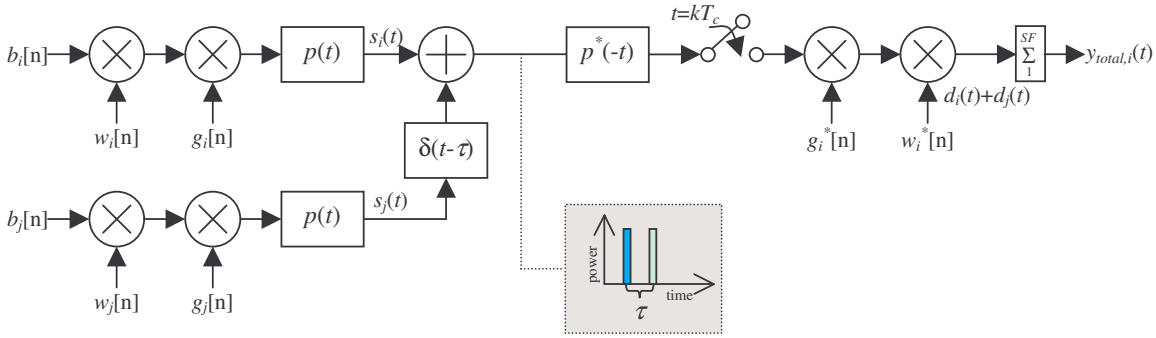

Figure 3.6. Block diagram of the equivalent base-band structure of the UMTS physical layer by considering only one interferer path in the receiver.

$$s_i(t) = \sum_{n=-\infty}^{+\infty} b_i[\mathrm{n}]\, p(t - T_c n)\, w_i[\mathrm{n}]\, g_i[\mathrm{n}],$$
$$s_j(t) = \sum_{n=-\infty}^{+\infty} b_j[\mathrm{n}]\, p(t - T_c n)\, w_j[\mathrm{n}]\, g_j[\mathrm{n}], \tag{3.9}$$

respectively, where T_c is the chip period, w_i and w_j, and g_i and g_j are the channelisation (Walsh) and scrambling (Gold) codes employed by UE #*i* and UE #*j*, respectively; and $p(t)$ is the impulse response of the transmit pulse shaping filter. For the case of UMTS, the transmission pulse shaping filter has an impulse response corresponding to a square root raised cosine filter with a roll-off factor β=0.22 [10]

$$p(t) = \frac{\sin\left(\pi \frac{t}{T_C}(1-\beta)\right) + 4\beta \frac{t}{T_C}\cos\left(\pi \frac{t}{T_C}(1+\beta)\right)}{\pi \frac{t}{T_C}\left(1-\left(4\beta \frac{t}{T_C}\right)^2\right)}. \tag{3.10}$$

The signals at the output of the despreading block associated with UE #*i* and UE #*j* can be expressed as

$$d_i[\mathrm{n}] = w_i^*[\mathrm{n}]\, g_i^*[\mathrm{n}] \left(s_i(t) \otimes p^*(-t)\right)_{t=nT_c},$$
$$d_j[\mathrm{n}] = w_i^*[\mathrm{n}]\, g_i^*[\mathrm{n}] \left(s_j(t-\tau) \otimes p^*(-t)\right)_{t=nT_c}, \tag{3.11}$$

respectively, where $(\,)^*$ stands for the complex conjugation and $a \otimes b$ is the convolution of a and b.

In the sequel, for the particular case in which UE #*j* uses the same scrambling code as UE #*i*, d_j is denoted $d_{j,same}$; for the case in which different scrambling codes are allocated to UE #*j* and UE #*i*, d_j is denoted $d_{j,different}$.

Let us finally define the function $\chi(\tau)$ between one path of a UE #*i* and another one from an interferer UE #*j* with relative delay τ as the average power received for UE #*i* coming from the single path of UE #*j* when both users have the same scrambling code but different channelisation codes divided by the average power received when they have different scrambling codes, i.e.

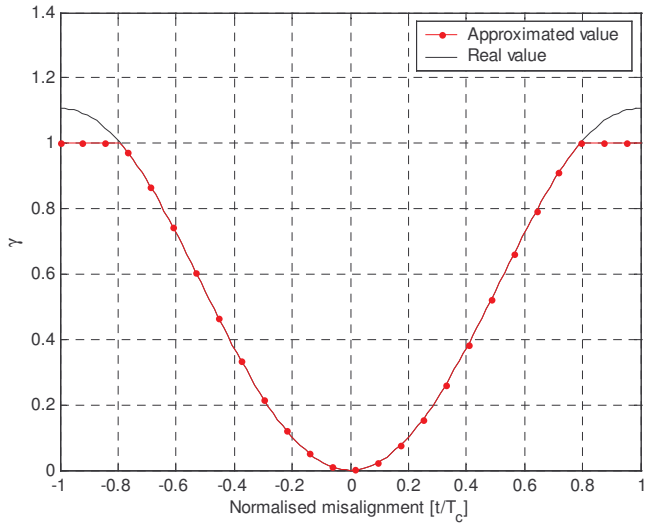

Figure 3.7. Evolution of the function γ with the misalignment.

$$\gamma(\tau)=\frac{\mathrm{E}\left[\left(\sum_{k=nSF}^{SF(n+1)-1} d_{j,same}\left(kT_c-\tau\right)\right)^2\right]}{\mathrm{E}\left[\left(\sum_{k=nSF}^{SF(n+1)-1} d_{j,different}\left(kT_c-\tau\right)\right)^2\right]}, \tag{3.12}$$

where *SF* is the spreading factor employed by UE #*i*.

Figure 3.7 shows the value $\gamma(\tau)$ as a function of the misalignment τ. Notice how for a misalignment error smaller than 1/4 of the chip period, the function γ remains below 0.16, whereas for an error smaller than 1/8 and 1/16 of chip period, γ remains below 0.04 and 0.01, respectively. For $|\tau|>1$, $\gamma(\tau)$ evolves oscillating around one. For simplicity, in the sequel γ will be considered to be one when the absolute value of the delay is greater than $0.8T_c$.

3.3.2 Effect of the Timing Control Resolution

The effect of the timing control resolution is analysed and characterised by means of the orthogonality factor.

3.3.2.1 Timing Control Resolution in a Flat Fading Channel

Let us assume that the UEs transmit through a flat fading channel, where the signal from a UE arrives at the BS as a single resolvable path. The delays of the arriving paths from different UEs with respect to the reference time at the BS are considered independent, identically distributed (iid). If the step size to update the UE transmission time is set to a certain value σ, and assuming no errors in the tracking process, then such delays are uniformly distributed between $-\sigma/2$ and $\sigma/2$.

According to this, the delay between the paths of any couple of UEs is the difference between two random variables uniformly distributed. The probability density function (PDF) of the difference of two iid random variables is calculated as the convolution of the individual PDFs.

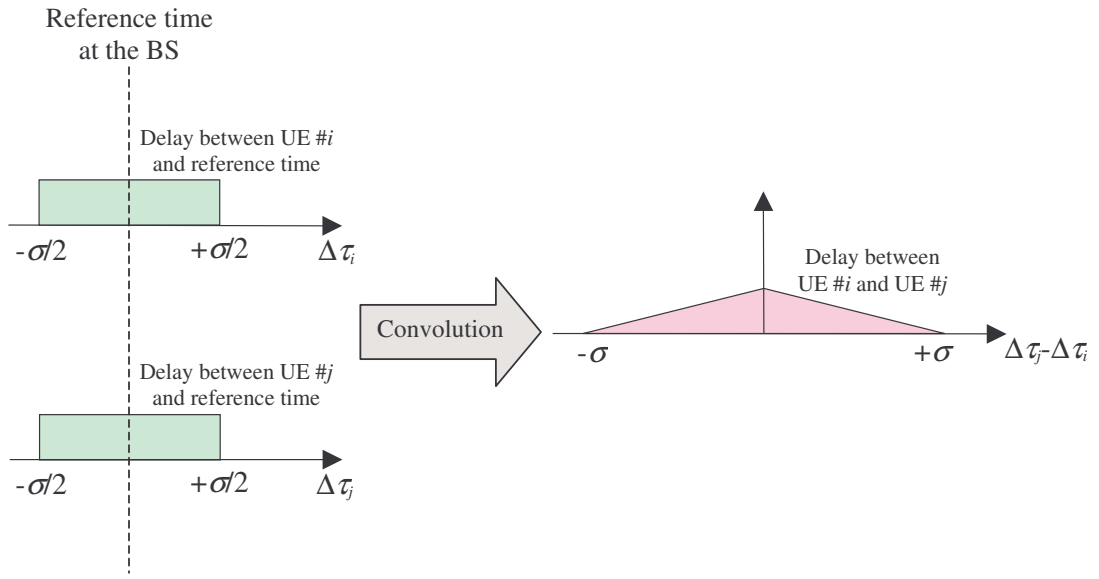

Figure 3.8. PDF of the delay between the first paths of two UEs for a step size σ.

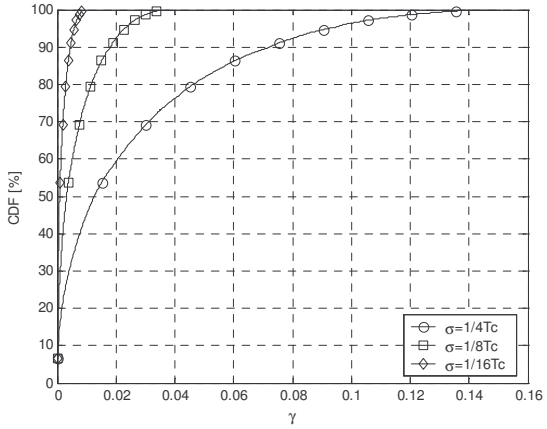

Figure 3.9. CDF of the values of the function γ between couples of paths from different UEs for different step sizes.

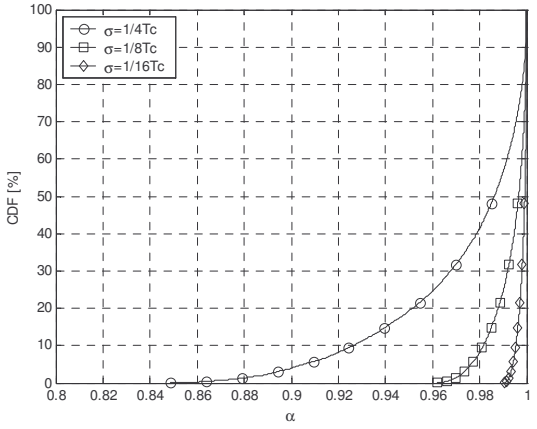

Figure 3.10. CDF of the orthogonality factor between couples of UEs under flat fading channel for different step sizes.

Hence, the delay between the paths of two UEs follows a distribution with a triangular PDF in the interval $[-\sigma,\sigma]$, as shown in Figure 3.8.

By assuming the time step size σ to be 1/4, 1/8 and 1/16 of the chip period, the function γ can be described by the cumulative distribution functions (CDF) represented in Figure 3.9. Notice that for low step sizes, like 1/8 or 1/16 of the chip time, the factor γ is very close to zero; 1/4 of the chip time is a more realistic value in practical implementations, but it still yields values of γ which are smaller than 0.07 in 90% of the cases, and smaller than 0.01 in 50% of the cases.

The orthogonality factor α is depicted in Figure 3.10 for a PDP consisting of one single path per user. For such a PDP, the orthogonality factor α between couples of UEs is exactly $1-\gamma$.

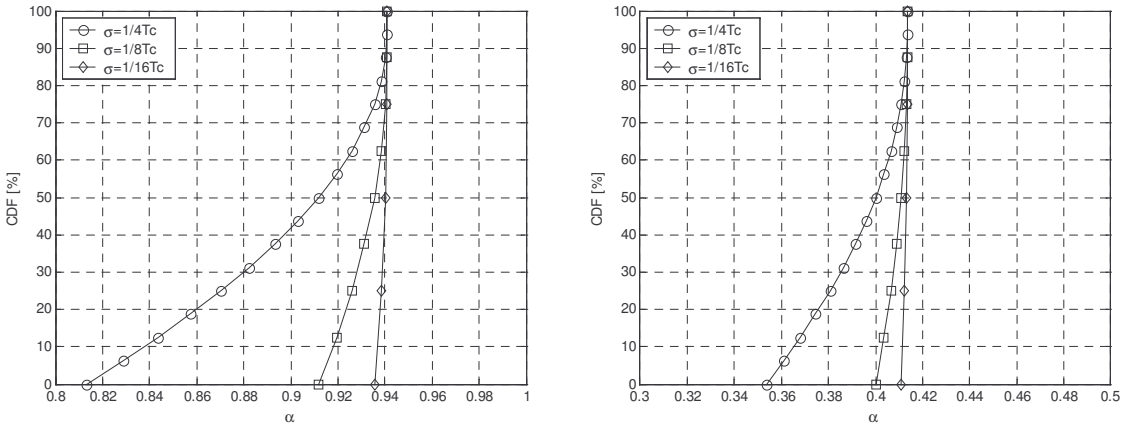

Figure 3.11. CDF of the orthogonality factor between two UEs for step sizes of 1/4, 1/8 and 1/16 of chip time for Pedestrian A (on the left) and Vehicular A (on the right) PDPs.

3.3.2.2 Timing Control Resolution in a Multi-Path Fading Channel

Next, the orthogonality factor is calculated for multi-path channels. Let us first assume the following approximation for the function γ between the *l*-th and the *m*-th paths of two different UEs

$$\gamma_{l,m} = \begin{cases} \gamma(d) & \text{if } l = m \\ \gamma(\tau_l - \tau_m) & \text{if } l \neq m \text{ and } |\tau_l - \tau_m| < 0.8T_c \\ 1 & \text{otherwise,} \end{cases} \tag{3.13}$$

where d is a random variable with a triangular PDF between $-\sigma$ and σ (σ is the step size for the tracking loop) as represented in Figure 3.8, and τ_l and τ_m are the relative delays for the *l*-th and the *m*-th paths, respectively. Let us recall that the employed model assumes the secondary paths arriving from different UEs to have the same relative delay with respect to the first path.

Figure 3.11 shows the CDF of the orthogonality factor for different step sizes in Pedestrian A and Vehicular A PDPs [43] by applying the equation (3.8) with the approximation made in (3.13).

Let us further assume no timing control resolution errors. Under this assumption, the function γ can be approximated as

$$\gamma_{l,m} = \begin{cases} 0 & \text{if } l = m \\ 1 & \text{otherwise.} \end{cases} \tag{3.14}$$

In this expression the relative delay between the first path of two UEs is assumed to be zero. Moreover, paths with different sequence numbers are considered completely non-orthogonal.

Table 3.1 shows the values of the orthogonality factor obtained for the PDPs defined in [43] by using the expression in (3.8) with the approximation in (3.14); only paths with a relative loss smaller than 15 dB with respect to the strongest one are considered. The table also includes the average orthogonality factor obtained with the function γ as defined in (3.13) for the case of σ=1/4T_c. Note that the difference between both approximations is very small. The approximation in (3.14) (i.e. no timing control resolution errors) will be used later on for the system level simulations in Chapter 4.

PDP	$E[\alpha]$ based on (3.13)	α based on (3.14)
Pedestrian A	0.90	0.89
Pedestrian B	0.31	0.32
Vehicular A	0.39	0.43
Vehicular B	0.46	0.48

Table 3.1. Average orthogonality factor for different PDPs.

Notice that the orthogonality factor is reduced in presence of multi-paths even with perfect synchronisation between UEs, since the paths arriving at different instants are not orthogonal.

3.3.3 Effect of the Errors in the Time Alignment Bits

As mentioned in Section 3.2.1, in USTS the TABs are sent by replacing one fast PC command bit every two frames. This means that the bit error rate (BER) for the TABs is the same as for the bits associated with fast PC reports.

The current 3GPP specifications do not allow changes in the transmission time in excess of ±1/4 chip every 200 ms period [34], which influences the synchronisation in USTS. Due to this the UEs do not update their transmission time after receiving every TAB (sent every 20 ms), but after collecting 10 of them. The TABs received throughout a 200 ms period are combined to take the decision on whether to advance or delay the transmission time. The way these TABs should be combined is not specified.

In [24] a very simple algorithm is proposed to take this decision, based on delay/advance commands. The problem of this algorithm is that the update is made even when the UE is perfectly synchronised. If the difference between the time of arrival of the signal and the reference at the BS is smaller than half the step size time, a new update would only make the time difference higher. To avoid this, let us propose a new algorithm based on three possible decisions: delay, advance and keep the transmission time unaltered. Note that this requires a sampling period of $\sigma/2$ for the BS at the reception. In this algorithm, the update is only made if the signal from the UE arrives with a delay which is longer than half a step size in absolute value. If no update is required, the BS sends the same number of 1s as of 0s during the 200 ms period.

In the case of a TAB report period of 20 ms, the UE will take the following decisions:

- if the number of received 0s is higher than 7, then the transmission time is advanced by 1/4 chip;
- if the number of received 1s is higher than 7, then the transmission time is delayed by 1/4 chip;
- in any other case the transmission time is not updated.

In this situation there are several types of errors when interpreting the TABs over a 200 ms report period. By assuming the errors in the TABs (i.e. errors in PC bits) to be independent, the probabilities of the different type of errors are:

a) the probability of interpreting “update” when “do not update” was sent is

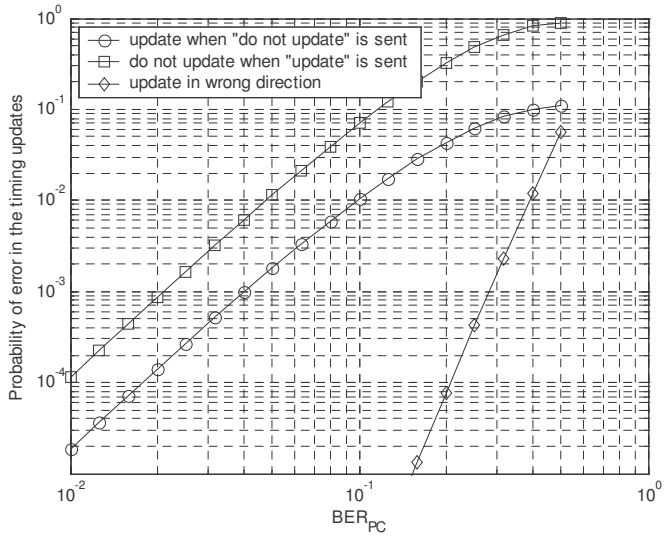

Figure 3.12. Probability of error in the timing updates for a TAB report period of 20 ms with the tracking algorithm based on delay/advance/keep.

$$p_{error\_update} = \sum_{n=3}^{7} (\mathrm{BER_{PC}})^n (1-\mathrm{BER_{PC}})^{10-n} \left[\binom{10}{n} - \sum_{m=\left\lfloor \frac{n-3}{2} \right\rfloor + 1}^{\left\lceil \frac{n+3}{2} \right\rceil - 1} \binom{5}{m} \binom{5}{n-m} \right], \tag{3.15}$$

where $\mathrm{BER_{PC}}$ is the BER associated with the fast PC command bits, $\lceil n \rceil$ stands for the smallest integer that is greater or equal to n, $\lfloor n \rfloor$ is the highest integer smaller or equal to n, and

$$\binom{N}{n} = \frac{N!}{n!(N-n)!}$$

are the n-combinations of N elements;

b) the probability of interpreting "do not update" when "update" was sent is

$$p_{error\_remain} = \sum_{n=3}^{7} \binom{10}{n} (\mathrm{BER_{PC}})^n (1-\mathrm{BER_{PC}})^{10-n}; \tag{3.16}$$

c) the probability of interpreting "update" in a wrong direction when "update" was sent is

$$p_{error\_direction} = \sum_{n=8}^{10} \binom{10}{n} (\mathrm{BER_{PC}})^n (1-\mathrm{BER_{PC}})^{10-n}. \tag{3.17}$$

The values of the different probabilities of errors are plotted in Figure 3.12 as a function of the error rate in the bits associated with PC. If the values of the BER for fast PC commands are low enough, then the impact of the errors on the TABs is practically negligible.

3.3.4 Timing Variation in the Received Signal Due to the Radio Channel Properties

Once the UE gets synchronised with the BS, a tracking loop is used to compensate for variations in the time of reception of the signal. These variations in the delay are due to

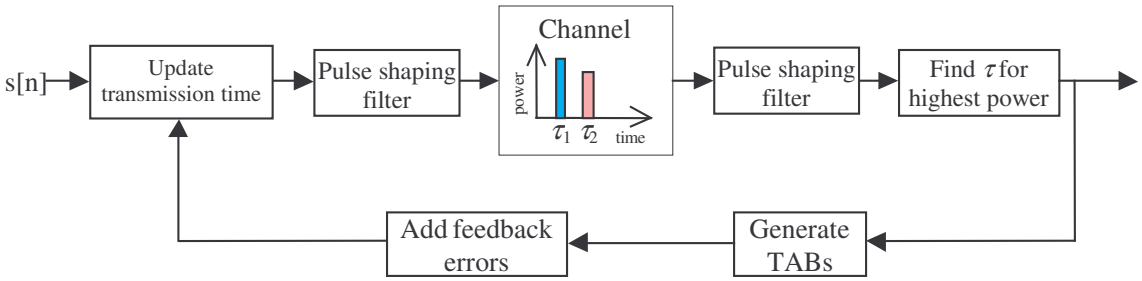

Figure 3.13 Equivalent block diagram of the closed-loop timing control scheme assuming perfect symbol synchroniser in the Rake receiver.

fluctuations in the radio channel, caused by the movement of both the UE and the rest of objects in the environment. If these time variations of the radio channel are too fast, it is likely that the UEs cannot maintain the synchronism; this might occur either because of the limit imposed by the maximum frequency of the tracking loop timing updates, or because of the maximum variation that the symbol synchroniser of every finger of the Rake receiver is able to track.

Next, the influence of radio channel variations in the orthogonality factor is investigated. Concretely, this study takes into account the RTPD fluctuations due to the UE movement and the time jitter experienced in a Rake finger when receiving two irresolvable paths. The results are obtained from simulations with several PDPs and UE speeds and include the effect of the errors in the TABs and the timing control resolution.

Let us assume a low dispersive environment with a radio propagation channel model consisting of a two-path PDP

$$h(\tau) = |\beta_1|^2 \delta(\tau - \tau_1) + |\beta_2|^2 \delta(\tau - \tau_2), \tag{3.18}$$

where β_1 and β_2, and τ_1 and τ_2 are the complex amplitude and the delay associated with the first and the second path, respectively.

Let us also assume that the path delays are constant, with a maximum separation of one chip time, which is the minimum period at which the Rake receiver can resolve different paths. Hence, the two paths are detected as one at the Rake receiver. The complex amplitudes are random variables following a Rayleigh distribution. Let us finally assume that the symbol synchroniser of the Rake receiver can perfectly track the variations of the maximum value of the signal. Under these assumptions, the closed-loop timing control scheme can be described with the block diagram of Figure 3.13, where the BS sends periodic reports to the UE so that the later one can update the transmission time to maintain the synchronism with respect to the reference time. The algorithm proposed in Section 3.3.3 based on delay/advance/keep is used to take the decisions on whether to update the transmission time or not. The step size to update the UE transmission time is set to $\sigma=1/4T_c$. A BER of 5% is assumed in the reception of the bits associated with the fast PC reports, which is in agreement with some of the values employed in the open literature [44], [45]. This yields the following probabilities for the different existing errors, based on the values plotted in Figure 3.12: p_{error_update}=0.2%; p_{error_remain}=1%; $p_{error\_direction}\approx 0$.

The variation of the channel has been analysed for two different PDPs:

a) $E[|\beta_1|^2]=E[|\beta_2|^2]$ and $\tau_2-\tau_1=0.5T_c$; and

b) $E[|\beta_1|^2]=9.3325E[|\beta_2|^2]$ and $\tau_2-\tau_1=0.42T_c$ (2 main paths of ITU Pedestrian A PDP).

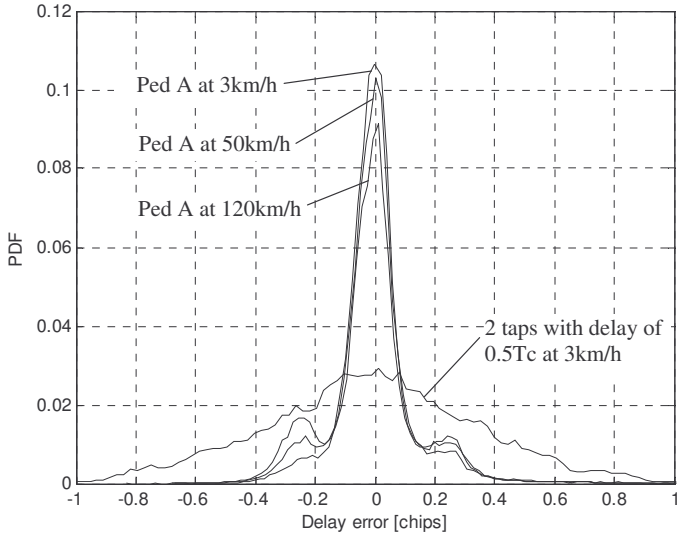

Figure 3.14. PDF of the delay between the signal from the UE and the reference time at the BS when using the closed-loop tracking algorithm.

Figure 3.14 shows the PDF of the delay of the received signal with respect to the reference time when the closed-loop tracking control algorithm is used in different environments, by assuming perfect initial acquisition. Notice that the closer the paths are within one chip period, the lower the variance of the delay. On the other hand, the speed does not have a crucial effect on the ability of the tracking algorithm to maintain the synchronism. However, it must not be forgotten that these results are obtained under the assumptions of perfect symbol tracking in the Rake receiver. The variation of the RTPD with the speed does not restrict the applicability of uplink synchronisation, as it is small even for high speeds; e.g. for a UE velocity of 120 km/h, the variation in the reception time at the BS every timing update period of 200 ms is smaller than $0.1T_c$.

Figure 3.15 shows the CDF of the orthogonality factor between two UEs for the considered two-path PDPs based on the delay depicted in Figure 3.14, i.e. the Rake receiver cannot resolve both paths separately. The average values of the orthogonality factor are summarised in Table 3.2, which fairly match those presented in Table 3.1 for the case of the ITU Pedestrian A PDP.

It should be mentioned that this orthogonality factor calculated in Figure 3.15 represents a pessimistic underestimation, since the real received pulses are the combination of the pulses from two paths and therefore have a higher width. This means that the same delay between the real received pulses would result in a higher orthogonality.

3.4 Conclusions

Uplink synchronisation has been presented as a method to reduce the MAI and therefore increase the capacity of WCDMA systems. To deploy this scheme in UMTS, the 3GPP standardisation body has proposed USTS for low mobility and low dispersive environments, which requires an initial acquisition and a closed-loop tracking control procedure for reaching the uplink synchronisation, as well as a new code allocation policy.

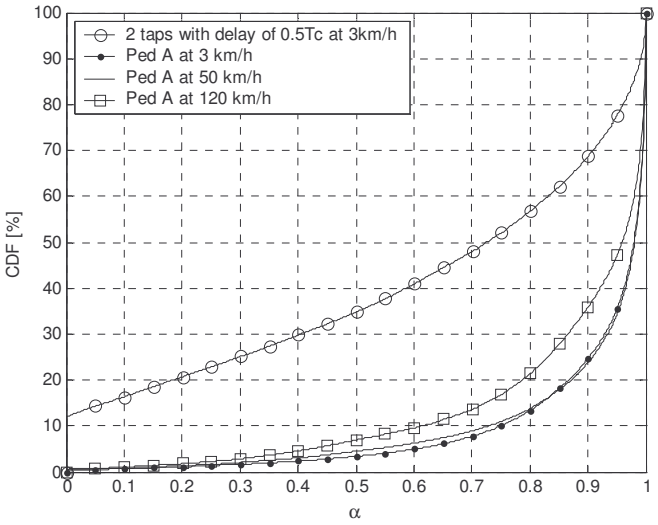

Figure 3.15. CDF of the orthogonality factor between couples of UEs when using the closed-loop tracking algorithm for PDPs consisting of two irresolvable paths.

PDP	Speed	E[α]
$E[\|\beta_1\|^2]=E[\|\beta_2\|^2]$ and $\tau_2-\tau_1=0.5T_c$	3 km/h	0.61
Pedestrian A	3 km/h	0.91
Pedestrian A	50 km/h	0.91
Pedestrian A	120 km/h	0.87

Table 3.2. Average orthogonality factor between couples of UEs when using the closed-loop tracking algorithm for PDPs consisting of two irresolvable paths.

The uplink orthogonality factor has been defined as a measure to characterise the impact of the lack of synchronism on the MAI cancellation over multi-path channels. If the variation of the channels allows synchronism with misalignment errors smaller than 1/4 of the chip period, an orthogonality factor of approximately 0.9 and 0.4 can be reached for Pedestrian A and Vehicular A PDPs, respectively. The results have been confirmed for the case of Pedestrian A by considering the influence of the radio channel variations and the errors in the closed-loop tracking algorithm.

The effect of the errors in the TABs implies a minor impact, since the UE uses the combined information from several of them in order to take the decision on whether to update the transmission time or not. On the contrary, the initial acquisition could represent a major issue since the UE might need up to 1.4 seconds to get initial synchronisation.

The variation of the radio channel also affects the degree of MAI cancellation that can be reached with uplink synchronous WCDMA. A rather high orthogonality factor between the synchronous UEs under the same scrambling code is obtained for low dispersive environments such as the ITU Pedestrian A PDP. The use of high UE velocities in a Pedestrian A has not been found to cause a major impact on the orthogonality factor. Therefore, the only argument that prevents high velocity UEs from using uplink synchronisation in low dispersive environment is the reduction of the fast PC updates, as 1 out

of 30 PC commands are used as TABs.

A higher synchronisation degree may be reached by adopting more sophisticate tracking algorithms, such as the one proposed in [38], which provides a timing accuracy better than $0.01T_c$ in the presence of severe multi-path fading. However, this kind of systems require complex computation, and enormous modifications in the 3GPP specifications would be necessary in order to support uplink synchronisation. Furthermore, the orthogonality factor obtained for low dispersive environments is already quite high with the simple closed-loop tracking algorithm; as it will be demonstrated in the next chapter, there are other factors that hide the high potential capacity gain of a perfect uplink synchronisation. In the case of a time dispersive environment, the orthogonality is very low even with perfect synchronisation, due to the multi-path effect.

Chapter 4

Performance of Uplink Synchronous WCDMA under Channelisation Code Constraints

4.1 Introduction

The potential capacity gain of uplink synchronised WCDMA (compared to asynchronous schemes) has already been evaluated in [25]. However, the study only concentrates on a single cell scenario and is based on quite ideal assumptions.

In this chapter we will quantify the capacity gain of uplink synchronised WCDMA in a multi cell environment, assuming that user equipments (UE) can only be synchronised to one cell. As it will be demonstrated, this assumption has impact on the potential performance gain of soft handover (SHO). The orthogonal codes used for own cell separation of UEs are assumed to be Walsh codes. This implies a finite set of orthogonal codes, which tends to limit the capacity gain of uplink synchronous WCDMA severely. Scenarios with single and dual antenna reception at the base station (BS) are addressed. The potential capacity gain of synchronous WCDMA is theoretically derived and evaluated by means of dynamic network simulations.

The chapter is organised as follows. Section 4.2 discusses various aspects at network level of an uplink synchronous WCDMA system. A theoretical analysis of the potential capacity gain of uplink synchronous WCDMA is presented in Section 4.3. The simulation methodology and the considered scenarios are described in Section 4.4. Both theoretical and simulation results

are presented and compared in Section 4.5. Concluding remarks and discussion are presented in Section 4.6.

4.2 Network Capacity Aspects of Uplink Synchronous WCDMA Systems

The application of synchronised WCDMA in radio channels without time dispersion completely cancels the own cell interference experienced at the BS (i.e. after despreading). The other cell interference is only suppressed by the basic processing gain, since UEs are assumed to be synchronised only to their serving cell. Hence, the potential capacity gain of synchronous WCDMA strongly depends on the other-to-own cell interference ratio, i.e. the gain in single cell is significantly larger than in multi cell environments. It is well known that in flat fading radio channels the use of dual antenna reception with maximal ratio combining (MRC) reduces the other-to-own cell interference ratio compared to single antenna reception [46]. In the later sections, results for both one and two antennas will be presented. Naturally, the capacity gain also depends on the degree of synchronisation. In this study, we will assume that the simple time delay tracking loop described in Section 3.2.1 is applied with a finite resolution of timing adjustments in the UE. It is also assumed that the timing error between the received signals at the BS is periodically estimated, and subsequently the UEs are informed via the downlink to advance or delay their transmission time. This is a very simple approach, which has proven to be sufficiently accurate for UEs at low speeds and a radio channel with marginal time-dispersion [24]. In environments with large time-dispersion the orthogonality of the signals at the BS is known to be degraded due to the misalignment of signals carried by different multi-path components. However, in radio channels with low time-dispersion such as the ITU Pedestrian A [43] power delay profile (PDP) the misalignment loss is marginal.

The fact that a UE can be synchronised to only one cell has an impact on the potential uplink SHO gain. In order to illustrate this, let us consider the following example where a UE is in SHO-mode with cell number one and cell number two, with the UE synchronised to cell number one only. The path loss towards both cells is the same, assuming equal wideband interference level at the two cells. The signal-to-interference ratio after despreading will therefore be higher at cell number one compared to cell number two, because the own cell interference in cell number one is orthogonal. In an asynchronous WCDMA system, the signal-to-noise ratio after despreading would have been equal in the two cells, indicating a significant SHO diversity gain by using either selection diversity combining or MRC. The loss of SHO gain for synchronous WCDMA is addressed in this study. Here it is assumed that a UE which enters SHO remains synchronised with its original serving cell during the SHO period. When the UE drops the connection with the original cell, it synchronises with the new serving cell.

In the following, the potential capacity gain of uplink synchronous WCDMA will be evaluated. Scenarios where only a certain percentage of UEs are operated in synchronous mode are addressed. The latter is of interest for an existing system like UMTS, where Uplink Synchronous Transmission Scheme (USTS) can potentially be introduced gradually, i.e. in the initial phase there will be a mixture of synchronous and asynchronous UEs.

4.3 Theoretical Analysis of the Capacity of Uplink Synchronous WCDMA

Let us derive a simple expression for the expected uplink capacity gain of a synchronous WCDMA system, where we assume that all the UEs have the same bit rate and are perfectly power controlled. In this context, perfect power control (PC) refers to the case where the transmission power of each UE is adjusted so that the energy-per-bit to noise ratio (Eb/No) at the BS equals a target value corresponding to a certain block error rate (BLER). For the sake of simplicity, we will not include cases where UEs are in SHO-mode in this simple theoretical analysis. SHO cases are instead studied by means of dynamic system level simulations in Section 4.4 and Section 4.5. We will define the maximum cell capacity as a function of the number of UEs that can be supported at a given noise rise (NR) at the BS. The NR at the BS is known to be a robust measure of the uplink load of a WCDMA system, which is often used by radio resource management (RRM) algorithms to control the uplink load [7], [8]. The NR is defined as

$$NR = \frac{P_{total}}{P_{noise}}, \tag{4.1}$$

where P_{total} is the total average received wideband power at the BS, and P_{noise} is the power of the background noise at the BS. The NR is related to the uplink load factor as [7]

$$\eta = \frac{NR - 1}{NR}, \tag{4.2}$$

where $\eta \in [0,1]$ is the uplink load factor. The system has reached its pole capacity when η approaches unity. Hence, the NR can be used to control how close the system is operated to the pole capacity. In deriving an expression for the NR, we will assume that there are N_{async} UEs in the cell of interest which are transmitting asynchronously. In addition, there are N^{j}_{sync} UEs in synchronous mode transmitting under scrambling code number j. Let us furthermore assume that the required Eb/No is identical for all the UEs. Under these assumptions, we can approximate the Eb/No for the UEs operating in asynchronous mode as

$$\rho = G\frac{P_{async}}{P_{total}}, \tag{4.3}$$

where G is the effective processing gain (ratio between the chip rate and the user bit rate), and P_{async} is the received power level at the BS from a UE in asynchronous mode. Similarly, we can express the Eb/No for synchronous UEs under scrambling code number j as

$$\rho = G\frac{P^{j}_{sync}}{P_{total} - N^{j}_{sync}P^{j}_{sync}\alpha}, \tag{4.4}$$

where P^{j}_{sync} is the received power level at the BS from a synchronous UE under scrambling code number j, and $\alpha \in [0,1]$ is the orthogonality factor as defined in Section 3.3, which expresses the degree of orthogonality between the signals received under the same scrambling code. Assuming a radio channel with marginal time-dispersion and perfect synchronisation at the BS, $\alpha \to 1$. On the contrary, if the synchronisation of the signals received at the BS completely fails due to erroneous adjustment of timing of the transmitted signals or excessive time-dispersion in the radio channel, then $\alpha \to 0$. Hence, assuming a perfectly synchronised

WCDMA system where the average PDP of the radio channel between all the UEs and their serving BS is the same, (4.4) is valid. Notice that (4.3) and (4.4) include the inter-path interference (IPI) from the own signal, although it is partially cancelled by the orthogonality factor like the rest of the own cell interference under the same scrambling code. From (4.3) and (4.4), the following expressions are obtained

$$P_{async} = \frac{\rho P_{total}}{G}, \tag{4.5}$$

$$P_{sync}^{j} = \frac{\rho P_{total}}{G + \rho N_{sync}^{j} \alpha}. \tag{4.6}$$

The total received power at the BS can be expressed as

$$\begin{aligned} P_{total} &= P_{own} + P_{other} + P_{noise} \\ &= P_{own}(1+i) + P_{noise}, \end{aligned} \tag{4.7}$$

where P_{own} is the own cell power, P_{other} is the other cell power, and $i=P_{other}/P_{own}$ is the other-to-own cell interference ratio. The own cell power equals

$$P_{own} = N_{async} P_{async} + \sum_{j=1}^{J} N_{sync}^{j} P_{sync}^{j}, \tag{4.8}$$

where J is the number of enabled scrambling code groups within the cell of interest. Combining (4.5), (4.6), and (4.8) yields

$$P_{own} = P_{total} \rho \left[\frac{N_{async}}{G} + \sum_{j=1}^{J} \frac{N_{sync}^{j}}{G + \rho N_{sync}^{j} \alpha} \right]. \tag{4.9}$$

An expression for the NR at the BS is subsequently obtained by combining (4.7) and (4.9), i.e.

$$NR = \frac{P_{total}}{P_{noise}} = \left(1 - (1+i) \rho \left[\frac{N_{async}}{G} + \sum_{j=1}^{J} \frac{N_{sync}^{j}}{G + \rho N_{sync}^{j} \alpha} \right] \right)^{-1}. \tag{4.10}$$

For systems where the UEs are not necessarily assumed to be transmitting all the time, we will introduce an activity factor $v \in [0,1]$. Hence, $v=1$ for UEs with constant transmission, while $v=0.5$ is equivalent to transmission during 50% of the time. Assuming that the average activity factor is identical for all the UEs, it can easily be shown that the expression in (4.10) is generalised to

$$NR = \frac{P_{total}}{P_{noise}} = \left(1 - (1+i) \rho \left[\frac{v N_{async}}{G} + \sum_{j=1}^{J} \frac{v N_{sync}^{j}}{G + v \rho N_{sync}^{j} \alpha} \right] \right)^{-1}. \tag{4.11}$$

The expression in (4.11) is employed to plot the NR in Figure 4.1 versus the number of UEs, conditioned on α=0.9, G=314 (3.84 Mcps/12.2 kbps), ρ=6.1 dB, v=0.5, and i=0.6. These parameter settings correspond to a typical micro cellular environment with 12.2 kbps speech users [7], assuming a chip rate of 3.84 Mcps. Results are presented for cases where all the UEs are either in asynchronous or synchronous mode. The curve labelled "no code limit" refers to the case where J=1, independently of the number of synchronous UEs, i.e. corresponding to an infinite number of channelisation codes under a single scrambling code.

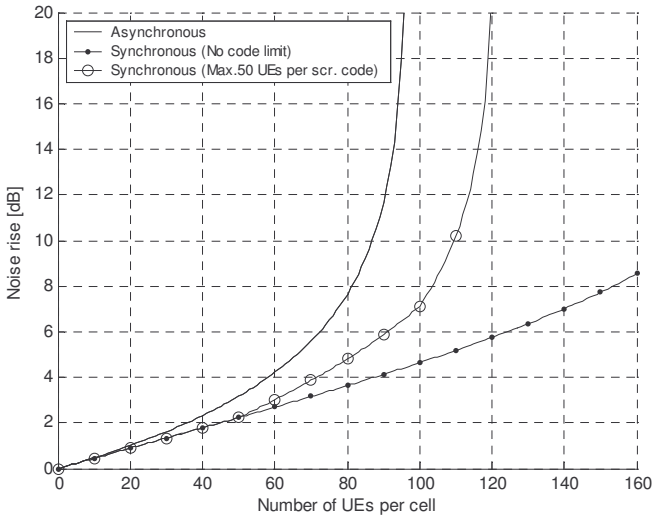

Figure 4.1. NR as a function of the number of UEs per cell (α=0.9, G=314, ρ=6.1 dB, v=0.5, and i=0.6).

The other curve for UEs in synchronous mode assumes a maximum of 50 UEs under each scrambling code [24]. For this scenario, UEs are first allocated under scrambling code number one. Once the number of UEs exceeds the maximum number of channelisation codes, the second scrambling code is enabled, and so forth. As an example, for 65 synchronised UEs, J=2 with N^1_{sync}=50 and N^2_{sync}=15. It is observed from Figure 4.1 that the NR increases rapidly for the case where all the UEs are operated in asynchronous mode, while the NR increases slower in the cases with synchronous UEs. This is equivalent to a capacity gain of uplink synchronous WCDMA compared to conventional asynchronous systems. The two NR curves for the synchronous cases are identical up to 50 UEs, whereafter the curve conditioned on a maximum number of UEs per scrambling code starts to increase much faster. This behaviour occurs because the synchronised UEs under different scrambling codes are non-orthogonal.

Let us define the capacity in a cell as the sum of the throughput transmitted by every UE in the cell. Hence, the capacity per cell in a synchronous and an asynchronous system equals

$$C_{async} = R_b \nu N_{async}, \tag{4.12}$$

$$C_{sync} = R_b \nu \sum_{j=1}^{J} N^j_{sync}, \tag{4.13}$$

respectively, where R_b is the bit rate for a single UE. The capacity gain of uplink synchronous WCDMA can then be expressed as

$$G_{sync} = \frac{C_{sync} - C_{async}}{C_{async}}. \tag{4.14}$$

By carrying out some manipulations, from (4.11), (4.12), (4.13) and (4.14) it is possible to derive the following expression for the capacity gain of uplink synchronisation

$$G_{sync} = \frac{1+i}{\eta}\left(\frac{\eta_J}{1+i-\eta\alpha} + \frac{\rho\nu}{G} N_{max}(J-1)\right) - 1, \tag{4.15}$$

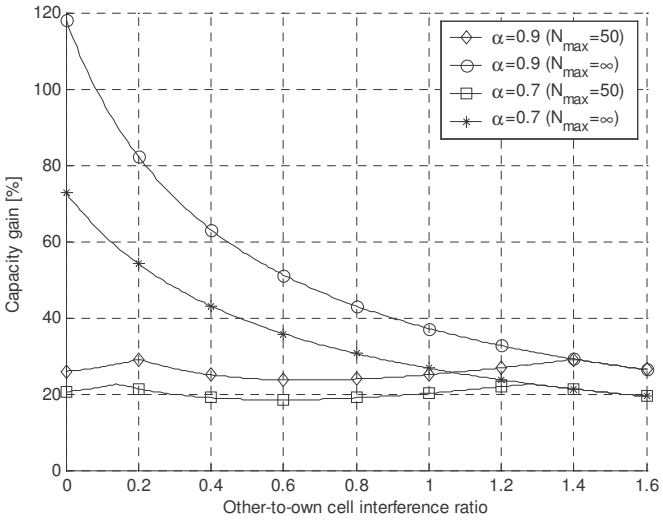

Figure 4.2. Capacity gain of uplink synchronous WCDMA for a NR target of 4.0 dB, a 12.2 kbps speech service and ρ=6.1 dB.

where N_{max} is the maximum number of UEs that can be allocated under the same scrambling code, and η_J is the load factor increase associated with the UEs in scrambling code number J; J and η_J can be calculated as

$$J = \left\lceil \eta \frac{G + \rho\nu\alpha N_{max}}{(1+i)\rho\nu N_{max}} \right\rceil, \tag{4.16}$$

$$\eta_J = \eta - \frac{(1+i)\rho\nu N_{max}(J-1)}{G + \rho\nu\alpha N_{max}}, \tag{4.17}$$

where $\lceil x \rceil$ denotes the smallest integer value that is bigger than x.

The capacity gain of synchronous WCDMA for a NR target of 4.0 dB is plotted in Figure 4.2 versus i for different values of α, with and without constraints on the maximum number of synchronised UEs under a single scrambling code. According to (4.2), NR=4.0 dB corresponds to η=0.60, which indicates that we are quantifying the capacity gain at 60% of the systems pole capacity. The remaining parameters are identical to the ones used in Figure 4.1. It is observed that the capacity gain decreases for increasing i. This is due to the fact that only the own cell interference is reduced by introducing synchronous WCDMA, and hence the gain decreases when the other cell interference starts to become dominant. Similarly, it is observed that the capacity gain decreases for decreasing values of α. In all the considered cases in Figure 4.2, the capacity gain is larger than or equal to 20%. The marginal variations in the capacity gain for the cases with a limited number of UEs per scrambling code is caused by a varying number of active scrambling codes (J) versus i.

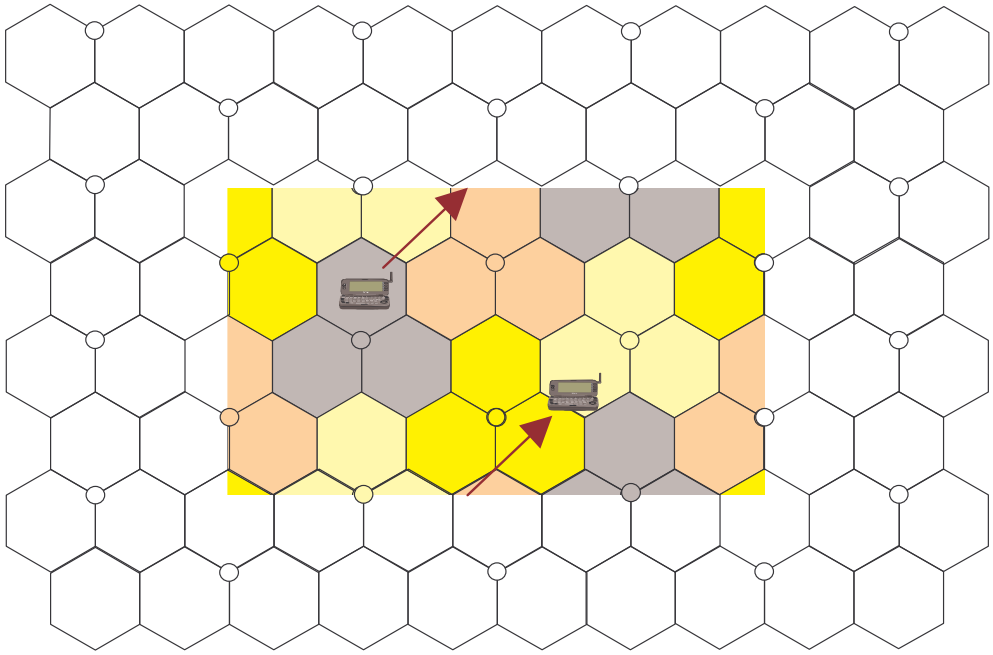

Figure 4.3. Network layout with wrap-around.

4.4 System Model for Dynamic Simulations

4.4.1 Overall Description

Dynamic network simulations are conducted for both single and multi cell environments, using the general simulation methodology outlined in [47]. As a reference, simulation parameters are selected according to the UMTS specifications, assuming that the synchronous WCDMA is implemented in coherence with the specifications of USTS [24]. The multi cell case simulations consider a network layout with 24 cells, grouped into three-sector BSs with 3 dB beam width antennas of 72 degrees. The cell grid is contained in a rectangle, where wrap-around is used to keep continuity, as shown in Figure 4.3; BSs only see UEs from the closest distance. UEs are uniformly distributed in the network, travelling with a fixed speed v=3 km/h in a random direction. A new UE entering the system automatically gets connected to the cell with a minimum path loss. The distance-dependent path loss is modelled according to the pedestrian model in [43]

$$L_d[\text{dB}] = 147 + 40\log d, \tag{4.18}$$

where d is the distance from the UE to the BS in km. Shadow fading is modelled as a lognormal distributed random variable, with an exponentially decaying spatial auto-correlation function; its variation along the time is generated based on a one-tap filter [48]

$$L_{SF}(nT) = L_{SF}((n-1)T)\cdot e^{-\frac{\Delta d}{d_0}} + \chi\cdot\sqrt{1-e^{-2\frac{\Delta d}{d_0}}}, \tag{4.19}$$

where $L_{SF}(nT)$ is the value of the shadow fading in decibels at instant nT, T is the time associated with consecutive samples of shadow fading, d_0 is the coherence distance, $\Delta d = vT$ is

Tap	Relative delay	Relative average gain	Amplitude distribution	Doppler spectrum
1	0	0 dB	Rayleigh	Classic
2	T_c	-12.8 dB	Rayleigh	Classic

Table 4.1. Modified ITU Pedestrian A PDP.

the distance covered by the UE since the calculation of the last sample of the shadow fading, and χ is a Gaussian random variable with zero mean and variance equal to the variance of the shadow fading.

Multi-path fading is modelled in compliance with a resampled version of the ITU Pedestrian A PDP [43]; this modified Pedestrian A PDP is equivalent to the one defined in [43] assuming the operation of a Rake receiver, where paths can only be resolved to a resolution of 1 chip. The relative average power of each multi-path component for the modified Pedestrian A model is summarised in Table 4.1. The amplitude of each path is assumed to be Rayleigh distributed, independent for each tap, with a classical Doppler spectrum.

The UEs are provided with speech service at 12.2 kbps. Once the users start a call, this is assumed to continue until the end of the simulation. Each simulation run corresponds to 200 seconds of real time. With the assumptions made and the wrap-around scheme shown in Figure 4.3, where the border effect is mitigated, all the cells provide the same statistics. Hence, it is possible to average over all the cells in the network to obtain the final statistical results per cell.

4.4.2 Interference and Block Error Rate Calculations

The time resolution of the dynamic network simulator is slot level (i.e. 0.66 ms). A conventional Rake receiver is assumed to be implemented in the BSs, and tracks the multi-path components within a window of 15 dB compared to the strongest path. Signals tracked by different Rake fingers are combined by using MRC. In every slot period the Eb/No is first computed for each individual Rake finger and UE, taking into account that the time-aligned interference from synchronised UEs within the cell is orthogonal. By assuming that the desired signal at every Rake finger is completely uncorrelated from the rest of the interference, the Eb/No after Rake finger combining is obtained as the sum of the Eb/Nos per Rake finger. Notice that this approximation also implies that the signals from the same UE, but associated with different paths, are completely uncorrelated. Under these assumptions, the Eb/No obtained at a certain BS from a UE #*i* is calculated as

$$\rho_i = G_i \sum_{l=1}^{L} \frac{P_i h_i a_{i,l}}{P_{noise} + \sum_{j=1}^{N} \sum_{m=1}^{L} P_j h_j a_{j,m} \chi_{i,j}(l-m)}, \tag{4.20}$$

where P_{noise} is the background noise power, P_i is the total power transmitted by the UE, h_i is the propagation gain from UE #*i* to the BS (considering path loss with distance, shadow fading and antenna gain), N is the number of UEs in the network, L is the number of paths defined for the channel model, $a_{i,l}$ is the relative gain associated with the l-th path of UE #*i*, and $\chi_{i,j}$ is a factor defined as

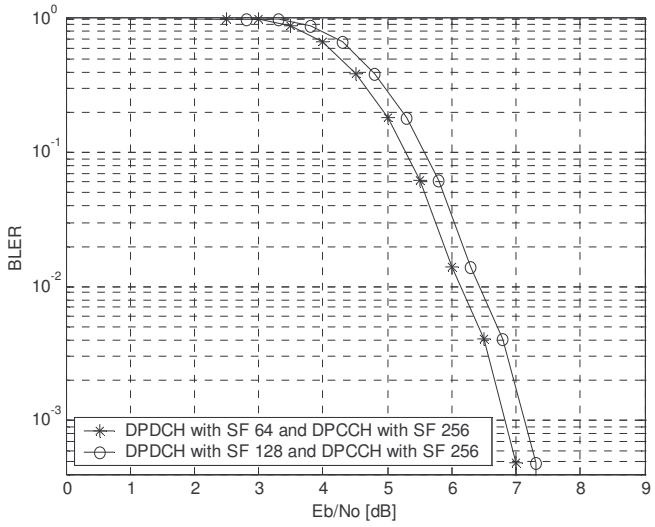

Figure 4.4. Function of BLER versus per block average Eb/No for Pedestrian A and a UE speed of 3 km/h [49].

$$\chi_{i,j}(k) = \begin{cases} 0 & \text{if } k = 0 \text{ and UE\#}i \text{ and UE\#}j \\ & \text{use the same scrambling code;} \\ 1 & \text{otherwise.} \end{cases} \tag{4.21}$$

Notice that the expression in (4.21) is defined to obtain an average orthogonality factor as in (3.14). In cases where dual antenna reception is used at the BS, the Eb/No is obtained as the sum of Eb/Nos per Rake finger, computed for each antenna branch. This approach is valid provided that the noise and interference at the two antennas are uncorrelated.

The BLER for each connection is computed via lookup tables, which map the geometrical average of Eb/Nos corresponding to one frame length into the BLER. This is a well-known approach, which is often applied in network simulators [50]. The aforementioned mapping table is obtained from link level simulations of a 12.2 kbps speech service with a 20 ms frame length, which can be supported with a spreading factor (SF) of 64 or 128. The mapping function is plotted in Figure 4.4. The results in Figure 4.4 include a Dedicated Physical Control Channel (DPCCH) with SF 256 and a Dedicated Physical Data Channel (DPDCH) with SF 64 or 128 [7]. The DPCCH and DPDCH are code multiplexed, so each UE uses two channelisation codes. Convolutional coding with a coding rate of 1/3 and an interleaver with either repetition or puncturing, depending on the SF of the DPDCH, is assumed. The overhead of the logical control channel, transmitted at 2.4 kbps, is included in the mapping table. Note that the configuration with a DPDCH with SF 128 allows more UEs under the same scrambling code compared to a DPDCH with SF 64. This is obtained at the expense of a 0.3 dB higher required Eb/No for a BLER of 1%.

4.4.3 Radio Resource Management Algorithms

A simplified admission control (AC) algorithm determines whether a new UE is allowed access to a cell. The average NR is computed over a period of 100 ms (corresponding to 150 slots), and if the NR is below a predefined NR target the UE is allowed access, otherwise the call is rejected. Only one UE is allowed to enter a cell per a 20 ms period. A UE in

synchronous mode which is granted capacity in a given cell is assigned a unique channelisation code for the DPDCH and another one for the DPCCH. If there are no free channelisation codes, an additional scrambling code is enabled for the cell so that more channelisation code resources are made available. This implies that a maximum number of 50 and 84 UEs can be supported under one scrambling code for DPDCHs with SF 64 and SF 128, respectively [24].

All the UEs are power controlled by their serving BS. A conventional closed-loop PC algorithm is implemented, where the UE transmission power is adjusted in steps of 1 dB at every slot period in coherence with the current Eb/No, compared to the Eb/No target [7]. The reception of transmit PC commands at the UEs is assumed to be error-free and subject to no delays. The Eb/No target is updated every frame period to obtain a BLER target of 1% according to the outer-loop PC algorithm in [51]. The maximum transmission power from each UE is limited to 24 dBm.

SHO is modelled in the simulator, assuming selection diversity combining between cells on different BSs and MRC between cells on the same Node B (i.e. softer handover). For the sake of simplicity, the maximum active set size is limited to two. A UE which enters SHO remains synchronised to its serving BS. Decisions on adding, replacing, or dropping a SHO leg are based on simple average path loss measurements from the UE to the BSs in the candidate set and/or the active set [52]. This is a well-known approach for implementation of a robust handover algorithm. The operation of the handover control (HC) is as follows: If the ratio between the strongest pilot measurement from a BS and the one received at another BS is smaller than the “window add” parameter, and the active set is not full, then this last BS is added to it. If the ratio between the strongest pilot measurement and the one received at a BS in the active set is higher than “window drop” during a predefined period of time, then this BS is dropped from the active set. If the active set is full, but a BS that does not belong to it receives a pilot measurement which is “window replace” times greater than another from the active set, the first one replaces the second one. All the relevant simulation parameters are summarised in Table 4.2.

4.5 Simulation Results

4.5.1 Single Cell Environment

Simulation results from a single cell scenario are presented in Figure 4.5 for various numbers of receive antennas and activity factors. For the single cell case, the omni directional antenna is assumed; the DPDCHs are transmitted at SF 64 for all the UEs. The average number of UEs per cell is reported for uplink synchronous and asynchronous WCDMA scenarios. The capacity gain of the synchronous WCDMA is observed to equal 45.7%, assuming one receiver antenna and an activity factor of one. Decreasing the activity factor to 0.5 results in a reduced capacity gain, i.e. the capacity gain drops to 26.1%. This is caused by the increase in the number of UEs, which requires additional active scrambling codes in order to avoid channelisation code shortages. Let us recall that a maximum of 50 UEs can be supported under each scrambling code. The capacity gain equals 13.0% in the case of two antennas at the BS, assuming an activity factor of 0.5. For this particular scenario, five scrambling codes are required on an average, where all the channelisation codes under four of the scrambling codes are fully utilised. Only a few channelisation codes under the fifth scrambling code are in use. Hence, for demodulation of the received signal from each UE, only approximately

Parameter		Value
System	Chip rate	3.84 Mcps
Cell Plan	Site-to-site distance	1040 m
	Number of receiver antennas per cell	1 or 2
	Noise level per receiver antenna	-102.9 dBm
Propagation	Path loss with distance d [km]	147.7+40log d dB
	Standard deviation for shadow fading	10 dB
	Coherence distance for shadow fading	50 m
	Receiver antenna gain	16 dBi
SHO	Window add / drop / replace	2 dB / 4 dB / 2 dB
	Time out to drop BS	0.02 s
	Maximum active set size	2
AC	Period between admissions	20 ms
	NR target	4 dB
PC	Fast closed-loop PC step size	1 dB
	Frequency of outer-loop PC updates	20 ms
	Outer-loop PC step size (up)	0.3 dB
	BLER target for outer-loop PC	1 %
UE	Effective bit rate (R_b)	12.2 kbps
	Speed (v)	3.0 km/h
	Activity factor (ν)	0.5 or 1.0
	Maximum transmission power	24 dBm

Table 4.2. Summary of the main simulation parameters.

25% of the total received interference is orthogonal. This results in the rather low capacity gain of 13.0%, compared to the capacity gain of 45.7% in the case of a single BS antenna and an activity factor of one. For systems with no constraints on the number of available channelisation codes the capacity gain would approximately equal 100% in all the four considered cases (in the particular case of two antennas and an activity factor of 0.5 the capacity gain increases from 13.0% to 102.1%). The simulation results in Figure 4.5 and the corresponding theoretical results in Table 4.3 are observed to be in agreement. The theoretical results are computed according to the expressions in Section 4.3 for ρ=6.1 dB (the value that corresponds to 1% BLER in Figure 4.4), α=0.94 (obtained by using the expression in (3.8) with the multi-path model in Table 4.1), a NR target of 4 dB, and i=0. In the case of two receive antennas ρ=3.1 dB (6.1-3.0).

4.5.2 Multi Cell Environment without Soft Handover

Multi cell simulation results are presented in Figure 4.6 for the case without SHO. The capacity gain for two antennas at the BS and an activity factor of 0.5 is equal to 10.8% under the channelisation code constraint. Hence, for this particular setup, the capacity gain is slightly lower than the capacity gain for the single cell scenario. This can be explained as follows: In the multi cell environment both the own cell and other cell interference are received at the BS. For the considered scenario, approximately an equal amount of own cell and other cell interference is received (i=0.8). From Figure 4.6 it is observed that three scrambling codes are required per cell, where the load of the third code equals 33% (17/50) on an average, while all the channelisation codes under the first two scrambling codes are in use. Hence, a UE transmitting under scrambling code number one or two is subject to approximately 43% orthogonal and 57% non-orthogonal own cell interference, plus the non-orthogonal other cell interference. This is equivalent to the single cell case, where

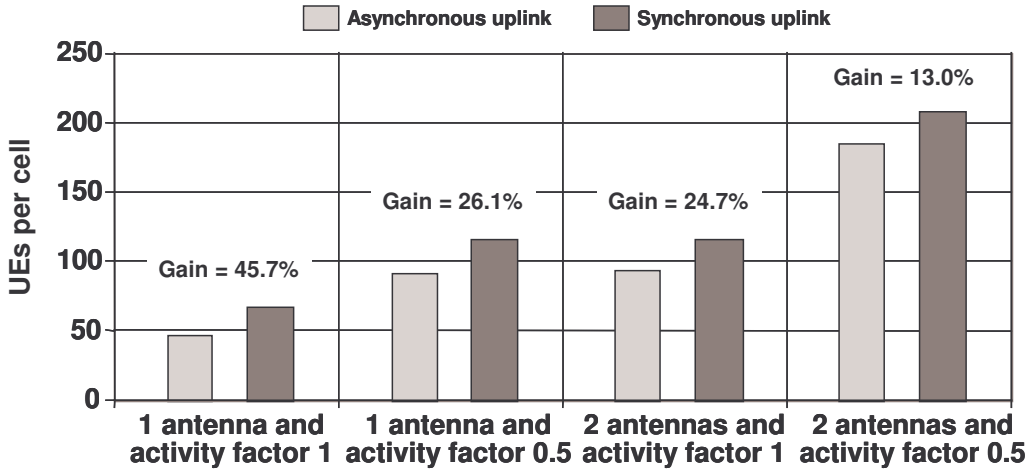

Figure 4.5. Average number of UEs per cell from simulations of a single cell environment (DPDCHs with SF 64).

No. of rx antennas	Activity factor	Number of asynchronous UEs	Number of synchronous UEs	Capacity gain
1	1.0	46	68	47.8%
1	0.5	93	117	25.8%
2	1.0	93	117	25.8%
2	0.5	185	211	14.1%

Table 4.3. Theoretical single cell results (DPDCHs with SF 64).

approximately 24% of the total received interference may be regarded as orthogonal. However, for the UEs transmitting under the third scrambling code, only 8% of the total received interference is orthogonal. For comparison, the corresponding theoretical findings are reported in Table 4.4. It is observed that the simulation results are in agreement with the theoretical findings. The theoretical results are calculated for i equal to 1.6 and 0.8 for one and two receive antennas, respectively; they correspond to the average values obtained from the simulations.

4.5.3 Multi Cell Environment with Soft Handover Enabled

In order to illustrate the impact of SHO on the performance of synchronous WCDMA, multi cell results with SHO enabled are presented in Figure 4.7. The used SHO parameter settings result in a scenario where 27% of the UEs are in two-way SHO.

Comparing the average number of UEs per cell in Figure 4.6 and Figure 4.7, it is observed that SHO provides a capacity gain for all the considered cases. However, due to the increase in the absolute number of UEs per cell, the load of the third scrambling code slightly increases for the case with SHO, which consequently maps to a marginal loss of the capacity gain of synchronous WCDMA. In the case of two BS antennas without SHO and an activity factor of 0.5, the capacity gain drops from 10.8% to 9.6%. This minor reduction of the capacity gain leads us to conclude that SHO does not provide a major obstacle for the capacity gain of synchronous WCDMA. Notice that a UE in SHO cannot synchronise with more than one cell simultaneously. On the other hand, the use of SHO reduces the other cell interference, which increases the performance of uplink synchronous WCDMA. To give an example, for a two branch reception diversity the average other-to-own cell interference ratio is 0.8 without SHO,

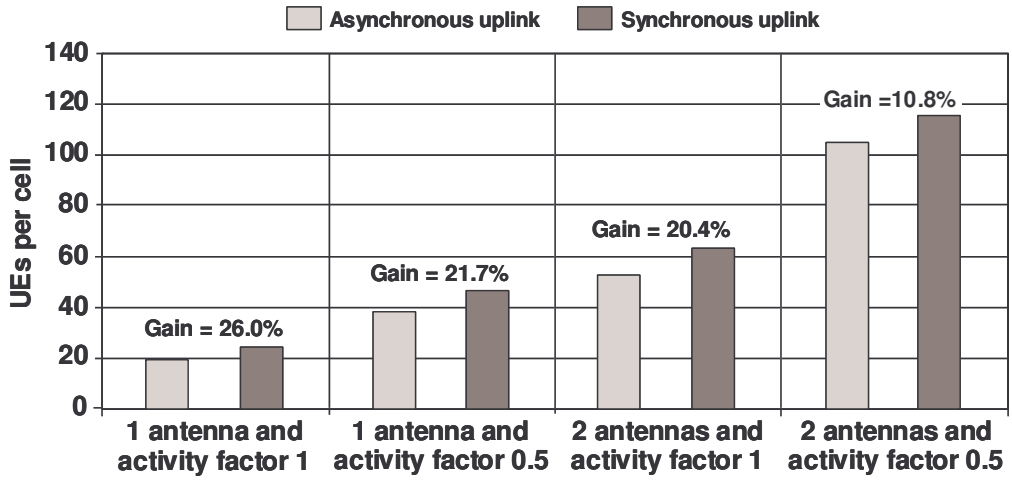

Figure 4.6. Average number of UEs per cell from simulations of a multi cell environment without SHO (DPDCHs with SF 64).

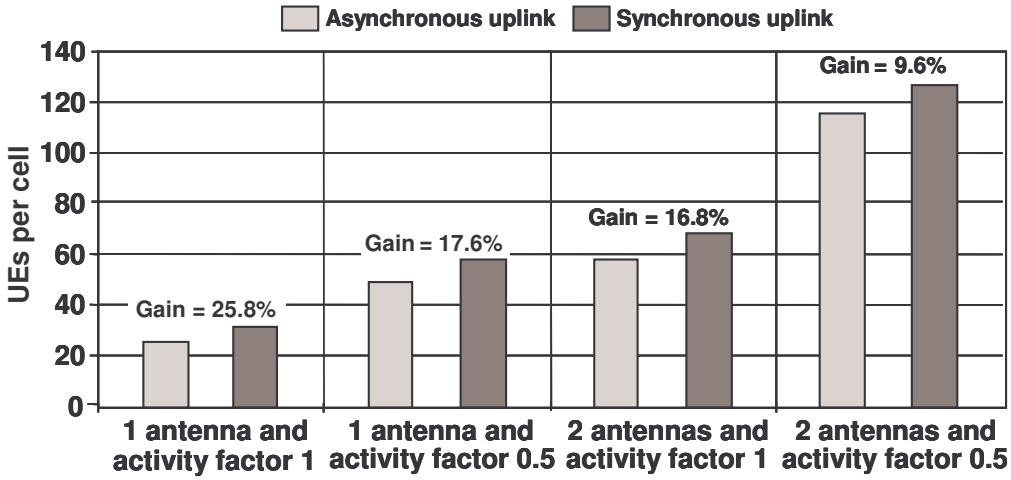

Figure 4.7. Average number of UEs per cell from simulations of a multi cell environment with SHO (DPDCHs with SF 64).

No. of rx antennas	Activity factor	Number of asynchronous UEs	Number of synchronous UEs	Capacity gain
1	1.0	18	22	22.2%
1	0.5	35	45	28.6%
2	1.0	51	64	25.5%
2	0.5	103	116	12.6%

Table 4.4. Theoretical multi cell results (DPDCHs with SF 64).

and 0.4 with SHO.

The main limitation is the relatively small number of available channelisation codes under a single scrambling code. Lifting the channelisation code constraint, our simulation results show that the capacity gain increases from 9.6% to 35.8%. This result clearly demonstrates that the capacity gain of synchronous WCDMA is limited by channelisation code shortage.

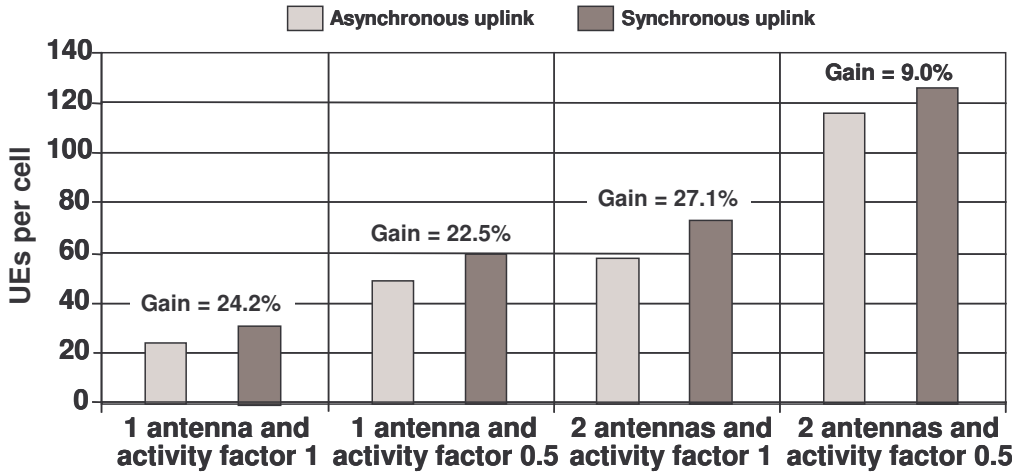

Figure 4.8. Average number of UEs per cell from simulations of a multi cell environment with SHO (DPDCHs with SF 128 for synchronous UEs and SF 64 for asynchronous UEs).

The number of available channelisation codes per scrambling code can be increased by using a higher SF for the DPDCHs, as discussed in Section 4.4 and further in Chapter 5. Changing the SF of the DPDCHs from 64 to 128, the maximum number of UEs per scrambling code increases from 50 to 84 [24], while maintaining the same effective bit rate. However, this is obtained at the expense of a 0.3 dB higher required Eb/No for a BLER of 1% (see Figure 4.4). The results pictured in Figure 4.8 correspond to the case where UEs in synchronous mode are operated with SF 128 and asynchronous UEs use SF 64. When comparing the results in Figure 4.7 and Figure 4.8, it is observed that this scheme only performs better than the case with SF 64 if the number of UEs per cell is higher than 50 and smaller than 84 (i.e. the maximum number of UEs under the same scrambling code for the SF 128 case). Hence, in the case of two receiver antennas and an activity factor of 0.5 there is no significant capacity gain from changing the SF of the DPDCHs from 64 to 128.

4.5.4 Capacity Gain versus the Penetration Rate of Synchronous UEs

The results in Sections 4.5.1-4.5.3 compare the capacity gain of a system with asynchronous UEs to a system where all the UEs are operated in synchronous mode. In the following we will present the results of a system with a mixture of UEs operated in either synchronous or asynchronous mode. The ratio between the number of synchronous UEs and the total number of UEs will be referred to as the penetration rate of synchronous UEs, i.e. a penetration rate of 50% is equivalent to an equal number of synchronous and asynchronous UEs. Figure 4.9 illustrates the evolution of the capacity gain of uplink synchronous WCDMA with the UE penetration rate. The presented results are obtained from simulations with a multi cell scenario with SHO enabled and DPDCHs with SF 64. The capacity gain is observed to increase gradually with the penetration rate. The dependency between the capacity gain and the penetration rate is non-linear, so a rather large penetration rate of synchronous UEs is required before a significant capacity gain is observed. The discontinuities on the presented curves are caused by introduction of additional scrambling codes.

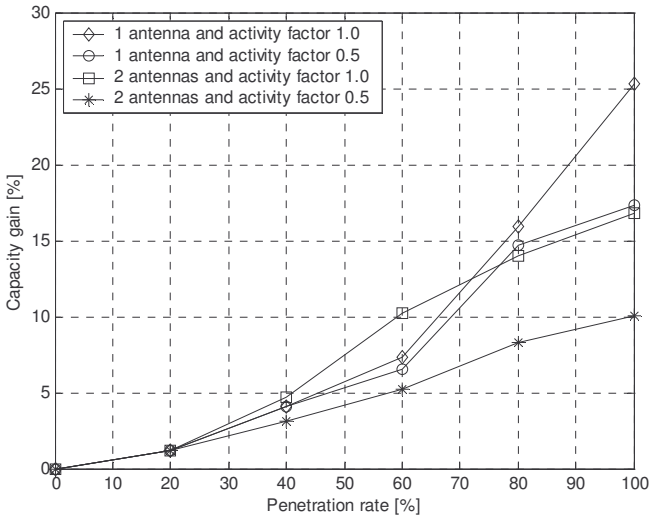

Figure 4.9. Capacity gain versus the penetration rate of synchronous UEs from simulations of a multi cell environment with SHO (DPDCHs with SF 64).

4.5.5 Capacity Gain Based on the Outage Probability

The NR is a good measurement of the load in the uplink of WCDMA systems, because it shows the amount of interference received at the BS for all the UEs. In general, the NR does not vary linearly with the number of UEs per cell, and therefore a NR target value is normally selected so that the stability is maintained with a certain margin of security. However, in synchronous uplink the potential NR increase due to the addition of new UEs is lower than in the asynchronous case, and the stability of the system is therefore higher for the same NR target. For instance, in an ideal case without other cell interference (i=0) and perfect orthogonality between UEs (α=1) the NR increases linearly with the number of UEs, and the unstable situation would never appear. An effective NR that considers this effect is presented in Appendix D as a practical measurement of the load in uplink synchronous WCDMA systems. In this subsection the outage probability is defined as an alternative reference measurement to calculate the real potential capacity gain with uplink synchronous WCDMA; this means that the NR level is no longer considered for the comparisons. The outage probability gives the probability that a UE is unsatisfied. In this study we define it as the probability that a UE experiences an average BLER greater than 1% along the speech call time. Let us further define the system capacity as the traffic throughput with a maximum outage probability of 5%.

The simulation results presented in this subsection are obtained by considering a fixed number of UEs in the network during the simulation time, with AC and outer-loop PC turned off. The values of the parameters are the same as in Table 4.2, except for those listed in Table

Parameter		**Value**
Cell Plan	Number of receiver antennas per cell	2
UE	Maximum transmitted power	21 dBm
	Eb/No target	7.0 dB

Table 4.5. Particular simulation parameters to obtain capacity results based on the outage probability.

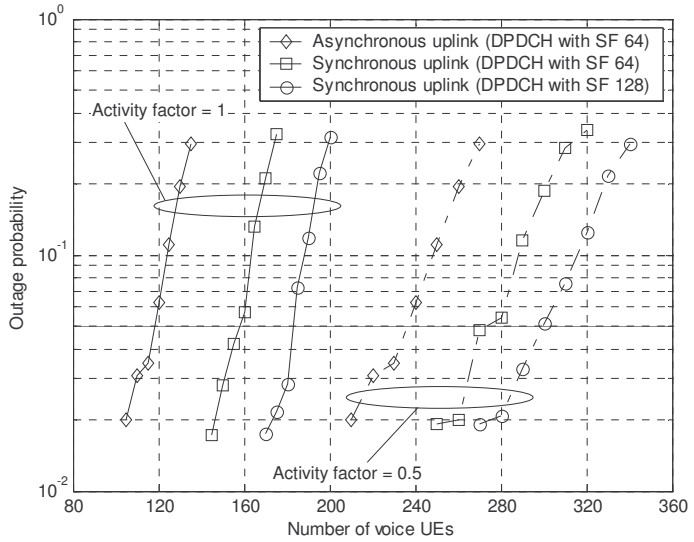

Figure 4.10. Outage probability as a function of average number of voice UEs per cell from simulations of a single cell environment.

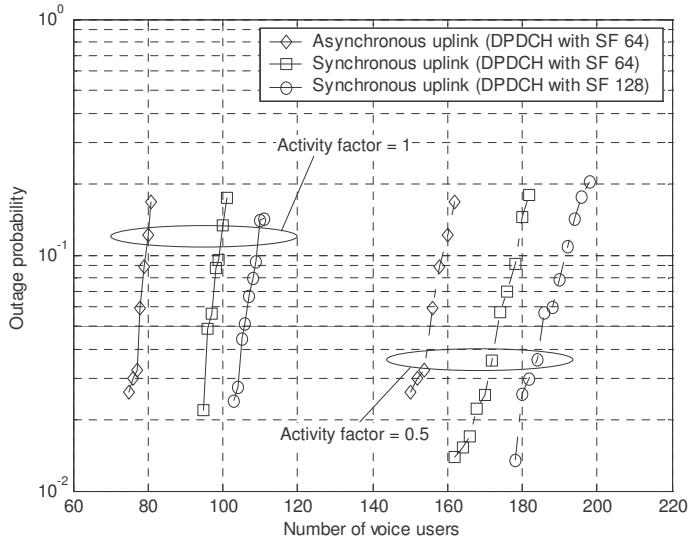

Figure 4.11. Outage probability as a function of average number of voice UEs per cell from simulations of a multi cell environment.

4.5.

For single cell environments (i.e. no other cell interference and no SHO) the simulations have again been run with an omni antenna. The results are shown in Figure 4.10. The results for the multi cell case with SHO are depicted in Figure 4.11. Both cases of DPDCHs with SF 64 and SF 128 are considered; the average number of UEs per cell and the capacity gain for a 5% outage probability are presented in Figure 4.12 and Figure 4.13.

In the single cell case the unique factors that limit the capacity gain are the orthogonality factor and the maximum number of available channelisation codes. Nevertheless, the number

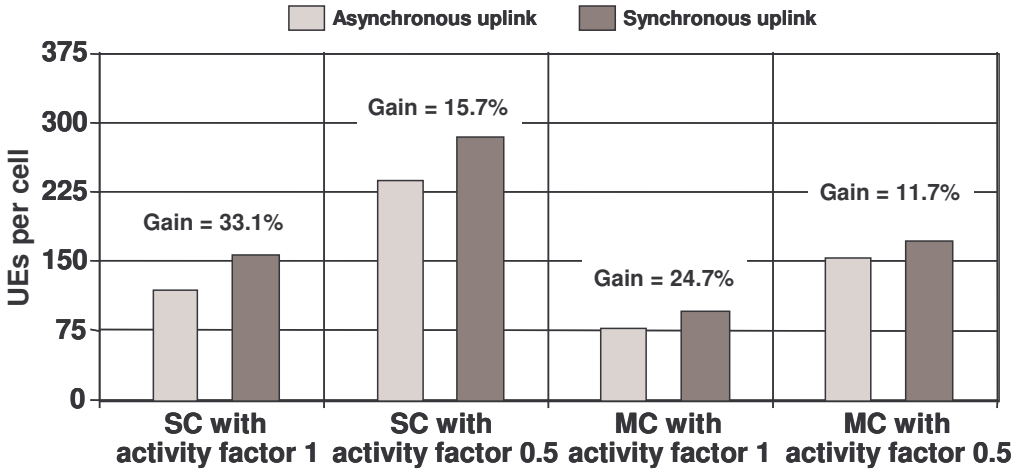

Figure 4.12. Average number of UEs per cell from simulations for a 5% outage probability (DPDCHs with SF 64).

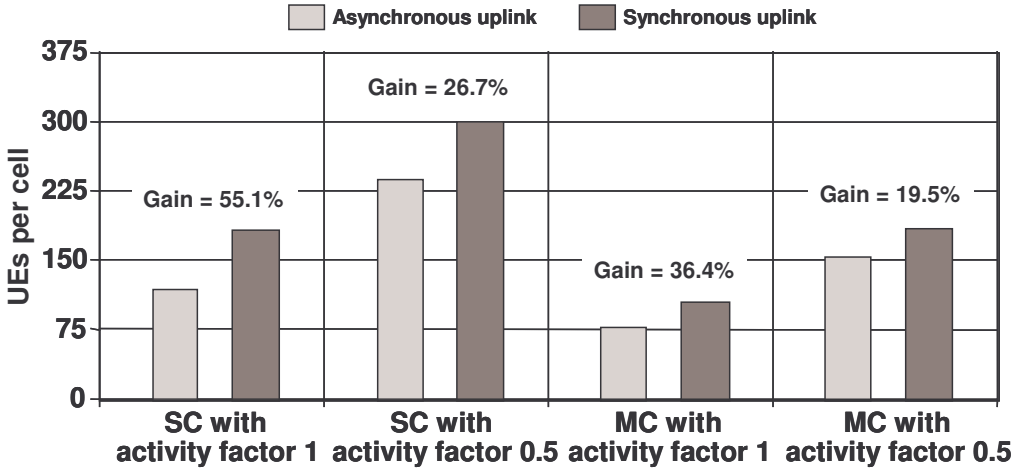

Figure 4.13. Average number of UEs per cell from simulations for a 5% outage probability (DPDCHs with SF 128 for synchronous UEs and SF 64 for asynchronous UEs).

of UEs per cell is so high that the effect of the orthogonality factor is eclipsed by the limit of codes for this particular case. Notice that up to six different scrambling codes are necessary in the case of SF 64 and a voice activity factor of 0.5. As the channelisation code restriction represents the main limit for the capacity gain of uplink synchronisation, the benefit of using a DPDCH with SF 128 instead of SF 64 is therefore greater in this case; e.g. in the case of an activity factor of 0.5, the capacity gain is 26.7% with SF 128 and 15.7% with SF 64.

The same idea applies to the multi cell case, where the number of required codes is so high that the reduction of the code utilisation per UE (with a DPDCH of SF 128) raises the capacity gain of the synchronous uplink by more than 10%.

It should be remarked that the same outage probability does not imply the same the NR level at BS, since quite different values are obtained for all the cases. For instance, for an activity factor of 1.0, the average NR is approximately 12.8 dB with asynchronous uplink, and 13.8 dB with synchronous uplink with SF 128 for the DPDCH. Anyway, these values reveal that the system is in a fairly loaded situation.

4.6 Concluding Remarks and Discussion

The performance of uplink synchronous WCDMA has been assessed in terms of the capacity gain relative to an equivalent asynchronous system in scenarios with low time dispersion. The capacity gain is evaluated theoretically and by means of dynamic system level simulations. The simulation results in the case where SHO is not considered are in agreement with the theoretical predictions. The maximum number of available channelisation codes turns out to be a major restriction for the capacity gain of an uplink synchronous WCDMA system, since the signals received from UEs allocated to different scrambling codes are non-orthogonal. Under the most realistic conditions, with a NR target of 4 dB (60% of the pole capacity), the capacity gain of an uplink synchronous WCDMA equals 9.6%, whereas in an ideal case without channelisation code restrictions, the capacity gain is 35.8%. If the capacity is calculated based on a 5% UE outage probability, the gain of uplink synchronous WCDMA raises to 19.5% when using DPDCHs with SF 128.

The use of dual antenna reception at the BS, SHO, and voice activity detection is found to decrease the capacity gain of an uplink synchronous WCDMA system, since the channelisation code limits are reached earlier when these capacity enhancing techniques are deployed. However, provided that the problems associated with the channelisation code shortage can be mitigated (e.g. by the use of higher order modulation), uplink synchronous WCDMA has been demonstrated to provide a significant potential capacity gain.

However, it should be noticed that uplink synchronisation in WCDMA requires changes of the current 3GPP specifications [24], and hence it may take years before a high penetration of USTS capable UEs is reached. This reduces the potential gain of USTS in the short term.

Chapter 5

Uplink Synchronous WCDMA Combined with Variable Modulation and Coding

5.1 Introduction

In Chapter 4, the performance of uplink synchronous WCDMA has been demonstrated to provide a potential capacity gain in the cases where there are no channelisation code restrictions. However, this seems to be one of the major challenges to unleash the full performance potential of synchronised uplink in WCDMA. An immediate solution to solve this problem is to allow the BSs to assign multiple scrambling codes in order to increase the number of available code resources per cell, as each scrambling code is associated with a channelisation code tree. However, since signals transmitted under different scrambling codes are non-orthogonal, the practical applicability of this approach is limited.

In this chapter, an alternative solution is proposed to increase the capacity in the uplink of a synchronised WCDMA system by introducing variable modulation and coding (VMC). A scheme where the user equipments (UE) are allowed to change their modulation and coding scheme (MCS) during the transmission has already been proposed in 3GPP for High Speed Downlink Packet Access (HSDPA) in the downlink [53]. A higher order modulation would support transmitting with a higher spreading factor (SF) while keeping the same throughput. To some extent, a similar effect could be obtained by increasing the effective channel-coding rate. Both features can be combined as shown in this chapter. The use of a higher SF while

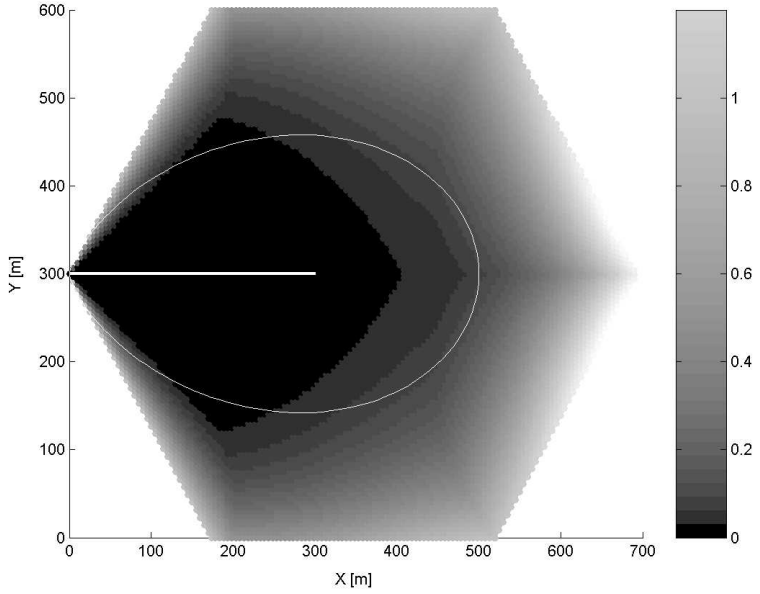

Figure 5.1. Effective other-to-own cell interference ratio per UE assuming pedestrian model for path loss with distance [43] and an antenna radiation pattern with a 3 dB beam width of 72 degrees.

keeping the same throughput has the benefit of decreasing the channelisation code consumption and thereby improve the capacity of uplink synchronous WCDMA. However, this is obtained at the expense of an increase in the required energy-per-bit to noise ratio (Eb/No) to achieve a certain block error rate (BLER). As proposed in this chapter, this problem can be minimised if the UEs experiencing a higher propagation attenuation are obliged to transmit with lower order modulation and coding rate, as a higher required Eb/No for these UEs is translated into a much higher inter cell interference in the system. Figure 5.1 shows the effective other-to-own cell interference ratio per UE, defined as the ratio of the power received at the closest neighbouring base station (BS) to power received at the serving BS. This parameter gives an idea of the user contribution to the total other-to-own cell interference ratio. As no fading is considered, the areas far from the BS correspond to higher values of the effective other-to-own cell interference ratio.

UEs with lower radio propagation attenuation would therefore be allowed to transmit with higher order modulation and coding rate, which, in spite of requiring a higher signal-to-interference ratio (SIR), provide a greater throughput.

The use of higher coding rate to decrease the channelisation code consumption has preliminarily been assessed in Chapter 4, where it has been shown to increase the capacity of uplink synchronous WCDMA in the cases where this method allows reduction of the number of active scrambling codes per cell.

New radio resource management (RRM) algorithms are required in order to employ a synchronous WCDMA scheme combined with VMC, which is described in this chapter.

The chapter is organised as follows: Section 5.2 describes the basics behind VMC to reduce the channelisation code utilisation. In Section 5.3, a theoretical analysis of the capacity gain of uplink synchronous WCDMA combined with VMC is presented. The model for simulations and the required RRM algorithms are described in Section 5.4. Both theoretical and simulation results are presented and discussed in Section 5.5. Concluding remarks are

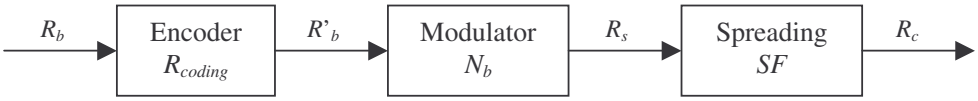

Figure 5.2. Physical layer transmission in WCDMA.

summarised in Section 5.6.

5.2 Higher Order Modulation and Coding Rate

This section describes how VMC can be used to improve the channelisation code utilisation, taking the particular case of UMTS Terrestrial Radio Access (UTRA) Frequency Division Duplex (FDD) mode as a reference. The benefits and drawbacks derived from the use of VMC are also addressed.

5.2.1 Structure of the Transmitter

As depicted in Figure 5.2, the information arriving at the physical layer of a WCDMA transmitter with a bit rate R_b goes through several blocks, which modify the data rate. First, redundant information is added with an effective coding rate R_{coding}; then, the modulator converts every N_b bits into one symbol. Finally, the signal is applied a spreading factor SF, acquiring the chip rate R_c

$$R_c = R_b \frac{SF}{N_b \cdot R_{coding}} = R_b \cdot G, \tag{5.1}$$

where G is the processing gain.

In the uplink of the UTRA FDD mode [7], the information associated with every single physical channel is Turbo encoded with a rate 1/3 or convolutional encoded with a rate 1/2 or 1/3 [54]. Puncturing or repetition is used for rate matching. Figure 5.3 shows the block diagram of the uplink transmitter after channel coding for one Dedicated Physical Data Channel (DPDCH) and one Dedicated Physical Control Channel (DPCCH) according to 3GPP [9]. The signals are multiplied by the channelisation code (c_d for data and c_c for control) and weighted by gain factors (β_d for DPDCH and β_c for DPCCH). The information from these channels is then BPSK modulated. The channels from the same UE are I-Q combined and multiplied by the complex scrambling sequence s_n in order to obtain a signal envelope similar to QPSK transmissions [7].

An example of an alternative scheme using higher order modulation is proposed in Figure 5.4, where the signal associated with the DPDCH is QPSK-modulated before applying the channelisation code. The signal associated with the DPDCH is multiplied by a channelisation code $\hat{c}_d$ with double SF compared to c_d. Both schemes in Figure 5.3 and Figure 5.4 provide the same bit rate $R_{b,d}$ for the DPDCH and $R_{b,c}$ for the DPCCH, but the one in Figure 5.4 uses half of the channelisation code resources for the DPDCH. Hence, a higher order modulation than BPSK (e.g. QPSK or 8PSK) can support either transmitting with a higher bit rate for the same SF or keeping the same bit rate with a reduced channelisation code consumption. The

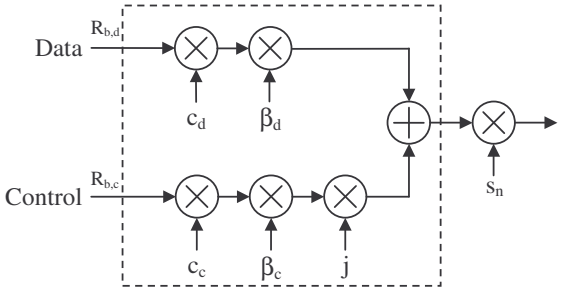

Figure 5.3. Transmission of data through one DPDCH and one DPCCH according to 3GPP.

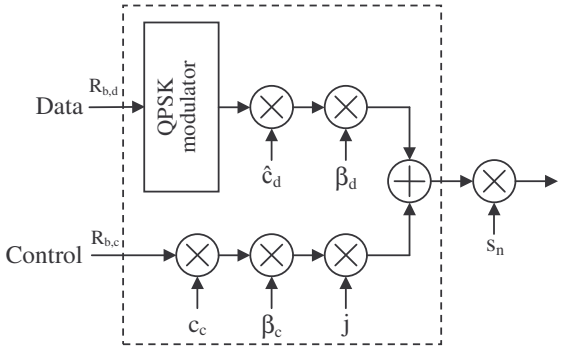

Figure 5.4. Equivalent scheme to the one in Figure 5.3 with higher order modulation.

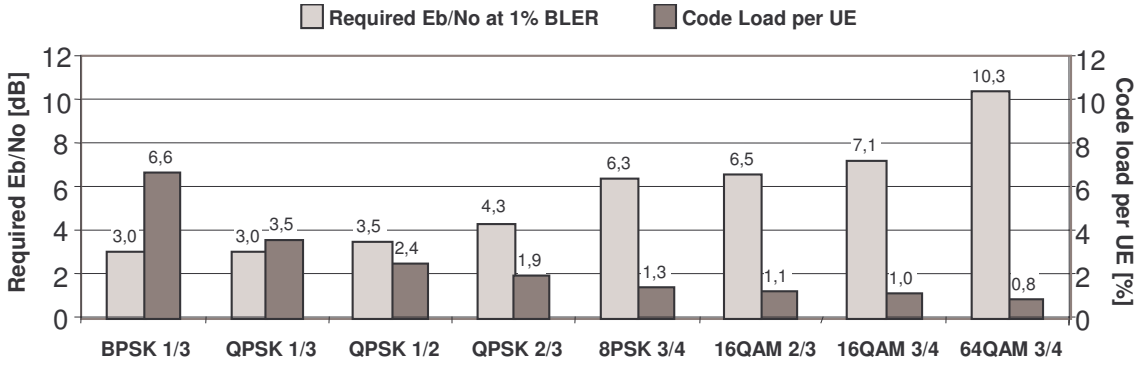

Figure 5.5. Required Eb/No versus channelisation code load for circuit-switched service at 64 kbps with a DPDCH and a DPCCH per UE in a Pedestrian A environment with a speed of 3 km/h.

same effect is obtained by increasing the channel coding rate.

Notice that Figure 5.4 is equivalent to using two I-Q combined DPDCHs with half the bit rate and the same channelisation code $\hat{c}_d$. This is already considered in [9] for the transmission of more than one DPDCH per UE, but in that case parallel DPDCHs are only allowed with a SF of 4.

5.2.2 Code Efficiency versus Required Energy per Link

Although the use of higher order modulation and/or higher coding rate results in a more efficient use of the channelisation code tree, the UEs will require a higher Eb/No for the same BLER, except for the case of going from BPSK to QPSK. In uplink synchronous WCDMA, higher order MCSs will therefore be employed only when the benefit of using just one scrambling code compensates for the extra energy required for the transmission. For DPDCHs with different MCSs, Figure 5.5 offers a comparison of the required Eb/No for 1% BLER with the code load (CL) per UE, defined as the allocated proportion of the channelisation code tree. The required Eb/No values are obtained from link level simulations for a circuit-switched service at 64 kbps in Pedestrian A environment, assuming a UE speed of 3 km/h, channel estimation based on the received pilot symbols and interference modelled as additive white Gaussian noise (AWGN). Further details on how these results were obtained are given in Appendix B. The code load is calculated assuming one DPDCH and one DPCCH per UE

as

$$CL = \frac{1}{SF_{data}} + \frac{1}{SF_{control}}, \tag{5.2}$$

where SF_{data} is the required SF associated with the DPDCH, and $SF_{control}$=256 is the SF for the DPCCH.

If QPSK is used instead of BPSK with the same coding rate for the DPDCH, there is no increment in the required Eb/No, while the code utilisation associated with the DPDCH is reduced by half. For the rest of the cases, increasing the coding rate gives a reduction of the CL at the expense of a higher required Eb/No.

5.2.3 Peak to Average Ratio

Using higher order modulation schemes for the DPDCH instead of BPSK causes a variation in the peak-to-average ratio (PAR) of the signal transmitted by the UEs in the uplink. The PAR of the signal is an important parameter that has to be taken into consideration, as it limits the maximum average power that can be transmitted by the UE in order not to reach the non-linear part of the transmit amplifier. A study on how to calculate the PAR associated with different transmit configurations is presented in Appendix C.

In the cases where sufficient bit rate can be achieved by using a single DPDCH with BPSK, the code efficiency obtained with QPSK comes at the cost of a PAR increase of 0.7 dB. This is expected to be of less concern in micro-cell environments, which is what the uplink synchronous WCDMA is intended for. As the UEs are designed to provide enough transmit power to fulfil the requirements for link budgets also in macro-cells, this leaves an even higher margin for micro-cell environments.

5.2.4 Link Budget Cost of Higher Order MCSs

The use of higher order MCSs has an impact on the link budgets. On one hand, a higher order MCS requires higher Eb/No, i.e. assuming a constant interference level the user must increase the power by the same amount as the required Eb/No. On the other hand, higher order modulations also present a higher PAR compared to BPSK, which limits the maximum power that the user is allowed to transmit. Table 5.1 presents the reduction of the allowed propagation loss for a cell range due to the use of higher order MCSs, considering the effect of both the higher required Eb/No and the PAR increase at 0.1% outage. Notice that, except for the case of QPSK with coding rate 1/3, in the rest of cases the cell range is significantly reduced compared to using BPSK with a coding rate 1/3. This is due to the fact that for the

MCS	Reduction of the allowed propagation loss
BPSK 1/3	0 dB
QPSK 1/3	0.7 dB
QPSK 1/2	4.0 dB
QPSK 2/3	4.8 dB
8PSK 3/4	6.6 dB

Table 5.1. Reduction of the allowed propagation loss for a cell range due to higher order MCSs with respect to BPSK with a coding rate 1/3, considering the required Eb/No at 1% BLER and the PAR increase at 0.1% outage; circuit-switched service at 64 kbps is assumed with 1 DPDCH and 1 DPCCH per UE over a Pedestrian A channel at 3 km/h.

same data rate, in such cases a higher spreading factor is used for the DPDCH. Hence, the power ratio of the DPDCH to the DPCCH is smaller, which makes the PAR higher.

5.3 Theoretical Analysis

5.3.1 System Model and Assumptions

A similar analysis as in Section 4.3 is presented to calculate the theoretical capacity gain of the synchronous WCDMA with VMC. The BSs can serve synchronous UEs with K possible MCSs. Every cell contains N^k_{sync} synchronous UEs with MCS #k. Additionally N_{async} asynchronous UEs are served per cell. For simplicity, all the UEs are assumed to transmit at the same bit rate; UEs with the same MCSs require the same Eb/No. Only one scrambling code is considered per cell. Ideal power control (PC) is assumed, so that the UEs always reach the required Eb/No. Soft handover (SHO) is not considered.

5.3.2 Calculation of the Power Level at the BS

The Eb/No reached by a UE in asynchronous mode can be approximated as in (4.3)

$$\rho_{async} = G\frac{P_{async}}{P_{total}}, \tag{5.3}$$

where G is the processing gain (defined as the ratio between the chip rate and the effective user bit rate), P_{async} is the power received at the BS from every UE in asynchronous mode, and P_{total} is the total power received at the BS.

Similarly, the Eb/No for UEs in synchronous mode with MCS #k can be written as

$$\rho^k_{sync} = G\frac{P^k_{sync}}{P_{total} - \left(P_{own} - N_{async}P_{async}\right)\alpha} \tag{5.4}$$

where P^k_{sync} is the power received at the BS from a UE served in synchronous mode with MCS #k, P_{own} is the power received at the BS from its own UEs, and $\alpha \in [0,1]$ is the orthogonality factor [42]. The total power received at the BS can be expressed as

$$P_{total} = P_{noise} + P_{own}\left(i+1\right), \tag{5.5}$$

where i is the other-to-own cell interference ratio and P_{noise} is the background noise power at the BS. The value of P_{async} and P^k_{sync} can be calculated from (5.3) and (5.4)

$$P_{async} = \frac{\rho_{async}P_{total}}{G}, \tag{5.6}$$

$$P^k_{sync} = \frac{\rho^k_{sync}}{G}\left(P_{total} - P_{own}\alpha + N_{async}P_{async}\alpha\right). \tag{5.7}$$

The own cell power at the BS is calculated as

$$P_{own} = N_{async}P_{async} + \sum_{k=1}^{K} N^k_{sync}P^k_{sync}. \tag{5.8}$$

Substituting (5.6) and (5.7) in (5.8) yields

$$P_{own} = \frac{P_{total}}{G}\left(\frac{GN_{async}\rho_{async} + (G + N_{async}\rho_{async}\alpha)\sum_{k=1}^{K}\left(N_{sync}^{k}\rho_{sync}^{k}\right)}{G + \alpha\sum_{k=1}^{K}\left(N_{sync}^{k}\rho_{sync}^{k}\right)}\right). \quad (5.9)$$

The noise rise at the BS can be expressed as

$$NR = \frac{P_{total}}{P_{noise}} = \left[1 - \frac{P_{own}}{P_{total}}(1+i)\right]^{-1} =$$
$$= \left[1 - \frac{1+i}{G}\left(\frac{GN_{async}\rho_{async} + (G + N_{async}\rho_{async}\alpha)\sum_{k=1}^{K}\left(N_{sync}^{k}\rho_{sync}^{k}\right)}{G + \alpha\sum_{k=1}^{K}\left(N_{sync}^{k}\rho_{sync}^{k}\right)}\right)\right]^{-1}. \quad (5.10)$$

5.3.3 Optimum Selection of Modulation and Coding Schemes

The capacity gain of uplink synchronous WCDMA with VMC depends on the criterion to assign MCSs to the UEs. This study considers two different approaches to reach an optimum selection of the MCSs so that the noise rise (NR) at the BS is minimised, assuming that all the UEs are capable of operating with uplink synchronous WCDMA and VMC:

- In the first one, multiple scrambling codes are allowed per BS, but all the UEs are assumed to adopt the same MCS. The performance of this approach can be theoretically evaluated by using the expression in (4.10).
- The second one consists of selecting the optimum combination of MCSs for the own cell UEs, but assuming that only one scrambling code is available at the BS. The theoretical performance of this approach is evaluated by obtaining the optimum values of the number of UEs using every MCS that minimise the NR, i.e.

$$\left\{\hat{N}_{sync}^{1}, \hat{N}_{sync}^{2}, ..., \hat{N}_{sync}^{K}\right\} = \min_{\left\{N_{sync}^{1}, N_{sync}^{2}, ..., N_{sync}^{K}\right\}} NR \text{ provided that } \sum_{k=1}^{K}\hat{N}_{sync}^{k} = N, \quad (5.11)$$

  where N is the total number of synchronous UEs in the cell, and NR is the noise rise calculated as in (5.10). The optimal parameters in (5.11) will be obtained by calculating the value of NR for all the possible combinations of $\{N^{1}_{sync}, N^{2}_{sync}, \ldots, N^{K}_{sync}\}$ with the MCSs included in Figure 5.5.

The NR is plotted in Figure 5.6 versus the number of synchronous UEs per cell for different MCSs by considering the first approach, i.e. assuming that all the UEs use the same MCS. The required Eb/No and the CL per UE are obtained by using the values shown in Figure 5.5 for circuit-switched service with a data rate of 64 kbps in a Pedestrian A channel at 3 km/h; the rest of parameters are taken from Table 5.2. In this case the maximum capacity gain with uplink synchronous WCDMA and VMC is obtained by finding the common MCS for all the UEs in the cell that minimises the NR. In Figure 5.6 the optimum selection for every load situation is plotted in bold. Notice that there are some MCSs which never turn out to be the optimum ones. This happens for modulations with higher order than QPSK, which are therefore not worth using because the loss from the required Eb/No increase is much higher than the gain obtained from the CL decrease.

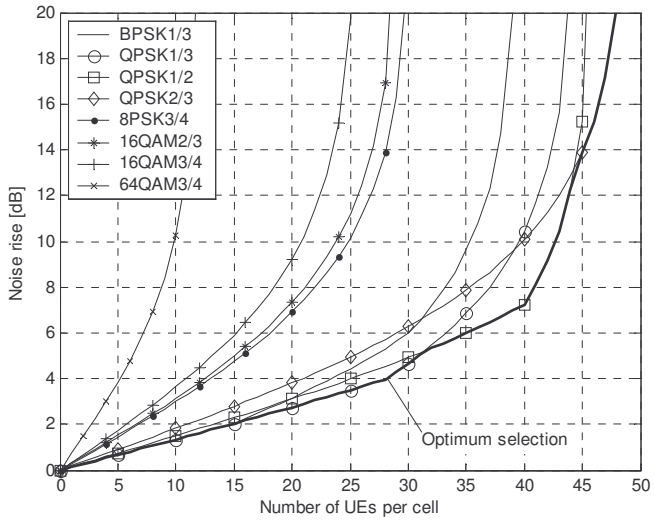

Figure 5.6. Noise rise versus number of UEs per cell with uplink synchronisation assuming the same MCS for all the UEs and multiple scrambling codes.

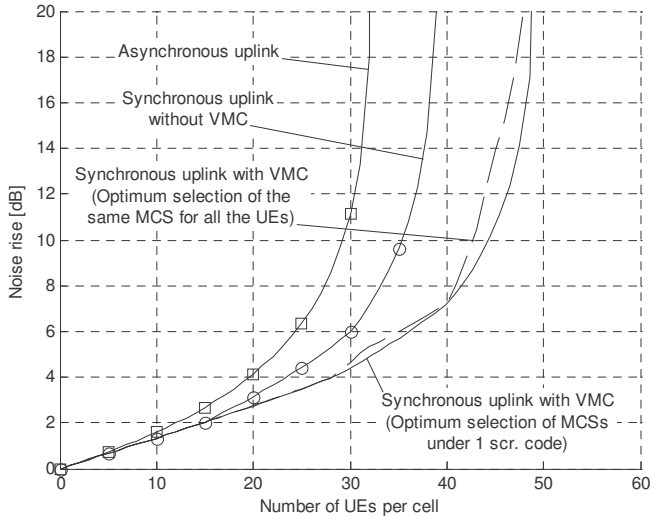

Figure 5.7. Noise rise versus number of UEs per cell with asynchronous uplink, synchronous uplink without VMC, and synchronous uplink with VMC.

It should be mentioned that the impact of a higher required Eb/No strongly depends on the other-to-own cell interference ratio and the orthogonality factor; e.g. in an ideal single cell case (i=0) with perfect orthogonality (α=1), the NR grows linearly when increasing the number of UEs per cell and there are no unstable states, even when increasing the required Eb/No due to higher order MCSs, as long as only one scrambling code is used.

Figure 5.7 compares the NR obtained with asynchronous uplink, synchronous uplink without VMC, and synchronous uplink with VMC (assuming optimum selection of a common MCS for all the UEs). It also includes the NR assuming the second approach, i.e. the optimum combination of MCSs for the UEs that minimises the NR at the BS under one scrambling

Parameter	Value
α	0.94
i	0.85
Number of receiver antennas	2 (The required Eb/No per antenna is 3 dB lower)
MCS for UEs without VMC	BPSK, 1/3

Table 5.2. Parameters for theoretical calculations in a Pedestrian A micro-cell environment (α is obtained as in Chapter 4; i is the average value from the simulation results in Chapter 4 without SHO).

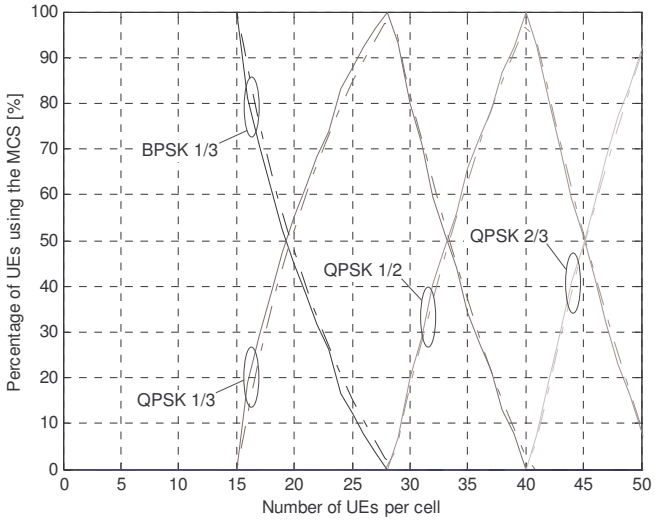

Figure 5.8. Theoretical optimum utilisation of different MCSs under the assumption of one available scrambling code per cell.

code (there is not a common MCS for all the UEs). The results are based on the same parameters as for Figure 5.6. Note that this approach gives a slightly better performance than the first one (using the same MCS for all the UEs).

Figure 5.8 plots the optimum percentage of UEs per MCSs that minimises the NR at the BS assuming one scrambling code per BS. The solid line corresponds to the method described above where all the possible combinations are considered. For instance, in a cell with 25 UEs, the NR is minimised if approximately 12% of the UEs use BSPK with a coding rate 1/3, and 88% of them use QPSK with a coding rate 1/3. The optimum case for a cell with 45 UEs corresponds to 50% UEs using QPSK with a coding rate 1/2 and 50% using QPSK with a coding rate 2/3. The dashed line is an approximation of the optimum case and is the result of assuming that only two MCSs, number n and n+1 (with the same sequence as in Figure 5.5), can be used simultaneously. An additional assumption made is that the CL is always fixed to one (i.e. the scrambling code is fully utilised). This is done by reallocating the necessary number of UEs from one to another MCS. This method is much simpler and reduces the complexity of the RRM algorithm required to select the MCS for every UE. As the results are almost identical to the optimum one, this approximation will be used in the sequel when referring to the theoretical optimum selection of MCSs.

Notice that the optimum values shown in Figure 5.8 are calculated under the assumption of an invariant other-to-own cell interference ratio with respect to allocation of the different MCSs.

5.4 System Model for Dynamic Simulations

Although the theoretical analysis provides a good description to understand the potential capacity gain with uplink synchronous WCDMA and VMC, dynamic system level simulations have been carried out to validate the results and also include the effect of dynamic algorithms for RRM.

5.4.1 System Model

The system model and assumptions for the dynamic system level simulator are the same as in Section 4.4. However, new advanced RRM algorithms are implemented in order to consider the possibility of UEs working with VMC as well as to improve the performance of uplink synchronisation with VMC. The new algorithms are described in Section 5.4.2.

Cases with all the UEs in asynchronous mode, all of them in synchronous mode without VMC, and all of them in synchronous mode with VMC are compared.

The parameters employed for the simulations are summarised in Table 5.3.

5.4.2 Radio Resource Management

5.4.2.1 Admission Control

The admission control (AC) decisions are made based on the measured received power at the serving BS [7] averaged over 100 ms. UEs are admitted in the system if

$$P_{rx} + \Delta P_{rx}^{est} < P_{target}, \tag{5.12}$$

where P_{rx} is the received power at the serving BS before the admission of the new UE, $\Delta P^{est}{}_{rx}$ is an estimate of the increase in the received power at the serving BS caused by the admission of the new UE, and P_{target} is a threshold set during the network planning phase. The calculation of $\Delta P^{est}{}_{rx}$ is done based on the expression derived in Appendix F.

5.4.2.2 Resource Manager

The resource manager (RM) is responsible for keeping the number of active scrambling codes as low as possible. The RM algorithm runs on a cell basis. Initially, UEs are allocated channelisation codes from the same scrambling code so that additional scrambling codes are not used until the first one is completely occupied. When more than one scrambling code are active in the cell, it is likely that some channelisation code resources from a full scrambling code are released, due to handovers or ended calls. When this happens, the RM performs a reallocation of the assigned codes, and UEs from the latest activated scrambling code are moved to the scrambling code with channelisation codes released. UEs with the highest CL that fits in the released gap are moved first. This operation is illustrated in Figure 5.9, and allows keeping the number of active scrambling codes per BS as low as possible.

For simulations with VMC, the RM also decides what MCS the UEs should use in order to minimise the number of active scrambling codes. The RM decides to increase the MCS

Parameter		Value
System	Chip rate	3.84 Mcps
Cell Plan	Number of cells	24
	Number of cells per site	3
	Site-to-site distance	1040 m
	Number of receiver antennas per cell	2
	Noise level per receiver antenna	-102.9 dBm
Propagation	Path loss with distance *d*[km]	147.7+40log *d* dB
	Standard deviation for shadow fading	10 dB
	Coherence distance for shadow fading	50 m
	Multi-path model	Pedestrian A
	Receiver antenna gain	16 dBi
SHO	Window add / drop / replace	2 dB / 4 dB / 2 dB
	Time out to drop BS	0.02 s
	Maximum active set size	2
AC	Period between admissions	20 ms
	NR target	4 dB
	Planned orthogonality factor for PIE	0.94
	Weight parameter for PIE	0.5
PC	Fast closed-loop PC step size	1 dB
	Frequency of outer-loop PC updates	10 ms
	Outer-loop PC step size (up)	0.3 dB
	FER target for outer-loop PC	1 %
RM	Period between RM actions	10 ms
	VMC updates per RM period	1
	CL target	93%
UE	Service	Circuit-switched
	Effective bit rate	64.0 kbps
	Speed	3.0 km/h
	Maximum transmission power by UE	24 dBm
	Available MCSs if supporting VMC	BPSK1/3, QPSK1/3, QPSK1/2, QPSK 2/3
	Default MCS if not supporting VMC	BPSK1/3
Simulation time		120 s

Table 5.3. Summary of the main simulation parameters.

number of one of the UEs in the cell if the CL for the first active scrambling code exceeds the CL target value set during the network planning phase. In the case considered for the simulations all the UEs transmit with the same bit rate, and the UE selected to use a higher order MCS that reduces the CL is the one with minimum transmission power; the UE transmission power is assumed to be known at the BS. With this criterion, the NR increase at the neighbouring BSs due to a higher required Eb/No is minimised.

No more than two MCSs are allowed to be active simultaneously for the same scrambling code, so if the UE with minimum transmission power has already changed its MCS, it cannot do it again until the rest of UEs have done so. This MCS allocation policy is in accordance with the theoretical optimum selection described in Figure 5.8. The theoretical calculations have shown that this simple algorithm behaves very close to the optimum one.

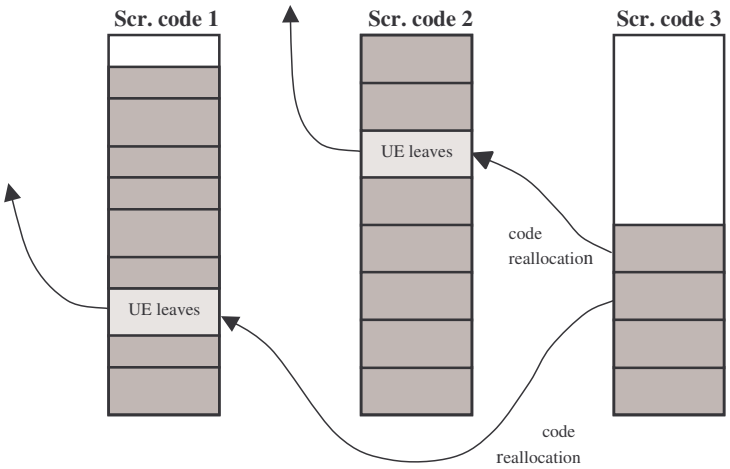

Figure 5.9. Channelisation code allocation.

5.5 Results

5.5.1 Results Based on the Noise Rise Level

The average NR versus the average number of UEs per cell from simulations without SHO are compared in Figure 5.10 with the theoretical calculations based on the values shown in Figure 5.5 and Table 5.2. Note that the simulation results match the expected values from the theoretical calculation.

The numbers of UEs per cell for a NR target of 4 dB obtained from simulation results and theoretical calculations are presented in Table 5.4. Simulation results show that in the case without SHO, uplink synchronisation with VMC provides approximately 20% extra capacity gain than uplink synchronisation without VMC, compared to the asynchronous case. With SHO the absolute capacity is higher in general, but the relative capacity gain of uplink synchronisation is lower, since UEs in SHO cannot maintain the synchronism with more than one cell simultaneously. The higher the absolute capacity is (and therefore the channelisation code utilisation), the larger the capacity gain of uplink synchronisation when combined with VMC. However, this is only true when the benefit of not using a second scrambling code compensates for the extra required energy for higher order MCSs. If additional scrambling codes are required, the gain of VMC does not increase with the absolute capacity. This is observed in Figure 5.11, where the capacity gain of uplink synchronous WCDMA is plotted as a function of the NR target. Since the NR grows slower in a synchronous scheme (see Figure 5.10), the capacity gain of uplink synchronisation (with and without VMC) increases with the NR target. The slope of the capacity gain curve starts reducing when additional

Case	Asynchronous	Synchronous without VMC	Synchronous with VMC
Simulations with SHO	24.8	28.0 (12.9% gain)	32.0 (29.0% gain)
Simulations without SHO	22.1	26.5 (19.9% gain)	30.9 (39.8% gain)
Theoretical without SHO	19.6	23.8 (21.8% gain)	28.1 (43.8% gain)

Table 5.4. Number of UEs per cell and capacity gain with uplink synchronisation.

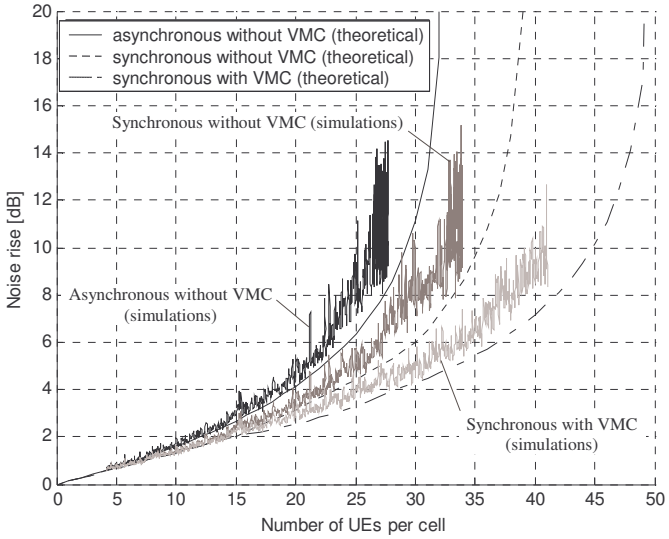

Figure 5.10. Noise rise versus average number of UEs per cell when SHO is disabled.

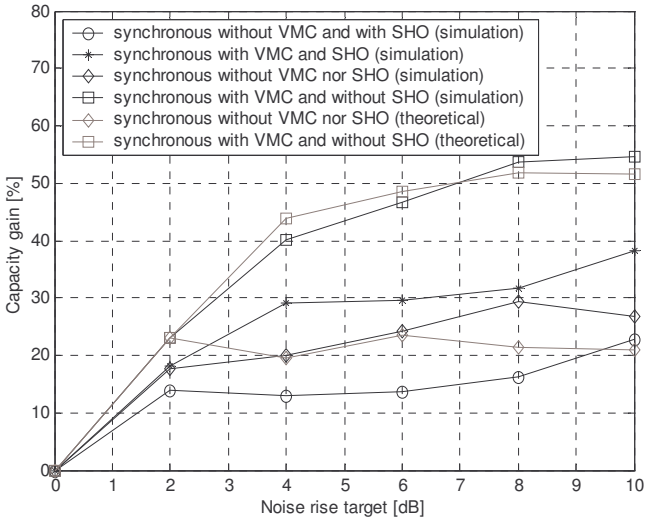

Figure 5.11. Capacity gain in terms of cell throughput as a function of the noise rise target.

scrambling codes have to be used. This occurs for higher values of the NR target when using VMC.

The percentage of MCS utilisation from the simulation results is depicted in Figure 5.12 as a function of the average number of UEs per cell. The results are similar to those in Figure 5.8, but the ones from the simulations include a big variance as they have been obtained by averaging the values corresponding to all the cells in the network. However, the tendency is similar to Figure 5.12, where once the first scrambling code in the cell is full with the first MCS, the UEs are gradually moved to the second MCS, and they are not moved to the third MCS while there are UEs still using the first one.

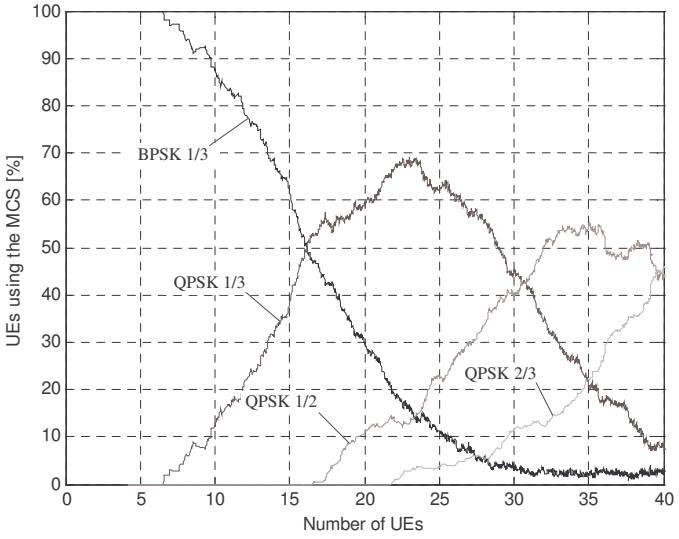

Figure 5.12. Average MCS utilisation as a function of the average number of UEs per cell from simulations without SHO.

5.5.2 Results Based on the Effective Noise Rise

In this subsection the effective NR is employed as a reference load measurement to calculate the theoretical capacity gain provided by uplink synchronous WCDMA combined with VMC. The effective NR is presented in Appendix D as a fairer load measurement when considering uplink synchronisation, as it gives information on the system stability by taking into account the orthogonality degree among the signals from the UEs. However, as stated in Appendix D, in the case of uplink synchronous WCDMA this information is only reliable when all the UEs transmit in synchronous mode.

Appendix D presents an overestimate of the effective NR for the case where all the UEs support synchronous mode and assuming that all the scrambling codes in the same cell generate the same interference power at the BS. With this assumption, the effective NR can be estimated by using the expression in (D.8)

$$NR^{eff,est} = NR\left(1-\frac{\alpha}{(1+i)J_{active}}\right)+\frac{\alpha}{(1+i)J_{active}}. \tag{5.13}$$

where NR is the noise rise at the BS, α is the orthogonality factor, i is the other-to-own cell interference factor and J_{active} is the number of active scrambling codes in the BS that are currently assigned to UEs.

Figure 5.13 presents the theoretical effective NR based on the expression in (5.13) compared to the results based on the NR with the same situation as in Figure 5.7. Let us recall that in the asynchronous case the effective NR equals the NR. Notice how the capacity gain at 4 dB effective NR target significantly increases when this new measurement is deployed. The capacity gain of uplink synchronisation without VMC grows from 21.8% to 34.5% when taking the effective NR as a reference instead of the NR. Correspondingly, the capacity gain grows from 43.8% to 86.5% in the case of synchronous WCDMA with VMC assuming optimum selection of MCSs for the UEs.

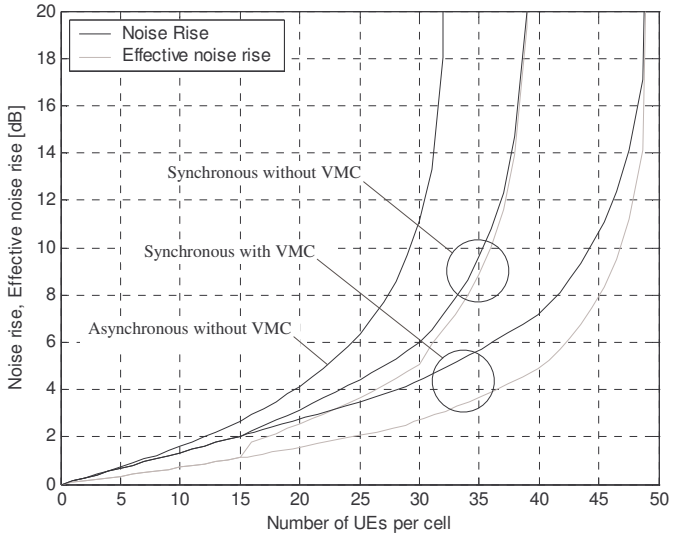

Figure 5.13. Theoretical NR and effective NR for synchronous and asynchronous WCDMA with and without VMC.

5.6 Conclusions

Variable modulation and coding rate has been presented as a complementary scheme for uplink synchronous WCDMA to decrease the channelisation code utilisation per UE. As it was demonstrated in Chapter 4, the channelisation code utilisation represented the main bottleneck in order to reach a high capacity gain with synchronous uplink.

The capacity gain of uplink synchronous WCDMA combined with VMC has been evaluated theoretically and with an extensive set of dynamic system level simulations in micro-cell environments with a low time-dispersion channel and a UE velocity of 3 km/h, showing a high capacity gain.

The outcome of the dynamic simulations matches quite well the results from the theoretical analysis. Simulation results for circuit-switched service at 64 kpbs with SHO and a NR target of 4 dB yield 12.9% higher throughput for uplink synchronisation without VMC, and 29.0% with VMC. In order to reach such a capacity gain, RRM algorithms for optimum selection of MCSs and channelisation code reallocation of the UEs are required. The necessary RRM algorithms to deploy this technology have been presented.

Further, the effective NR presented in Appendix D has been used as a reference measurement to evaluate the uplink capacity. The main advantage is that this new parameter gives a better idea of the uplink stability level of the BS when all the UEs are synchronised. However, as mentioned in Appendix D, it is an average measurement that does not consider the degree of instability that may be caused by asynchronous UEs; i.e. the effective NR is only feasible under full synchronous UE penetration conditions. For an effective NR target of 4 dB, the theoretical capacity gain of uplink synchronous WCDMA combined with VMC equals 86.5% when SHO is deactivated.

As mentioned in Chapter 1, M-branch receive antenna diversity [18], [19], or/and multi-user

detection (MUD) at the BS [22], [21], [23] are alternative methods to improve the uplink capacity in WCDMA systems. The latter uplink capacity enhancing techniques do not require changes in the UEs, i.e. no legacy UE problems. Thus, despite of the potential gain of uplink synchronisation, implementation of Uplink Synchronous Transmission Scheme (USTS) in WCDMA at this stage should be considered carefully.

Chapter 6

Capacity Enhancing Strategies Based on Fast Packet Scheduling

6.1 Introduction

The packet scheduler (PS) is responsible for the management of the available resources for non-real time (NRT) services. Packet data services are suitable for interactive and background traffic classes, since they do not require any strictly guaranteed data rates and delays. However, they can also be utilised for streaming class, which, in spite of requiring a minimum guaranteed bit rate, tolerates some delay [7].

In the downlink the transmission is started from a common entity, the base station (BS), whereas in the uplink it is distributed among the users. This complicates the PS algorithm in the uplink, as it is more complicated to control the received power from all the users, unlike the downlink, where the BS controls the transmitted power. Furthermore, the BS does not have instantaneous information about the amount of data to transmit. The information required by the BS about the state of the data buffer in the user equipments (UE) adds additional scheduling load to the system [55].

So far, most of the previous research on packet scheduling has focused on the downlink due to the nature of the traffic. However, there is a potential increase in the uplink traffic related to high data rate reverse control channels associated with the downlink or the growth of other services such as ftp or image/data upload. As a consequence some research has been done on the subject of the uplink packet scheduling.

In [56] the problem of uplink packet scheduling is addressed, describing the desired properties

for a PS algorithm; the proposals are mainly intended for common channels. One of the desired properties is that the PS assigns resources on demand in order to maximise the multiplexing gain. This approach is considered in [29], [31] for WCDMA systems. The proposed algorithms are run centralised at the Radio Network Controller (RNC). In [29] it is concluded that a potential capacity improvement exists when using faster scheduling; however, this requires moving the PS from the RNC to the Node B.

The RNC-controlled scheduling brings long delays associated with the Radio Resource Control (RRC) signalling between the RNC and the UE, i.e. network layer (L3) signalling. This makes it a hard task to rapidly reallocate data rates depending on the instantaneous requirements of the UEs. If the PS decisions are taken in the Node B and the signalling between the Node B and the UEs is made at physical layer (L1), the delay can be considerably reduced. The use of distributed (i.e. Node B located) scheduling requires changes in the location of the algorithm according to Figure 1.5; i.e. the PS would have to be moved from the RNC to the Node B.

The first investigations towards a distributed uplink packet access were initiated by the 3GPP2, i.e. intended for cdma2000 systems. Two different packet control mechanism concepts are currently being discussed for cdma2000: A dynamic variable control rate where the base transceiver station (BTS[2]) sends an "up" or a "down" command to the UEs to either increase or decrease its data rate by one step is compared to a purely scheduled control system based on time division multiplexing (TDM) [57], [58], [59], [60]. Scheduling algorithms can better track the channel variations, but they are more sensitive to an imperfect knowledge of the channel in terms of the propagation loss. In [60] a scheme where the radio resource management (RRM) is shared between the base station controller (BSC[3]) and the BTS is considered. The results show that this hybrid scheme outperforms the corresponding centralised and distributed PS algorithms. However, this is done under the assumption of a short scheduling period even for the centralised scheduling (30 ms).

Further, several scheduling policies based on TDM for the uplink of cdma2000 are evaluated in [61] in terms of the average queue length. The main findings from this study is that it is more advantageous on the uplink to schedule users with a strong received power at the BS one-at-a-time, and users with weak receive power in larger groups. However, the results are obtained for a single cell scenario with power control (PC) disabled. In [55] a high capacity gain is shown for a hybrid CDMA/TDMA system compared to a pure CDMA system in a dual-class multi cell scenario. No fluctuations in the other cell interference are considered.

In this chapter, several strategies are proposed to perform PS over dedicated channels (DCH) at the Node B for WCDMA systems. The performance of the different algorithms is evaluated by means of system level simulations in terms of cell throughput, compared to a reference RNC PS. A Node B PS based on blind data rate detection (BRD) is evaluated, which does not require any explicit signalling from the UE with information about its buffer occupancy. A Node B PS algorithm based on TDM is also proposed, which exploits the different instantaneous channel quality experienced by the users. Multi-user diversity allows increasing the cell throughput by reducing the other cell interference.

Another promising candidate feature to enhance the uplink capacity for packet access in WCDMA systems is the use of Hybrid ARQ (HARQ). Node B controlled HARQ with fast L1 retransmissions of erroneously received data units reduces the number of link layer (L2) retransmissions and the associated delays. Furthermore, with low retransmission delays, the

[2] The term BTS is equivalent to Node B within 3GPP2.
[3] The term BSC is equivalent to RNC within 3GPP2.

UEs can afford operating at higher block error probability. Although HARQ has already been demonstrated to provide gain in capacity and cell range for the downlink case [62], [63], [64], [65], [66], only a few investigations consider HARQ for the uplink case; see e.g. cdma2000 [58], [59], [60]. The performance of L1 HARQ is further assessed in this study by means of both theoretical calculations and system level simulations. The combination of HARQ with a fast PS algorithm is finally considered, including the use of uplink synchronisation.

The chapter is structured as follows. The reference RNC packet scheduler is described in 6.2. The HARQ scheme is presented in Section 6.3, as well as a theoretical analysis to calculate the capacity gain with such a scheme. Section 6.4 describes a Node B scheduling concept based on BRD. In Section 6.5, a Node B scheduling concept based on TDM is described. The use of uplink synchronisation for packet services to increase the system capacity is discussed in Section 6.6. Section 6.7 describes the system model and the parameters employed for the simulations. The results are presented and discussed in Section 6.8. The conclusions are given in Section 6.9.

6.2 RNC Packet Scheduler

This section summarises the basics of the reference PS implemented in the system level simulator to facilitate the use of packet services over DCHs. The PS is meant to operate in the context of 3GPP/Release 99, which means that it is located at the RNC. The algorithm is proposed in [29]. During the connection establishment, a Transport Format Combination Set (TFCS) is initially allocated to the UEs. The PS algorithm modifies the allocated TFCS based on the traffic volume measurements (TVM) reported by the UEs to the RNC, and the interference level at the BS. In the TVM message the UE reports its Radio Link Control (RLC) buffer payload, among other relevant information [67]. The TFCS allocation requires a relatively large amount of signalling over the Iub interface. This should be considered when selecting the minimum period between two consecutive TFCS modifications for the same UE.

6.2.1 Packet Data Access in the RNC PS

The procedure associated with the allocation and selection of the TFCs is summarised in Figure 6.1. The UE sends TVM reports to the PS in the RNC when the buffer size exceeds a threshold obtained from the network. In our implementation the event is interpreted at the PS as a capacity request. All the UEs are assumed to have a minimum allocated bit rate, which applies if no other allocation has been made by the PS. Moreover, this minimum allocated bit rate is kept even when the UE does not transmit any data.

The outcome of the scheduling process is the maximum Transport Format Combination (TFC) that the UE is allowed to use in the following scheduling period. The TFCS can be simplified to a set of allocated data rates. A TFCS allocation corresponds to the allocation of an index pointing at the maximum allowed data rate. All the data rates below the allocated one can also be selected at the UE side.

A TFC elimination algorithm [32], [34], [68] is implemented in order to set the maximum TFC the UE is able to use without reaching transmission power limitations. The algorithm basically consists of eliminating the TFCs (data rates) that require higher transmission power than the maximum at the terminal. This prevents the UEs from using data rates that cannot be correctly received due to coverage limitations. A TFC is eliminated when it is estimated to run into a coverage limitation for “X” slots within a window that includes the last “Y” slots.

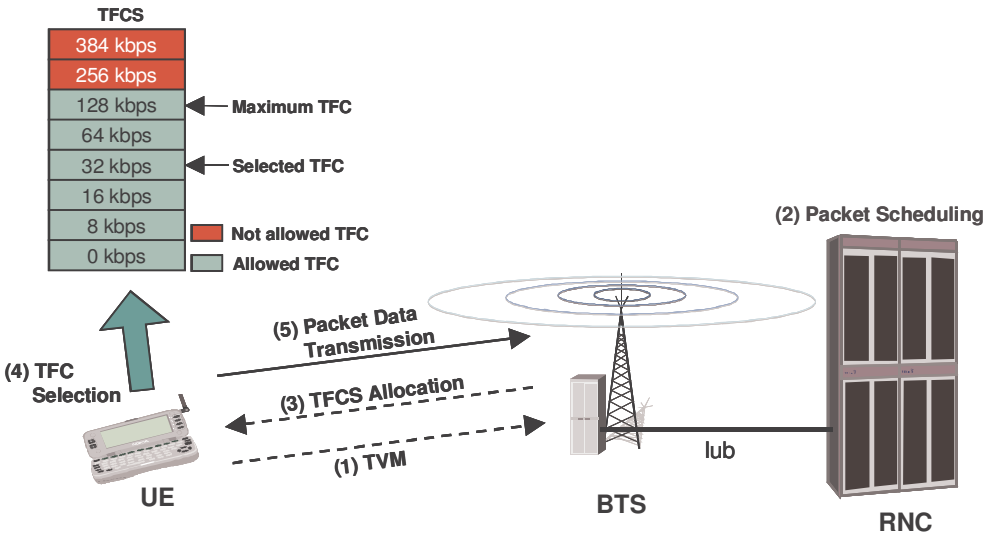

Figure 6.1. Packet data access in the RNC PS based on TVMs.

This estimation is performed by rescaling the current transmission power according to the data rates associated with every TFC. An eliminated TFC can be recovered when the estimated required transmission power for such a TFC does not exceed the maximum value during "Z" consecutive slots.

Notice that in Figure 6.1, the maximum TFC is calculated as the minimum value between the TFC allocated by the RNC and the maximum allowed by the TFC elimination algorithm.

6.2.2 Packet Scheduling Algorithm Based on TVMs

The PS algorithm performs both upgrading and downgrading of the data rate allocated to the users. Upgrading is performed based on the capacity requests made by the users, whereas the downgrading actions are carried out based on inactivity detection. The inactivity is detected at the Node B by monitoring the received data rate. The data rate downgrading takes place before the capacity request process associated with the data rate upgrading.

The flow chart in Figure 6.2 gives a general overview of the part of the RNC PS algorithm in charge of the data rate upgrading. The capacity request processing is a recursive procedure where, at each scheduling period, the process in Figure 6.2 is executed a number of times. The table at the top of Figure 6.2 shows a list where each row represents a TVM. The PS processes the requests in ascending order based on the currently allocated data rate (TFC_{TEMP} column), i.e. the requests from UEs with the currently lowest allocated data rates are served first. The algorithm performs the scheduling according to a fair resource policy. The algorithm to process the capacity request consists of the following:

- At every iteration, the PS estimates the increase in the total received power at the Node B caused by moving the UE with the currently lowest allocated data rate to the next higher data rate.
- If the estimated power does not exceed the target value P_{target}, then the request is accepted and reinserted in the queue with the information on the new allocation, still keeping the ordering criterion. Notice that the P_{target} corresponds to the noise rise value NR_{target} considered in previous chapters for admission control (AC).

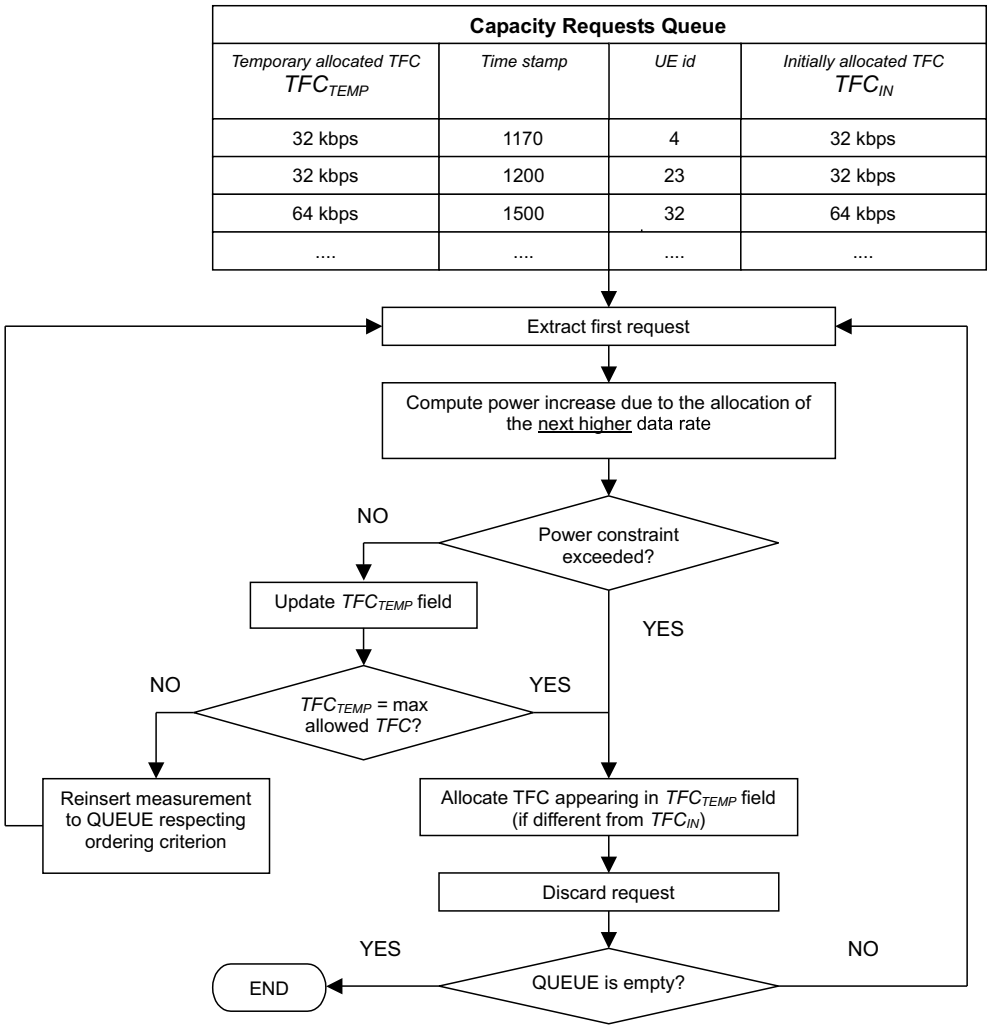

Figure 6.2. Capacity request processing in the RNC PS based on TVMs.

- The process is then repeated until eventually either the estimated power exceeds the target value or all the requests are fulfilled, i.e. all the UEs issuing a capacity request are allocated the maximum data rate.
- Once the process is over the allocations are signalled to the UEs and subsequently applied. In a real implementation the RNC applies a random delay to the allocation signal for every user, in order to avoid overloading the Iub interface. In this study all the allocations are assumed to be known at all the UEs simultaneously once the TFC modification period has elapsed.

A TVM report remains in the scheduling queue for subsequent scheduling instants, unless the maximum data rate has been allocated to the UE issuing the request, or the TVM report has been in the queue for longer than the time set by the *Queuing timer* parameter. In this sense the *Queuing timer* can be interpreted as the maximum lifetime of a TVM report in the RNC queue. While a TVM report is in the queue the UE issuing the corresponding request is not allowed to send a new report. Nevertheless, as soon as the TVM report is deleted from the queue the corresponding UE is free to send another request. In general, the UE will send a TVM report only if the following three conditions are fulfilled:

- the buffer content exceeds the preset threshold value (4 kbytes),
- the UE is currently allocated less than the maximum possible data rate, and
- there is currently no request being processed for that particular UE.

In the reference RNC PS, the data rate downgrading is performed based on an inactivity timer. Whenever data packets have not been received from a particular UE for longer than the time set by the *Inactivity timer* parameter, the PS reduces the UE allocated data rate to the minimum allowed. This somehow simulates the switching to RACH/FACH mode [69].

It should be mentioned that in real implementations, when the UE switches to RACH/FACH mode, the allocated DCH is released, and no data rate is guaranteed for this UE. In our implementation no DCH establishment/release procedures are simulated, and the UEs are always assumed to keep a minimum allocated data rate.

Load control (LC) is executed if the total received power at the BS exceeds the target value by an amount corresponding to the LC offset, i.e. if the total noise rise (NR) exceeds the threshold value NR_{TH}, and the BS operates in the overload area, as depicted in Figure 2.2. The LC functionality performs data rate downgrades according to the proceeding of Figure 6.2, but starting from those UEs with the highest allocated data rate. LC actions are terminated when the estimated received power is below P_{target}, and the BS is predicted to operate in the feasible load area again.

6.3 HARQ Controlled by the Node B

This section presents a fast HARQ mechanism controlled by the Node B. A distinction is made between HARQ Type I (without soft combining) and HARQ Type II/III (with soft combining) schemes [62], [70]. In the Type III, every retransmission is self-decodable, whereas in general this is not the case with the Type II. In this study no distinction is made between HARQ Type II and Type III, and the same link level performance is assumed for both.

When using HARQ, there is an optimal block error rate (BLER) operating point where the system capacity becomes maximal, both in the case of Type I and Type II/III. In [71] it is shown that with a fast Node B controlled protocol, the BLER target can be increased from 1% to approximately 10-20% without any significant degradation in the average delay performance. However, operating with an excessive high error probability can drastically deteriorate the packet delay and throughput performance despite of the fast Node B controlled retransmission mechanism.

Although the system capacity gain with Type I and Type II/III HARQ schemes is presented in Section 6.8 based on system level simulation results, a simple theoretical analysis is presented in the current section.

In this study, the retransmission delays due to either L1 or L2 ACK/NACK signalling are neglected, and no distinction is made between the case in which the entity handling the retransmission protocol is placed at the RNC or at the Node B. The focus will therefore be on the system throughput more than on the users' delay performance.

6.3.1 Theoretical Analysis

Let us define the cell throughput for this study as

$$C = (1 - BLER)\sum_{k=1}^{N_{UEs}} R_{b,k}, \tag{6.1}$$

where *BLER* is the ratio of the total number of correctly received blocks to the total number of sent blocks, N_{UEs} is the number of UEs in the cell, and $R_{b,k}$ is the bit rate associated with UE #*k*. Notice that the term (1-*BLER*) gives the proportion of correctly received data.

Let us now assume a system where all the UEs require the same energy-per-bit to noise ratio (Eb/No) target ρ and the same data rate R_b. By keeping the system assumptions made in Section 4.3, the cell throughput in (6.1) can be calculated by using the expression (4.5), (4.7) and (4.8) with $N_{async}=N_{UEs}$ and $N^j_{sync}=0\ \forall j$

$$C = (1 - BLER)(1 - NR^{-1})\frac{R_c}{\rho(1+i)}. \tag{6.2}$$

In (6.2), R_c is the chip rate, *i* is the other-to-own cell interference ratio and *NR* is the noise rise at the BS. Note that this expression is obtained by including the desired signals as part of the rest of the interference.

In the case of Type I HARQ, the block error rate value *BLER* corresponds to the target value $BLER_{target}$ associated with ρ. In the case of Type II/III HARQ, *BLER* decreases as the number of retransmission increases, due to the soft combining. For Type II/III HARQ the *BLER* value to calculate the cell capacity with the expression in (6.2) can be obtained as

$$BLER = \frac{\sum_{n=1}^{N}\prod_{m=1}^{n} BLEP_m}{1+\sum_{n=1}^{N-1}\prod_{m=1}^{n} BLEP_m}, \tag{6.3}$$

where *N* is the maximum number of L1 transmissions for which soft information can be accumulated at the receiving entity, and $BLEP_n$ is the block error probability associated with the *n*-th transmission. The value of $BLEP_n$ is calculated from AVI tables that map the Eb/No into the BLER, considering the cumulated Eb/No from the previous transmissions

$$BLEP_n = f\left(Eb/No_{cum,n}\right), \tag{6.4}$$

where *f* is a function that takes one Eb/No value as an input and gives the resulting BLER value as output based on the AVI tables, and $Eb/No_{cum,n}$ is the cumulated Eb/No after *n* transmissions, calculated as

$$Eb/No_{cum,n} = \begin{cases} f^{-1}\left(BLER_{target}\right) & \text{if } n = 1 \\ \dfrac{Eb/No_{cum,n-1} + f^{-1}\left(BLER_{target}\right)}{L_{comb}} & \text{if } n > 1. \end{cases} \tag{6.5}$$

L_{comb} is set to 1.05 (0.2 dB) [63], and is a combining loss which is added every time the received Eb/No is summed to the cumulated one[4], and f^{-1} is the inverse function of *f*. Hence, the Eb/No for every single transmission is also calculated from the AVI tables, assuming the same BLER value $BLER_{target}$ for all of them.

[4] This value is associated with the data channel, whereas the AVI tables employed in this study include the effect of both the control and the data channel; see Appendix H for considerations on the influence of the control channel.

6.4 Node B Packet Scheduler Based on BRD

According to the Release 99 of the 3GPP specifications, the scheduling decisions at the RNC are taken based on TVM reports, which are sent by the UEs either periodically or event-triggered [67]. These reports are exchanged between the UE and the network through RRC signalling. Hence, a fast Node B based scheduling algorithm cannot use the information contained in these reports, as they are only available at the RNC.

The first approach considered in this chapter to perform PS at the Node B is based on BRD [71]. Node B observes the instantaneous data rate selected by each active UE at every transmission time interval (TTI) of 10 ms, and compares it to the maximum data rate that the UE is allowed to use. This information is then used at the next scheduling periods to reallocate the available resources according to the users' actual needs. In this study, each Node B is assumed to be in complete control of the allocation of the TFCS to the UEs.

The Node B scheduling algorithm is defined based on the resource utilisation factor (RUF). The RUF gives the number of the last consecutive transmissions with either selected data rate equal to zero (in this case the RUF has a negative value) or selected data rate corresponding to the maximum allocated TFC (the RUF has a positive value). Notice that the UE can select data rates within a range from zero to the maximum allocated data rate. The Node B takes the data rate information from the uplink Transport Format Combination Indicator (TFCI) field, transmitted every TTI on the Dedicated Physical Control Channel (DPCCH). The RUF is updated at TTI basis. The pseudo-code for the calculation of the value of RUF at TTI #t (RUF_t) is

```
if (data rate == 0 kbps)
{
      if (RUF_{t-1} < 0)    RUF_t = RUF_{t-1} − 1;
         else   RUF_t = −1;
}
else   if (data rate == max. allocated data rate at Node B)
{
      if (RUF_{t-1} > 0)   RUF_t = RUF_{t-1} + 1;
         else   RUF_t = 1;
}
else   RUF_t = 0;
```

A minimum allocated data rate is always guaranteed. This is necessary since the scheduling is performed based on the users' activity information. Otherwise, the PS could not distinguish the inactivity state from the case where the UE has data in the buffer but it cannot transmit because a minimum data rate has not been allocated.

The Node B PS based on BRD divides the active UEs into three groups, depending on whether the maximum data rate must be decreased, increased or kept the same. Figure 6.3 illustrates the decision regions for data rate allocation based on the different possible values of the RUF. The decision rules for the considered algorithm are defined as follows:

DOWN UEs without any activity during the averaging period of the received power measurement do not contribute to the power measured at the Node B. Therefore they are considered as part of the NRT inactive traffic. In order to

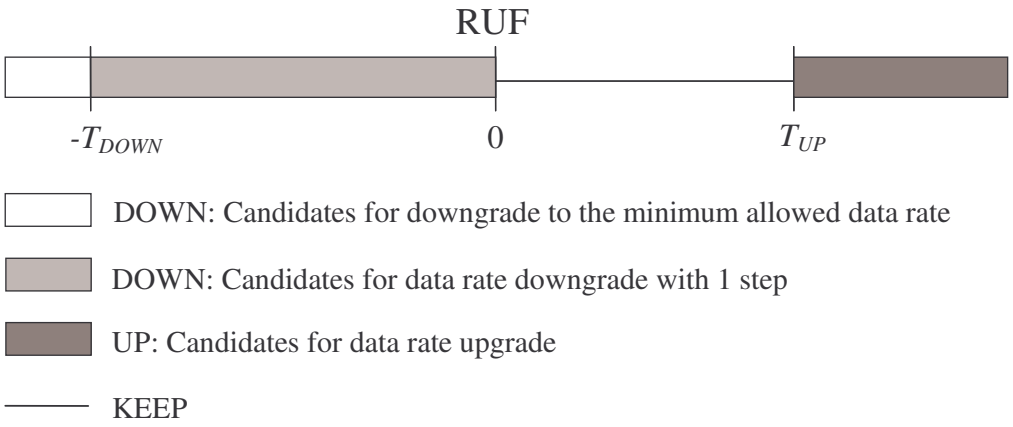

Figure 6.3. Decision regions for data rate allocation based on the value of the RUF.

reduce the data rate allocated to these users, a UE is downgraded to the minimum allowed value when $RUF \leq -T_{DOWN}$, where T_{DOWN} is set accordingly with the averaging period for the received power. Moreover, in order not to allocate higher data rates than the ones the UE require, UEs with $-T_{DOWN} < RUF \leq 0$ are downgraded by using a downgrading step of one, i.e. the TFC is decreased to the next lower value. A non-positive value of the RUF is an indication that the UE is not using the maximum allocated data rate.

UP A UE is selected as a candidate for data rate upgrade if $RUF \geq T_{UP}$. In the upgrading procedure, the UEs can be upgraded up to the maximum possible data rate, provided that the estimated received power does not exceed P_{target}, and keeping the priority established in the capacity request queue. As for the RNC PS case, a higher priority is given to those UEs to which lower data rates are allocated.

KEEP No actions are taken for this class of UEs (except under overload conditions).

The task sequence performed by the Node B PS based on BRD is similar as for the PS based on TVMs. First, the downgrading actions are carried out. Then, the candidate UEs are upgraded following the same procedure as in Figure 6.2 and keeping a priority sequence based on the momentary allocated data rate and the RUF parameter. The LC algorithm is performed exactly as in the RNC based case.

For the UEs operating in soft handover (SHO) mode the scheduling algorithm performed at the Node B does not have information on the data rate allocated by the rest of the Node Bs in the active set. This information would have to be transferred through the RNC, with all the associated delays. In the solution included in our simulations, when a UE is in SHO every BS performs the allocation as if it was the only one in the active set. If for a certain UE, the BSs in the active set allocate different data rates, then the UE must select the minimum of them. Another possible option is to select the maximum of them, or allow only one of the BSs in the active set to perform PS for these UEs. However, in such cases there might be BSs in the active set receiving with higher data rates than the ones actually allocated. Hence, these BSs would not be under control of part of their intra cell interference.

In Section 6.8 simulation results are presented to compare the performance of the Node B PS based on BRD to the RNC PS based on TVMs presented in Section 6.2.

6.5 Node B Packet Scheduler Based on TDM

The other approach proposed in this chapter to perform packet scheduling at the Node B is to combine the code allocation with a time division scheme, where only a subset of the UEs is allocated data rates at every TTI of 2 ms. The time division concept for packet scheduling is already employed for the downlink of WCDMA in High Speed Downlink Packet Access (HSDPA) [6], although in such a scheme only one user is allocated at a time.

6.5.1 Implications of the Use of a Time Division Based PS

With this scheme, it is possible to allocate very high data rates during short periods, which can potentially increase the system capacity [72].

With a fast allocation mechanism based on instantaneous buffer occupancy information it is possible to keep the resource utilisation closer to the planned target, i.e. the users will transmit at data rates close to the allocated ones. This improvement in the radio resource utilisation reduces the variance of the NR at the BS, which results in a higher capacity and therefore a better spectral efficiency. A similar effect is obtained with the multi cell AC approach presented in Chapter 2; by using information from the neighbouring cells the received interference at the BSs gets more stable, and more users can be added in the system without reaching an overload state.

Furthermore, a TDM approach is able to exploit the differences in the instantaneous channel quality among the users. If the allocation decisions are based on the channel conditions, the time division scheduling can potentially reduce the interference generated to other cells and introduce some multi-user diversity gain, by scheduling the UEs with better channel conditions at a time.

The disadvantage from deploying a PS based on TDM is the necessity of achieving uplink synchronisation, so that at every scheduling period the Node B only receives the signals from the scheduled UEs.

One option is to synchronise the downlink frames for UEs served by the same Node B, and then use the time of arrival in the downlink to set the uplink frame timing. This would anyway require some guard time, as the lack of synchronism due to the different RTPDs of the UEs in the cell implies some capacity loss. When two UEs are not completely synchronised they may use the same code simultaneously for a certain instant. The required guard time can be set by considering the round trip propagation delay (RTPD) for a UE in the cell border. For a macro-cell with maximum distance from the UE to the Node B of 1 km, the misalignment error is smaller than 0.33% relative to a 2 ms TTI, and for a micro-cell with a maximum distance of 300 m smaller than 0.1%.

The deployment of Node B PS based on TDM would be more attractive if it is jointly deployed with the uplink synchronisation concept investigated in Chapters 3 to 5 to achieve uplink orthogonality. Although uplink orthogonality requires a higher synchronisation degree than a time division PS, the combined capacity gain resulting from deploying both schemes may compensate for the necessary changes to reach uplink synchronisation.

In this study the required synchronisation to perform PS based on TDM is assumed, although the current 3GPP specifications do not consider such a possibility yet.

The fast allocation of a low number of simultaneous UEs at a time introduces fast variations in the other cell interference, and deteriorates the performance of the fast PC. Furthermore, the UEs transmit in a discontinuous basis, which obliges them to continuously adjust the transmission power. This problem has previously been addressed in [55]. The associated changes in the transmission power to allow the fast increases/decreases of high data rates cannot be carried out with a high accuracy. The influence of this inaccuracy can be reduced with the use of HARQ.

In this study, the Node B is assumed to receive instantaneous information on whether the buffers of the UEs are empty or not. This requires a minor increase in the signalling from the UE to the Node B, which has not been considered. A constant delay is assumed when applying the allocated data rate at the UE, which is supposed to cover processing delays at both the Node B and the UE, and the delay in actually signalling the allocation to the UE. The associated downlink signalling is assumed to be operational, but the implications for the downlink are not considered in this study.

The PS algorithm based on TDM can be summarised as follows.

- At each TTI the PS estimates the reduction in the total received power at the BS from setting all the current data rate allocations to 0 kbps. The estimation is made by using the power decrease estimator (PDE) in Appendix G.
- Afterwards, the scheduler constructs a queue including all the active users with non-empty buffer. The queue is then ordered according to a scheduling policy.
- By keeping the sequence established in the queue, the PS tries to allocate the maximum data rate to the UEs provided that the estimated received power does not exceed the target value. If it succeeds, it continues with the next UE in the queue. If according to the power increase estimator (PIE) no available power is left, then lower data rates are allocated.
- The procedure finalises when either all the UEs in the queue have been scheduled or no more power is available for new allocations.

In order to support SHO, only the serving BS is allowed to perform scheduling decisions associated with a certain UE. In our implementation, from all the BSs in the active set, the serving BS is considered to be the one with the lowest average radio propagation attenuation to the UE, calculated based on the pilot measurement. The ideal option would be to coordinate all the BSs in the active set of a UE in SHO to schedule it at the same time. However, this is not possible with a distributed PS mechanism. On the other hand, if several BSs were allowed to independently perform the scheduling for the UEs in SHO, then the effective scheduling period would be reduced for these users.

6.5.2 Allocation Strategies

Three different allocation strategies are defined to set the UE sequence for data allocation: round-robin fair throughput (RRFT), proportional fair throughput (PFT) and maximised transmit power efficiency (MTPE).

- **Round-Robin Fair Throughput Scheduler**

  The UEs are scheduled by keeping a sequence order according to a round-robin approach. Hence, this scheduling strategy is not channel-dependent.

- **Maximised Transmit Power Efficiency Scheduler**

  In this case, the PS allocates resources to the UEs with the best channel conditions. In order to evaluate the channel quality of the link between the UEs and the BS, the Node B utilises the uplink channel quality information (UCQI) at every TTI. The UCQI at a TTI #*n* for UE #*k* is defined as

$$UCQI_k[n] = \frac{R_k[n]}{P_k[n]} = \frac{SIR_k[n]}{P_k[n]} \cdot \frac{R_c}{\rho}, \tag{6.6}$$

  where $R_k[n]$ and $P_k[n]$ are the data rate and the power transmitted by UE #*k* at TTI #*n*, respectively, $SIR_k[n]$ is the signal to total wideband interference ratio, R_c is the chip rate and, ρ is the required Eb/No. While the user is not scheduled the data rate and the power are obtained from the associated DPCCH. All these parameters are available at the Node B, except the instantaneous power transmitted by the UE. This information can be signalled from the UE to the UMTS Terrestrial Radio Access Network (UTRAN) [36]. The Node B could in principle update this information with the power control commands, although this cannot be done during SHO.

  With this scheduling policy, the resource allocation allows reducing the other cell interference, which is normally degraded by UEs under bad channel conditions. However, this algorithm does not provide fairness among the active UEs. It can be considered as the uplink version of the Max C/I PS method for HSDPA [6], [73].

- **Proportional Fair Throughput Scheduler**

  This scheduling strategy provides fair throughput in the sense that the same throughput is allocated to all the UEs on average. However, it also considers the instantaneous channel quality, and the UEs are not scheduled during deep fades; i.e. a UE is only allocated resources when experiencing good channel conditions compared to its average channel quality. The approach of selecting the UEs with the highest relative instantaneous channel quality has already been considered in the proportional fair PS method for HSDPA [6], [73]. PFT scheduling allows user fairness while increasing the cell capacity.

  In order to take the scheduling decisions, the Node B keeps track of the average value of UCQI over the last *N* TTIs. From the set of active users, UEs are selected based on the relative UCQI, defined as

$$\overline{UCQI}_k[n] = \frac{UCQI_k[n]}{\frac{1}{N}\sum_{i=1}^{N} UCQI_k[n-i]}. \tag{6.7}$$

Figure 6.4 illustrates the operation of the three proposed allocation strategies by considering a hypothetical scenario with two candidate UEs in which only one UE is scheduled at a time.

6.6 Time-Rate Scheduling Combined with Uplink Synchronisation

Let us propose a simple procedure to allow the use of the uplink synchronous WCDMA concept studied in Chapters 3 to 5 together with a PS based on TDM. The main idea behind

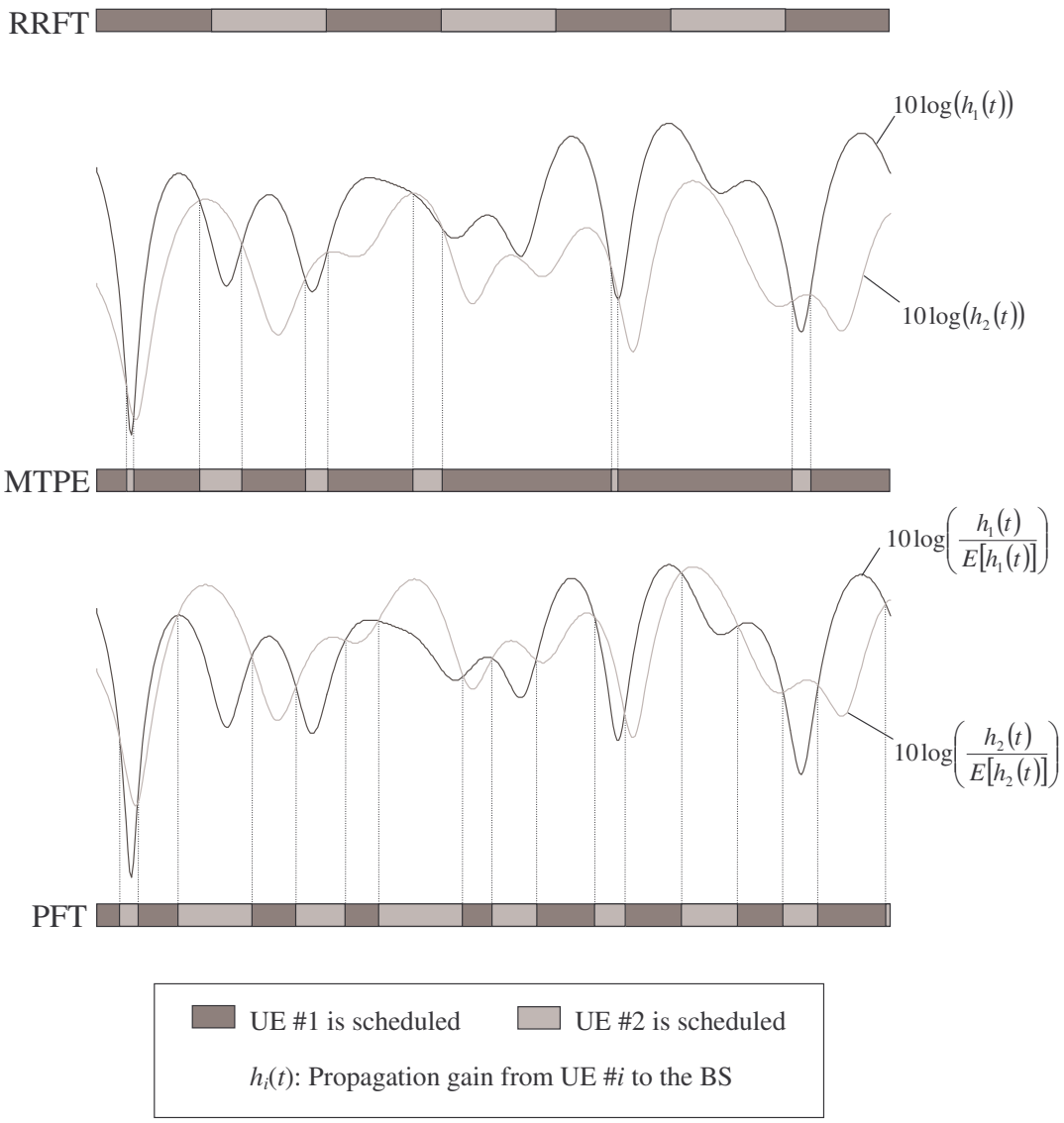

Figure 6.4. Different allocation policies for TDM PS in a scenario with two candidate UEs where only one is scheduled at a time; the same Eb/No target and data rate is assumed for both UEs.

uplink synchronous WCDMA was to obtain uplink orthogonality and thus reduce the multiple access interference (MAI) from synchronised users under a common scrambling code.

In order to support a PS based on TDM combined with uplink synchronous WCDMA, two main changes to the 3GPP specifications are required. On one hand the specifications must contemplate the possibility for the UEs to use uplink synchronisation, e.g. the mechanism proposed for Uplink Synchronous Transmission Scheme (USTS). On the other hand, it is necessary a fast code allocation mechanism to deallocate the orthogonal codes from the non-scheduled UEs and allocate them to the scheduled UEs at every TTI. At the BSs, some processing would be necessary to decide what code to allocate for every UE. Furthermore, extra signalling is needed in the downlink direction for code allocation notification. The use of the fast code allocation mechanism also allows a better utilisation of the allocated channelisation codes, and therefore maximises the code utilisation efficiency. All these advanced features are assumed to be available in this study, in order to assess the potential

Bit rate	**UEs per scr. code with uplink synchr. (BPSK for DPDCH)**	**UEs per scr. code with uplink synchr. (QPSK for DPDCH)**
8 kbps	85	128
16 kbps	51	85
32 kbps	28	51
64 kbps	15	28
128 kbps	7	15
256 kbps	3	7
384 kbps	3	7

Table 6.1. Number of UEs that can share a common scrambling code simultaneously in the uplink, assuming one DPCCH with SF 256 and one DPDCH per UE [24].

gain of uplink synchronisation combined with a PS based on TDM.

With the purpose of minimising the signalling overhead, only one active common scrambling code is allowed per BS. Let us recall that a low capacity increase is expected from allowing more than one active common scrambling code per BS, since the signals under different scrambling codes are not orthogonal.

Every time the BS carries out the notification of a new TFCS allocation, it also sends information on the code the UE must use for the uplink transmission. The use of the active common scrambling code is reserved for the UEs that have been allocated the maximum data rate. According to Table 6.1, with a maximum data rate of 384 kbps and QPSK modulation for the data channel, up to seven different UEs can be allocated under the same scrambling code. The information on the code to use can therefore be coded with three bits, reserving one of the codes to notify the UE that it is not allowed to use the common scrambling code; i.e. it must use its own scrambling code, which was fully allocated to it during the connection establishment.

With the fast scheduling concept it is not possible to share information between Node Bs regarding the codes allocated to the users, and therefore the UEs in SHO are not eligible to use the common scrambling code. This is of minor concern, as in Chapter 4 it was explained that the UEs in SHO do not get much benefit from uplink synchronisation.

The users under the common scrambling code can cancel part of the interference, and will therefore be able to reduce their transmission power. Hence, the common scrambling code is preferably allocated to the UEs under the worst channel conditions, as they generate higher interference to the neighbouring cells. However, different priority policies for code and data rate allocation would complicate the resource allocation algorithm; e.g. the power increase is different with and without uplink orthogonality. Hence, this study assumes that the common scrambling code is allocated to the UEs by keeping the same priority as with the scheduling policy to allocate the data rates.

Small performance differences are expected for the PFT and MTPE scheduling strategies with respect to a scheme that prioritises UEs under the worst channel conditions. In the case of MTPE the UEs with the worst channel quality are almost never scheduled. With PFT, UEs with bad absolute channel conditions have on average the same priority as the rest. Furthermore, the UEs with the worst channel conditions are normally in SHO mode, which means that they are not eligible for the common scrambling code anyway. On the other hand, the number of simultaneous UEs that can be allocated under the same scrambling code seems to be large enough to include all the UEs which are not in SHO mode; e.g. assuming QPSK modulation for the Dedicated Physical Data Channel (DPDCH), according to Table 6.1 up to

2.7 Mbps can be allocated for users in non-SHO mode.

With the interference reduction provided by uplink synchronisation, the UEs can decrease their transmission power while keeping the same required Eb/No, and the whole system benefits. However, this requires a fast mechanism for the adjustment of the transmission power, since the codes are only allocated during one TTI. This study utilises a simple approach to adjust the transmission power in the mentioned situation, by assuming the same required Eb/No for all the UEs under the active scrambling code

$$\rho = G\frac{P_{CSC}}{P_{total} - \alpha \cdot N_{CSC} \cdot P_{CSC}} = G\frac{P_{NO\_CSCs}}{P_{total} - P_{NO\_CSCs}}, \tag{6.8}$$

where G is the processing gain, P_{total} is the total received power at the Node B, α is the orthogonality factor, N_{CSC} is the maximum number of UEs that can be accommodated under the common scrambling code, P_{CSC} is the required received power for a UE under the common scrambling code, and P_{NO_CSCs} is the required received power for that UE if it did not use the common scrambling code. From (6.8) it is possible to derive an expression to calculate the new transmission power when the UE switches from a non-common scrambling code to the common scrambling code and vice versa

$$\frac{P_{CSC}}{P_{NO\_CSCs}} = \frac{1}{1+\rho\dfrac{N_{CSC}\alpha - 1}{G+\rho}}. \tag{6.9}$$

Assuming a channel model with low time dispersion, $\alpha \approx 1$, and

$$\frac{P_{CSC}}{P_{NO\_CSCs}} \approx \frac{1}{1+\rho\dfrac{N_{CSC} - 1}{G+\rho}}. \tag{6.10}$$

This simplified expression is not completely accurate and is expected to have direct impact on the system performance. On one hand, if a user transmits with excessive lower power than required, all the blocks will arrive erroneously at the BS. On the other hand, an excessive transmission power might guarantee the correct reception of the blocks, but it would create extra interference that has impact on the total cell throughput. Nevertheless, as already mentioned the system can rely on HARQ to compensate for the power inaccuracy.

6.7 Scenario for System Level Simulations

The network model for the system level simulations is basically the same as the one employed in Chapter 4 and Chapter 5. Both micro-cell and macro-cell scenarios are considered. Uplink data traffic between the UEs and the BS has been implemented according to the modified gaming model described in Appendix I. A weighted combination of the PIEs presented in Appendix E is employed. For uplink synchronisation the PIEs are performed based on the algorithm described in Appendix F.

PDEs are also employed when required, based on the expression derived in Appendix G.

The capacity gain of the proposed schemes is measured in terms of the cell throughput. The cell throughput is obtained by considering only the successfully received packets, averaging over all the cells in the network and the whole simulation time.

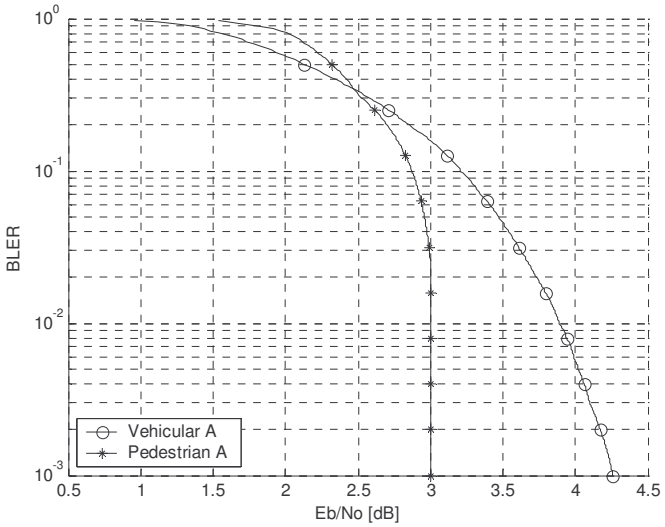

Figure 6.5. Function of BLER versus per block average Eb/No for Vehicular A and Pedestrian A with UE speed of 3 km/h and a circuit-switched service at 64 kbps [49].

The gain obtained with the different capacity enhancing strategies is calculated from the system level simulations by comparing cases with the same system load and quality of service (QoS). The system load is measured as the NR per cell at a 5% outage; the quality of service is determined by the UE throughput per packet call at a 10% outage. In our study, the NR outage is considered to occur for NR values over 6 dB. The UE outage is considered to occur for a throughput per packet call smaller than 64 kbps.

Each simulation performed in this investigation has been carried out by computing a minimum of 5000 packet calls. This means that the QoS is calculated by considering a minimum of 500 packet calls for the 10% outage. In the case of the NR, the accuracy is much higher, as the outage is computed by considering one sample per slot and per BS.

The system level model and the parameters employed for the simulations are summarised in Table 6.2 and Table 6.3. The AVI tables to map the system level results into link level results are plotted in Figure 6.5. The specific default parameters employed for the simulation of the RNC PS based on TVMs are collected in Table 6.4. Table 6.5 presents the specific default parameters for the simulations with the Node B PS based on BRD. Table 6.6 comprises the default settings for the Node B PS based on TDM.

It should be mentioned that in a real implementation, the PS normally manages the rest of the received power up to the target value once the real time (RT) services have been accommodated. However, in order to calculate the full potential of the schemes, this study assumes that all the available own cell received power is intended for NRT services, i.e. the PS takes full control of all the resources. Hence, with this approach the influence of the circuit-switched traffic on the packet-switched traffic and vice versa is not considered.

Parameter		Micro-cell	Macro-cell
Cell Plan	Number of cells	24	24
	Cells per site	3	3
	Site-to-site distance	1040 m	3232 m
	Number of receiver antennas per cell	2	2
	Noise level per receiver antenna	-102.9 dBm	-102.9 dBm
Propagation	Path loss [dB] with distance *d* [km]	147.7+40log *d*	128.1+37.6log *d*
	Standard deviation for shadow fading	8 dB	8 dB
	Coherence distance for shadow fading	100 m	100 m
	Multi-path model	Pedestrian A [43]	Vehicular A [43]
	BS antenna gain	16 dBi	16 dBi

Table 6.2. Cell plan and propagation parameters for micro-cell and macro-cell environments.

Parameter				Value
SHO	Window add / drop / replace			2 dB / 4 dB / 2 dB
	Time out to drop BS			0.05 s
	Maximum active set size			2
PC	Fast closed-loop PC step size			1 dB
	Frequency of outer-loop PC updates			1 TTI
	Outer-loop PC step size (up)			0.3 dB
UE	Possible data rates			0,8,16,32,64,128,256 and 384 kbps
	Modulation for the DPDCHs	without uplink synchron.		BPSK
		with uplink synchronisation		QPSK
	Speed			3.0 km/h
	Maximum transmission power			21 dBm
	UE antenna gain			0 dBi
	Link to system level interface			AVI for 64 kbps [49][5]
TFC Selection [32]	Notify delay (MAC-d to higher layers)			15 ms
	Modify delay (higher layers to MAC-d)			10 ms
	Processing delay (physical layer)			15 ms
	TFC Elimination algorithm		X	15 slots
			Y	30 slots
			Z	30 slots
Traffic model	Packet Call	Distribution of duration		Exponential (mean: 5s)
		Distribution of reading time		Exponential (mean: 5s)
	Datagram	Distribution of inter-arrival time		Log-normal (mean: 40ms, std: 38ms)
		Size		1152 bytes
Simulation time				180 s

Table 6.3. Summary of the main system model and simulation parameters.

[5] See Appendix H for considerations on the use of the AVI tables for 64 kbps with other different data rates.

Parameter	Value
TTI size	10 ms
PS period	200 ms
TFCS modification period	600 ms
NR offset (for LC)	1 dB
Minimum data rate allocated by the PS	8 kbps
Maximum data rate	384 kbps
Inactivity timer	2 s
Queuing timer	2 s
TVM report period	1 TTI
TVM report threshold	4 kbytes
Power measurement averaging window at the BS	100 ms
HARQ	L2 Type I
BLER target	1%

Table 6.4. Specific default parameters for the simulation of the RNC PS based on TVMs.

Parameter		Value
TTI size		10 ms
PS period		100 ms
TFCS modification period		100 ms
Inactivity timer		400 ms
NR offset (for LC)		1 dB
Minimum data rate allocated by the PS		8 kbps
Maximum data rate		384 kbps
RUF threshold for data rate upgrade (T_{UP})		5 TTIs
RUF threshold for data rate downgrade (T_{DOWN})		10 TTIs
Observation period to calculate RUF		200 ms
Power measurement averaging window at the BS		100 ms
HARQ	Type	L1 Type II/III
	L1 retransmissions (N)	5
	Combining loss (L_{comb})	0.2 dB
BLER target		10%

Table 6.5. Specific default parameters for the simulation of the Node B PS based on BRD.

6.8 Simulation Results

6.8.1 Performance of HARQ

The performance of using HARQ Type I and Type II/III is compared in Figure 6.6 in terms of cell throughput for different target values of the BLER. The figure includes both theoretical and simulation results. The theoretical results are based on equations (6.2) and (6.3), and correspond to a Vehicular A power delay profile (PDP) without SHO. The simulation results are performed with a Node B PS based on BRD and SHO in macro-cell environment.

HARQ Type II/III is performed by assuming a combining loss of 0.2 dB and a maximum of 5

Parameter		Value
TTI size		2 ms
PS period		2 ms
Minimum data rate for scheduled UEs		128 kbps
UCQI calculation (only MTPE and PFT)		slot basis
NR offset (for LC)		1 dB
Minimum data rate allocated by the PS		0 kbps
Maximum data rate		384 kbps
UCQI averaging window (only PFT)		100 ms
Power measurement averaging window at the BS		100 ms
Allocation delay (also includes the rest of UE delays)		3 TTIs
HARQ	Type	L1 Type II/III
	L1 retransmissions (N)	5
	Combining loss (L_{comb})	0.2 dB
BLER target		10%

Table 6.6. Specific default parameters for the simulation of the Node B PS based on TDM.

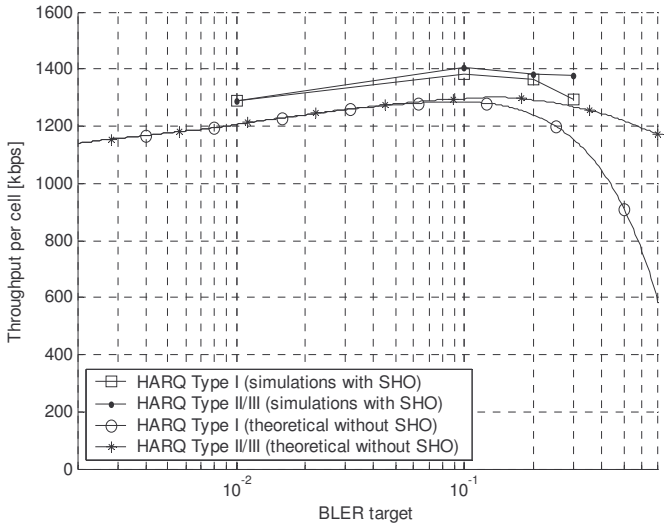

Figure 6.6. Throughput per cell with HARQ from simulations in macro cell environment and from theoretical calculations (i=0.76, 2 receive antennas, AVI table for Vehicular A PDP and SHO off).

transmissions of the same block. After the forth retransmission all the received information from that block is discarded. The tendency is very similar in both the theoretical and simulation results, however the theoretical ones do not include SHO, and the absolute throughput is therefore lower.

In both the theoretical and the simulation results the optimum performance is obtained for a BLER target close to 10% in both cases of HARQ Type I and Type II/III. By considering the simulation results, there is a 9.1% cell throughput gain from using HARQ Type II/III with 10% BLER target with respect to HARQ Type I with a 1% BLER target.

By comparing cases with the same BLER target, the capacity gain between HARQ Type II/III and Type I increases for high values of the BLER target; however, for the optimum value of the BLER target the simulation results only show a marginal gain of 1.5%.

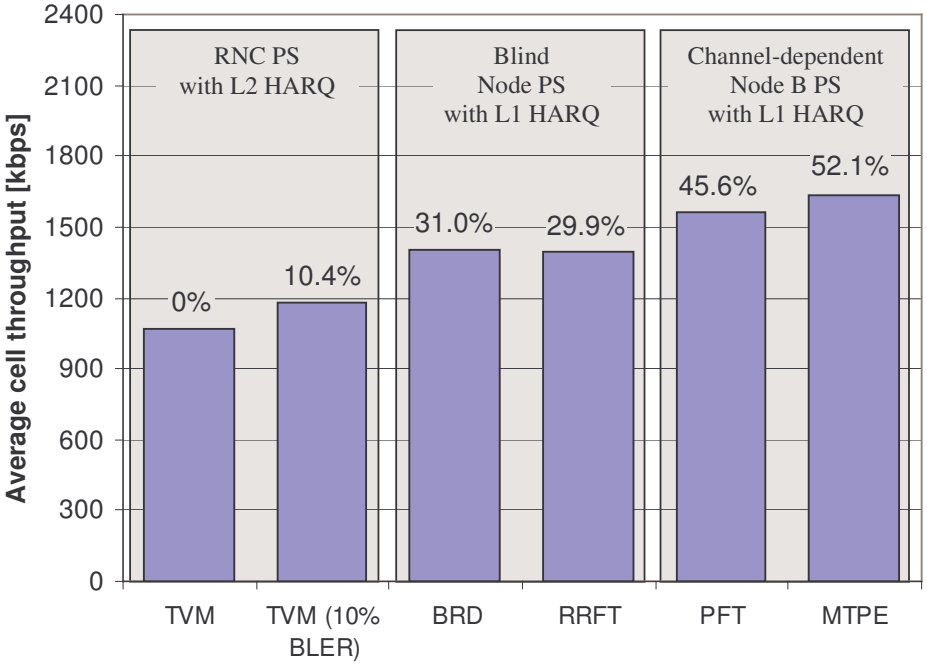

Figure 6.7. Average throughput per cell for the different scheduling algorithms based on simulations of a macro-cell environment.

6.8.2 Performance of the Node B Packet Schedulers

Figure 6.7 plots the throughput per cell obtained from the simulations of a macro-cell environment with both the Node B PS based on BRD and the Node B PS based on TDM with the three proposed scheduling strategies. The results are compared in terms of cell throughput relative to the RNC PS based on TVMs with a 1% BLER target. Although the use of a BLER target of 10% would require fast retransmissions, the RNC PS based on TVMs with a BLER target of 10% is considered as well. The aim is to make a difference between the gain due to HARQ and the one due to the fast scheduling.

Compared to the RNC PS algorithm based on TVMs without L1 HARQ and a BLER target of 1%, the Node B PS based on BRD with L1 HARQ provides a capacity increase of 31% in terms of cell throughput for the macro-cell environment. Notice that the gain with respect to the RNC PS with a BLER target of 10% is 18.7%; this is approximately the gain provided by the fast scheduling algorithm.

The performance of RRFT is very similar to BRD, since in both cases the resource allocation is carried out by giving the same priority to all the UEs. However, with PFT and MTPE, there is an additional capacity gain from using the channel quality information for the resource allocation decisions. MTPE provides the highest capacity gain from all the proposed schemes, since it only allocates resources to the UEs with the highest UCQI, i.e. with the lowest required transmission power per bit-per-second of data transmission. Hence, MTPE gets a higher reduction in the interference to other cells. Furthermore, the probability that a scheduled UE is subsequently scheduled in the following PS periods is much higher with MTPE. This means that with MTPE the abrupt changes in the transmission power from the UEs occur less frequently; hence, the influence of an inaccurate power adjustment is reduced.

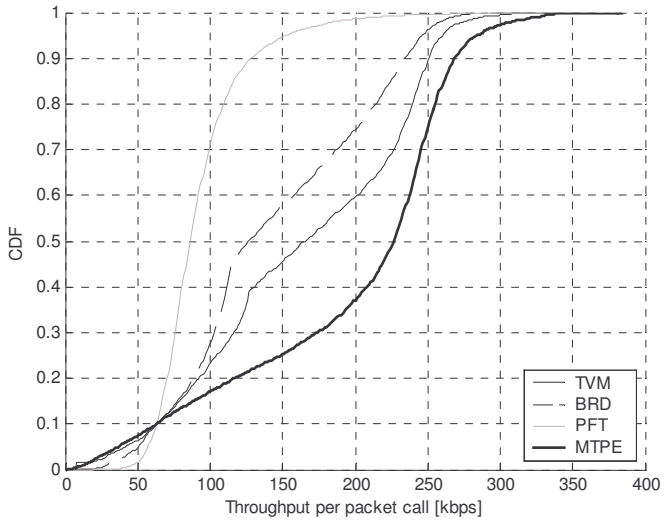

Figure 6.8. CDF of the throughput per packet call experienced by the UEs for different scheduling algorithms from simulations of a macro-cell environment.

Figure 6.8 depicts the cumulative distribution function (CDF) of the throughput per packet call for the different scheduling strategies in the macro-cell environment. Notice that, although MTPE provides a higher throughput per cell, it introduces high differences among the packet calls in terms of the obtained throughput. On the other hand, by providing a slightly smaller throughput per cell, PFT presents a more fair distribution of the throughput for all the packet calls. Although the throughput with PFT should theoretically be the same for all the packet calls, the results in Figure 6.8 are biased, in the sense that they are influenced by the traffic model. As the source data rate is not constant, as well as the packet call duration, some packet calls might require much higher or lower throughput than the average.

Figure 6.9 plots the average throughput per UE during the active periods as a function of the average path gain to the BS with the best radio link in a macro-cell environment. The purpose is to describe how the different scheduling algorithms behave with respect to the channel conditions of the link between the UEs and the BS. The MTPE provides the most unfair distribution of the throughput among the UEs. Notice that for average path gains over -110 dB the throughput per UE is approximately constant with a value close to the average source data rate (250 kbps). This roughly means that UEs with a path gain higher than -110 dB are always scheduled. The resources that are left after scheduling these UEs are then allocated to the following users with the highest path gain. Therefore, MTPE may have presented even more unfair results with a traffic model that provided a higher source data rate.

The rest of the considered scheduling strategies provide fair throughput for all the UEs within a higher cell range. However, PFT provides a better utilisation of the available resources, keeping the UE throughput closer to 64 kbps, i.e. the value selected for the UE outage criterion in Section 6.7.

The same cases as in Figure 6.7 are plotted in Figure 6.10 for a micro-cell environment. Although the tendency is very similar, the gain of using any of the schemes compared to the RNC PS with a 1% BLER target is higher than in the macro-cell case. Part of the extra capacity gain obtained for micro-cells with respect to a macro-cell scenario comes from the use of HARQ (Type I or Type II/III) with a higher BLER target. With the RNC PS based on TVMs the throughput increases by 20.2%, whereas in the macro-cell scenario the increase

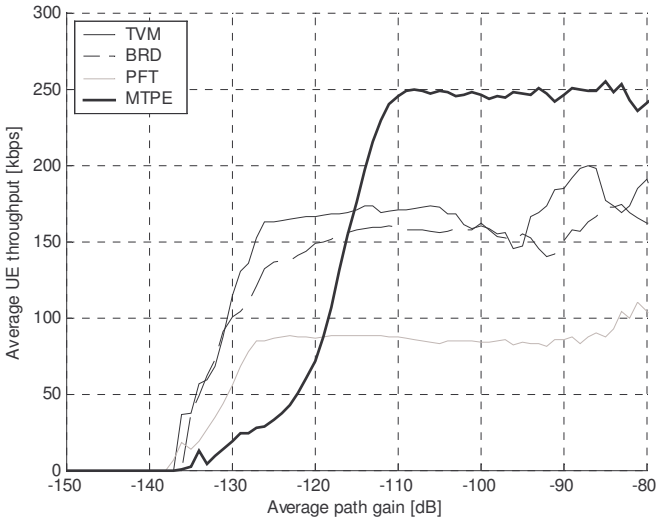

Figure 6.9. Average throughput per active UE versus the average path gain to the BS with the best link in a macro-cell environment.

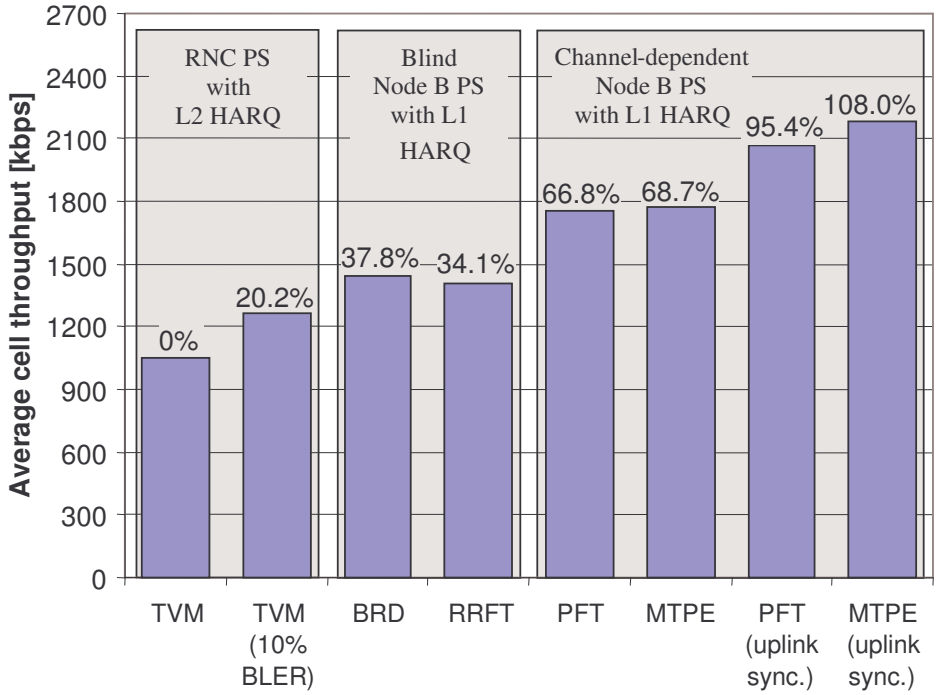

Figure 6.10. Average throughput per cell for the different scheduling algorithms based on simulations of a micro-cell environment.

was 10.4%.

The capacity gain of HARQ mainly originates from the fact that operating at a higher BLER target requires much less received energy than the loss due to the retransmissions. However, in the case of the Pedestrian A PDP, used to model the micro-cell case, the required Eb/No hardly varies when increasing the BLER target, as illustrated in Figure 6.5 (0.3 dB from 1%

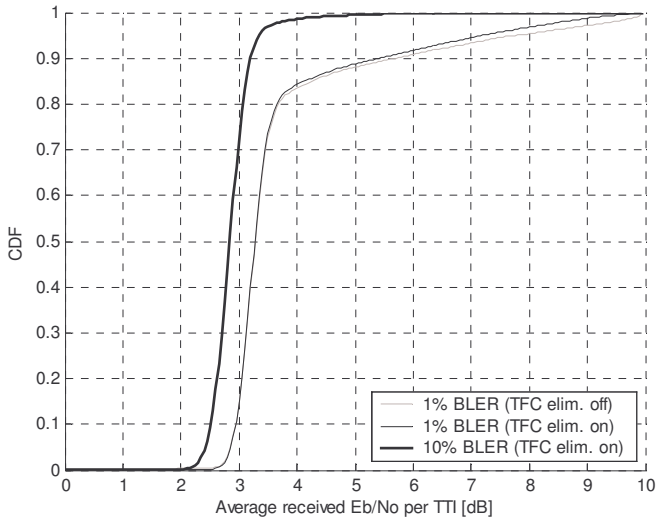

Figure 6.11. CDF of the average received Eb/No per TTI from simulations with the RNC PS based on TVMs in a micro-cell scenario.

to 10%, which corresponds to a linear decrease of 7%). Therefore, essentially no energy reduction is obtained to outweigh the retransmissions.

Nevertheless, in low dispersive environment such as the Pedestrian A PDP it is not possible to exploit the multi-path diversity, and they are more coverage limited. Hence, the UEs close to the cell border will have more problems fulfilling the Eb/No target. If this happens, and the distance between deep fades makes it impossible to reach the required BLER target, the use of outer-loop PC will increase the Eb/No target, which indeed makes the situation worse. As it can be seen in Figure 6.11, the mentioned situation occurs for the simulations with the RNC PS based on TVMs for a BLER of 1%. From the figure it can be concluded that there is a number of UEs under coverage constraints, which have set a much higher Eb/No target than the rest. Notice that although the difference in the median value of the Eb/No between the case of BLER target of 1% and 10% is around 0.5 dB, the mean is much higher, due to the contribution of the UEs with coverage problems. Increasing the BLER target to 10% gives the system the opportunity to recover from the deep fades. The figure also includes the case in which the TFC elimination algorithm is disconnected. Although the algorithm does not appear to give any benefit seen from Figure 6.11, in Figure 6.12 it is shown how it actually helps the users under coverage constraints reach their 1% BLER target, compared to the case without TFC elimination. With the use of such an algorithm, the UE only transmits at data rates which require a transmission power that the terminal can provide.

From the results it can be concluded that the use of HARQ does not only provide a capacity gain in terms of cell throughput due to the reduction of the required Eb/No, but also a gain derived from solving the coverage problems, in the cases where they occur. This is done by reducing the influence of the errors in the selection of the new BLER target value, i.e. in the outer-loop PC algorithm.

Another aspect that should be highlighted from Figure 6.10 is the fact that the cell throughput increase of PFT and MTPE with respect to the rest of PS strategies is higher in micro-cell than in macro-cell environments. Although the coverage problem is solved with the use of HARQ and PS based on BRD or RRFT, there is still some potential from exploiting the higher dynamic range of channels with of a low time dispersion such as the Pedestrian A

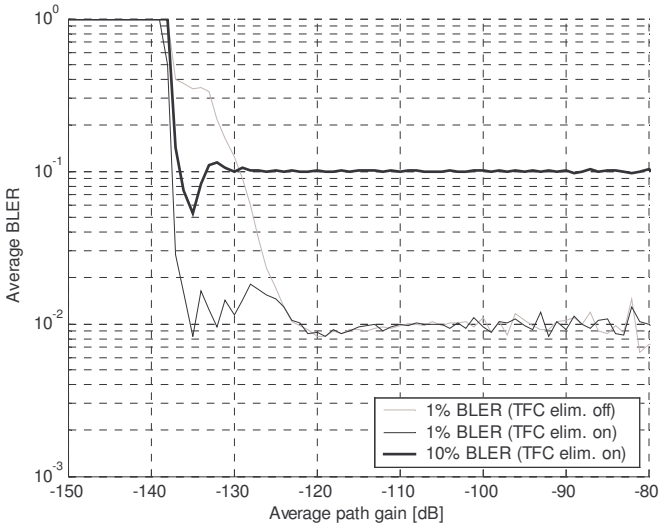

Figure 6.12. Average BLER per active UE versus average path gain to the closest BS from simulations with the RNC PS based on TVMs in a micro-cell scenario.

PDP.

Figure 6.10 also includes the capacity gain provided by the combined use of the Node B PS based on TDM with uplink synchronisation and either PFT or MTPE. Notice how the full gain provided by uplink synchronisation is added to the previous capacity increase derived from deploying the Node B PS based on TDM. Such a gain provided by uplink synchronisation is slightly higher with MTPE (23.3%) than with PFT (17.8%). The reason is that with MTPE the scheduling policy is based on the absolute channel quality, which reduces the allocation frequency for the UEs in SHO. As UEs in SHO do not benefit from uplink orthogonality, the overall gain is higher in this case. Furthermore, with this type of allocation policy, most of the scheduled UEs during a certain TTI are very likely scheduled for the next TTIs as well. This is expected to reduce the frequency of the power updates due to the change from non-orthogonal mode to orthogonal mode and vice versa; therefore the error associated with the use of the approximated equation in (6.10) is smaller.

Figure 6.13 shows the median value of the other-to-own cell interference ratio (i factor) obtained from the simulations for the different considered cases. Notice that changing the scheduling policy provides different values of the i factor. A decrease in the i factor is directly translated into a capacity gain in Figure 6.7 and Figure 6.10. In the case of the micro-cell scenario, the i factor experiments a considerable reduction when using PFT and MTPE, as the difference between the bad and the good channel quality experienced by the UEs is higher than in the macro-cell scenario.

However, not all the capacity gain comes from direct translation of the i factor reduction. Let us recall that in the simulations with the TVM PS, part of the obtained capacity gain originates from using a 10% BLER target instead of 1%. In macro-cell, the i factor remains unaltered, while in the micro-cell environment the variation is small, and it is not responsible for the whole 20.2% cell throughput gain.

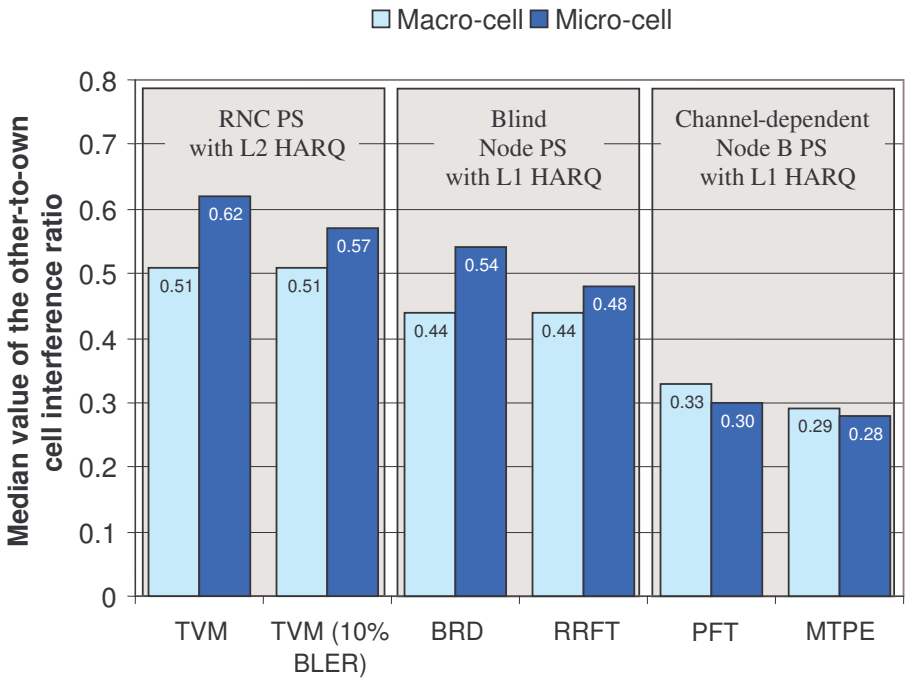

Figure 6.13. Median value of the other-to-own cell interference ratio from simulations with the different scheduling algorithms.

6.9 Conclusions

In this chapter various proposals for capacity enhancement of uplink packet access over DCHs have been presented and analysed for WCDMA systems. All the strategies are mainly based on moving part of the RNC functionality to the Node B, in order to circumvent the bottleneck caused by the signalling delay through the Iub interface.

The performance of L1 HARQ and Node B scheduling based on BRD and on TDM has been evaluated in terms of cell throughput, by means of system level simulations in low mobility environments. Some of these techniques can also be combined in order to obtain a higher gain. The combined use of the PS based on TDM with uplink synchronisation has been evaluated as well.

A theoretical approach to calculate the capacity with HARQ has been presented, which provides results in agreement with the simulations. For the simulated cases in a macro-cell scenario, the optimum BLER target has been found to be 10% for both HARQ Type I and Type II/III, where the capacity gain in terms of cell throughput compared to a BLER target of 1% is 7.5% and 9.1%, respectively. The throughput difference between HARQ Type II/III and Type I is much higher for larger values of the BLER target, but the difference is marginal at 10%.

Although the theoretical gain in the required Eb/No when increasing the BLER is smaller with a micro-cell scenario and an ITU Pedestrian A PDP, in this case the use of HARQ provides a higher capacity gain by improving the coverage.

The simulation results with the Node B PS based on BRD have shown a 31.0% and 37.8%

capacity gain in macro-cell and micro-cell scenarios, respectively, when combined with HARQ.

With the Node B PS based TDM, the WCDMA air interface capacity intended for NRT services is divided in the time domain. This means that only a few UEs are allowed to transmit at every time interval, set to 2 ms. Three different UE allocation policies have been presented and analysed: round-robin fair throughput (RRFT), proportional fair throughput (PFT) and maximised transmit power efficiency (MTPE). With RRFT no distinction is made among UEs, and therefore it provides a similar performance as PS based on BRD. PFT and MTPE take into account measurements of the channel quality of the UEs, and provide considerable gain with respect to the rest of schemes both in macro-cell and micro-cell environments. Although the capacity gain is slightly higher with MTPE, PFT provides a fairer resource sharing.

The use of uplink synchronisation with only one active common scrambling code over a PS based on TDM increases the capacity gain by 17.8% for PFT and 23.3% for MTPE in a micro-cell environment.

As previously mentioned, some of the proposed techniques can be combined. Compared to the reference RNC PS based on TVMs, a Node B PS based on TDM with HARQ and uplink synchronisation in the micro-cell scenario provides a 96.6% capacity gain with a PFT allocation policy, and 108.0% with MTPE.

Notice that although the potential gain of these techniques is quite significant, it should also be considered the effect of the extra signalling load added when deploying them. In the case of the Node B PS based on TDM, extra signalling load is required both in the uplink and the downlink. The information on the buffer occupancy at the UEs has to be transmitted through the uplink. Although such information is necessary at every frame, it is only required one effective bit to indicate a change in the buffer status (empty/full), and this bit is only sent whenever the buffer status of the UE changes. On the other hand, fast allocation messages have to be sent from the BS to the UEs with information on whether they are allowed to transmit or not at every scheduling period. One solution to minimise such a signalling load is to only send messages to the scheduled users at every PS period. Hence, no significant degradations are expected due to the extra signalling load.

The use of a channel-dependent scheduling algorithm based on TDM is therefore recommended as an efficient method to increase the capacity for uplink packet access. This type of scheduling is especially attractive in environments with low time dispersion, where it can be combined with uplink synchronous WCDMA, increasing the capacity by a factor of two. Notice that this gain is added to the one provided by other capacity enhancing techniques employed in uplink, such as the use of SHO or two receive antenna diversity.

Chapter 7

Conclusions

7.1 Summary

In this Ph.D. thesis various capacity enhancing techniques have been investigated for the uplink of WCDMA: multi cell admission control, uplink synchronisation and fast scheduling strategies for packet services.

The dissertation has provided an evaluation of the system level performance and the achievable capacity gain with these techniques. Furthermore, the required radio resource management (RRM) algorithms to deploy the different concepts has been considered.

The research relies on extensive simulations. Theoretical analyses have also been carried out to validate the results obtained with the simulations and to provide an easier way to assess the influence of certain factors in the overall performance.

In the following sections, a summary of the whole thesis is given, drawing the main conclusions from each chapter of the dissertation. Finally, a future scope of investigation is proposed.

7.2 Multi Cell Admission Control for Uplink

Chapter 2 has presented an uplink power based multi cell (MC) admission control (AC) approach to increase the system capacity and stability in networks with high-speed data users.

An MC power increase estimator (PIE) has been derived in order to make the operation of the MC AC algorithms possible. A simulation procedure has been developed to compare the operation and efficiency of the MC AC algorithm with respect to a reference single cell (SC) AC algorithm. The probability of AC errors that lead to an overload situation is smaller than when using the SC AC algorithm. This makes it possible to increase the threshold used for taking the admission decisions so that, having the same probability of reaching an overload situation, the MC AC algorithm provides a higher capacity.

In homogeneous load cases the MC AC algorithm does not give any gain. The same is concluded from the results in the hot spot load case with low data rate users. However, a significant capacity increase is obtained under non-homogeneous load conditions with respect to a SC AC scheme when considering a mixed situation with both low and high data rate users (34% more cell throughput for a 5% probability of reaching an overload situation).

According to the results provided in this Ph.D. thesis, the use of MC AC is recommended for scenarios with high coupling between cells, where the system may potentially operate under hot spot load situations and offering real time (RT) services that require high data rates. However, the gain provided by the MC approach may be reduced in mixed scenarios that also include non-real time (NRT) services, as they do not require a minimum guaranteed data rate. In these situations the received power can be decreased by reducing the data rate allocated to NRT, instead of dropping connections associated with RT services.

7.3 Uplink Synchronisation in WCDMA

Chapter 3 has presented uplink synchronisation as a method to reduce the multiple access interference (MAI) by means of exploiting the uplink orthogonality and thereby increase the capacity of WCDMA systems. To deploy this scheme in UMTS, the 3GPP standardisation body has proposed the Uplink Synchronous Transmission Scheme (USTS) for environments with a low time dispersion and a low mobility. USTS requires an initial acquisition and a closed-loop tracking control procedure for reaching the uplink synchronisation, as well as a new code allocation policy.

The time variability properties of the channels have a major impact on the degree of orthogonality reached with uplink synchronisation. The uplink orthogonality factor has been defined as a measure to characterise the impact of the lack of synchronism on the MAI cancellation over multi-path channels. The orthogonality factor can have values between 0 (non-orthogonality at all) and 1 (full orthogonality).

By assuming that the variation of the channels allows synchronism with misalignment errors smaller than 1/4 of the chip period, an orthogonality factor of approximately 0.9 and 0.4 can be reached for Pedestrian A and Vehicular A power delay profiles (PDP), respectively. The results have been confirmed for the case of Pedestrian A by considering the influence of the radio channel variations and the errors in the closed-loop tracking algorithm. Hence, a quite high orthogonality between the synchronous user equipments (UE) under the same scrambling code is obtained for low time-dispersive environments such as the ITU Pedestrian A PDP. On the contrary it is not worth using uplink synchronisation for high dispersive environments such as the Vehicular A channel, as the multi-path components reduce the orthogonality. The use of high UE velocities in a Pedestrian A channel has not been found to have a major impact on the orthogonality factor.

7.4 Uplink Synchronous WCDMA under Channelisation Code Constraints

In Chapter 4, the performance of uplink synchronous WCDMA has been assessed in terms of the capacity gain relative to an equivalent asynchronous system. The capacity gain has been evaluated theoretically and by means of dynamic system level simulations for scenarios with low time dispersion. The simulation results without soft handover (SHO) are in agreement with the theoretical predictions. The maximum number of available channelisation codes turns out to be a major limitation for the capacity gain of an uplink synchronous WCDMA system. Although the whole set of channelisation codes can be reused by employing a different scrambling code, the signals under different scrambling codes are non-orthogonal. Under the most realistic conditions, with a noise rise (NR) target of 4 dB (60% of the pole capacity) the capacity gain of an uplink synchronous WCDMA equals 9.6%. If the capacity is calculated for a 5% probability of unsatisfied UEs, the gain of uplink synchronous WCDMA rises to 19.5%. In an ideal case without channelisation code restrictions, the capacity gain with a NR target of 4 dB is 35.8%.

The use of the existing strategies for capacity improvement, such as dual antenna reception at the Node B, and voice activity detection, has been found to decrease the capacity gain of an uplink synchronous WCDMA system. The reason for this is that the channelisation code limitation is reached earlier when these capacity enhancing techniques are deployed. However, provided that the problems associated with the channelisation code shortage can be mitigated (e.g. by the use of higher order modulation), uplink synchronous WCDMA has been demonstrated to provide a significant capacity gain.

7.5 Uplink Synchronous WCDMA Combined with Variable Modulation and Coding

Variable modulation and coding (VMC) has been presented in Chapter 5 as a complementary scheme for uplink synchronous WCDMA to decrease the channelisation code utilisation per UE.

The capacity gain of uplink synchronous WCDMA combined with VMC has been evaluated theoretically and with an extensive set of dynamic system level simulations in micro-cell pedestrian environments. The results from the dynamic simulations are in agreement with the theoretical calculations. The simulation results for circuit-switched service at 64 kpbs with SHO and a NR target of 4 dB yield a 12.9% capacity gain for uplink synchronisation without VMC, and 29.0% with VMC.

Further, the effective NR was presented in Appendix D as a measurement to evaluate the uplink capacity. The effective NR gives a better idea of the uplink stability level of the base station (BS) when all the UEs are synchronised. However, the effective NR is only feasible under full UE penetration conditions. For an effective NR target of 4 dB and no SHO the theoretical capacity gain of uplink synchronous WCDMA combined with VMC equals 86.5%.

Multi-branch receive antenna diversity or/and multi-user detection (MUD) at the BS are alternative methods to improve the uplink capacity in WCDMA systems. The latter uplink capacity enhancing techniques do not require changes in the UEs, i.e. no legacy UE problems. Thus, despite of the potential gain of uplink synchronisation, the implementation in WCDMA should be considered carefully.

7.6 Capacity Enhancing Strategies Based on Fast Packet Scheduling

The capacity gain of HARQ and fast Node packet scheduling based on blind rate detection (BRD) and time division multiplexing (TDM) has been evaluated in Chapter 6 in terms of cell throughput, by means of system level simulations. Some of these techniques can also be combined with uplink synchronisation in order to obtain a higher gain.

A theoretical approach to calculate the capacity gain with HARQ has also been presented, which provides results in agreement with the simulations. The use of HARQ has proven to increase the capacity in Vehicular A environments, where it has been shown that increasing the block error rate (BLER) target can be translated into a much smaller required Eb/No. Although this does not happen with a Pedestrian A channel, HARQ is able to provide a higher capacity gain by improving the performance of outer-loop PC when operating under coverage constraints.

For the simulated cases in a macro-cell scenario with a Vehicular A PDP, the optimum BLER target value has been found to be 10% for both HARQ Type I and II/III, where the capacity gain with respect to a BLER target of 1% is 7.5% and 9.1%, respectively.

Two different scheduling concepts have been proposed based on moving the packet scheduler (PS) functionality from the Radio Network Controller (RNC) to the Node B. The first of them is based on BRD, and the simulations results have shown 31.0% and 37.8% higher cell throughput in macro-cell and micro-cell channels, respectively, when combined with HARQ, and assuming a UE velocity of 3 km/h.

In the second one the WCDMA resources dedicated to packet access are divided in the time domain, which means that only a few UEs are allowed to transmit at every time interval, set to 2 ms. Three different UE allocation policies have been presented and analysed: round-robin fair throughput (RRFT), proportional fair throughput (PFT) and maximise transmit power efficiency (MTPE).

With RRFT no distinction is made among the UEs, and therefore provides a similar performance as the PS based on BRD.

PFT and MTPE exploit the multi-user diversity by taking into account the channel quality of the UEs. These strategies provide considerable gain with respect to the rest of schemes both in macro-cell and micro-cell scenarios. MTPE allocates resources to the users experiencing the best absolute instantaneous channel quality, and provides the highest capacity gain. However, PFT provides a fairer resource sharing by allocating resources to the UEs with the highest instantaneous channel conditions compared to their average channel quality.

As previously mentioned, some of the proposed techniques can be combined. Compared to the reference RNC PS based on traffic volume measurement (TVM), a PS based on TDM with HARQ and uplink synchronisation in a micro-cell scenario provides a 96.6% capacity

gain with a PFT allocation policy, and 108.0% with MTPE.

The associated required changes in both the BSs and the UEs to adopt uplink synchronous WCDMA may represent an issue in spite of the existing potential for capacity increase. On the other hand, once the users are synchronised it is also possible to deploy fast packet scheduling based on TDM. The combined use of uplink synchronisation with a channel-dependent scheduling algorithm based on TDM is therefore recommended as an efficient method to increase the capacity for uplink packet access. This type of scheduling is especially attractive in environments with low time dispersion, where it can be combined with uplink synchronous WCDMA, increasing the capacity by a factor of up to two. Notice that this gain is added to the one provided by other capacity enhancing techniques employed in uplink, such as the use of SHO or two receive antenna diversity.

HARQ and fast Node B PS are currently been discussed in the 3GPP forum as techniques to support the uplink evolution of the packet access in WCDMA, the Enhanced Dedicated Channel (E-DCH). This is an indication that they currently represent a hot topic at the end of this Ph.D. research.

As a final recommendation, a hybrid mechanism to control the interference in the uplink a combined solution is suggested due the nature of the traffic expected for WCDMA systems, mainly based on high data rate users. Such a mechanism consists of combining a multi cell admission control centralised at the RNC for the initial admission of users, with a fast Node B PS that controls the fast variations of the interference level.

7.7 Future Research

This section addresses some proposals to continue the investigations performed in this Ph.D. study.

The results obtained in this thesis have provided a quite realistic picture of the potential of MC AC and especially uplink synchronous WCDMA, and no more investigation should be required in these fields. However, there are some open areas to continue the investigations of the fast scheduling concepts presented in Chapter 6.

One of them is the effect of the signalling overhead that the proposed Node B PS algorithms with physical layer HARQ and uplink synchronisation would require in the radio interface (Uu). Although little degradation is expected in the performance of the strategies introduced in Chapter 6, the influence of this extra signalling and the associated delay requires further study.

The results provided for the PS based on TDM are obtained for short scheduling periods (i.e. 2 ms), with the purpose of taking advantage of the multi-user diversity. However, the real influence of selecting other PS periods has not been addressed. In principle, increasing the scheduling period should not influence the performance of the PS for low velocity terminals, since the channel quality has a lower variability. However, fast channel fluctuations can reduce the multi-user diversity gain. Only low user velocities are considered in the system level simulations performed in this Ph.D. thesis. An assessment of the performance with higher speeds would provide extra information to understand the full potential for the different considered schemes.

Another topic that requires further investigation is the impact of the traffic model on the performance of the proposed fast scheduling strategies. The modified gaming traffic has been

chosen as the only reference model for this Ph.D. Due to its bursty properties and the high required data rate, it is very suitable for the study of the advanced packet access. However, it would be interesting to consider other traffic models associated with services that will very likely come into the picture with the new 3G multimedia applications, such as file transfer or multimedia messaging service (MMS).

Although multi-user detection (MUD) or other techniques listed in Chapter 1 have already been investigated in detail, there is some potential for the research of combined features, e.g. MUD and/or antenna arrays with HARQ and/or uplink synchronisation.

This thesis has provided an idea of the potential for the uplink evolution of the UMTS, but it would be quite interesting to get results on the performance of a full evolution of 3G systems, considering both the uplink and the downlink simultaneously, i.e. HSDPA with E-DCH, and also combining NRT and RT services.

Appendix A

Multi cell Admission Control for Downlink

A.1 Scope

In this appendix, the multi cell (MC) admission control (AC) study made in Chapter 2 for uplink is extended for the downlink case. With the aim of supporting the MC AC operation, two new methods to estimate the power increase in the neighbouring BSs due to the admission of the new user equipments (UE) are derived for the downlink case.

A.2 Power Based Multi Cell Admission Control for Downlink

As in the uplink case, the power is commonly used in the downlink of WCDMA systems as a measurement of the system load. The level of transmitted power by the BSs is therefore employed in downlink AC, where a UE is normally admitted if

$$P_{serv} < P_{max} \tag{A.1}$$

where P_{serv} is the power transmitted by the serving base station (BS) before the admission and P_{max} is maximum level of power that can be transmitted by the BS. Notice that (A.1) is the equivalent expression for downlink as in (2.1) for the uplink case. Keeping the same

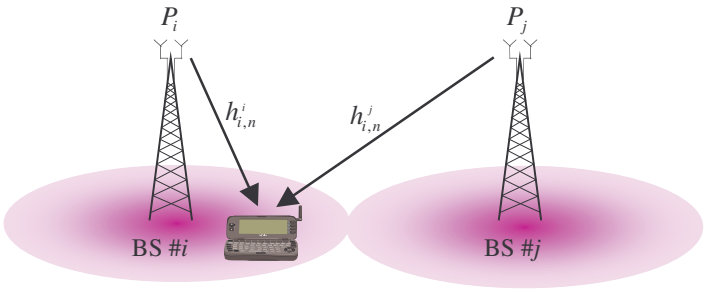

Figure A.1. Scenario where a UE receives signals from its serving BS and from a neighbouring one.

reasoning as in the uplink case, downlink single cell (SC) AC and MC AC algorithms are based on the following conditions, respectively

$$P^{est}_{serv} < P_{max} - P_{offset} = P_{target}\ [\text{dB}]; \tag{A.2}$$

$$\begin{aligned} &P^{est}_{serv} < P_{target}, \text{ and} \\ &P^{est}_{neigh,j} < P_{target} \quad \forall j \,|\, 1 \le j \le N_{adj}, \end{aligned} \tag{A.3}$$

where $P^{est}{}_{serv}$ is an estimate of P_{serv}, and $P^{est}{}_{neigh,j}$ is an estimate of $P_{neigh,j}$, which is defined as the power transmitted by the neighbouring BS #*j*. In (A.2) and (A.3), P_{target} is a practical threshold P_{offset} times smaller than P_{max}, employed as a security margin.

A.2.1 Downlink Multi Cell Power Increase Estimator

In this study, two methods are proposed to estimate the power increase that the admission of a new UE causes in the neighbouring BSs. The first one is based on the pilot measurement reported by all the UEs belonging to the implicated cells. The second estimation is very simple and is based on the approximation that the power increase in the neighbouring BSs is proportional to the power increase in the serving BS.

Figure A.1 shows the main signals that relate a UE to its serving BS (#*i*) and one of the neighbouring BSs (#*j*). Let us denote the path loss from a certain BS #*j* to the *n*-th UE served by BS #*i* as $h^j_{i,n}$, the power transmitted by BS #*i* as P_i, and the power from BS #*i* associated with its *n*-th UE as $P_{i,n}$.

A.2.1.1 Downlink Multi Cell Power Increase Estimator Based on the Pilot Reports

Let us assume that a new UE makes a request at BS #*i* to enter the system.

The energy-per-bit to noise ratio (Eb/No) for the *n*-th UE served by a neighbouring BS #*k* before the admission of the new UE can be expressed as

$$\rho_{k,n} = G_{k,n} \frac{P_{k,n} h^k_{k,n}}{P_{noise} + P^{other}_{k,n} + \left(P_k - P_{k,n}\right) h^k_{k,n} \left(1 - \alpha_{k,n}\right)}, \tag{A.4}$$

where $G_{k,n}$ is the processing gain, P_{noise} is the background noise power, $P^{other}{}_{k,n}$ is the power received from other BSs different from the serving one, and $\alpha_{k,n}$ is the orthogonality factor; all these factors are associated with the *n*-th UE served by BS #*k*.

Let us call the power increase caused by the admission of the new UE in BS #*i* as ΔP_i, and the

estimated value as $\Delta P^{est}{}_i$. Once the new UE is admitted in BS #*i* and after all the UEs have performed power control (PC) and the system is stabilised, the new Eb/No for the *n*-th UE of BS #*k* is

$$\rho_{k,n}^{new} = G_{k,n} \frac{\left(P_{k,n} + \Delta P_{k,n}\right) h_{k,n}^{k}}{P_{noise} + \left(P_{k,n}^{other} + \Delta P_{k,n}^{other}\right) + \left[\left(P_k + \Delta P_k\right) - \left(P_{k,n} + \Delta P_{k,n}\right)\right] h_{k,n}^{k} \left(1 - \alpha_{k,n}\right)}, \tag{A.5}$$

where $\Delta P_{k,n}$, $\Delta P^{other}{}_{k,n}$, ΔP_k are the increment in the values of $P_{k,n}$, $P^{other}{}_{k,n}$ and P_k after the admission of the UE, respectively.

Let us assume that the power increase from other cells is only originated by BS #*i*, i.e.

$$\Delta P_{k,n}^{other} \approx \Delta P_i \, h_{k,n}^{i}. \tag{A.6}$$

$\Delta P^{other}{}_{k,n}$ is therefore an underestimation of the real value.

In order to maintain the quality of service (QoS) requested for all the UEs, the Eb/No should remain the same after the admission for all of them, which means that

$$\rho_{k,n}^{new} = \rho_{k,n} \quad \forall k, n. \tag{A.7}$$

By substituting (A.4) and (A.5) in (A.7) with the approximation in (A.6) and making some manipulations

$$\Delta P_{k,n} = P_{k,n} \frac{\Delta P_i \, h_{k,n}^{i} + \Delta P_k \, h_{k,n}^{k} \left(1 - \alpha_{k,n}\right)}{P_{noise} + P_{k,n}^{other} + P_k \, h_{k,n}^{k} \left(1 - \alpha_{k,n}\right)}. \tag{A.8}$$

From (A.4) it is possible to derive that

$$P_{noise} + P_{k,n}^{other} + P_k h_{k,n}^{k} \left(1 - \alpha_{k,n}\right) = \frac{G_{k,n}}{\rho_{k,n}} P_{k,n} h_{k,n}^{k} + P_{k,n} h_{k,n}^{k} \left(1 - \alpha_{k,n}\right), \tag{A.9}$$

which can be substituted in (A.8) and yields

$$\Delta P_{k,n} = P_{k,n} \frac{\Delta P_i \, h_{k,n}^{i} + \Delta P_k \, h_{k,n}^{k} \left(1 - \alpha_{k,n}\right)}{\frac{G_{k,n}}{\rho_{k,n}} P_{k,n} h_{k,n}^{k} + P_{k,n} h_{k,n}^{k} \left(1 - \alpha_{k,n}\right)} = \frac{\Delta P_i \, \frac{h_{k,n}^{i}}{h_{k,n}^{k}} + \Delta P_k \left(1 - \alpha_{k,n}\right)}{\frac{G_{k,n}}{\rho_{k,n}} + \left(1 - \alpha_{k,n}\right)}. \tag{A.10}$$

Let us recall that the energy-per-chip to interference-power-density ratio (Ec/Io) contained in the pilot report associated with every link starting from a BS #*p* and ending in the *n*-th UE of BS #*q* can be described in the following way

$$\rho_{q,n}^{pilot,p} = \frac{P_p^{pilot} h_{q,n}^{p}}{P_{q,n}^{rx}}, \tag{A.11}$$

where $P^{pilot}{}_p$ is the pilot power transmitted by BS #*p* and $P^{rx}{}_{q,n}$ is the total wideband power received by the *n*-th UE of BS #*q*. From (A.11) it is possible to derive the value of the quotient between the path losses from BS #*i* and BS #*k* to the *n*-th UE of BS #*k*

$$\frac{h_{k,n}^{i}}{h_{k,n}^{k}} = \frac{\rho_{k,n}^{pilot,i} P_k^{pilot}}{\rho_{k,n}^{pilot,k} P_i^{pilot}}, \tag{A.12}$$

which can be used in (A.10) and gives

$$\Delta P_{k,n} = \frac{\Delta P_i \dfrac{\rho_{k,n}^{pilot,i} P_k^{pilot}}{\rho_{k,n}^{pilot,k} P_i^{pilot}} + \Delta P_k \left(1-\alpha_{k,n}\right)}{\dfrac{G_{k,n}}{\rho_{k,n}} + \left(1-\alpha_{k,n}\right)}. \tag{A.13}$$

The increase of power transmitted by the neighbouring BS #*k* after the admission of the new UE in BS #*i* can be calculated as the sum of the increases of power associated with every one of its UEs, i.e.

$$\Delta P_k = \sum_{n=1}^{N_k} \Delta P_{k,n} = \sum_{n=1}^{N_k} \frac{\Delta P_i \dfrac{\rho_{k,n}^{pilot,i} P_k^{pilot}}{\rho_{k,n}^{pilot,k} P_i^{pilot}} + \Delta P_k \left(1-\alpha_{k,n}\right)}{\dfrac{G_{k,n}}{\rho_{k,n}} + \left(1-\alpha_{k,n}\right)}, \tag{A.14}$$

where N_k is the number of UEs served by BS #*k*.

From (A.14) it is possible to derive the value of the increment of power transmitted by BS #*k*

$$\Delta P_k = \Delta P_i \frac{P_k^{pilot}}{P_i^{pilot}} \frac{\displaystyle\sum_{n=1}^{N_k} \frac{\rho_{k,n}^{pilot,i}}{\rho_{k,n}^{pilot,k}\left(\dfrac{G_{k,n}}{\rho_{k,n}} + \left(1-\alpha_{k,n}\right)\right)}}{1 - \displaystyle\sum_{n=1}^{N_k} \frac{1-\alpha_{k,n}}{\dfrac{G_{k,n}}{\rho_{k,n}} + \left(1-\alpha_{k,n}\right)}}. \tag{A.15}$$

By using the estimation of the power increase at the serving BS #*i*, the same average value of the orthogonality factor α for all the UEs, and the same transmitted pilot power P^{pilot} for all the BSs, the increase of power at the neighbouring BS #*k* can be estimated by

$$\Delta P_k^{est} = \Delta P_i^{est} \frac{\displaystyle\sum_{n=1}^{N_k} \frac{\rho_{k,n}^{pilot,i}}{\rho_{k,n}^{pilot,k}\left(\dfrac{G_{k,n}}{\rho_{k,n}} + 1 - \alpha\right)}}{1 - (1-\alpha)\displaystyle\sum_{n=1}^{N_k} \frac{1}{\dfrac{G_{k,n}}{\rho_{k,n}} + 1 - \alpha}}. \tag{A.16}$$

A.2.1.2 Multi Cell Power Increase Estimator Based on a Coupling Factor

This method basically assumes the existence of a coupling factor μ between neighbouring BSs, which gives information on the influence of an increase of the power transmitted by the a BS in the neighbouring cells. This factor is set based on network planning dimensioning. The power increase in a neighbouring BS #*k* after the admission of the new UE in a serving BS #*i* can be estimated as

$$\Delta P_k^{est} = \mu \Delta P_i^{est}. \tag{A.17}$$

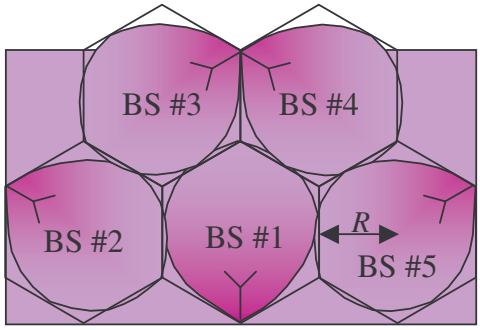

Figure A.2. Cell layout for downlink MC AC simulations.

A.2.2 Single Cell Power Increase Estimator

Although the goal of this document is not to look into a new power increase estimator (PIE) for SC, it is necessary to use one for this study. Let us employ a similar expression for single transmit antenna to the one presented in for beam-forming antenna array in downlink [74]

$$\Delta P_i^{est} = P_i \beta \left[1 + \frac{\left(1-\alpha_{i,N_i+1}\right)\rho_{1,N_i+1}}{G_{i,N_i+1}} \right] + \frac{\rho_{i,N_1+1}}{G_{i,N_1+1}} \left[\frac{P^{pilot}}{\rho_{i,N_i+1}^{pilot,i}} - P_i \right], \tag{A.18}$$

where the serving BS is the one labelled as #i, and the new user is numbered as N_i+1.The factor β can be calculated in an approximate way according to the expression

$$\beta = 1 + \frac{\rho_{i,N_i+1}}{2G_{i,N_i+1}}. \tag{A.19}$$

A.3 Model for Simulations

A.3.1 System Model and Parameters

The cell grid employed for the simulations is composed of 5 cells, as shown in Figure A.2, everyone equipped with a sector antenna that covers 120 degrees. The downlink orthogonality factor (α) for every user is assumed to be Gaussian distributed, but only considering positive values. The mean value of α is assumed to be known to the PIE. The rest of the cellular system model and the associated assumptions are the same as those described in Section 2.3 for the corresponding uplink case. Table A.1 summarises the parameter set employed for the downlink simulations.

A.3.2 System Load

The operation of the simulator is also as described in Figure 2.5. The UEs' data rate is modelled according to the traffic case 1 defined in Section 2.3.3 for the uplink case. Let us define the fractional load factor in a BS for the downlink case as the quotient between the total power transmitted by the BS and P_{max}. For this downlink study, only the case of initial non-homogeneous load (Figure 2.6) is considered, which is the one where all the capacity gain is expected. The initial load factor is 0.10 at BS #1, and 0.35 at BSs #2-#7.

Parameter		Value
Cell radius (R)		667 m
Antenna radiation pattern		$\begin{cases}(\cos(\phi))^{3.2} & \text{if } \lvert\phi\rvert < 90 \\ 0 & \text{otherwise}\end{cases}$
Antenna gain		13 dBi
Standard deviation for shadow fading		8 dB
Radio prop. attenuation with distance		137.4+35.2log(d) [dB]
Mean and standard deviation of α [7]	ITU Pedestrian A	E[α]=0.9; σ_α=0.1
	ITU Vehicular A	E[α]=0.6; σ_α=0.2
Fast PC iterations between admissions		30
Fast PC step size		1 dB
Required Eb/No for UEs (ρ)		8 dB
Background noise level (P_{noise})		-99.9 dBm
Standard deviation of pilot report error		1 dB
Mean value of the pilot report error		0 dB
Maximum transmit power		15 w
Power offset (P_{offset}) range for AC		0 – 5 dB
Pilot power (P^{pilot})		1 w

Table A.1. Parameters employed for the downlink simulations.

A.4 Simulation Results

A.4.1 Results on the Performance of the Power Increase Estimators

Figure A.3 shows the estimation error for the different MC PIEs. The errors for 10% and 90% of the cumulative distribution function (CDF) are summarised in Table A.2. The best estimations are performed by the pilot report based PIE, although this method requires extensive computation. Thus, the coupling factor based PIE can provide only a little worse estimations with almost no computation cost.

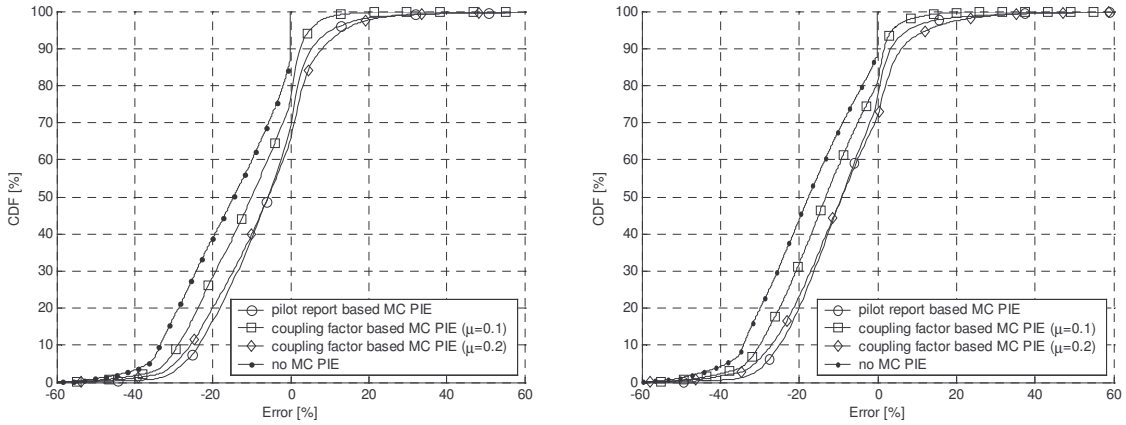

Figure A.3. CDF of the estimation error when using different MC PIE approaches for Pedestrian A (on the left) and Vehicular A (on the right) environments.

MC PIE	Pedestrian A		Vehicular A	
	CDF at 10%	CDF at 90%	CDF at 10%	CDF at 90%
Pilot report based	-23.6 %	5.5 %	-25.0 %	3.4 %
Coupling factor based (μ=0.1)	-28.9 %	2.4 %	-30.1 %	1.7 %
Coupling factor based (μ=0.2)	-25.8 %	8.2 %	-27.1 %	6.1 %
No MC PIE	-33.5 %	-0.1 %	-34.2 %	-0.1 %

Table A.2. Estimation error for CDF values of 10 and 90%.

MC PIE for AC	Capacity gain		Type 3 errors reduction	
	Pedestrian A	Vehicular A	Pedestrian A	Vehicular A
Pilot report based	39.5 %	34.4 %	28.9 %	58.1 %
Coupling factor based (μ=0.1)	34.8 %	31.0 %	21.0 %	50.4 %
Coupling factor based (μ=0.2)	33.5 %	31.7 %	24.8 %	48.7 %

Table A.3. Capacity increase and reduction in the percentage of Type 3 errors measured at 5% probability of Type 1 errors with different MC AC approaches with respect to SC AC.

A.4.2 Results on the Performance of the Multi Cell Admission Control Algorithm

The simulation results on the performance of the MC AC algorithm based on the different MC PIE approaches are depicted from Figure A.4 to Figure A.6 for Pedestrian A and Vehicular A environments. The throughput increase and the reduction in the number of Type 1 errors due to AC errors in an adjacent BS at 5% probability of reaching an overload situation with the different MC AC algorithms with respect to the SC AC are summarised in Table A.3. The capacity gain is slightly higher for Pedestrian A environments. This is due to the fact that the orthogonality factor suffers from less variations and a better estimation is possible. Nevertheless, the greatest reductions of the probability of Type 3 errors with respect to the Type 1 errors are obtained in Vehicular A, since most of the errors come from the SC PIE.

A.5 Conclusions

The MC AC concept introduced in Chapter 2 for the uplink has been extended for the downlink case. First, a MC PIE based on the pilot report sent by the UEs was derived to calculate the interference that a new UE causes to the neighbouring BSs. A second MC PIE was proposed by assuming the increment of power in the neighbouring BSs to be a constant fraction of the increase in the serving BS.

The performance of the MC AC algorithm with both MC PIEs has been tested by means of Monte Carlo simulations and compared to an equivalent SC scheme that does not consider MC information. The results show slightly higher capacity gain than in the uplink case under non-homogeneous conditions: 39.5% in Pedestrian A and 34.4% in Vehicular A. The performance of the second MC PIE is slightly worse (34.8% capacity gain in Pedestrian A and 31.0% in Vehicular A), but its simplicity makes it more appropriate from the practical point of view.

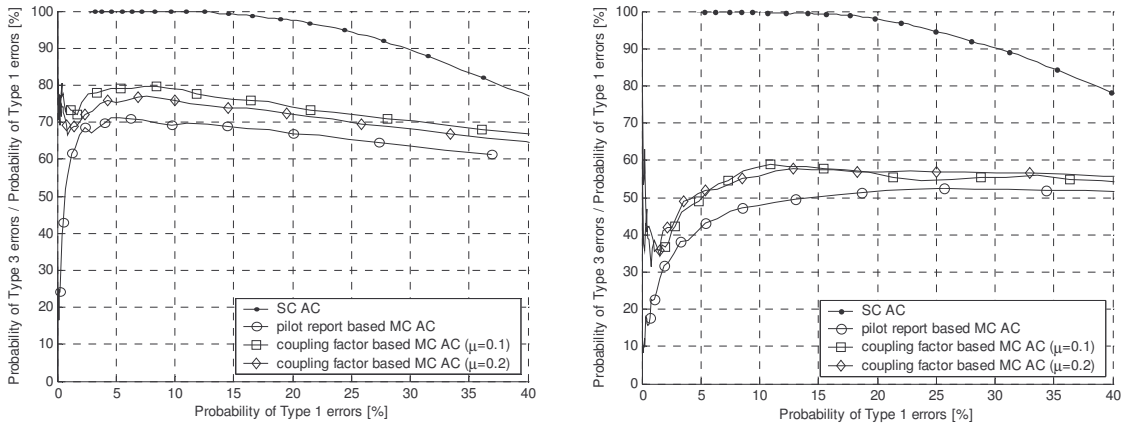

Figure A.4. Ratio of the probability of Type 3 errors to the probability of Type 1 errors when using different AC approaches for Pedestrian A (on the left) and Vehicular A (on the right) environments.

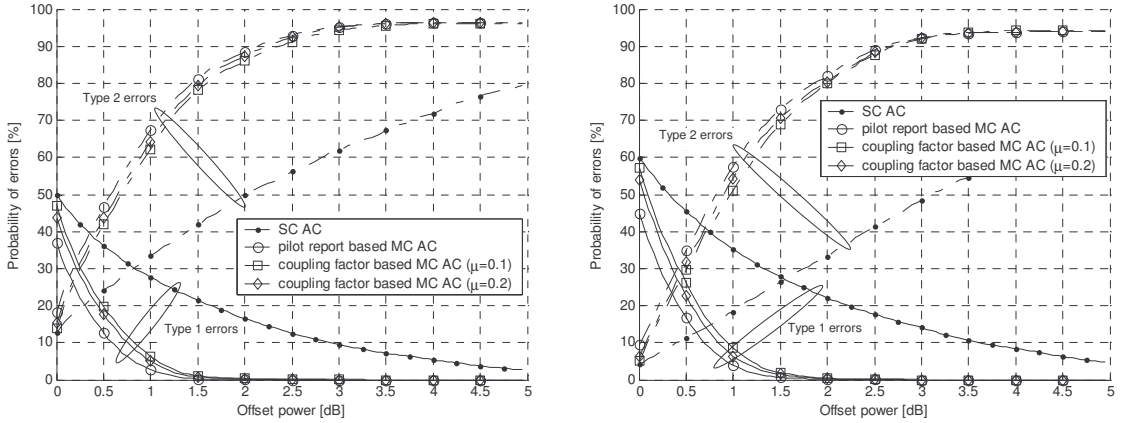

Figure A.5. Probability of Type 1 and Type 2 errors when using different AC approaches for Pedestrian A (on the left) and Vehicular A (on the right) environments.

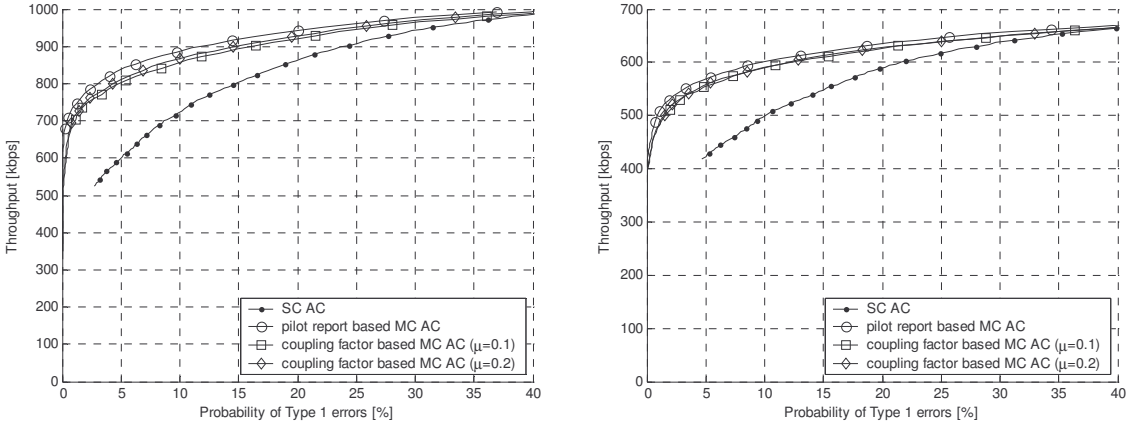

Figure A.6. Average throughput at BS #1 when using different AC approaches for Pedestrian A (on the left) and Vehicular A (on the right) environments.

Appendix B

Generation of Uplink AVI Tables for Different MCSs

The actual value interface (AVI) is a way to connect link and system level simulations. The performance of the link level algorithms, such as decoding, are not measured or analysed in the system level simulations, but they are included based on AVI tables [50].

The generation of these AVI tables is out of the scope of this Ph.D. thesis. However, the use of such tables is crucial in order to perform reliable system level simulations.

Making use of a set of uplink AVI tables for different modulation and coding scheme (MCS) is essential to accomplish the simulation study in Chapter 5. However, they were not immediately available when this Ph.D. investigation was been carried out. At that point, most of the work in this area was concentrated on the downlink part, and in this respect, link level studies with different MCSs were dedicated to provide AVI tables for High Speed Downlink Packet Access (HSDPA) [75].

In this appendix the steps used to obtain approximate uplink AVI tables for different MCSs are presented. These AVI tables for different MCSs are obtained from a reference uplink AVI table associated with BPSK with coding rate 1/3, and based on the relative offset between the downlink AVI values for the desired MCSs and the values for BPSK with coding rate 1/3. This is possible by assuming the relative difference (in dB) between the AVI tables for different MCSs to be the same in downlink and uplink.

There are several ways of measuring the ratio between the received level of the desired signal and the level of the interference, depending on where they are taken. Figure B.1 shows several points where to take measurement of the ratio of signal to interference based on the basic block diagram of a WCDMA receiver. SIR is the total wideband signal-to-interference power ratio at the input of the receiver, $(Eb/No)_{bd}$ and $(Es/No)_{bd}$ are the energy-per-bit to noise ratio

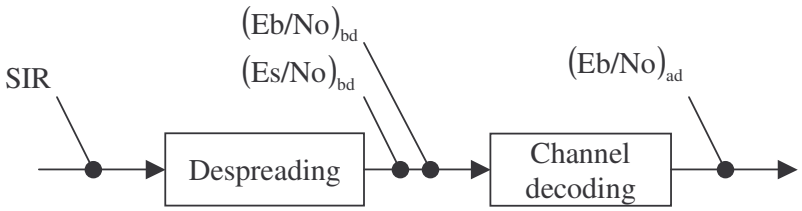

Figure B.1. Different possible measurements of the ratio between the received level of the desired signal and the interference.

(Eb/No) and the energy-per-symbol to noise ratio (Es/No) before the channel decoding block, respectively, and $(\text{Eb/No})_{\text{ad}}$ is the Eb/No after the channel decoding block.

The AVI functions in Figure B.2 were generated in [75] for different MCSs in downlink, and they give the block error rate (BLER) as a function of the $(\text{Es/No})_{\text{bd}}$. In this case the energy per symbol is referred to coded data, and is measured at the input of the receiver, and the Es/No is obtained by

$$(\text{Es/No})_{\text{bd}} = \text{SIR SF}, \tag{B.1}$$

where SF is the spreading factor, defined as

$$\text{SF} = \frac{R_c}{R_s}, \tag{B.2}$$

where R_c is the chip rate and R_s is the symbol rate measured before the channel decoding block.

The Eb/No before channel decoding can be obtained as

$$(\text{Eb/No})_{\text{bd}} = (\text{Es/No})_{\text{bd}} \frac{R_s}{R_{b,bd}} = \text{SIR} \frac{R_c}{R_{b,bd}}, \tag{B.3}$$

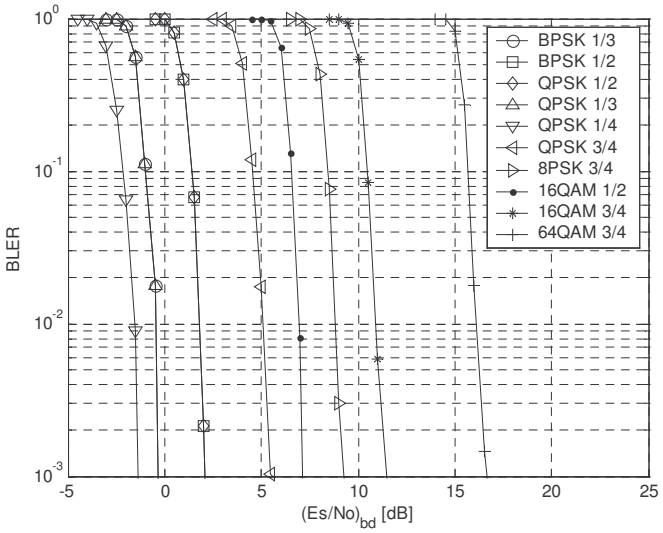

Figure B.2. AVI tables for downlink in a Pedestrian A environment: BLER as a function of the Es/No measured before channel decoding.

where $R_{b,bd}$ is the bit rate measured before the channel decoding block.

From these curves it is possible to obtain the relative Es/No offset at e.g. 1% BLER for all the MCSs with respect to the reference case, i.e. BPSK with coding rate 1/3. The relative $(\text{Es/No})_{\text{bd}}$ offset for MCS #*k* is

$$\Delta(\text{Es/No})_{\text{bd}}^{\text{k}} = \frac{(\text{Es/No})_{\text{bd}}^{\text{k}}}{(\text{Es/No})_{\text{bd}}^{\text{ref}}}, \tag{B.4}$$

where $(\text{Es/No})_{\text{bd}}^{\text{k}}$ and $(\text{Es/No})_{\text{bd}}^{\text{ref}}$ are the required $(\text{Es/No})_{\text{bd}}$ at 1% BLER for MCS #*k* and for BPSK with coding rate 1/3, respectively.

However, the input to the AVI tables normally employed in network simulators is the Eb/No at the input of the channel decoding block, but referred to the bit rate at the output of such a block, calculated as

$$(\text{Eb/No})_{\text{ad'}} = \text{SIR}\,\frac{R_c}{R_{b,ad}}, \tag{B.5}$$

where $R_{b,ad}$ is the bit rate measured at the output of the channel coding block, calculated as

$$R_{b,ad} = R_{b,bd} R_{coding}, \tag{B.6}$$

where R_{coding} is the coding rate.

Notice that $(\text{Eb/No})_{\text{ad'}}$ is different from $(\text{Eb/No})_{\text{ad}}$ because it does not include the coding gain. The coding gain is on the contrary included in the AVI tables.

A relation between $(\text{Eb/No})_{\text{ad'}}$ and $(\text{Es/No})_{\text{bd}}$ can be obtained from (B.3), (B.5) and (B.6)

$$(\text{Eb/No})_{\text{ad'}} = (\text{Es/No})_{\text{bd}}\,\frac{R_s}{R_{b,bd}}\,\frac{1}{R_{coding}}. \tag{B.7}$$

The relative Eb/No offset after channel decoding with MCS #*k* referred to the case of BPSK and coding rate 1/3 is

$$\Delta(\text{Eb/No})_{\text{ad'}}^{\text{k}} = \frac{(\text{Eb/No})_{\text{ad'}}^{\text{k}}}{(\text{Eb/No})_{\text{ad'}}^{\text{ref}}} = \frac{(\text{Es/No})_{\text{bd}}^{\text{k}}\,\dfrac{R_s^k}{R_{b,bd}^k}\,\dfrac{1}{R_{coding}^k}}{(\text{Es/No})_{\text{bd}}^{\text{ref}}\,\dfrac{1}{1/3}} = \Delta(\text{Es/No})_{\text{bd}}^{\text{k}}\,\frac{N_b^k}{3R_{coding}^k}, \tag{B.8}$$

where $(\text{Eb/No})^{\text{k}}_{\text{ad'}}$ and $(\text{Eb/No})^{\text{ref}}_{\text{ad'}}$ are the required $(\text{Eb/No})_{\text{ad}}$ at 1% BLER for MCS #*k* and for BPSK with coding rate 1/3, respectively; R^k_s, $R^k_{b,bd}$ and R^k_{coding} are the values of R_s, $R_{b,bd}$ and R_{coding} for MCS #*k*, respectively; and N^k_b is the number of bits per symbol with MCS #*k*. Notice that in BPSK, the symbol rate equals the bit rate.

Since the offset values were assumed to be equal in downlink and in uplink, the AVI curves for the different MCSs in uplink can be obtained by applying the calculated offset to the reference curve for BPSK with coding rate 1/3 [49].

This thesis considers the case where the user equipments (UE) transmit over one Dedicated Physical Data Channel (DPDCH) and one Dedicated Physical Control Channel (DPCCH). In that case it is not possible to directly apply the offset in (B.8) to obtain the AVI tables for different MCSs based on the curves plotted in Figure B.2, since in such curves the DPCCH (with BPSK modulation) is not considered. It is therefore necessary to derive a method to

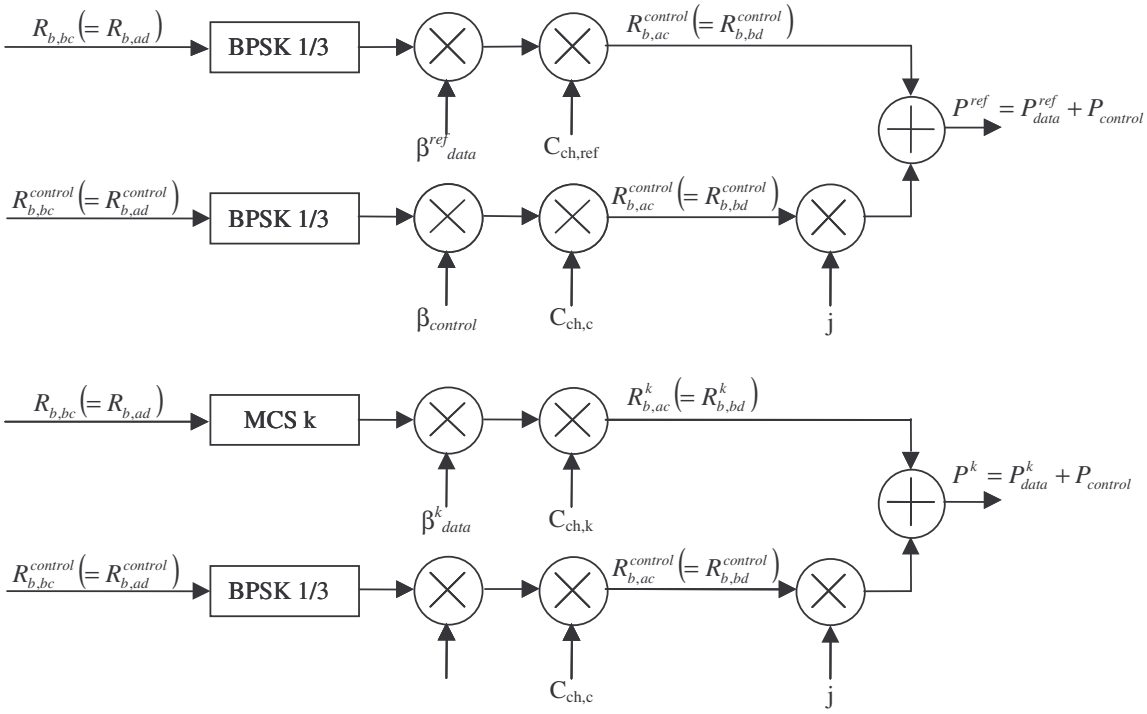

Figure B.3. Uplink transmission schemes based on one DPDCH and one DPCCH.

convert the offset without DPCCH into an offset where the effect of a DPCCH is considered.

Let us assume the transmission schemes shown in Figure B.3. In Figure B.3, $R^{control}_{b,bd}$ and $R^{control}_{b,ad}$ are the control bit rate before and after channel decoding, respectively, P^{ref} and P^{k} are the total required transmission power for UEs using BPSK with 1/3 for control and BPSK with coding rate 1/3 and MCS *#k* for data, respectively, R^{ref}_{data} and R^{k}_{data} are the required transmission power for data when using BPSK with coding rate 1/3 and MCS #*k*, respectively, $P_{control}$ is the required transmission power for control information when using BPSK with coding rate 1/3, and $c_{ch,c}$, $c_{ch,k}$ and $c_{ch,ref}$ are the channelisation codes employed for the control channel and for data channels with MCS #*k* and BPSK 1/3, respectively; β^{ref}_{data}, β^{k}_{data} and $\beta_{control}$ are weight factors to obtain the required final control-to-data power ratio. Notice that the subscripts *bc* and *ac* stand for "before channel coding" and "after channel coding", respectively, and are equivalent to *ad* and *bd*, respectively ("after channel decoding" and "before channel decoding") when referring to bit rates.

The power penalty from transmitting data bits with MCS *#k* with respect to BPSK with coding rate 1/3 is

$$\varepsilon^{k}_{data}=\frac{P^{k}_{data}}{P^{ref}_{data}}. \tag{B.9}$$

The factor ε^{k}_{data} is the power efficiency of using BPSK with coding rate 1/3 for data instead of MCS #*k*. The ratio of power required for control with respect to data when using BPSK with coding rate 1/3 is

$$p=\frac{P_{control}}{P^{ref}_{data}}. \tag{B.10}$$

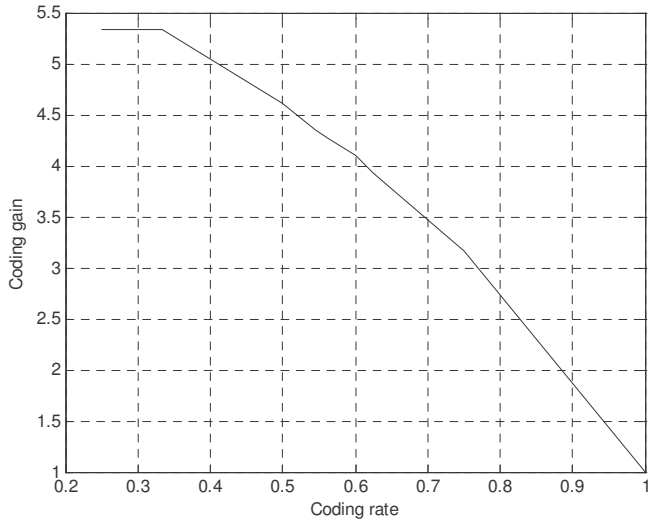

Figure B.4. Coding gain versus the coding rate obtained at 1% BLER from to the AVI tables in Figure B.2.

The quotient between the total power at the output of both schemes is

$$\varepsilon^k = \frac{P^k}{P^{ref}} = \frac{P^k_{data} + P_{control}}{P^{ref}_{data} + P_{control}} = \frac{\varepsilon^k_{data} + p}{1+p}. \tag{B.11}$$

The factor ε^k_{data} is actually a measure of the extra required energy per bit after channel decoding to reach the same BLER when using MCS #*k* instead of BPSK with coding rate 1/3 for the DPDCH. The factor ε^k_{data} is therefore equivalent to $\Delta(\text{Eb/No})^k_{ad'}$. The factor ε^k gives the extra energy per bit after channel decoding when using MCS #*k* instead of BPSK with coding rate 1/3 considering one DPDCH and one DPCCH per UE

$$\Delta(\text{Eb/No})^k_{ad',DPCCH} = \varepsilon^k = \frac{\Delta(\text{Eb/No})^k_{ad'} + p}{1+p} = \frac{\Delta(\text{Es/No})^k_{bd}\dfrac{N^k_b}{3R^k_{coding}} + p}{1+p}. \tag{B.12}$$

It is also possible to generate AVI tables for MCSs with coding rates different from the ones presented in Figure B.2. This can be done before including the effect of the DPCCH based on the $(\text{Es/No})_{bd}$ required for another scheme with the same modulation

$$(\text{Es/No})^k_{bd} = (\text{Es/No})^m_{bd}\frac{G^m_{coding}}{G^k_{coding}}\frac{R^k_{coding}}{R^m_{coding}}, \tag{B.13}$$

where *k* and *m* refer to MCSs with the same modulation, and G^k_{coding} and G^m_{coding} are the coding gains obtained by applying the coding rate associated with MCSs #*k* and #*m*, respectively. The values of the coding rates can be calculated from the curve in Figure B.4. The coding gain is defined as the gain in the required $(\text{Eb/No})_{ad}$ when a coding rate different from one is applied to the signal while maintaining the same effective throughput. Notice from Figure B.4 that there is no gain from changing the coding rate from 1/3 to 1/4. The reason is that the values of the coding gain plotted in this figure do not correspond to the optimum cases where the best coding algorithm is selected (e.g., the particular case of coding rate of 1/4 was performed by adding some repetition to the output of an encoder with a rate of

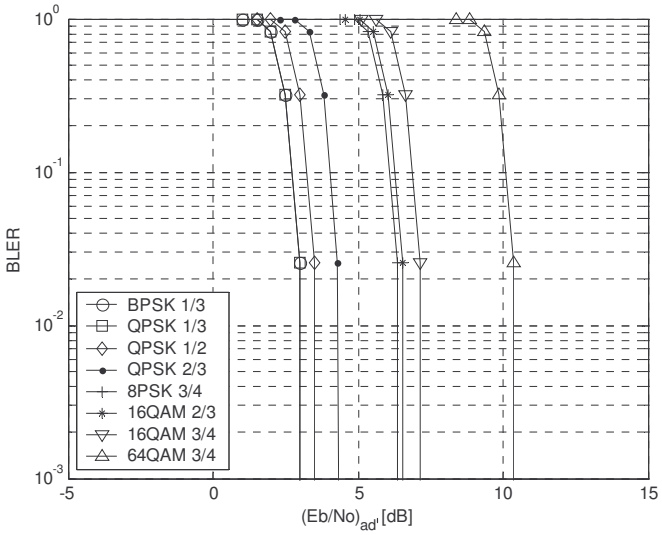

Figure B.5. Approximate uplink AVI tables for different MCSs: BLER as a function of the Eb/No measured before channel decoding, but referred to the bit rate at the output of such a block.

1/3).

The AVI tables shown in Figure B.5 have been generated for different MCSs in uplink, based on the procedure described in this appendix, starting from the curve for BPSK with coding rate 1/3 presented in [49] (Figure B.5) for a circuit-switched service at 64kbps with one DPDCH and one DPCCH in Pedestrian A environment and a UE speed of 3 km/h. In this case, p=-5.46 dB [49].

Appendix C

Impact of High Order Modulations on the PAR

C.1 Introduction

Using higher order modulation schemes for the Dedicated Physical Data Channels (DPDCH) instead of BPSK causes a variation in the peak-to-average ratio (PAR) of the signal transmitted by the user equipments (UE) in the uplink. The same effect is present when using BPSK with several parallel DPDCHs [76]. The PAR of the signal is an important parameter that has to be taken into consideration, as it limits the maximum average power that can be transmitted by the UE in order not to reach the non-linear part of the transmit amplifier. An increase in the PAR may saturate the power amplifier and cause out-of-band interference. This can be solved with the use of amplifiers designed with large back-off factor; however this reduces their efficiency and the battery life, and increases the costs.

The PAR is therefore a very important issue for the design of UE terminals, which has previously been investigated for CDMA systems in [77], [78], [79], [80].

This appendix studies the impact on the PAR caused by the use of higher order modulations than BPSK for the DPDCHs. The value of the PAR is calculated for several transmit configurations.

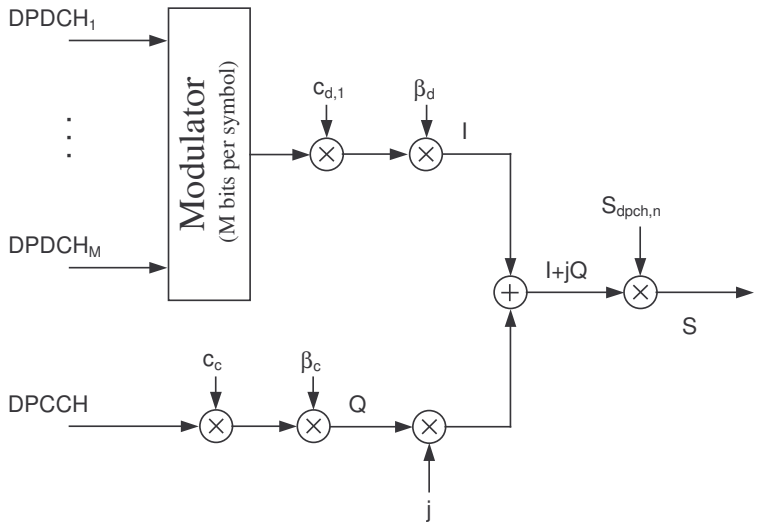

Figure C.1. Alternative transmission scheme with higher order modulation.

C.2 Characterisation of the PAR

The generic structure of an uplink transmitter according to 3GPP [10], [9] was presented in Figure 1.2. Notice that the 3GPP specifications only allow the use of parallel DPDCHs for a spreading factor (SF) of 4. An equivalent WCDMA transmitter equipped with a higher order modulator for the DPDCHs could have the block diagram proposed in Figure C.1. Notice that the use of higher order modulations with a single DPDCH can be utilised instead of both an equivalent scheme with parallel DPDCHs or an equivalent scheme with only one DPDCH and higher SF.

The PAR is defined as the ratio of the peak envelope power to the average envelope power. In this study, the PAR is measured at the output of the root raised cosine pulse shape filter [10]. This definition is consistent with the results provided in [76], [77], [81]. For the calculation of the values of the PAR presented in this appendix, the pulsing shape filter is run at a sampling rate 64 times faster than the chip time (T_c); the impulse response is non-zero for time values within the range [$-5T_c$,$5T_c$]. The PAR is normally represented in probabilistic terms; in the literature it is used the value of the PAR that is not exceeded with probability of 0.1% [76], [77], [81].

C.3 PAR with Higher Order Modulations

As it has already been mentioned, the use of a DPDCH with higher order modulation than BPSK is proposed as an alternative method to the use of several parallel DPDCHs or to the use of a single DPDCH with lower SF; in this Ph.D. thesis, the purpose is in both cases to reduce the channelisation code utilisation per UE.

Total data rate	Structure of the transmitter	PAR at 0.1% outage
384 kbps	1 DPDCH with BPSK	2.9 dB
768 kbps	2 DPDCHs with BPSK	3.4 dB
	2 DPDCHs with QPSK	3.4 dB
1152 kbps	3 DPDCHs with BPSK	5.0 dB
	3 DPDCHs with 8PSK	3.3 dB
1536 kbps	4 DPDCHs with BPSK	5.1 dB
	4 DPDCHs with 16QAM	5.0 dB

Table C.1. PAR at 0.1% outage for several uplink transmit configurations with a SF of 4 for the DPDCHs.

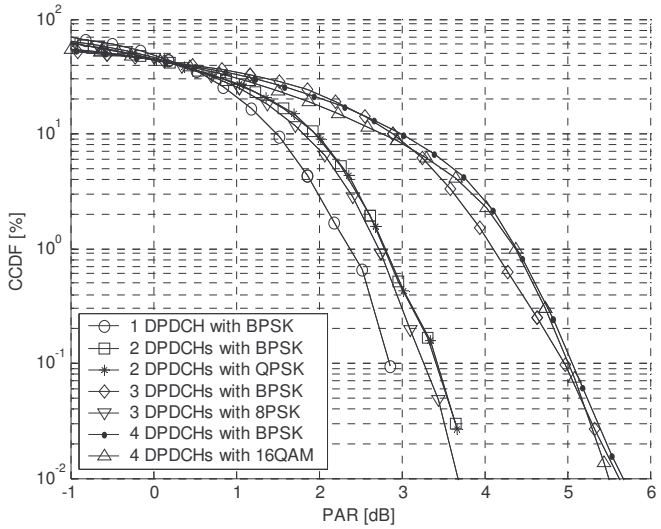

Figure C.2. CCDF of the PAR for several uplink transmit configurations with a SF of 4 for the DPDCHs.

C.3.1 PAR with Higher Order Modulations instead of Several Parallel DPDCHs

Figure C.2 shows the complementary cumulative distribution function (CCDF) of the PAR for several transmit configurations, where the channelisation code is applied with a SF of 4 to the data channels. Notice that the same coding rate is assumed for all the cases, with such a value that allows transmitting with a bit rate of 384 kbps per DPDCH. All the cases include a control channel with a Dedicated Physical Control Channel (DPCCH) to DPDCH power ratio of -10 dB [81]. The PAR corresponding to the values of the CCDF of 0.1% are presented in Table C.1. An important point that should be stressed is the fact that the cases of 2 DPDCHs with both BPSK and QPSK modulation present the same curve of the PAR. The reason is that such cases are actually the same, since, according to 3GPP, when using parallel DPDCHs with BPSK modulation, the scrambling codes should be shared by every couple of them: since both of them are I-Q multiplexed, this corresponds to QPSK modulation in terms of signalling shape, PAR and spectral efficiency.

Notice that, the higher the number of DPDCHs per UE with BPSK modulation is, the greater the PAR. This also happens when using higher order modulations. However, the PAR at 0.1%

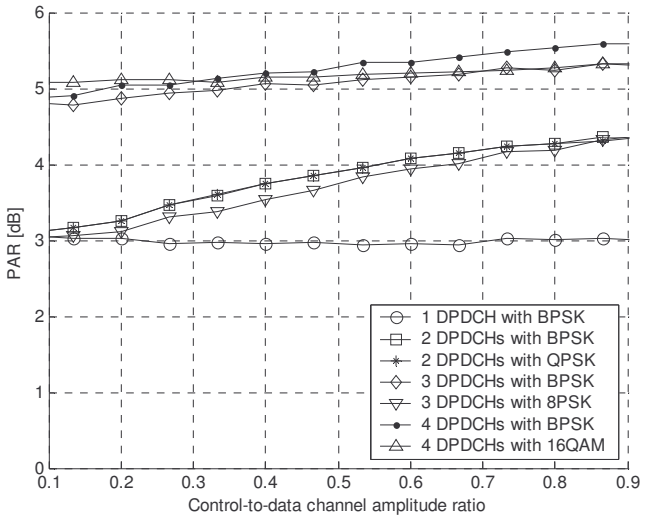

Figure C.3. PAR at 0.1% outage as a function of the control-to-data amplitude ratio for several uplink transmit configurations.

outage with parallel DPDCHs and higher order modulations is never higher than the corresponding cases with BPSK modulation. In fact, the use of 8PSK for 3 parallel DPDCHs drastically improves the PAR compared to BPSK, and also even to the case of 2 parallel DPDCHs.

Figure C.3 summarises the PAR at 0.1% outage as a function of the ratio of the amplitude of control channel to the data channels for several modulation schemes. For the case of one single DPDCH with BPSK, the PAR does not vary with the ratio between control and data power. However, with several parallel DPDCHs, the PAR increases when the control-to-data channel power ratio is higher. Since a higher value of such ratio corresponds to a low data rate, and vice versa, from Figure C.3 it is concluded that the use of 2 or 3 parallel DPDCHs with either BPSK or a higher order modulation would have a negligible effect on the PAR for high data rates.

C.3.2 PAR with Higher Order Modulations Instead of One Single DPDCH with Lower Spreading Factor

Figure C.4 plots the CCDF of the PAR for the transmit configurations presented in Figure 5.3 and Figure 5.4 assuming a circuit-switched service with a data rate of 64 kbps, which corresponds to the cases of 1 DPDCH with BPSK modulation (SF 16) and QPSK modulation (SF 32), respectively. Moreover, both cases include 1 DPCCH with a SF of 256. These situations are those considered in Chapter 5. The channelisation code utilisation per UE is reduced with use of QPSK at the expense of an increase of 0.7 dB in the PAR at the 0.1% level of the CCDF.

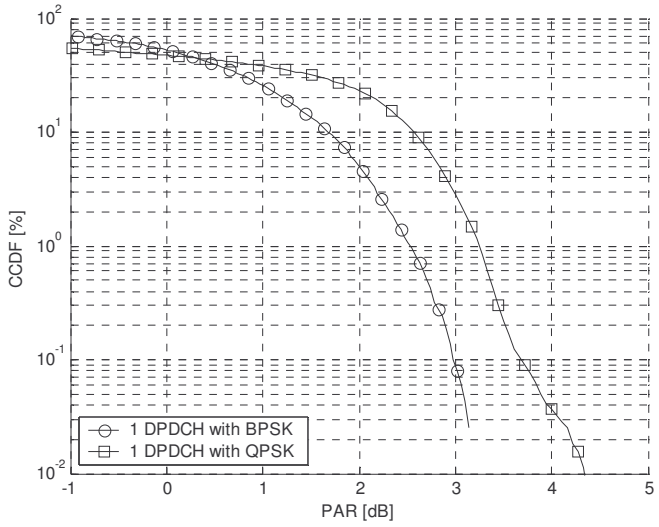

Figure C.4. CCDF of the PAR for two different uplink transmit configurations corresponding to circuit-switched service at 64 kbps.

Appendix D

Effective Noise Rise for Synchronous Uplink

As it has repeatedly been stated throughout this Ph.D. thesis, the noise rise (NR) is a good measurement of the load in uplink asynchronous WCDMA, because it shows the amount of interference received at the base station (BS) from all the user equipments (UE). Nevertheless, as in synchronous uplink the NR grows with lower slope than in the asynchronous case, the stability of the system is higher for the same NR target (see e.g. Figure 4.1). This is due to the fact that the received power increase caused by the admission of a new synchronous UE is partly cancelled by the rest of UEs under the same scrambling code. The relative increase in the power transmitted by these UEs to again fulfil their energy-per-bit to noise ratio (Eb/No) requirements will be smaller than the power from the rest.

A higher NR target for uplink synchronisation than for an equivalent asynchronous scheme could keep the same system stability margin while providing capacity gain. An effective NR that considers this effect is presented in this appendix as a measure of the load in uplink synchronous WCDMA systems.

Let us define the effective interference power at a BS associated with a synchronous UE with scrambling code #*j* as the wideband interference power that cannot be cancelled after despreading and is only reduced by the processing gain, i.e.

$$P_j^{eff} = P_{total} - P_{scr,j}\alpha_j, \tag{D.1}$$

where $P_{scr,j}$ is the power received at the BS from all the UEs under scrambling code #*j*, and α_j is the orthogonality factor associated with the UEs under scrambling code #*j*. For asynchronous UEs, the orthogonality factor equals zero. In the sequel, the same value of the

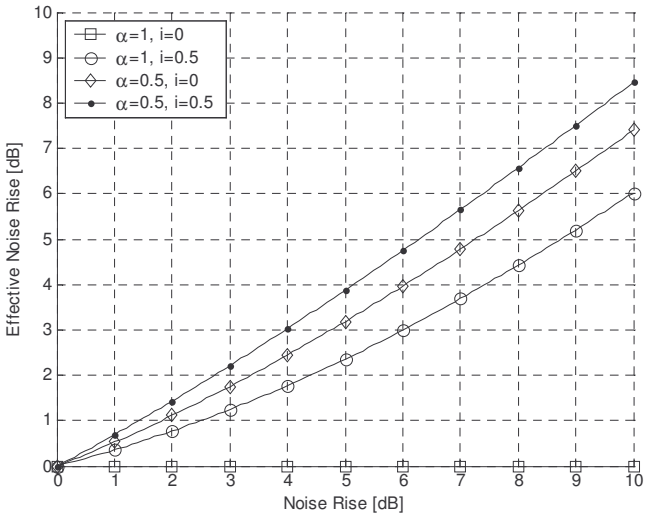

Figure D.1. Effective NR versus NR for synchronous WCDMA assuming one scrambling code per BS.

orthogonality factor α will be assumed for all the synchronous UEs with the same scrambling code.

The effective interference power in a BS is calculated as the average effective interference power associated with all the UEs of the BS, pondered according to the power they generate at the BS

$$P_{total}^{eff} = \sum_{j=1}^{J}\left(\frac{P_{scr,j}}{P_{own}} P_j^{eff}\right) = P_{total} - \alpha \sum_{j=1}^{J} \frac{P_{scr,j}}{P_{own}} P_{scr,j}, \tag{D.2}$$

where J is the number of active scrambling codes at the BS, and P_{own} is the own cell power received at the BS.

From (5.5), the power from the UEs of the own cell can be expressed as

$$P_{own} = \frac{P_{total} - P_{noise}}{i+1}, \tag{D.3}$$

where P_{noise} is the background noise power and i is the other-to-own cell interference ratio.

The effective NR can be calculated by introducing (D.3) in (D.2)

$$NR^{eff} = \frac{P_{total}^{eff}}{P_{noise}} = NR - \frac{\alpha(1+i)}{NR-1} \sum_{j=1}^{J} \left(NR_{scr,j}\right)^2, \tag{D.4}$$

where

$$NR = \frac{P_{total}}{P_{noise}}, \text{ and} \tag{D.5}$$

$$NR_{scr,j} = \frac{P_{scr,j}}{P_{noise}}. \tag{D.6}$$

The effective NR is plotted as a function of the NR in Figure D.1 for several cases, assuming

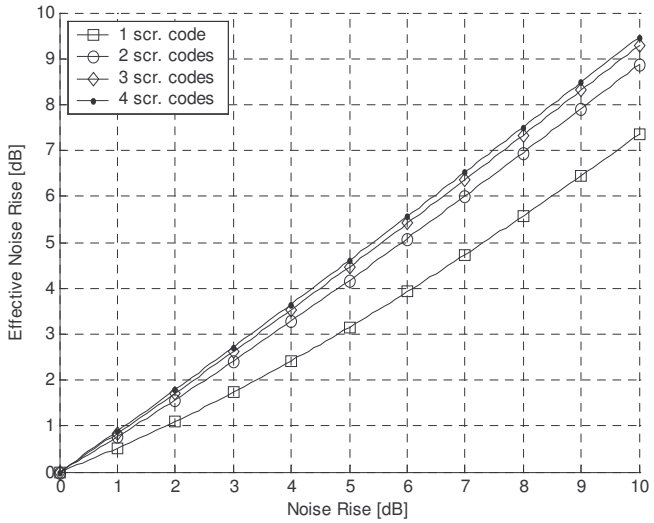

Figure D.2. Overestimated effective NR versus NR for synchronous WCDMA with α=0.96, i=0.86, and various numbers of scrambling codes per BS.

that there is one only active scrambling code per BS.

An overestimate of the effective NR for the case where all the UEs support synchronous mode can be obtained by assuming that all the scrambling codes allocated to own cell UEs generate the same interference power at the BS, i.e.

$$P_{scr,j} = P_{scr} = \frac{P_{own}}{J_{active}}. \tag{D.7}$$

where J_{active} is the number of active scrambling codes in the BS that are currently assigned to UEs.

With this assumption, the effective NR can be estimated by using the expression

$$NR^{eff,est} = NR\left(1 - \frac{\alpha}{(1+i)J_{active}}\right) + \frac{\alpha}{(1+i)J_{active}}. \tag{D.8}$$

Based on (D.8), the overestimation of the effective NR is plotted as a function of the NR in Figure D.2 for different numbers of active scrambling codes per BS.

The expression in (D.8) can be extended for the case where not all the UEs in the cell are in synchronous mode,

$$NR^{eff,est} = NR\left(1 - \frac{\alpha\eta_{own,sync}}{(1+i)J_{active}}\right) + \frac{\alpha\eta_{own,sync}}{(1+i)J_{active}}, \tag{D.9}$$

where $\eta_{own,sync}$ is the proportion of the own cell power that is generated by synchronous UEs.

Notice that the definition of the effective NR made in (D.4) gives an idea of the average interference that every UE in the BS is suffering, although it is possible that the real interference values is much higher for some of them. This happens for UEs whose signal has in general a smaller degree of orthogonality with respect to the rest of the interference, due to the channel conditions, the allocation of a low loaded scrambling code or simply because it

does not support uplink synchronisation. In this sense, (D.4) is a good measurement of the uplink load level, but it does not give very accurate information on the degree of stability of the system when both synchronous and asynchronous UEs are served in the BS. On the other hand, the value of the conventional NR is a more conservative measure of the stability of the system, but it does not give such good information of the load level with uplink synchronisation.

An explanation to why it is not reliable to use the effective NR can be given from the expression in (D.9). For a same value of the NR, different fractions of the own cell power coming from synchronous UEs will provide different values of the effective NR.

However there still exist very good reasons for using the effective NR, since this parameter let get a better use of the available capacity with uplink synchronous WCDMA. From the previous results in Section 4.5.4, it is known that the benefit of uplink synchronisation grows gradually with the percentage of synchronous UEs at the BS, which means that for low percentages of synchronous UEs in the BS the capacity gain is very small, and it is not worth deploying such a scheme in the system. Therefore, if this scheme was adopted in WCDMA systems, a minimum percentage of synchronous UEs per cell must be guaranteed. Then, a target value for the effective NR target value could be selected from network planning to keep the system stable under a certain probability. Furthermore, in order to ensure a certain degree of liability for the effective NR as a stability measurement of the network, a more or less conservative value of the average orthogonality factor can be used.

Appendix E

Power Increase Estimator for Uplink

E.1 Introduction

This appendix summarises the description of the power increase estimator (PIE) for uplink made in [26], which is employed throughout this Ph.D. thesis.

E.2 Problem Formulation

The target of the uplink admission control (AC) algorithm is to prevent the overload of the WCDMA system and to guarantee the quality of the existing connections and the planned coverage area of the system. Before a new user is admitted to the system, the AC algorithm estimates the increase in the total interference level due to a new user as shown in Figure E.1.

In Figure E.1, P_{rx} and $P_{rx,new}$ are the total received power before and after the admission of the new user, respectively; the power increase after the admission of the new user is denoted ΔP_{rx}; η and η_{new} are the load factors before and after the admission of the new user, respectively. The load factor is defined as

$$\eta = \frac{P_{rx} - P_{noise}}{P_{rx}}, \tag{E.1}$$

where P_{noise} is the background noise power received at the base station (BS).

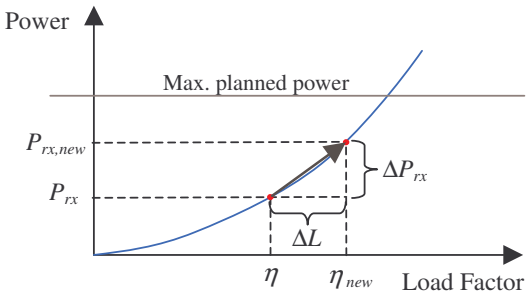

Figure E.1. Uplink admission control and power increase estimation.

The difference between η_{new} and η is approximately the load factor ΔL of the new user requesting resources in the radio access network

$$\Delta L = \frac{1}{1+\frac{R_c}{R_b \rho}}, \tag{E.2}$$

where R_c is the chip rate, R_b is the requested bit rate and ρ is the estimated required energy-per-bit to noise ratio (Eb/No) for that service.

E.3 Uplink Power Increase Estimation

The value of P_{rx} is obtained from (E.1)

$$P_{rx} = \frac{P_{noise}}{1-\eta}. \tag{E.3}$$

Based on this expression, two different PIEs for uplink are derived, a derivative PIE and an integrative PIE.

E.3.1 Derivative PIE

$$\begin{aligned} &\frac{dP_{rx}}{d\eta} = \frac{d}{d\eta}\left(\frac{P_{noise}}{1-\eta}\right) = \frac{P_{noise}}{(1-\eta)^2} \Leftrightarrow \\ &\frac{dP_{rx}}{d\eta} = \frac{P_{noise}}{\left(1-\frac{P_{rx}-P_{noise}}{P_{rx}}\right)^2} = \frac{{P_{rx}}^2}{P_{noise}} = \frac{1}{1-\eta} P_{rx}; \end{aligned} \tag{E.4}$$

$$\begin{aligned} &\Delta P_{rx} \approx \frac{dP_{rx}}{d\eta}\Delta L \Leftrightarrow \\ &\Delta P_{rx} \approx \frac{\Delta L}{1-\eta} P_{rx}. \end{aligned} \tag{E.5}$$

E.3.2 Integrative PIE

$$\Delta P_{rx} = \int_{\eta}^{\eta+\Delta L} dP_{rx} = \int_{\eta}^{\eta+\Delta L} \frac{P_{noise}}{(1-\eta)^2} d\eta \Leftrightarrow$$

$$\Delta P_{rx} = \frac{P_{noise}}{1-\eta-\Delta L} - \frac{P_{noise}}{1-\eta} = \frac{\Delta L}{1-\eta-\Delta L}\frac{P_{noise}}{1-\eta} \Leftrightarrow \tag{E.6}$$

$$\Delta P_{rx} = \frac{\Delta L}{1-\eta-\Delta L} P_{rx}.$$

Appendix F

PIE for Uplink Synchronous WCDMA

A power increase estimator (PIE) is derived for BSs serving both asynchronous and synchronous user equipments (UE) simultaneously. Let us assume a base station (BS) serving both synchronous and asynchronous UEs, where a new synchronous UE makes a request to be served. The BS receives a total wideband power denoted P_{rx} before the admission and $P_{rx,new}$, after it. The BS determines that the UE should be allocated scrambling code #*j* if it was finally admitted in the system.

Let us denote η^{j}_{sync} and $\eta^{j}_{sync,new}$, respectively, the fractions of P_{rx} and $P_{rx,new}$ generated by the UEs under the scrambling code #*j*. The required energy-per-bit to noise ratio (Eb/No) for the *i*-th UE using scrambling code #*j* can be expressed based on the power before and after the admission of the new UE as

$$\rho_{j,i} = G_{j,i}\frac{P^{j,i}}{P_{rx}\left(1-\alpha\eta^{j}_{sync}\right)}, \text{ and}$$
$$\rho_{j,i} = G_{j,i}\frac{P^{j,i}_{new}}{P_{rx,new}\left(1-\alpha\eta^{j}_{sync,new}\right)}, \tag{F.1}$$

respectively, where $P^{j,i}$ and $P^{j,i}{}_{new}$ are the received power at the BS from the *i*-th UE under scrambling code #*j* before and after the admission of the new UE, respectively, $G_{j,i}$ is the processing gain for the *i*-th UE under scrambling code #*j* and α is the orthogonality factor between synchronous UEs using the same scrambling code. For simplicity, the same orthogonality factor is assumed for all the synchronous UEs.

From (F.1) it is possible to derive the fractions of P_{rx} and $P_{rx,new}$ generated by the i-th UE with scrambling code #j, which are respectively

$$L^{j,i} = \frac{P^{j,i}}{P_{rx}} = \frac{\rho_{j,i}}{G_{j,i}}\left(1-\alpha\eta^{j}_{sync}\right),$$
$$L^{j,i}_{new} = \frac{P^{j,i}_{new}}{P_{rx,new}} = \frac{\rho_{j,i}}{G_{j,i}}\left(1-\alpha\eta^{j}_{sync,new}\right). \tag{F.2}$$

From (F.2), the proportion of the total received power from UEs with scrambling code #j before and after the admission can be expressed as

$$\eta^{j}_{sync} = \sum_{i=1}^{N_j} L^{j,i} = \left(1-\alpha\eta^{j}_{sync}\right)\sum_{i=1}^{N_j}\frac{\rho_{j,i}}{G_{j,i}}, \text{ and}$$
$$\eta^{j}_{sync,new} = \sum_{i=1}^{N_j+1} L^{j,i}_{new} = \left(1-\alpha\eta^{j}_{sync,new}\right)\sum_{i=1}^{N_j+1}\frac{\rho_{j,i}}{G_{j,i}}, \tag{F.3}$$

respectively, where N_j is the number of UEs under scrambling code #j before admitting the new UE. Notice that the candidate UE is referred to as the (N_j+1)-th user under scrambling code #j. By combining the equations in (F.3), we can express $\eta^{j}_{sync,new}$ as

$$\eta^{j}_{sync,new} = \frac{\eta^{j}_{sync} + \Delta L}{1+\alpha\Delta L}, \tag{F.4}$$

where

$$\Delta L = \left(1-\alpha\eta^{j}_{sync}\right)\frac{\rho_{j,N_j+1}}{G_{j,N_j+1}}. \tag{F.5}$$

Let us also denote η^{j}_{async} and $\eta^{j}_{async,new}$ the fractions of P_{rx} and $P_{rx,new}$ from the rest of UEs in the network that do not use scrambling code #j. In this sense,

$$\eta = \eta^{j}_{sync} + \eta^{j}_{async} \quad \forall j,$$
$$\eta_{new} = \eta^{j}_{sync,new} + \eta^{j}_{async,new} \quad \forall j, \tag{F.6}$$

where η and η_{new} are the load factors before and after the admission of the new UE, respectively, defined as

$$\eta = \frac{P_{rx} - P_{noise}}{P_{rx}},$$
$$\eta_{new} = \frac{P_{rx,new} - P_{noise}}{P_{rx,new}}, \tag{F.7}$$

where P_{noise} is the background noise power received at the BS. From (F.7) it is easy to derive

$$P_{rx} = \eta P_{rx} + P_{noise}, \tag{F.8}$$

$$P_{rx,new} = \eta_{new} P_{rx,new} + P_{noise}.$$

The power increase at the BS after the admission of the new synchronous UE under the scrambling code #*j* is

$$\begin{aligned} \Delta P_{rx} &= P_{rx,new} - P_{rx} = \eta_{new} P_{rx,new} - \eta P_{rx} = \\ &= \left(\eta^{j}_{async,new} + \eta^{j}_{sync,new}\right)\left(P_{rx} + \Delta P_{rx}\right) - \left(\eta^{j}_{async} + \eta^{j}_{sync}\right)P_{rx}. \end{aligned} \tag{F.9}$$

Let us assume $\eta^{j}_{async,new}=\eta^{j}_{async}$. With this approximation the other cell interference is assumed to grow in the same proportion as the interference from the own cell UEs under scrambling codes different from #*j*. By applying this assumption in (F.9), the power increase at the BS can be (over) estimated as

$$\Delta P^{over}_{rx} = \frac{\eta^{j}_{sync,new} - \eta^{j}_{sync}}{1 - \eta^{j}_{async} - \eta^{j}_{sync,new}} P_{rx}. \tag{F.10}$$

The final expression of the PIE is obtained by substituting (F.4) in (F.10)

$$\Delta P^{over}_{rx} = \frac{\Delta L\left(1 - \alpha \eta^{j}_{sync}\right)}{1 - \eta - \Delta L\left(1 - \alpha\left(1 - \eta^{j}_{async}\right)\right)} P_{rx}. \tag{F.11}$$

This results is only valid if the stability condition $\eta_{new}<1$ is fulfilled, i.e.

$$\eta^{j}_{async} + \frac{\eta^{j}_{sync} + \Delta L}{1 + \alpha \Delta L} < 1. \tag{F.12}$$

By making $\alpha=0$, $\eta^{j}_{async}=\eta$ and $\eta^{j}_{sync}=0$, (F.11) and (F.12) can also be used to estimate the power increase caused by asynchronous UEs.

Let us recall that the expression in (F.11) gives an overestimation of the power increase, since it assumes the other cell interference to increase proportionally to the increase of the own cell power from UEs under scrambling codes different from #*j*.

An underestimation of the power increase could be calculated by assuming that the other cell interference does not increase after the admission of the new UE. Equation (F.9) can be approximated as

$$\begin{aligned} \Delta P^{under}_{rx} &= \left(P^{own}_{rx,new} + P^{other}_{rx} + P_{noise}\right) - \left(P^{own}_{rx} + P^{other}_{rx} + P_{noise}\right) = \\ &= \left(\eta^{j}_{async,own} + \eta^{j}_{sync,new}\right)\left(P_{rx} + \Delta P_{rx}\right) - \left(\eta^{j}_{async,own} + \eta^{j}_{sync}\right)P_{rx}. \end{aligned} \tag{F.13}$$

where P_{rx}^{own} and $P_{rx,new}^{own}$ are respectively the own cell power before and after the admission of the new UE, P_{rx}^{other} is the other cell interference before the admission of the new UE, and $\eta^{j}_{async,own}$ is the fraction of P_{rx} generated by the own cell UEs under scrambling codes different from *j*, and is calculated as

$$\eta^{j}_{async,own} = \frac{\eta}{i+1} - \eta^{j}_{sync}, \tag{F.14}$$

where *i* is the other-to-own cell interference ratio.

By substituting (F.4) and (F.14) in (F.13) it yields

$$\Delta P_{rx}^{under} = \frac{\Delta L\left(1-\alpha\eta_{sync}^{j}\right)}{\left(1-\frac{\eta}{i+1}\right)\left(1+\alpha\Delta L\right)-\Delta L\left(1-\alpha\eta_{sync}^{j}\right)} P_{rx}. \tag{F.15}$$

As the estimated value of η_{new} is smaller in this underestimation than in the overestimation made to obtain the expression in (F.11), the condition in (F.12) is sufficient to consider the value calculated in as valid.

The power increase can be estimated as an intermediate value, pondering the over and the underestimation as follows

$$\Delta P_{rx}^{est} = \omega\Delta P_{rx}^{over} + (1-\omega)\Delta P_{rx}^{under}. \tag{F.16}$$

where $\omega \in [0,1]$ is a weight parameter that can be determined adaptively or can be kept constant with a value depending on network planning. In order to take admission control decisions, the stability condition in (F.12) must also be fulfilled, which is the most conservative one.

Appendix G

Power Decrease Estimator for Uplink

G.1 Introduction

The use of a power increase estimator (PIE) is essential for power based admission control (AC) and packet scheduler (PS). In the PS and load control (LC) algorithms, power decrease estimators (PDE) are also necessary, in order to know the power available after deallocating resources to user equipments (UE), and therefore assign it to other users.

Although the PIE algorithms are sometimes used as PDEs, this is not completely optimal. In this case the PDE would give an estimation based on an erroneous initial load. This can be explained with the help of Figure G.1. Let us denote ΔP_{rx} the power decrease caused by the

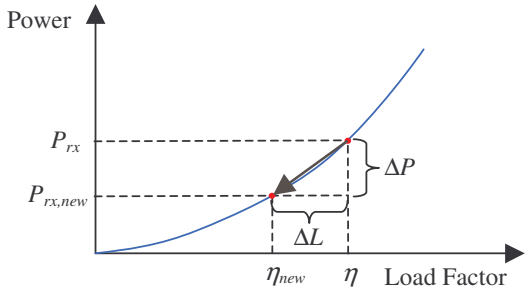

Figure G.1. Power and load factor decrease due to resource deallocation.

deallocation of resources associated with a proportion ΔL of the total received power P_{rx}. The initial load factor is η, ending up with a final load factor η_{new}. The load factor is defined as in (E.1). This value ΔP_{rx} is lower than the one that would be obtained by starting from the same load factor η and adding ΔL, instead of subtracting it, since the growth of the power is not lineal.

In this appendix, several PDEs are calculated based on the integrative and derivative versions of the PIE presented in [26] and the PIE for uplink synchronisation derived in Appendix F.

G.2 PDE for Non-Orthogonal Uplink

G.2.1 Derivative Method

According to the derivative method employed in [26], the power increase caused by the allocation of resources that would generate a load increase of ΔL in a BS with a load factor η_{new} is estimated as

$$\Delta P_{rx} = P_{rx,new} \frac{\Delta L}{1-\eta_{new}}. \tag{G.1}$$

This power increase is the same as the power decrease when deallocating ΔL with an initial load factor of η. The inconvenient is that for the case of the power decrease, η_{new} and $P_{rx,new}$ are not known before hand, but they can be calculated from η and P_{rx}:

$$\begin{aligned} P_{rx,new} &= P_{rx} - \Delta P_{rx}, \\ \eta_{new} &= \eta - \Delta L. \end{aligned} \tag{G.2}$$

The derivative version of the PDE is therefore

$$\begin{aligned} \Delta P_{rx} &= \left(P_{rx} - \Delta P_{rx}\right)\frac{\Delta L}{1-\left(\eta-\Delta L\right)} \\ &= P_{rx}\frac{\Delta L}{1-\eta+2\Delta L}. \end{aligned} \tag{G.3}$$

The expression calculated in (G.3) is valid if

$$\Delta P_{rx} \le P_{rx} - P_{noise} \Leftrightarrow \Delta L \le \eta \frac{1-\eta}{1-2\eta}. \tag{G.4}$$

G.2.2 Integrative Method

Let us assume the situation depicted in Figure G.1, where the base station (BS) initially operates under a load factor η; then, the BS decides to dellocate resources which generate a proportion ΔL of the total received power, as defined in (2.11). The final load factor decrease is higher than ΔL, since once the resources are dellocated, the rest of UEs in the system will transmit with lower power, since the interference associated with them decreases. The power decrease after deallocating the resources is

$$\Delta P_{rx} = P_{rx} - P_{rx,new}. \tag{G.5}$$

By using the approximation η-η_{new}=ΔL as shown in Figure G.1, the expression in (G.5) can be written as

$$\begin{aligned}\Delta P_{rx} &= \left(P_{rx}\eta - P_{noise}\right) - \left(P_{rx,new}\eta_{new} - P_{noise}\right) \\ &= P_{rx}\eta - P_{rx,new}\eta_{new} \\ &= P_{rx}\eta - \left(P_{rx} - \Delta P_{rx}\right)\left(\eta - \Delta L\right) \\ &= P_{rx}\Delta L + \Delta P_{rx}\eta - \Delta P_{rx}\Delta L \Leftrightarrow \\ \Delta P_{rx} &= P_{rx}\frac{\Delta L}{1-\eta+\Delta L}.\end{aligned} \tag{G.6}$$

The expression calculated in (G.6) is valid if

$$\Delta P_{rx} \le P_{rx} - P_{noise} \Leftrightarrow \Delta L \le \eta. \tag{G.7}$$

G.3 PDE for Uplink Synchronisation

Let us calculate a PDE for uplink synchronisation by keeping a similar approach as for the PIE in (F.11).

The power decrease at the BS after deallocating resources from synchronous UE with scrambling code #*j* is

$$\begin{aligned}\Delta P_{rx} &= \left(P_{rx}\eta - P_{noise}\right) - \left(P_{rx,new}\eta_{new} - P_{noise}\right) \\ &= P_{rx}\left(\eta^{j}_{async} + \eta^{j}_{sync}\right) - P_{rx,new}\left(\eta^{j}_{async,new} + \eta^{j}_{sync,new}\right),\end{aligned} \tag{G.8}$$

where η^{j}_{async}, $\eta^{j}_{async,new}$, η^{j}_{sync} and $\eta^{j}_{sync,new}$ are defined as in Appendix F.

By making $\eta^{j}_{async,new}$=η^{j}_{async}, the other cell interference is assumed to decrease proportionally to the reduction of the interference from the own cell UEs under scrambling codes different from #*j*

$$\begin{aligned}\Delta P_{rx} &= P_{rx}\left(\eta^{j}_{async} + \eta^{j}_{sync}\right) - \left(P_{rx} - \Delta P_{rx}\right)\left(\eta^{j}_{async} + \eta^{j}_{sync,new}\right) \\ &= P_{rx}\frac{\eta^{j}_{sync} - \eta^{j}_{sync,new}}{1-\eta^{j}_{async} - \eta^{j}_{sync,new}} \\ &= P_{rx}\frac{\Delta L\left(1-\alpha\eta^{j}_{sync}\right)}{1-\eta+\Delta L\left(1-\alpha\eta^{j}_{sync}\right)}.\end{aligned} \tag{G.9}$$

In this case, the expression is valid if

$$\Delta P_{rx} \le P_{rx} - P_{noise} \Leftrightarrow \Delta L \le \frac{\eta}{1-\alpha\eta^{j}_{sync}}. \tag{G.10}$$

Appendix H

Influence of the DPCCH in AVI Tables Intended for DPDCHs

H.1 Introduction

This appendix analyses the effect of using the AVI tables that include the effect of one Dedicated Physical Data Channel (DPDCH) and one Dedicated Physical Control Channel (DPCCH) in the simulations performed with HARQ Type II/III, i.e. with soft combining. The appendix also addresses the impact of using the same AVI tables for different data rates.

H.2 Effect in Calculations for HARQ

As explained in Appendix B, the AVI tables employed in this Ph.D. thesis to map the link level simulations into system level simulations include the combined operation of one DPDCH and one DPCCH, i.e. they provide one unique block error rate (BLER) value associated to the data part by giving as input one value of energy-per-bit to noise ratio (Eb/No) that corresponds to the sum of the contributions from both the DPDCH and the DPCCH.

In HARQ Type II/III, the received signal from retransmissions of a packet is combined with the previous received versions of the same packet. Assuming soft combining, the received Eb/No is added to the cumulated Eb/No from the previous transmissions, including a certain combining loss. The cumulated Eb/No is then used as an input for the AVI tables in order to

obtain the new BLER. However, the Eb/No for every single retransmission includes the energy from both the data and the control, whereas the soft combining is only intended for the data part.

In the following, a description is provided on how to obtain the Eb/No associated to the data channel from the Eb/No that includes both the data and the control channel.

The Eb/No including the data and the control channel can be expressed as

$$\begin{aligned}\left(\text{Eb/No}\right)_{data+control} &= G\cdot\left(\text{SIR}\right)_{data+control}\\ &= G\frac{P_{data}+P_{control}}{I}h,\end{aligned} \tag{H.1}$$

where $(\text{SIR})_{data+control}$ is the signal-to-interference ratio (SIR) including both the DPDCH and the PDCCH as the desired signal, G is the processing gain, P_{data} and $P_{control}$ are the transmission power associated with the DPDCH and the DPCCH, respectively, h is the path gain from the user equipment (UE) to the base station (BS), and I is the interference power.

The Eb/No including only the data channel is

$$\begin{aligned}\left(\text{Eb/No}\right)_{data} &= G\cdot\left(\text{SIR}\right)_{data}\\ &= G\frac{P_{data}}{I}h\\ &= \left(\text{Eb/No}\right)_{data+control}\frac{P_{data}}{P_{data}+P_{control}},\end{aligned} \tag{H.2}$$

where $(\text{SIR})_{data}$ is the SIR including only the DPDCH as the desired signal. Hence, the loss when translating the Eb/No including data and control channel into an Eb/No including only the data channel is

$$L_{control}=\frac{\left(\text{Eb/No}\right)_{data+control}}{\left(\text{Eb/No}\right)_{data}}=\frac{P_{data}+P_{control}}{P_{data}}. \tag{H.3}$$

For example, according to [49] the ratio of power for control to power for data channel is –5.46 dB for a circuit-switched service at 64 kbps, which yields $L_{control}$=1.09 dB.

Notice from equation (6.5) the combining loss was added to the whole cumulated Eb/No. However, the loss due to excluding the contribution of the control channel in the AVI tables only applies to the Eb/No associated with the new single retransmission, i.e.

$$\left(\text{Eb/No}\right)_{cum,n}=\begin{cases}\left(\text{Eb/No}\right)_{data+control,n} & \text{if } n=1\\ \left(\text{Eb/No}\right)_{cum,n-1}+\dfrac{\left(\text{Eb/No}\right)_{data+control,n}}{L_{control}} & \\ \hline L_{comb} & \text{if } n>1,\end{cases} \tag{H.4}$$

where $(\text{Eb/No})_{cum,n}$ is the cumulated Eb/No after n transmissions, $(\text{Eb/No})_{data+control,n}$ is the value of $(\text{Eb/No})_{data+control}$ at the n-th transmission of the same block and L_{comb} is the combining loss.

By assuming the same received Eb/No for all the transmissions of the same packet, it is possible to translate this loss per single transmission into a loss for the cumulated Eb/No. For the case of $L_{control}$=1.09 dB, a total loss in the cumulated Eb/No of 0.51 dB should be applied if $(\text{Eb/No})_{data+control}$ is employed for the first retransmission, 0.18 dB after the second retransmission, 0.10 dB after the third retransmission, and 0.06 dB after the forth one.

Data Rate	$(Eb/No)_R/(Eb/No)_{64kbps}$
64 kbps	0.00 dB
128 kbps	-0.51 dB
256 kbps	-0.78 dB
384 kbps	-0.89 dB

Table H.1. Offset in the required Eb/No for different data rates with respect to the value obtained with the AVI tables for 64 kbps.

Notice that for higher data rates $L_{control}$ is lower, as the ratio of control to data power decreases. For example, a data rate of 256 kbps would require four times less power for the control channel than with a data rate of 64 kbps, which yields $L_{control}$ =0.30 dB.

H.3 Use of the AVI Tables for Different Data Rates

The AVI tables employed for the simulations associated with the study carried out in Chapter 6 correspond to a circuit-switched service at 64 kbps. However in such study a higher set of available data rates is considered, and the same AVI tables are utilised for all the cases. In this section, the impact of employing AVI tables for different data rates is addressed.

Provided that the AVI tables only include the effect of the data channel, they are independent of the data rate. However, as far as they include the effect of the associated dedicated control channel, there exist some variations due to the different ratio of control-to-data power. By using the expression in (H.1) for the required Eb/No including both the control and the data channel, it is possible to calculate the value $(Eb/No)_R$ associated with a certain data rate R as a function of the reference value $(Eb/No)_{64kbps}$ associated with a data rate of 64 kbps

$$(Eb/No)_R = (Eb/No)_{64kbps} \frac{1+p_R}{1+p_{64kbps}}, \quad \text{(H.5)}$$

where p_R and p_{64kbps}=-5.46 dB are the ratio of control-to-data power associated with data rate R and 64 kbps, respectively.

If the change in the data rate is carried out by only varying the spreading factor (e.g. other option could have been to vary the coding rate), the ratio of control-to-data power is inversely proportional to the data rate. Based on this, the offset in the required Eb/No for different data rates when employing the AVI tables for 64 kbps is presented in Table H.1.

Notice that the required Eb/No with AVI tables for higher data rates is smaller than with the AVI tables for 64 kbps for the same BLER target. On the other hand, lower data rates than 64 kbps normally require the same ratio of power for control to power for data channels [49].

Appendix I

Data Traffic Model for System Level Simulations

This appendix summarises the source uplink traffic model associated with the input of the Radio Link Control (RLC) buffer implemented for the system level simulations with packet services in Chapter 6. The chosen traffic model corresponds to the modified gaming model described in [32], and its mechanism is illustrated in Figure I.1.

The parameters are compiled in Table I.1, and correspond to an average source data rate of 250 kbps during a packet call. The model is implemented by assuming infinite user RLC buffer size as well as infinite lifetime of a packet in the buffer.

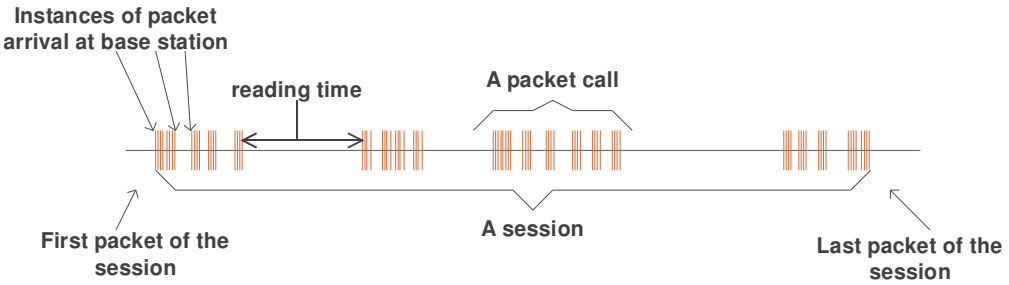

Figure I.1. Source packet data model with packets (datagrams) arriving as part of a packet call [32].

Parameter		Distribution	Values
Packet call	Duration	Exponential	mean: 5 s
	Reading time	Exponential	mean: 5 s
Datagram	Inter-arrival time	Log-normal	mean: 40 ms; std: 38 ms
	Size	-	1152 bytes

Table I.1. Parameter setting for the modified gaming traffic model.

Bibliography

[1] J. De Vriendt, P. Laine, C. Lerouge and X. Xiaofeng, "Mobile network evolution: a revolution on the move", *IEEE Communications Magazine*, Vol. 40, Issue 4, pp. 104-111, April 2002.

[2] www.3gpp2.com

[3] www.3gpp.com

[4] S. Parkvall, E. Dahlman, P. Frenger, P. Beming, and M. Persson, "The high speed packet data evolution of WCDMA", *IEEE International Symposium on Personal, Indoor and Mobile Radio Communications*, Vol. 2, pp. G27-G31, San Diego (USA), October 2001.

[5] P. Chaudhury, W. Mohr, "The 3GPP proposal for IMT-2000", *IEEE Communications Magazine*, Vol. 37, No. 12, pp. 72-81, December 1999.

[6] T. E. Kolding, K. I. Pedersen, J. Wigard, F. Frederiksen, and P. E. Mogensen, "High Speed Downlink Packet Access: WCDMA Evolution", *IEEE Veh. Technol. Society News*, Vol. 50, No. 1, pp. 4-10, February 2003.

[7] H. Holma and A. Toskala (Editors), "WCDMA for UMTS. Radio Access for Third Generation Mobile Communications", *John Wiley & Sons, Ltd*, England, 2000.

[8] E. Dahlman, P. Beming, J. Knutsson, F. Ovesjo, M. Persson and C. Roobol, "WCDMA-the radio interface for future mobile multimedia communications", *IEEE Transactions on Vehicular Technology*, Vol. 47, No. 4, pp. 1105-1118, November 1998.

[9] 3rd Generation Partnership Project, "Spreading and modulation (FDD)", TS 25.213, Version 4.3.0, Release 4, Available at www.3gpp.org, June 2002.

[10] 3rd Generation Partnership Project, "UE Radio Transmission and Reception (FDD)", TS 25.101, Version 5.0.0, Release 5, Available at www.3gpp.org, September 2001.

[11] W.C.Y. Lee, "Power control in CDMA", *IEEE Vehicular Technology Conference*, pp. 77-80, St Louis (Missouri), May 1991.

[12] T.S. Rappaport, "Wireless communications: principles and practice", *Prentice Hall PTR*, Upper Saddle River (New Jersey), 1996.

[13] G. Fock, J. Baltersee, P. Schulz-Rittich, and H. Meyr, "Channel tracking for RAKE receivers in closely spaced multipath environments", *IEEE Journal on Selected Areas in Communications*, Vol. 19, Issue 12, pp. 2420-2431, December 2001.

[14] Telecompetition, Inc., "3G Wireless Data Traffic Characteristics. Commercial Report", June 2001.

[15] H. Holma and A. Tolli, "Simulated and measured performance of 4-branch uplink reception in WCDMA", *IEEE Vehicular Technology Conference*, Vol. 4, pp. 2640-2644, Rhodes (Greece), May 2001.

[16] A. Jalali and P. Mermelstein, "Effects of multipath and antenna diversity on the uplink capacity of a CDMA wireless system", *IEEE Global Telecommunications Conference*, Vol. 3, pp. 1660-1664, Houston (Texas), November 1993.

[17] J. Ramiro, “System level performance analysis of advanced antenna concepts in WCDMA”, Ph.D. Thesis, University of Aalborg (Denmark), July 2003.

[18] J. H. Winters, “Smart antennas for wireless systems”, *IEEE Personal Communications*, Vol. 5, pp. 23-27, February 1998.

[19] R. Kohno, “Spatial and temporal communication theory using adaptive antenna array”, *IEEE Personal Communications*, Vol. 5, pp. 28-35, February 1998.

[20] A. F. Naguib, A. Paulraj, and T Kailath, “Capacity improvement with base-station antenna arrays in cellular CDMA”, *IEEE Transactions on Vehicular Technology*, Vol. 43, No. 3, pp. 691-698, August 1994.

[21] S. Moshavi, “Multi-user detection for DS-CDMA communications”, *IEEE Communications Magazine*, Vol. 34, pp. 124-136, October 1996.

[22] A. Duel-Hallen, J. Holtzman, and Z. Zvonar, “Multiuser detection for CDMA systems”, *IEEE Personal Communications*, Vol. 2, pp. 46-58, April 1995.

[23] S. Verdu, “Multiuser detection”, *Cambridge University Press*, 1998.

[24] 3rd Generation Partnership Project, "Study report for Uplink Synchronous Transmission Scheme (USTS)", TR 25.854, Version 5.0.0, Release 5, Available at www.3gpp.org, December 2001.

[25] D.K. Kim, S.H. Hwang, E.K. Hong and S.Y. Lee, “Capacity estimation for an uplink synchronised CDMA system with fast TPC and two-antenna diversity reception”, *IEICE Transactions on Communications*, Vol. E84-B, No. 8, pp. 2309-2312, August 2001.

[26] H. Holma and J. Laakso, “Uplink Admission Control and Soft Capacity with MUD in CDMA”, *IEEE Vehicular Technology Conference*, Vol. 1, pp. 431-435, Amsterdam (Netherlands), September 1999.

[27] J. Kuri and P. Mermelstein, “Call Admission on the Uplink of a CDMA System based on Total Received Power”, *IEEE International Conference on Communications*, Vol. 3, pp. 1431-1436,Vancouver (Canada), June 1999.

[28] S. Kumar and S. Nanda, “High Data-Rate Packet Communications for Cellular Networks Using CDMA: Algorithms and Performance”, *IEEE Journal on Selected Areas in Communications*, Vol. 17, No. 3, pp. 472-492, March 1999.

[29] K. Dimou, C. Rosa, T. B. Sørensen, J. Wigard and P. E. Mogensen, “Performance of uplink packet services in WCDMA”, *IEEE Vehicular Technology Conference*, Vol. 3, pp. 2071-2075, Jeju (Korea), April 2003.

[30] Z. Liu and M. Zarki, “SIR-Based Call Admission Control for DS-CDMA Cellular Systems”, *IEEE Journal on Selected Areas in Communications*, Vol. 12, No. 4, pp. 638-644, May 1994.

[31] E. Villier, P. Legg and S. Barrett, “Packet data transmissions in a W-CDMA network - Examples of uplink scheduling and performance”, *IEEE Vehicular Technology Conference*, Vol. 3, pp. 2449-2453, Tokyo (Japan), May 2000.

[32] 3rd Generation Partnership Project, “Feasibility Study for Enhanced Uplink for UTRA FDD”, TR 25.896, Version 6.0.0, Release 6, Available at www.3gpp.org, September 2003.

[33] B. Timus and J. Pettersson, “Uplink admission control for conversational services using information from many cells”, *IEEE Proc. of Veh. Technol. Conference*, Vol. 2, pp. 1068-1072, Rhodes (Greece), May 2001.

[34] 3rd Generation Partnership Project, “Requirements for Support of Radio Resource Management (FDD)”, TS 25.133, Version 4.2.0, Release 4, Available at www.3gpp.org, September 2001.

[35] J. Outes, L. Nielsen, K. Pedersen and P. Mogensen, “Multi-Cell Admission Control for UMTS”, *IEEE Vehicular Technology Conference*, Vol. 2, pp. 987-991, Rhodes (Greece), May 2001.

[36] 3rd Generation Partnership Project, “Physical layer - Measurements (FDD)”, TS 25.215, Version 4.2.0, Release 4, Available at www.3gpp.org, September 2001.

[37] Y. Wei, J. Krogmeier and S. Gelfand, “Reliable uplink code-timing synchronization for cellular DS-CDMA", *IEEE Sixth International Symposium on Spread Spectrum Techniques and Applications*, Vol. 2, pp. 628-632, Parsippany (New Jersey), 2000.

[38] R.D.J. van Nee, “Timing aspects of synchronous CDMA”, *IEEE International Symposium on Personal, Indoor and Mobile Radio Communications*, Vol. 2, pp. 439-443, The Hague (Netherlands), September 1994.

[39] K.I. Pedersen and P.E. Mogensen, “The Downlink Orthogonality Factors Influence on WCDMA System Performance”, *IEEE Vehicular Technology Conference*, pp. 2061-2065, Vancouver (Canada), September 2002.

[40] T. Klingenbrunn, “Downlink capacity enhancement of UTRA FDD networks”, Ph.D. Thesis, University of Aalborg (Denmark), January 2001.

[41] W. Jakes, “Microwave mobile communications”, *IEEE Press*, New Jersey, January 1994.

[42] C. Passerini and G. Falciasecca, “Correlation between delay-spread and orthogonality factor in urban environments”, *IEE Electronics Letters*, Vol. 37, No. 6, pp. 384-386, March 2001.

[43] Universal Mobile Telecommunications System (UMTS), “Selection procedures for the choice of radio transmission technologies of the UMTS”, TR 101 112 version 3.2.0 (UMTS 30.03 version 3.2.0), Available at www.3gpp.org, April 1998.

[44] P. Pirinen, “Impact of mobility and closed-loop power control to received signal statistics in Rayleigh fading channels”, *IEEE Vehicular Technology Conference*, Vol. 4, pp. 2859-2863, Rhodes (Greece), May 2001.

[45] S. Parkvall, M. Karlsson, M. Samuelsson, L. Hedlund, and B. Goransson, “Transmit diversity in WCDMA: link and system level results”, *IEEE Vehicular Technology Conference*, Vol. 2, pp. 864-868, Tokyo (Japan), May 2000.

[46] J. Laiho, A. Wacker and T. Novosad (Editors), “Radio Network Planning and Optimisation for UMTS”, *John Wiley & Sons, Ltd*, England, 2002.

[47] S. Hämäläinen, H. Holma and K. Sipilä, “Advanced WCDMA Radio Network Simulator”, *IEEE International Symposium on Personal, Indoor and Mobile Radio Communications*, Osaka (Japan), September 1999.

[48] M.M. Zonoozi and P. Dassanayake, "Shadow fading in mobile radio channel", *IEEE International Symposium on Personal, Indoor and Mobile Radio Communications*, Vol. 2, pp. 291-295, Taipei (Taiwan), October 1996.

[49] Nokia internal document, "Actual value interface tables for Wallu simulator".

[50] S. Hämäläinen, P. Slanina, M. Hartman, A. Lappeteläinen, H. Holma and O. Salonaho, "A Novel Interface Between Link and System Level Simulations", *Proc. of ACTS Summit 1997*, pp. 509-604, Aalborg (Denmark), October 1997.

[51] A. Sampath, P.S. Kumar and J. M. Holtzman, "On setting reverse link target SIR in a CDMA system", *IEEE Vehicular Technology Conference*, Vol. 2, pp. 929-933, Phoenix (Arizona), May 1997.

[52] N. Binucci, K. Hiltunen and M. Caselli, "Soft handover gain in WCDMA", *IEEE Vehicular Technology Conference*, Vol. 3, pp. 1467-1472, Boston (Massachusetts), September 2000.

[53] 3rd Generation Partnership Project, "High Speed Downlink Packet Access (HSDPA); Overall Description", TR 25.308, Version 5.4.0, Release 5, Available at www.3gpp.org, March 2003.

[54] 3rd Generation Partnership Project, "Multiplexing and channel coding (FDD)", TS 25.212, Version 4.2.0, Release 4, Available at www.3gpp.org, September 2001.

[55] S. Ramakrishna and J.M. Holtzman, "A scheme for throughput maximization in a dual-class CDMA system", *IEEE Journal on Selected Areas in Communications*, Vol. 16, No. 6, pp. 830-844, August 1998.

[56] E.G. Barrantes-Sliesarieva and A.F. Lobo, "Scheduling in third generation wireless networks", *Proc. of Southcon'95*, pp. 273-278, Fort Lauderdale (Florida), March 1995.

[57] 3rd Generation Partnership Project 2, "Comparison of rate control and scheduling in terms of throughput", TSG-C WG3 C30-20030616-075, Available at www.3gpp2.org, San Diego (California), June 2003.

[58] 3rd Generation Partnership Project 2, "Performance of rate control on 1xEV-DV reverse link", TSG-C WG3 C30-20030704-042, Available at www.3gpp2.org, San Francisco (California), July 2003.

[59] R.T. Derryberry and Z. Pi, "1x evolved high-speed integrated data and voice (1xEV-DV): Reverse link overview and performance", *Telecommunications Review*, Vol. 13, No. 6, pp. 881-893, December 2003.

[60] Z. Pi and R.T. Derryberry, "CDMA2000 1x EV-DV reverse link system design", *IEEE Wireless Communications and Networking Conference*, Vol. 1, pp. 514-519, New Orleans (Louisiana), March 2003.

[61] K. Kumaran and L. Qian, "Uplink scheduling in CDMA packet-data systems", *IEEE INFOCOM 2003 Conference*, Vol. 1, pp. 292-300, San Francisco (California), April 2003.

[62] E. Malkamäki, D. Mathew, D and S. Hamalainen, "Performance of hybrid ARQ techniques for WCDMA high data rates", *IEEE Vehicular Technology Conference*, Vol. 4, pp. 2720-2724, Rhodes (Greece), May 2001.

[63] F. Frederiksen and T.E. Kolding, "Performance and modeling of WCDMA/HSDPA transmission/H-ARQ schemes", *IEEE Vehicular Technology Conference*, Vol. 1, pp. 472-476, Vancouver (Canada), September 2002.

[64] L. Zhang, F. Li and J. Zhu, "Performance analysis of multiple reject ARQ theme at RLC layer in 3G", *IEEE Vehicular Technology Conference*, Vol. 4, pp. 2056-2060, Vancouver (Canada), September 2002.

[65] X. Peng, F.P.S. Chin, Y.C. Liang and M. Motani, "Performance of hybrid ARQ techniques based on turbo codes for high-speed packet transmission", *IEEE Seventh International Symposium on Spread Spectrum Techniques and Applications*, Vol. 3, pp. 682-686, Prague (Czech Republic), September 2002.

[66] M. Raitola and H. Holma, "Wideband CDMA packet data with hybrid ARQ", *IEEE Fifth International Symposium on Spread Spectrum Techniques and Applications*, Vol. 1, pp. 318-322, Sun City (South Africa), September 1998.

[67] 3rd Generation Partnership Project, "RRC Protocol Specification", TS 25.331, Version 4.2.0, Release 4, Available at www.3gpp.org, September 2001.

[68] 3rd Generation Partnership Project, "MAC protocol specification", TS 25.321, Version 4.7.0, Release 4, Available at www.3gpp.org, December 2002.

[69] 3rd Generation Partnership Project, "Interlayer procedures in connected mode, TS 25.303, Version 3.12.0, Release 1999, Available at www.3gpp.org, June 2002.

[70] 3rd Generation Partnership Project, "Report on Hybrid ARQ Type II/III", TS 25.835, Version 1.0.0, Release 2000, Available at www.3gpp.org, September 2000.

[71] C. Rosa, J. Outes, K. Dimou, et al: "Performance of Fast Node B Scheduling and L1 HARQ Schemes in WCDMA Uplink Packet Access", to be published at the *IEEE Vehicular Technology Conference*, Milan (Italy), May 2004.

[72] 3rd Generation Partnership Project, "On the Potential Gains with Uplink Scheduling", TSG RAN WG1 #32-03-0453, Available at www.3gpp.org, EuroDisney (France), May 2003.

[73] P.J. Ameigeiras, "Packet scheduling and quality of service in HSDPA", Ph.D. Thesis, University of Aalborg (Denmark), October 2003.

[74] K. I. Pedersen and P. E. Mogensen, "Directional power-based admission control for WCDMA systems using beamforming antenna array systems", *IEEE Transactions on Vehicular Technology*, Vol. 51, No. 6, pp. 1294-1303, November 2002.

[75] Nokia internal document, "2G HSDPA AVI tables (rev. 1.0). Documentation and basic verification".

[76] 3rd Generation Partnership Project, "Channelization code allocation in uplink multi-code transmissions", TSG RAN WG1 #6-99-828, Available at www.3gpp.org, Espoo (Finland), July 1999.

[77] R. Ratasuk and A. Ghosh, "Performance analysis of time-multiplexed services for UMTS W-CDMA reverse link", *IEEE Vehicular Technology Conference*, Vol. 3, pp. 1607-1611, Vancouver (Canada), September 2002.

[78] K. Laird, N. Whinnett and S. Buljore, "A peak-to-average power reduction method for third generation CDMA reverse links", *IEEE Vehicular Technology Conference*, Vol. 1, pp. 551-551, Houston (Texas), May 1999.

[79] R. Attar, "On the Peak-to-Average Ratio (PAR) of an IS-856 (cdma2000 1xEV) Forward Link", *IEEE Conference on Mobile and Wireless Communication Networks*, Rezife (Brazil), August, 2001

[80] J. Kim, S. Park and D.K. Sung, "Spreading Modulation for Reduction of Peak-to-Average Radio in DS/CDMA Systems", *4th International Symposium on Multi-Dimensional Mobile Communications*, Pori (Finland), June 2001.

[81] 3rd Generation Partnership Project, "On the peak to average issues in the UL", TSG RAN WG1 #32-03-0574, Available at www.3gpp.org, Paris (France), May 2003.